frontiers | Research Topics

Ocean artificial upwelling – ecological responses and biogeochemical impacts

Edited by
Ulf Riebesell, Javier Arístegui, Nina Bednarsek, Angelicque White and Ricardo Maria Letelier

Published in
Frontiers in Marine Science

ISSN 1664-8714
ISBN 978-2-8325-4746-5
DOI 10.3389/978-2-8325-4746-5

About Frontiers

Frontiers is more than just an open access publisher of scholarly articles: it is a pioneering approach to the world of academia, radically improving the way scholarly research is managed. The grand vision of Frontiers is a world where all people have an equal opportunity to seek, share and generate knowledge. Frontiers provides immediate and permanent online open access to all its publications, but this alone is not enough to realize our grand goals.

Frontiers journal series

The Frontiers journal series is a multi-tier and interdisciplinary set of open-access, online journals, promising a paradigm shift from the current review, selection and dissemination processes in academic publishing. All Frontiers journals are driven by researchers for researchers; therefore, they constitute a service to the scholarly community. At the same time, the *Frontiers journal series* operates on a revolutionary invention, the tiered publishing system, initially addressing specific communities of scholars, and gradually climbing up to broader public understanding, thus serving the interests of the lay society, too.

Dedication to quality

Each Frontiers article is a landmark of the highest quality, thanks to genuinely collaborative interactions between authors and review editors, who include some of the world's best academicians. Research must be certified by peers before entering a stream of knowledge that may eventually reach the public - and shape society; therefore, Frontiers only applies the most rigorous and unbiased reviews. Frontiers revolutionizes research publishing by freely delivering the most outstanding research, evaluated with no bias from both the academic and social point of view. By applying the most advanced information technologies, Frontiers is catapulting scholarly publishing into a new generation.

What are Frontiers Research Topics?

Frontiers Research Topics are very popular trademarks of the *Frontiers journals series*: they are collections of at least ten articles, all centered on a particular subject. With their unique mix of varied contributions from Original Research to Review Articles, Frontiers Research Topics unify the most influential researchers, the latest key findings and historical advances in a hot research area.

Find out more on how to host your own Frontiers Research Topic or contribute to one as an author by contacting the Frontiers editorial office: frontiersin.org/about/contact

Ocean artificial upwelling – ecological responses and biogeochemical impacts

Topic editors

Ulf Riebesell — GEOMAR Helmholtz Center for Ocean Research Kiel, Helmholtz Association of German Research Centres (HZ), Germany

Javier Arístegui — University of Las Palmas de Gran Canaria, Spain

Nina Bednarsek — Oregon State University, United States

Angelicque White — University of Hawaii at Manoa, United States

Ricardo Maria Letelier — Oregon State University, United States

Citation

Riebesell, U., Arístegui, J., Bednarsek, N., White, A., Letelier, R. M., eds. (2024). *Ocean artificial upwelling – ecological responses and biogeochemical impacts*. Lausanne: Frontiers Media SA. doi: 10.3389/978-2-8325-4746-5

Table of contents

04 Effect of Intensity and Mode of Artificial Upwelling on Particle Flux and Carbon Export
Moritz Baumann, Jan Taucher, Allanah J. Paul, Malte Heinemann, Mari Vanharanta, Lennart T. Bach, Kristian Spilling, Joaquin Ortiz, Javier Arístegui, Nauzet Hernández-Hernández, Isabel Baños and Ulf Riebesell

21 Numerical Flow Modeling of Artificial Ocean Upwelling
Jost Kemper, Ulf Riebesell and Kai Graf

34 Artificial Upwelling in Singular and Recurring Mode: Consequences for Net Community Production and Metabolic Balance
Joaquin Ortiz, Javier Arístegui, Jan Taucher and Ulf Riebesell

44 Oligotrophic Phytoplankton Community Effectively Adjusts to Artificial Upwelling Regardless of Intensity, but Differently Among Upwelling Modes
Joaquin Ortiz, Javier Arístegui, Nauzet Hernández-Hernández, Mar Fernández-Méndez and Ulf Riebesell

59 Expected Limits on the Potential for Carbon Dioxide Removal From Artificial Upwelling
David A. Koweek

73 Response of plankton community respiration under variable simulated upwelling events
Isabel Baños, Javier Arístegui, Mar Benavides, Markel Gómez-Letona, María F. Montero, Joaquín Ortiz, Kai G. Schulz, Andrea Ludwig and Ulf Riebesell

85 The importance of the dissolved organic matter pool for the carbon sequestration potential of artificial upwelling
Markel Gómez-Letona, Marta Sebastián, Isabel Baños, María Fernanda Montero, Clàudia Pérez Barrancos, Moritz Baumann, Ulf Riebesell and Javier Arístegui

102 Nutrient composition (Si:N) as driver of plankton communities during artificial upwelling
Silvan Urs Goldenberg, Jan Taucher, Mar Fernández-Méndez, Andrea Ludwig, Javier Arístegui, Moritz Baumann, Joaquin Ortiz, Annegret Stuhr and Ulf Riebesell

117 Counteracting effects of nutrient composition (Si:N) on export flux under artificial upwelling
Moritz Baumann, Silvan Urs Goldenberg, Jan Taucher, Mar Fernández-Méndez, Joaquin Ortiz, Jacqueline Haussmann and Ulf Riebesell

130 Microzooplankton communities and their grazing of phytoplankton under artificial upwelling in the oligotrophic ocean
Kristian Spilling, Mirian Arellano San Martín, Mira Granlund, Kai G. Schulz, Carsten Spisla, Mari Vanharanta, Silvan Urs Goldenberg and Ulf Riebesell

frontiers in Marine Science

ORIGINAL RESEARCH
published: 27 October 2021
doi: 10.3389/fmars.2021.742142

Effect of Intensity and Mode of Artificial Upwelling on Particle Flux and Carbon Export

Moritz Baumann[1], Jan Taucher[1], Allanah J. Paul[1], Malte Heinemann[2], Mari Vanharanta[3,4], Lennart T. Bach[5], Kristian Spilling[3,6], Joaquin Ortiz[1], Javier Arístegui[7], Nauzet Hernández-Hernández[7], Isabel Baños[7] and Ulf Riebesell[1]*

[1] Marine Biogeochemistry, Biological Oceanography, GEOMAR Helmholtz Centre for Ocean Research Kiel, Kiel, Germany, [2] Institute of Geosciences, Kiel University, Kiel, Germany, [3] Marine Research Centre, Finnish Environment Institute, Helsinki, Finland, [4] Tvärminne Zoological Station, University of Helsinki, Hanko, Finland, [5] Institute for Marine and Antarctic Studies, University of Tasmania, Hobart, TAS, Australia, [6] Centre for Coastal Research, University of Agder, Kristiansand, Norway, [7] Oceanografía Biológica, Instituto de Oceanografía y Cambio Global, Universidad de Las Palmas de Gran Canaria, Las Palmas de Gran Canaria, Spain

Reduction of anthropogenic CO_2 emissions alone will not sufficiently restrict global warming and enable the 1.5°C goal of the Paris agreement to be met. To effectively counteract climate change, measures to actively remove carbon dioxide from the atmosphere are required. Artificial upwelling has been proposed as one such carbon dioxide removal technique. By fueling primary productivity in the surface ocean with nutrient-rich deep water, it could potentially enhance downward fluxes of particulate organic carbon (POC) and carbon sequestration. In this study we investigated the effect of different intensities of artificial upwelling combined with two upwelling modes (recurring additions vs. one singular addition) on POC export, sinking matter stoichiometry and remineralization depth. We carried out a 39 day-long mesocosm experiment in the subtropical North Atlantic, where we fertilized oligotrophic surface waters with different amounts of deep water. The total nutrient inputs ranged from 1.6 to 11.0 μmol NO_3^- L^{-1}. We found that on the one hand POC export under artificial upwelling more than doubled, and the molar C:N ratios of sinking organic matter increased from values around Redfield (6.6) to ∼8–13, which is beneficial for potential carbon dioxide removal. On the other hand, sinking matter was remineralized at faster rates and showed lower sinking velocities, which led to shallower remineralization depths. Particle properties were more favorable for deep carbon export in the recurring upwelling mode, while in the singular mode the C:N increase of sinking matter was more pronounced. In both upwelling modes roughly half of the produced organic carbon was retained in the water column until the end of the experiment. This suggests that the plankton communities were still in the process of adjustment, possibly due to the different response times of producers and consumers. There is thus a need for studies with longer experimental durations to quantify the responses of fully adjusted communities. Finally, our results revealed that artificial upwelling affects a variety of sinking particle properties, and that the intensity and mode with which it is applied control the strength of the effects.

Keywords: artificial upwelling, export flux, particle properties, sinking velocity, remineralization rate, remineralization depth, carbon sequestration, mesocosm study

OPEN ACCESS

Edited by:
Angelicque White, University of Hawai'i at Mānoa, United States

Reviewed by:
Chin-Chang Hung, National Sun Yat-sen University, Taiwan
Bieito Fernández Castro, University of Southampton, United Kingdom

****Correspondence:***
Moritz Baumann
mbaumann@geomar.de

Specialty section:
This article was submitted to Marine Biogeochemistry, a section of the journal Frontiers in Marine Science

Received: *15 July 2021*
Accepted: *05 October 2021*
Published: *27 October 2021*

Citation:
Baumann M, Taucher J, Paul AJ, Heinemann M, Vanharanta M, Bach LT, Spilling K, Ortiz J, Arístegui J, Hernández-Hernández N, Baños I and Riebesell U (2021) Effect of Intensity and Mode of Artificial Upwelling on Particle Flux and Carbon Export. Front. Mar. Sci. 8:742142. doi: 10.3389/fmars.2021.742142

INTRODUCTION

To limit global warming to between 1.5 and 2°C as committed in the Paris Climate Agreement, reducing carbon dioxide (CO_2) emissions alone will most likely not suffice. Negative emission technologies, which actively remove CO_2 from the atmosphere, will be needed to achieve net zero CO_2 emissions (IPCC, 2018). Many such technologies focus on the ocean (GESAMP, 2019), which has the capacity to potentially store large amounts of extra carbon (Sabine et al., 2004). The world ocean has already absorbed roughly a third of cumulated anthropogenic CO_2 emissions (Khatiwala et al., 2013), thereby mitigating a substantial part of global warming. The ocean's storage capacity might be further enhanced by strengthening the carbon flux from the air-sea-interface to the deep ocean. One component of this flux is the biological carbon pump, which mediates the transport of organic carbon produced in the euphotic zone to the deep ocean. Once the carbon reaches the deep ocean, it remains out of touch with the atmosphere for decades to centuries (i.e., sequestered, Boyd et al., 2019). Some negative emission technologies focus on strengthening the biological carbon pump to enhance this natural carbon sink. In the oligotrophic ocean, increased vertical mixing and resulting nutrient-upwelling can enhance carbon fluxes to the deep ocean (Pedrosa-Pàmies et al., 2019). This principle is utilized by a negative emission technology called "artificial upwelling," an approach in which nutrient- and CO_2-rich deep ocean water is pumped to the surface layer with the goal of enhancing primary production and hence, carbon export.

The feasibility of artificial upwelling as a CO_2-sequestration technique has been disputed by several modeling studies. Although it has the potential to sequester additional atmospheric carbon (Yool et al., 2009), Pan et al. (2015) found this potential to be rather small and connected to very high efforts; i.e., the upwelling of massive amounts of water (117 Sv) from 1,000 m depth would achieve an additional oceanic CO_2 uptake of 1 Gt C yr^{-1}. For comparison, in the year 2008 the oceans took up ∼2.5 Gt of anthropogenic carbon (Khatiwala et al., 2009). Furthermore, modeling studies have suggested that geophysical ocean-atmosphere feedbacks might lead to undesirable side-effects, e.g., that stopping artificial upwelling after several decades of large-scale operation would increase global temperatures to levels higher than if it had not been applied at all (Oschlies et al., 2010; Keller et al., 2014; Kwiatkowski et al., 2015). Beside such geophysical feedbacks, other major unknowns are the biological and biogeochemical responses of pelagic communities to artificial upwelling. Basically all our knowledge about potential effects of artificial upwelling is based on models with a low degree of ecological complexity and simplified biogeochemistry (e.g., constant stoichiometry and particle properties). So far, there is little empirical research on the effects of artificial upwelling on the ecology and biogeochemistry of pelagic plankton communities.

The limited number of experimental studies so far have shown that artificial upwelling can significantly increase phytoplankton biomass in oligotrophic waters (McAndrew et al., 2007; Strohmeier et al., 2015; Giraud et al., 2016, 2019; Casareto et al., 2017). However, studies considering its effect on the export production and carbon sequestration processes are scarce, mostly due to the methodological difficulties of simulating artificial upwelling under close-to-natural conditions. Svensen et al. (2002) carried out a mesocosm nutrient enrichment experiment, in which they found that nutrient enrichment increases particulate organic carbon (POC) sedimentation and that the effect size is dependent on the frequency of nutrient additions. However, no study so far has examined in detail the properties of sinking particles, particularly sinking velocity and degradation rates, which together determine the remineralization depth and thus the potential for deep carbon export.

To create a net carbon sink using artificial upwelling, the export flux needs to overcompensate for the CO_2 upwelled with deep water (Pan et al., 2016). The most important export conditions determining carbon sequestration potential are (i) elemental stoichiometry of sinking particles and (ii) the remineralization depth of these particles. While artificially upwelled deep water usually contains more nitrogen and phosphorus than the surface water, it also contains more dissolved inorganic carbon (DIC), which could potentially outgas to the atmosphere. Hence, for artificial upwelling to increase the ocean's function as a net carbon sink, more carbon must be sequestered than is brought up as excess DIC (excess DIC = deep water DIC – surface water DIC). Carbon sequestration is thereby promoted by a high C:N ratio of sequestered particulate material (POC:PON). How much of the exported matter reaches the sequestration depth (i.e., the depth at which sinking material is regarded as sequestered) is determined by the remineralization length scale (RLS). It is a proxy for how deep particles can sink before being remineralized. Both parameters are dependent on the plankton community that develops as a response to artificial upwelling. Plankton community composition shapes not only the magnitude and C:N stoichiometry of the mass flux (Taucher et al., 2021), but also the characteristics of the sinking particles, such as their sinking velocities (SV) and carbon-specific remineralization rates (C_{remin}) (e.g., Legendre and Rivkin, 2002; Iversen and Ploug, 2010; Henson et al., 2012b; Turner, 2015; Bach et al., 2019). Community composition and succession are in turn controlled by the amount of added nutrients and the frequency with which they are supplied (Leibold et al., 1997; Jakobsen et al., 2015). This is why the intensity of artificial upwelling, as well as the mode of the application (i.e., the frequency of deep water addition) are important parameters that impact the export of organic matter.

Here, we present results from a mesocosm experiment where we studied the impact of different intensities and modes of artificial upwelling on arising food web dynamics and particulate matter export. We addressed the question whether increasing intensity of artificial upwelling leads to a higher mass flux and increased potential for carbon sequestration. Additionally, we compared the particle properties and their implications for deep carbon export of a singular upwelling event with a recurring mode of upwelling. The singular upwelling mode resembled an application of artificial upwelling that fertilizes each patch of water only once, e.g., by means of a moored wave pump (see e.g., Liu et al., 1999; Fan et al., 2016). The recurring mode on the

other hand resembled an approach where the upwelling device drifts within a patch of water and fertilizes it over longer periods of time. Mesocosms are useful to study effects on whole pelagic communities, since they incorporate the responses of multiple trophic levels of a food web and allow for the assessment of a variety of ecological and biogeochemical parameters in an enclosed and well-characterized (eco-) system. Our study is the first to analyze the combined effects of upwelling intensity and upwelling mode on pelagic communities.

MATERIALS AND METHODS

Experimental Setup

The mesocosm experiment was conducted from 5th of November 2018 and lasted for 39 days. Nine Kiel Off-Shore Mesocoms for Ocean Simulations (KOSMOS, see Riebesell et al., 2013 for technical information) were deployed in Gando Bay off the east coast of Gran Canaria (27°55.673′ N, 15°21.870′ W). They enabled us to monitor the temporal development of the enclosed pelagic communities at *in situ* conditions. The mesocosms contained a 15 m long water column with a volume of ∼38 m^3. We simulated artificial upwelling by replacing part of the oligotrophic mesocosm water with nutrient rich deep water. Our experimental design comprised one mesocosm as a control (i.e., no deep water addition), while the remaining eight received deep water additions in different modes and intensities. Four of these mesocosms were fertilized once with one big addition at the beginning of our study, i.e., the "singular treatments." The other four were fertilized eight times throughout the experiment with lower amounts of deep water per addition, but comparable total amounts of deep water summed up over the study period, i.e., the "recurring treatments." Both addition modes had four different levels of mixing ratio (low, medium, high, and extreme), with two respective mesocosms of different modes receiving similar amounts of deep water in total (**Table 1**).

We collected deep water for fertilization off the coast of Gran Canaria using a deep water collector, an opaque synthetic bag with 100 m^3 carrying capacity (see Taucher et al., 2017 for technical details), and moored it at the mesocosm site after each of two collections. The water was supposed to originate from ∼600 m depth, where NO_3^- concentrations are as high as 20–25 μmol L^{-1} (Llinás et al., 1994), in order to enhance primary and export production. However, due to loss of equipment under rough conditions we could not as planned collect water from that depth. Instead, we collected water from 330 m depth on the 26th of October 2018 (experimental day −10 = T-10) and from 280 m depth on the 28th of November (T23). Therefore, to reach the macronutrient concentrations necessary to achieve our planned experimental fertilization, we added nitrate (NO_3^-), phosphate (PO_4^{3-}) and silicate [$Si(OH)_4$] to the deep water prior to the first addition, resulting in concentrations of 25, 1.38, and 12.1 μmol L^{-1}, respectively. We calculated the amount of new N added to the mesocosms in the course of the whole experiment (**Table 1**) by calculating and adding up the net N inputs of each deep water replacement. For more details on the experimental setup and mesocosm activities (see Sswat et al., in prep.).

Sampling Procedure and Maintenance

Sampling for various parameters was generally carried out every second day (see **Figure 1**). A higher sampling frequency was pursued at the beginning of the experiment in order to cover the biological responses to the first two deep water additions in higher temporal resolution. The samples were either analyzed at our on-shore lab facilities at the Oceanic Platform of the Canary Islands (PLOCAN), the Marine Science and Technology Park (Parque Cientiìfico Tecnoloìgico Marino, PCTM) or the University of Las Palmas (ULPGC), or transported back to Kiel for analysis at the GEOMAR Helmholtz Centre for Ocean Research Kiel.

A CTD60M (Sea & Sun Technology GmbH, Trappenkamp, Germany) was cast to get depth profiles for temperature, salinity, density, pH, turbidity, oxygen (O_2) and photosynthetically active radiation. Bulk samples from the upper 13 m of the water column (WC) were taken for the analysis of primary productivity, chlorophyll *a* (Chl *a*), photosynthetic pigments, phyto- and microzooplankton analysis, prokaryotic heterotrophic production (PHP), and for the analysis of suspended particulate matter (PM_{wc}). The latter was composed of particulate organic and inorganic carbon (POC_{wc}/PIC_{wc}), particulate organic nitrogen (PON_{wc}) and phosphorus (POP_{wc}), and biogenic silica (BSi_{wc}). Bulk samples were collected with integrated water samplers (HYDRO-BIOS Apparatebau GmbH, Kiel, Germany), which performed depth-integrated sampling from the upper 13 m of the water column. On each sampling day, around 40–60 L of bulk samples (i.e., 8–12 water samplers) were sampled per mesocosm. These were filled into 10 L carboys and stored dark and cool until arrival in the on-shore labs. Dissolved nutrients and carbonate chemistry (DIC and total alkalinity) were also sampled from the integrated water samplers.

Sedimented particulate matter was pumped out of the sediment trap (depth = 15 m) with a manual vacuum pump, not exceeding 0.3 bar during the process. Sediments were collected in 5 L glass bottles (Schott Scandinavia A/S, Kgs. Lyngby, Denmark) and stored in darkness until arrival in the lab, where they were subsampled for various parameters. The bottles were gently rotated to resuspend the material before homogeneous subsamples were taken. These subsamples were used for particle sinking velocity measurements and measurements of carbon-specific remineralization rates. For the latter, seven glass bottles (Schott, 310 mL volume) were additionally sampled with mesocosm water without headspace. They were used for incubating the sediment subsamples. The remaining sediment sample was weighed and analyzed for particulate carbon, nitrogen, phosphorus and biogenic silica content (see Boxhammer et al., 2016 for details of the method).

To prevent wall growth on the inside walls of the mesocosms, a ring-shaped wiper was pulled through each mesocosm roughly every 10 days (see **Figure 1**). This counteracted nutrient consumption by fouling organisms and their alteration of incoming light. For the latter reason, also the outside walls were cleaned twice during the study by divers equipped with brushes.

The sediment tubes of all mesocosms detached from the sediment traps on T30 due to strong winds and currents. They were reinforced and refitted on T31, however, no sediment

TABLE 1 | Treatment overview indicating different upwelling modes and intensities, mean net volume exchange of surface water with nutrient-rich deep water per addition and the total amount of new nitrogen that was added via the addition of deep water throughout the experiment.

Upwelling mode	Control	Singular				Recurring			
Upwelling intensity	–	Low	Medium	High	Extreme	Low	Medium	High	Extreme
Volume exchange per addition (%)	0	6.4	12.0	22.4	39.2	0.8	1.6	3.2	6.4
Total new N added (μmol L^{-1})	0	1.6	3.1	5.6	9.8	1.6	3.1	6.2	11.0

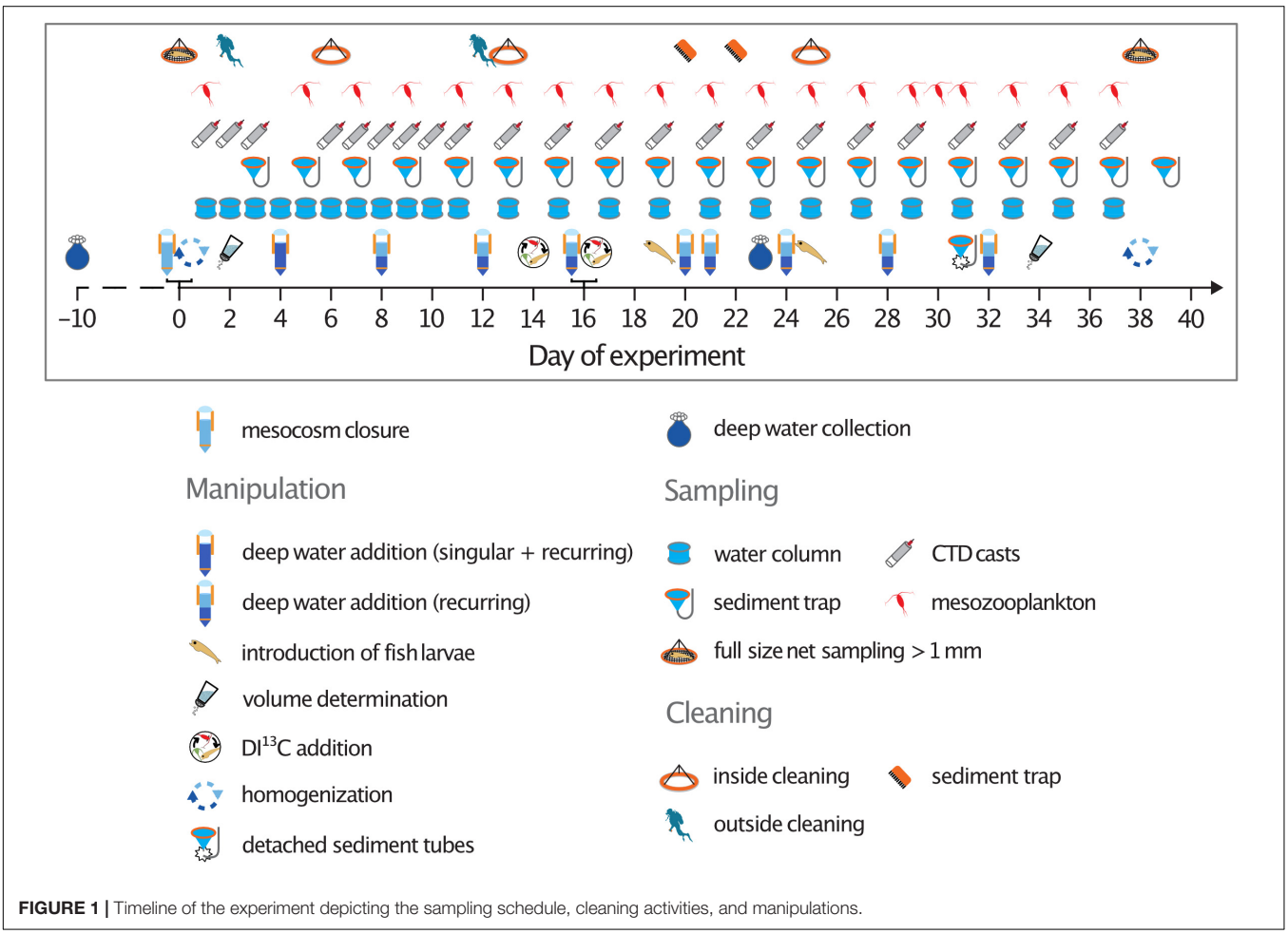

FIGURE 1 | Timeline of the experiment depicting the sampling schedule, cleaning activities, and manipulations.

samples could be recovered that day and thus sedimented matter elemental composition, sinking velocity and remineralization rate could not be measured on T31. The tubes of the singular medium and high treatments and of the recurring extreme treatment disconnected again and had to be reattached a second time on T33. We were not able to sample the singular medium treatment that day, and the singular high and recurring extreme treatments had short incubation periods of only 18 h between the T33 and T35 samplings. We discarded all sinking velocity measurements from these days, since they showed systematically higher values than the measurements of the surrounding days. The mean seawater density inside all mesocosms between 0.5 and 15 m was slightly higher than in the surrounding water (1025.69 ± 0.11 and 1025.42 kg m^{-3} on T31, respectively), so that we assume no Atlantic water entered the small opening at the base of the sediment trap (ø ∼1 cm). An outflow of mesocosm water into the surrounding seems more likely under these circumstances. Nevertheless, we cannot rule out the possibility that e.g., due to wave and current action some Atlantic water entered the mesocosms. The surrounding water was, however, oligotrophic, and had substantially lower POC concentrations than any of the mesocosms on T33 according to our measurements (7.9 μmol POC L^{-1} in the Atlantic water compared to 35.7 ± 21.4 μmol POC L^{-1} in the mesocosms). This makes an influential contamination with biogenic material and/or species from the outside less probable, even if Atlantic water had entered the mesocosms. At the end of the experiment the water column in the mesocosms was mixed by pumping

compressed air through the sediment hose. This might have altered the sediment flux and quality of the last sampling on T39.

Sample Processing and Measurement

Sediment Trap Material

At PLOCAN the sediment trap (ST) material was prepared for elemental analysis of POC_{ST}, PON_{ST}, and BSi_{ST} by first of all separating the particles from the seawater. 3 mol L^{-1} ferric chloride ($FeCl_3$) were added to each 5 L bottle of sediment material to enhance flocculation and coagulation, followed by 3 mol L^{-1} NaOH addition to compensate for the decrease in pH (as described in detail in Boxhammer et al., 2016). After letting the material settle for 1 h, the supernatant was gently decanted. The remaining flocculated material was then centrifuged for 10 min at ∼5,200 *g* in a 6–16KS centrifuge (Sigma Laborzentrifugen GmbH, Osterode am Harz, Germany). An additional 10 min centrifugation step at ∼5,000 *g* in a 3K12 centrifuge (Sigma) resulted in compact sediment pellets, which were frozen at −20°C and transported to Kiel for further processing. In Kiel, the pellets were freeze-dried to remove any leftover moisture and then ground in a cell mill (Edmund Bühler GmbH, Bodelshausen, Germany) to a fine homogeneous powder that was suitable for subsampling and further elemental analysis (Boxhammer et al., 2016). Subsamples for POC/N were weighed into tin capsules, acidified with 1 mol L^{-1} HCl, dried over night at 50°C, and then measured in duplicate on a CN analyzer (Euro EA-CN, HEKAtech GmbH, Wegberg, Germany) according to Sharp (1974). To determine BSi concentrations, ∼2 mg subsamples of the sediment powder were measured spectrophotometrically following Hansen and Koroleff (1999).

The sediment powder was stored dark and cool in glass vials. As some samples required multiple vials due to their high amounts, subsamples from all bottles were measured for each variable. If they differed among each other in elemental composition, the sample was pooled, homogenized, split up and remeasured until all bottles yielded the same results.

Water Column Samples

Water column samples were subsampled for elemental (POC_{WC}/PON_{WC}) and pigment analysis (Chlorophyll *a*/Chl *a*) by collection on pre-combusted glass fiber filters (0.7 μm, Whatman) in our on-shore labs. POC and PON filters were acidified for ∼2 h to remove inorganic carbon, using 1 mol L^{-1} HCl, and dried over night at 60°C in pre-combusted glass petri dishes. Filters for total particulate carbon (TPC) were dried without prior acidification. All filters were packed in tin cups (8 × 8 × 15 mm, LabNeed GmbH, Nidderau, Germany) and measured back in Kiel on a CN analyzer (Euro EA-CN, HEKAtech) as described for sediment C and N content above. Due to sample handling and/or measurement errors, measured POC_{wc} concentrations were sometimes higher than those of TPC_{wc}. Whenever the difference was greater than 10%, we report the TPC_{wc} instead of the POC_{wc} concentration (i.e., assuming that no PIC was present). Samples for Chl *a* were stored at −80°C in cryovials until analysis in Kiel. They were extracted in acetone (100%) and homogenized with glass beads in a cell mill. After centrifugation (10 min, 5,200 rpm, 4°C) they were filtered through 0.2 μm PTFE filters (VWR International GmbH, Darmstadt, Germany). Phytoplankton pigments, including Chl *a* in the supernatant were measured by an HPLC Ultimate 3,000 (Thermo Scientific GmbH, Schwerte, Germany).

Primary productivity was measured in the on-shore labs using a modified Nielsen (1952) ^{14}C uptake method described by Cermeño et al. (2012). Four water column subsamples (70 mL) per mesocosm were prefiltered and peaked with $2.96{\cdot}10^5$ Bq of ^{14}C-labeled sodium bicarbonate solution ($NaH^{14}CO_3$, PerkinElmer Inc., Waltham, United States). They were subsequently incubated *in vitro* for 24 h in a 12 h dark-light cycle. One of the subsamples was thereby covered with an opaque foil in order to measure the dark carbon uptake. Light intensity and temperature were set to *in situ* conditions based on CTD measurements. Thereafter, size fractions were filtered, the PIC and DIC fractions removed through acidification and the filters and filtrates were treated with a scintillation cocktail (Ultima Gold XR). Disintegrations per minute were counted on a scintillation counter (Beckmann LS-6500, Beckman Coulter Inc., Brea, United States). From these, knowing the concentration of added ^{14}C isotope and the measured *in situ* DIC concentration (see paragraph on DIC below), primary productivity rates (μmol C L^{-1} d^{-1}) were calculated. For a more detailed description of the sampling and measurement procedure see Ortiz et al. (submitted).

PHP was estimated from rates of protein synthesis determined by the incorporation of tritiated leucine [(^3H)leucine; Perkin Elmer] using the centrifugation method (Smith and Azam, 1992). Four subsamples (1 mL) and two trichloroacetic acid killed blanks were dispensed into screw-cap Eppendorf tubes. They were spiked with [^3H]leucine (final concentration: 20 nmol L^{-1}, specific activity 123 Ci $mmol^{-1}$) and incubated at *in situ* temperature (21°C) in the dark for 2–3 h. After the incubation, 100 μL of 50% trichloroacetic acid were added to the subsamples, which were kept with the blanks at −20 °C until centrifugation at 12 000 rpm for 20 min. The supernatant was carefully removed, and 1 mL of scintillation cocktail (Ultima Gold XR) was added to the Eppendorf tubes. They were stored in darkness for 24 h, after which the incorporated radioactivity was determined on a scintillation counter (Beckmann LS-6500). PHP was calculated using a conservative theoretical conversion factor of 1.55 kg C mol^{-1} Leu assuming no internal isotope dilution (Kirchman and Ducklow, 1993).

Samples for dissolved inorganic nutrients were filtered (0.45 μm Sterivex filters, Merck KGaA, Darmstadt, Germany) upon arrival in the on-shore lab. Nitrate (NO_3^-), nitrite (NO_2^-), ammonium (NH_4^+), phosphate (PO_4^{3-}) and silicic acid [$Si(OH)_4$] concentrations were subsequently measured spectrophotometrically on a five channel continuous flow analyzer (QuAAtro AutoAnalyzer, SEAL Analytical Inc., Mequon, United States).

Samples for DIC measurements were filtered to remove particulate inorganic carbon (0.7 μm, Whatman) with an overflow of 1.5 times the volume of the filtrate. Inclusion of air in the filtration process was carefully avoided. The filtrate was fixed with mercuric chloride ($HgCl_2$). DIC

concentrations were measured in triplicate on an AIRICA system (MARIANDA, Kiel, Germany) in Kiel, using a LI-COR LI-7000 Analyzer (LI-COR Biosciences GmbH, Bad Homburg, Germany). Certified reference materials (CRM batch 142, supplied by A. Dickson, Scripps Institution of Oceanography, United States) were used to determine the accuracy of DIC measurements.

Dissolved organic carbon (DOC) samples were filtered through pre-combusted GF/F filters (450°C, 6 h) into polypropylene copolymer Nalgene^{TM} bottles (Thermo Scientific), and stored at −20°C. Prior to analysis, samples were acidified to a pH < 2 to remove inorganic carbon. Subsequently, DOC concentrations were measured by high temperature catalytic oxidation on a total organic carbon analyzer (TOC-V, Shimadzu Europa GmbH, Duisburg, Germany). The instrument was calibrated daily using potassium hydrogen phthalate (99.95–100.05%, p.a., Merck), which yielded an analytical precision of ± 1 μmol C L^{-1}. The accuracy was determined using certified reference materials (provided by D. A. Hansell, University of Miami, United States). Measured CRM concentrations were 43.39 ± 0.92 μmol C L^{-1} (n = 33), at a reference value of 42–45 μmol C L^{-1}.

Sinking Velocity of Sediment Trap Particles

Sinking velocity and remineralization rates of sedimented particulate matter were measured in a temperature-controlled on-shore lab at PCTM. Sinking velocity was determined by video microscopy using the method described in Bach et al. (2012). Sediment subsamples were diluted with filtered seawater according to their particle density (1:25–1:100) and injected to a sinking chamber (a cuvette with the dimensions: 10 × 10 × 350 mm), which was mounted vertically on a FlowCam 8000 (Fluid Imaging Technologies Inc., Scarborough, United States). Gravitational settling of particles in the cuvette was subsequently monitored for 20 min. Measurements were carried out at *in situ* temperatures (∼21°C) under ventilation to prevent a temperature gradient around the sinking chamber. Particles between 25 and 1,000 μm were identified at a frame rate of 15–20 fps. The FlowCam measures more than 60 visually assessed parameters, which were read into MATLAB (version R2018b) for data analysis. The MATLAB script described by Bach et al. (2012 see: "Evaluation of sinking velocities") was adjusted for the more recent FlowCam version and used for calculation of sinking velocities. By finding multiple captures of the same particle on a y-position-gradient and applying a linear regression model against time, sinking velocities were calculated. They were corrected for wall effects of the sinking chamber according to the equation given by Ristow (1997). Further data analysis was carried out with the programming software R (R Core Team, 2017) using RStudio (version 1.3.959) and the package "tidyverse" (Wickham et al., 2019). An optical proxy for particle porosity (P_{int}) was calculated according to Bach et al. (2019). It is essentially a measure of the brightness of a particle, scaled with its size.

Analysis of the distribution of sinking particle volume showed that most of the volume was contained in a small fraction of particles with high equivalent spherical diameter (ESD) in all measurements (largest 10% accounted for > 75% of total particle biovolume). The smaller size fractions, however, constituted the majority of particle counts (∼90% in the 25–200 μm fraction). To not give the more numerous small particles undue weight, we calculated a "weighted SV." It gives more weight to the high-volume, but underrepresented bigger particles, which consequently contain more biomass (see **Supplementary Figure 2** for an illustration of weighted SV calculation). In order to do so, we determined the ESD for which at least 25% of the summed-up particle volume was contained in the smaller particles and 75% in the bigger ones. For this "weighted ESD" we calculated the corresponding "weighted SV" by fitting a linear model to the mean sinking velocities as a function of their ESD across different size classes (log-spaced). We used size class means to—again—not give the numerous small particles undue weight. This weighted sinking velocity (hereinafter referred to as sinking velocity or SV) is thus the sinking velocity that corresponds to the ESD which segments the measurement into two particle volume fractions containing 25 and 75% of the total particle volume. We calculated the "weighted particle porosity" in the same way (hereinafter referred to as porosity or P_{int}). We used the weighted SV for all following sinking velocity dependent calculations such as the remineralization length scale (see below).

Remineralization Rates of Sinking Particles

Remineralization rates were determined every 4–6 days. We therefore took water column samples, collected in four replicate and three control bottles per mesocosm [(4 + 3) bottles × 9 mesocosms = 63 bottles in total]. They were transported back to the temperature-controlled lab (set to *in situ* temperature based on CTD measurements), where they acclimatized in a water bath for 2 h. Then, 0.5–3 mL of sediment subsample of the respective mesocosm were added to the four replicate bottles. The control bottles were left untreated. To examine the rate at which sedimented POC was remineralized back to DIC, all bottles were incubated in the dark on a rotating plankton wheel (∼1 rpm) and Oxygen depletion over time was measured. O_2 measurements were carried out using a handheld optical measurement device (Fibox4 Trace, PreSens—Precision Sensing GmbH, Regensburg, Germany), measuring non-invasively on PSt3 optodes (PreSens) mounted inside the bottles. O_2 measurements were automatically corrected for temperature (measured in a dummy bottle) and atmospheric pressure by the Fibox4. We adjusted the optode salinity correction according to the daily observed salinity measurements of the CTD cast. The second O_2 measurement was carried out after the bottles had been mixed properly, about 2 h after the incubation start, and were repeated continuously in 2–6 h intervals. The incubations lasted between 19 and 43 h, during which O_2 measurements were done at least 7 and up to 16 times. Particles in the incubation bottles were then collected on pre-combusted glass fiber filters (0.7 μm, Whatman) and

analyzed for their POC content the same way as the water column POC filters.

By dividing the O_2 consumption rate (r in μmol O_2 L^{-1} d^{-1}) of the sedimented matter by its POC content at the end of the incubation (μmol C L^{-1}), the carbon-specific remineralization rate of the sedimented particulate matter (C_{remin} in d^{-1}) was calculated according to:

$$C_{remin} = \frac{(r * RQ)}{(POC + r * RQ * \Delta t)}$$

where RQ is the respiratory quotient (μmol C μmol $O_2{}^{-1}$), which is commonly used as 1-mol CO_2 produced:1-mol O_2 consumed (= 1) (Ploug and Grossart, 2000; Iversen and Ploug, 2013; Bach et al., 2019) and Δt (d) as the time interval from the start of the incubation until the start of the filtration. In order to distinguish the response of the sedimented matter from any background seawater oxygen consumption, the C_{remin} rates of the sediment-containing bottles were corrected for the mean C_{remin} rates in the blank bottles.

Calculation of Export Flux and Remineralization Depth

The mass flux to the sediment trap (POC_{ST}, PON_{ST}, BSi_{ST}) was calculated for each element from the amount measured in the sediment powder. The total content per sample was calculated and normalized to the volume of the mesocosm and the time between sample collection (48 h), which yielded the daily mass flux in μmol per liter mesocosm water (μmol L^{-1} d^{-1}). Ten data points were missing due to the detachment of the sediment trap hoses on and around T30 (all mesocosms on T31 and the singular medium mesocosm on T33, see section "Sampling Procedure and Maintenance"). To calculate the cumulative POC_{ST} flux (ΣPOC_{ST}), daily POC_{ST} fluxes were summed up, whereby the missing data points were interpolated using the two surrounding data points (T29 and T33, or T29 and T35 for the singular medium treatment). Cumulative mass fluxes are reported in μmol L^{-1}.

To find out how much of the produced organic carbon had been exported from the water column until a specific experimental day (Tx), total organic carbon in the water column (TOC_{WC}) was calculated, subtracted by the initial TOC_{WC} concentration on T01 (= ΔTOC_{WC}), and finally compared to the cumulative POC_{ST} flux (ΣPOC_{ST}).

$$\frac{\Delta TOC_{WC}(Tx)}{POC_{ST}(Tx)} = \frac{(POC_{WC}(Tx)+DOC_{WC}(Tx))-(POC_{WC}(T01)+DOC_{WC}(T01))}{POC_{ST}(Tx)}$$

Finally, the remineralization length scale (RLS, i.e., remineralization depth) was calculated, which is the quotient of sinking velocity and carbon specific remineralization rate.

$$RLS = \frac{SV}{C_{remin}}$$

It is the depth (m) by which 63% of the sinking organic particle flux have been remineralized (Cavan et al., 2017) and thus a proxy for the POC transfer efficiency to depth.

RESULTS

Primary Production, Export Flux, and Stoichiometry

Primary productivity as well as Chl *a* and POC_{WC} concentrations increased in all treatment mesocosms following the first deep water addition on T4. Phytoplankton blooms dominated by diatoms (Ortiz et al., submitted) developed in the singular treatments with intensity and duration depending on their upwelling intensity. The highest phytoplankton biomass (measured as Chl *a* concentration) was observed in the extreme singular treatment (11.2 μg L^{-1} on T9). Recurring upwelling sustained more stable phytoplankton biomass and productivity compared to singular upwelling. In the high and extreme recurring treatments primary productivity rates increased until well into the second half of the experiment (**Figures 2A,B**). Note that in most mesocosms a large fraction of produced organic matter was retained in the water column as suspended POC_{wc} at the end of the experiment (**Figure 2C**). This was particularly evident in the recurring treatments, which received nutrients until T32. In the extreme recurring treatment, the amount of POC_{WC} at the end of the experiment was higher than its total cumulative POC mass flux (**Figures 2C,E**: 102 μmol L^{-1} POC_{WC} vs. 82 μmol L^{-1} of cumulative POC_{ST}, on T39).

The treatment differences observed in Chl *a* and primary productivity were mirrored in the POC mass flux. A post-bloom export event occurred in the singular treatments 4–10 days after their bloom peak in the water column, with the time lag being longer at higher intensities of deep water addition. This is based on visual inspection (comparison of **Figures 2B,D**, e.g., extreme singular treatment bloom peak on T9, highest POC_{ST} flux between T17–T21), since the temporal variation in the POC_{ST} data did not allow a reliable calculation of time lags as e.g., in Stange et al. (2017). In contrast, the recurring mode led to POC_{ST} maxima 20–30 days after initial fertilization (**Figure 2D**). In both modes, the overall cumulated POC_{ST} at the end of the experiment correlated positively with the cumulated primary productivity (**Figure 2F**). The control mesocosm was excluded from this regression analysis, because it had unexplainably high export rates, although it did not receive any new N via deep water addition. When comparing the total amount of dissolved and particulate N at the beginning and end of the study period in the control, we found that approx. 4.2 μmol L^{-1} N sank out to the sediment trap, which were not accounted for in the initial N pools, according to our measurements. Apparently, there was an N source (or multiple) in the control, which we did not capture, e.g., fouling residues on the inside walls of the sediment trap or large swimmers (zooplankton, small fish), which were initially present but not accounted for. Other causes for the discrepancy might have been methodology-related, e.g., inaccurate sampling of patchily distributed PON_{WC}. Regarding the test statistics, removing the control from the quantitative regression analysis in **Figure 2F** decreased the *p*-values (from 0.014 to 0.044 in the singular and from 0.015 to 0.060 in the recurring upwelling mode) and did not considerably affect the *R*-values (from 0.90 to

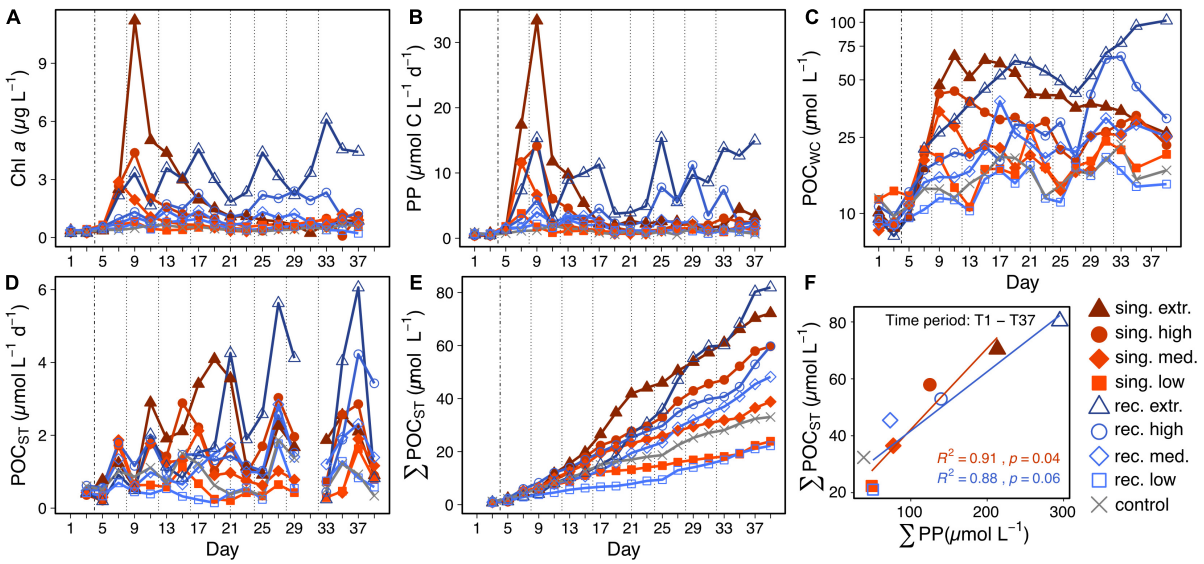

FIGURE 2 | Chl a concentration **(A)**, primary productivity **(B)**, suspended POC concentration in the water column **(C)**, POC mass flux to the sediment trap **(D)**, and cumulative mass flux **(E)** during the 39 day experiment. The vertical lines indicate the deep water additions with the dashed one on the left representing the one for the singular and recurring treatment, the dotted ones being the following recurring additions. **(F)** Shows the correlation between the cumulative POC flux and the cumulative primary productivity on T37. Regression lines are plotted in the color of the corresponding upwelling mode (singular or recurring) and exclude the control data point. Regression equations are provided in **Supplementary Table 1**.

0.91 in the singular and from 0.89 to 0.88 in the recurring upwelling mode).

The peaks in POC_{ST} on T7 and T27 (**Figure 2D**) in all mesocosms likely occurred due to the preceding cleaning of the inside mesocosm walls on T6 and T25, respectively. It appears that a carbon-rich biofilm was growing on the walls, which was removed during cleaning and subsequently sank into the sediment traps. This is also indicated by the high C:N ratios of POC flux on these days (compare **Figures 2D**, **3A**). On T33 and T39, POC_{ST} was lower than expected for most mesocosms, contrasting the time points before and after these days. For T33, the reason for this was probably a lower than usual accumulation period of material due to the preceding sediment tube detachments (see section "Sampling Procedure and Maintenance"). Many large and heavy particles might have sunk out before the reattachment of the tubes, leaving a higher proportion of slower sinking particles with lower POC content for the accumulation period. Regarding T39, the final fish net haul and the mixing of the water column through the sediment hose on T38 likely caused lower sedimentation rates of organic matter. The fish net haul by removing large and sticky aggregates, the mixing by resuspending already settled material.

In all treatment mesocosms except for the recurring low treatment more organic carbon was retained in the water column as POC and DOC than exported to the sediment trap as POC (ratio between ΣPOC_{ST} and $\Delta TOC_{WC} < 1$). The ratios did not substantially differ among the singular treatments, whereas they decreased with increasing upwelling intensity in the recurring mode (**Table 2**).

In the singular upwelling treatments, the C:N ratios in the suspended particulate matter pool generally increased to higher than Redfield ratios on T11, 1 week after the deep water addition (**Figure 3B**). This occurred precisely when the blooming phytoplankton communities became nutrient limited (see **Supplementary Figure 1** for inorganic nutrient concentrations), and was particularly prominent under high upwelling intensities. In the recurring treatments, the C:N ratios of POM_{WC} showed a high temporal variation, they, however, tended to increase throughout the study period.

The C:N ratio of the mass flux was higher than the canonical Redfield ratio of 6.6 in all mesocosms throughout the experiment (**Figure 3A**). Increasing amounts of deep water addition, however, enhanced the mass flux C:N ratios further. We found a positive correlation between N addition and the C:N of the mass flux in the singular treatment between T11 and T21, when most of the post-bloom flux occurred (**Figure 3C**). Furthermore, the Si:C ratio during this time was higher in the singular treatments compared to the recurring ones and the control (**Figure 3D**).

Particle Properties and Remineralization Depth

Remineralization rates of sinking particles ranged from 0.09 to 0.12 d^{-1} initially, and peaked in most mesocosms a week after the first deep water addition (T11). Thereafter, they decreased in all treatments (**Figure 4A**). Sinking velocities were generally lower in the singular treatments than in the recurring ones (**Figure 4B**). This difference between the two modes was confirmed by a *t*-test for mean sinking velocities calculated for days T7–T15 [two-sample $t(6) = -4.019$, $p = 0.007$]. Low sinking velocities in the singular mode were accompanied by high porosities in

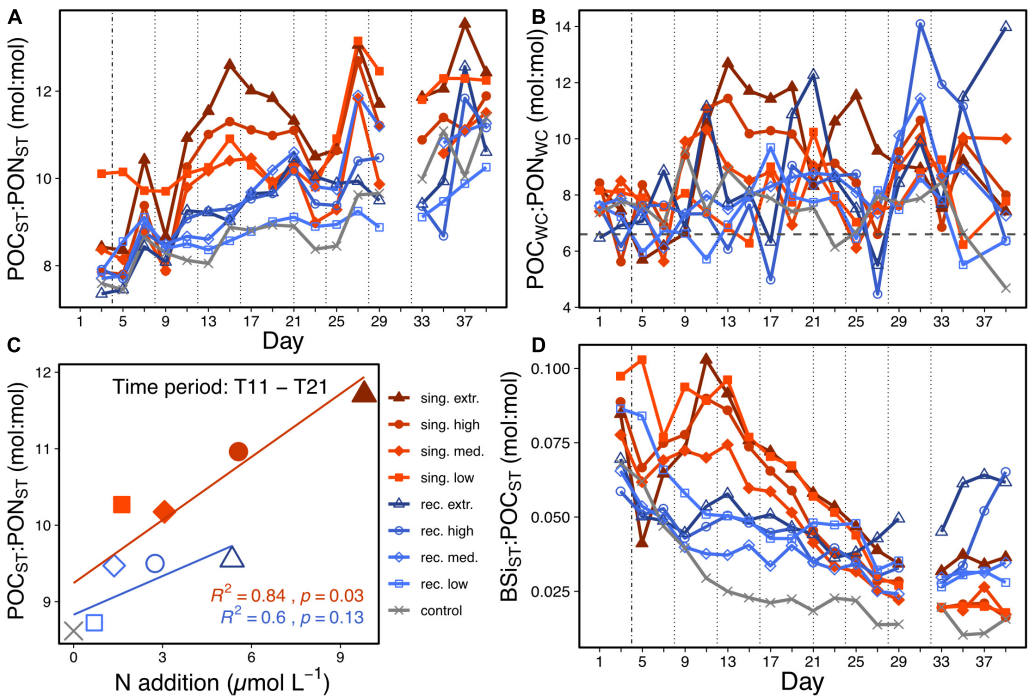

FIGURE 3 | C:N ratios of the mass flux to the sediment trap **(A)** and suspended particulate matter C:N ratios **(B)** over time. The horizontal line in **(B)** indicates the C:N Redfield ratio of 6.6. **(C)** Displays the correlation between the mean C:N ratio of the mass flux and the mean cumulative N addition. It considers the time frame of the singular bloom export event (T11–T21), from which means over time were calculated. Regression lines are plotted in the color of the corresponding upwelling mode (singular or recurring). Regression equations are provided in **Supplementary Table 1**. **(D)** Shows the mass flux Si:C ratios over time. The vertical lines are used as described in **Figure 2**.

TABLE 2 | Mean ΔTOC_{WC} and ΣPOC_{ST} values, as well as ΔTOC_{WC}:ΣPOC_{ST} ratios calculated from T33, T35, and T39.

Upwelling mode	**Control**	**Singular**				**Recurring**			
Upwelling intensity	**–**	**Low** ●	**Medium** ●	**High** ●	**Extreme** ●	**Low** ●	**Medium** ●	**High** ●	**Extreme** ●
ΔTOC_{WC} (μmol L^{-1})	20.5	29.1	47.0	58.7	85.6	17.0	50.3	83.1	149.3
ΣPOC_{ST} (μmol L^{-1})	30.6	20.4	34.5	53.0	66.5	19.5	42.0	48.3	70.1
ΣPOC_{ST}:ΔTOC_{WC} (mol:mol)	1.49	0.70	0.73	0.90	0.78	1.15	0.84	0.58	0.47

Data for T37 is missing because POC_{WC} was not measured on that day.

particles > 90 μm (**Figure 4D**). The difference in porosity between particles sinking under different upwelling modes is highlighted by the visual assessment of FlowCam pictures from T11 (**Figure 4E**).

Altogether, the singular treatments exported sedimented particulate matter which was carbon- and biogenic silica-rich and sank slowly during the export event. Particles > 100 μm were more porous compared to those in the recurring treatments. In contrast, the recurring treatments generally produced sinking particles which had lower C:N ratios, sank faster and were less porous than the ones in the singular treatments throughout the experiment.

We found that upwelling intensity had significant effects on sinking particle properties and on the remineralization depth during the time we observed increased mass flux (T11–T39, **Figures 5A–C**). Particles sampled from the sediment trap sank slowest and were remineralized most rapidly in mesocosms with high and extreme upwelling intensities. The fast remineralization rates correlated with high PHP in the water column during the same time period (**Figure 5D**). The RLS, as the quotient of SV and C_{remin}, also decreased with increasing deep water fertilization.

DISCUSSION

Temporal Decoupling of Biomass Production and Particulate Organic Carbon Export

We found that increased intensities of artificial upwelling resulted in higher primary productivity and POC export from the surface. However, upwelling also resulted in a temporal decoupling between biomass production (ΔTOC_{WC}) and POC

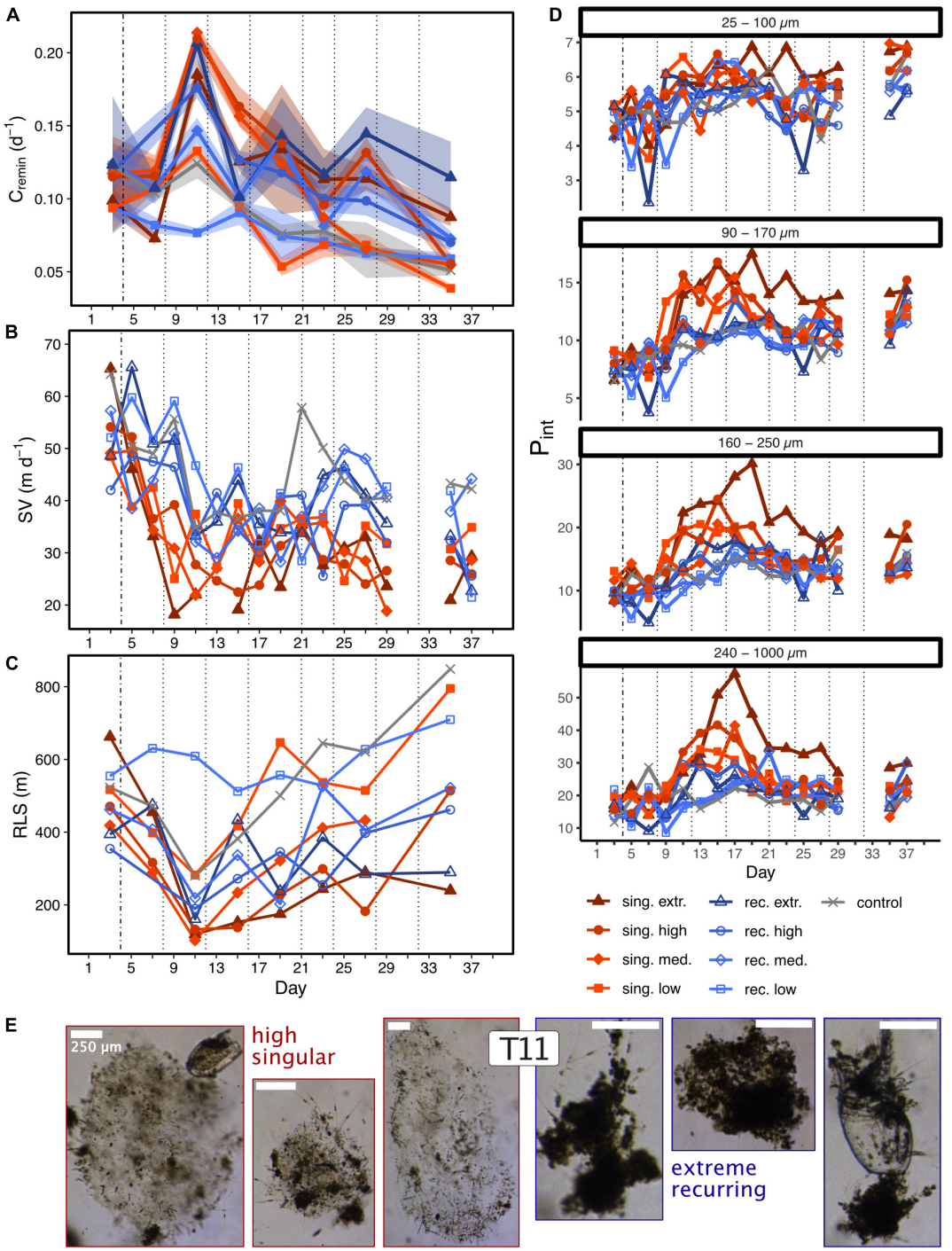

FIGURE 4 | Carbon-specific remineralization rates **(A)**, sinking velocities **(B)**, remineralization length scale **(C)** and particle porosities in four different size classes **(D)** during the 39 days of experiment. Shaded areas in **(A)** depict the standard deviation of measurements (n = 4). Mind the different y-axis scales in **(D)**. The vertical lines are used as described in **Figure 2**. **(E)** Shows a selection of FlowCam pictures illustrating sinking aggregates from the high singular (three pictures on the left side) and the extreme recurring treatment (three pictures on the right side) on T11. The scale bar depicts 250 μm.

export (cumulative POC_{ST}). We found that less than half of the produced organic carbon was exported in most of our upwelling treatments during our experimental duration, while the rest was retained in the water column (see **Table 2**). This is consistent with findings by Taucher et al. (2017), who also fertilized Gran Canarian oligotrophic communities with a single pulse of nutrient-rich deep water, and found that roughly half of the produced particulate carbon was retained in the water

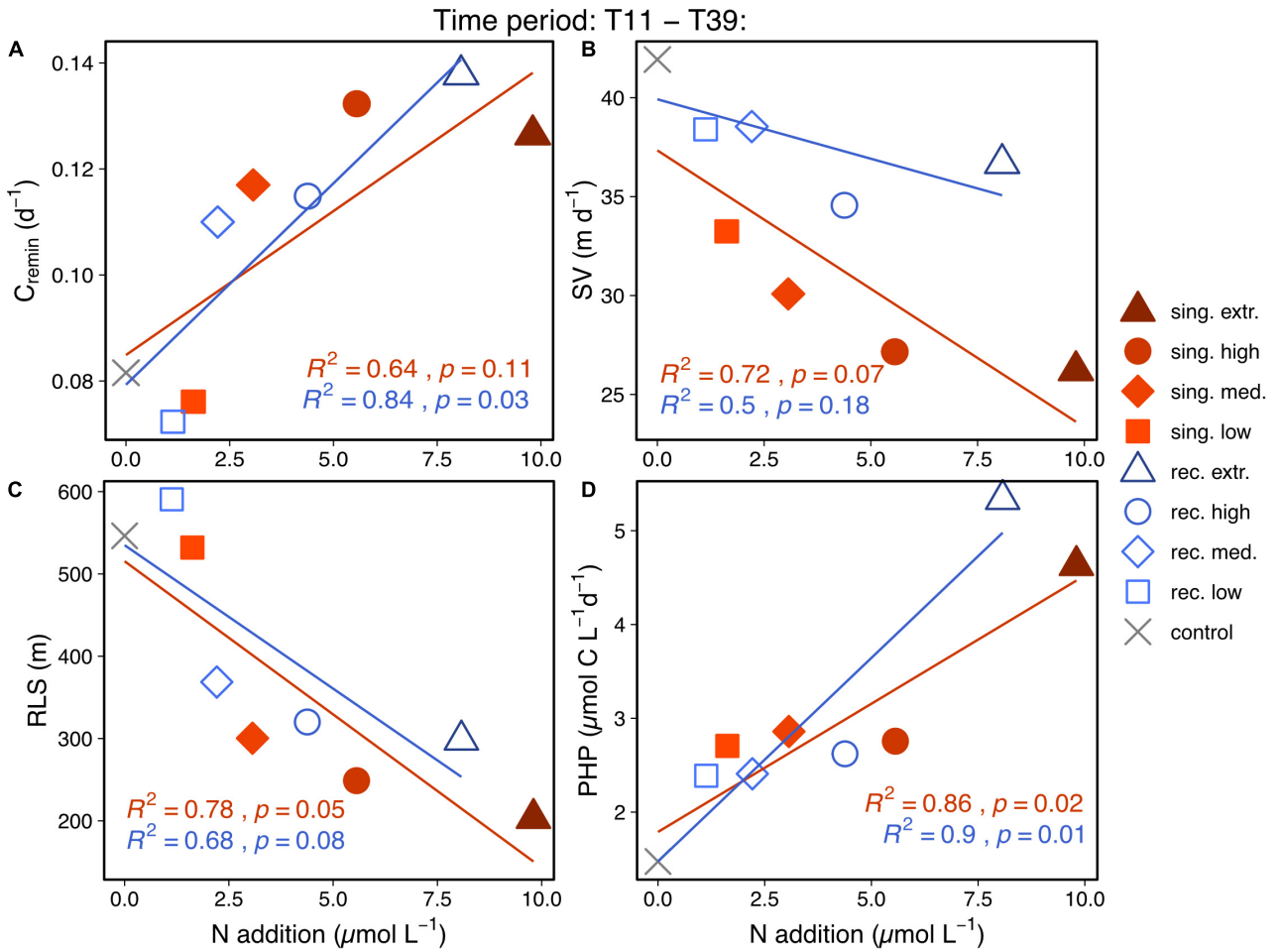

FIGURE 5 | Correlations between mean carbon-specific remineralization rate **(A)**, mean sinking velocity **(B)**, mean remineralization length scale **(C)** and mean prokaryotic heterotrophic production **(D)** against cumulative N addition. It considers the time frame starting with the singular bloom export event until the end of the experiment (T11–T39), for which means of each of the parameters shown on y-axes were calculated. Since the recurring treatments received multiple deep water additions over time, mean cumulative N additions were calculated for the considered time period. Regression lines are plotted in the color of the corresponding upwelling mode (singular or recurring) and include the control treatment. Regression equations are provided in **Supplementary Table 1**.

column for at least 25 days after the fertilization. Seemingly, artificial upwelling in oligotrophic surface waters does thus not lead to rapid export of most of the produced organic matter in the time scale of weeks.

Such decoupling between production and export occurs in a variety of oceanic regions (Cavan et al., 2015; Henson et al., 2019; Laws and Maiti, 2019), including eastern boundary upwelling systems (e.g., Kelly et al., 2018; Bach et al., 2020). It is thus no peculiarity of artificial upwelling. In natural upwelling systems reasons for a temporal decoupling can be e.g., persistent phytoplankton species in the water column (Bach et al., 2020) or weak trophic links in the planktonic food web (Stukel et al., 2011). A tight coupling of primary production and zooplankton consumers can generally lead to the export of high amounts of fast sinking fecal pellets, which can increase the POC export efficiency (Stukel et al., 2011; Le Moigne et al., 2016) and its transfer efficiency to depth (Steinberg and Landry, 2017). In our study, the response of the mesozooplankton community to the deep water fertilization was not very pronounced. Although a treatment effect on mesozooplankton biomass established toward the end of the experiment, values mostly stayed on a similar or lower level compared to before the first fertilization (~20 µg C L^{-1} or lower, Spisla et al., in prep.). We also rarely observed fecal pellets in the FlowCam measurements of the sediment subsamples. The low mesozooplankton biomass and fecal pellet abundances indicate a limited impact of the mesozooplankton community on the POC flux. This hints at a potential caveat of short-term artificial upwelling as a tool for enhancing C sequestration: The fauna adapted to oligotrophic systems may not be able to readily consume great amounts of primary produced biomass and efficiently channel it into the export pathway. The dilution effect of the deep water addition amplifies the zooplankton handicap, making it even more difficult for them to catch up with the rapid phytoplankton reproduction.

Another factor that delayed the sedimentation of primary produced matter was surface microbial recycling.

Le Moigne et al. (2016) and Henson et al. (2019) found high bacterial abundances to be associated with high primary production and low export efficiency (i.e., only a small fraction of primary produced biomass is exported). Microbial recycling can channel particulate organic matter into the dissolved organic matter pool, thereby making it unavailable for metazoan consumers. Hence the breakdown of POC into DOC reduces the chances for either direct sinking of particles or incorporation and active transportation by zooplankton (Legendre and Le Fèvre, 1995). We found similar patterns of microbial activity as the above mentioned studies associated to the decoupling of primary production and export. Microbial production increased significantly with upwelling intensity in both upwelling modes (**Figure 5D**), thereby retaining organic matter in the surface microbial loop and making it unavailable for immediate export.

Due to the retention of organic matter in the water column, we were not able to capture the whole export response of our fertilized mesocosms, especially of the recurring highly fertilized ones. We argue that the high amounts of suspended POC (see **Figure 2C**) in the high and extreme recurring treatments at the end of the experiment represented a high potential for POC export, e.g., by particle aggregation and gravitational settling. Nevertheless, the retention of organic matter in the water column makes a quantitative mass flux comparison between the two upwelling modes difficult. Laws and Maiti (2019) found that the decoupling between primary and export production at the ALOHA time-series station disappears when taking into account data of monthly time intervals. We argue that the same is needed in future artificial upwelling studies. The experimental duration must be long enough to allow for the quantitative assessment of export fluxes as well as the long-term response of higher trophic levels to the enhanced surface primary production.

Upwelling Mode Shapes Sinking Particle Properties

The export events in the singular treatments were strongly linked to the preceding diatom blooms, as indicated by the elevated BSi:POC ratios in the sedimented matter (**Figure 3D** and **Supplementary Figure 1**). They featured relatively porous particles, which sank slower than the ones in the recurring treatments (**Figures 4B,D**), and hence resulted in a low RLS (**Figure 4C**). Multiple studies have shown that diatom blooms typically result in inefficient particle transfer to depth (e.g., Guidi et al., 2009; Henson et al., 2012a; Maiti et al., 2013), potentially due to the associated high particle porosities (Lam et al., 2011; Puigcorbé et al., 2015; Bach et al., 2019). Our data supports these observations, stressing the importance of a particle's porosity for its sinking velocity and thus for its potential to be transported to depth.

The influence of transparent exopolymer particles (TEP) may explain the low sinking velocities and high porosities in the singular treatments. TEP are exuded by microbial cells and facilitate the formation of aggregates (Passow, 2002; Engel et al., 2004). They can lower particle density and increase porosity, which in turn reduces particle sinking velocity (Azetsu-Scott and Passow, 2004; Mari et al., 2017). TEP production is favored by high primary productivity and nutrient limitation (Obernosterer and Herndl, 1995), both of which occurred in the higher singular treatments on T9 (**Figure 2B** and **Supplementary Figure 1**). Additionally, the POC:PON ratio in the water column increased by > 60% from T9–T11 in the three highest singular treatments (mean values: 7.3 on T9–12.2 on T11, see **Figure 4C**), which indicates potentially enhanced TEP exudation. The same scenario has already been observed in a previous mesocosm experiment off Gran Canaria (Taucher et al., 2017), in which TEP concentrations were measured. During that experiment, TEP increased when the blooming phytoplankton community became nutrient limited (compare Taucher et al., 2017, 2018). We thus argue that also in our experiment increased TEP exudation was likely the cause for the reduction of particle sinking velocity in the singular upwelling mode, rendering it less efficient regarding the potential for deep POC export than the recurring mode.

Besides sinking velocity, respiration of sinking matter was another equally important factor determining the remineralization depth of sinking particles in our experiment. The temporal changes in C_{remin} were equally high (about fourfold) as the changes in sinking velocity over time. We measured the highest remineralization rates during the initial export event on T11, shortly after phytoplankton communities had shifted to diatom dominance (T7–T9, Ortiz et al., submitted). This is in accordance with earlier studies, which speculated that the structure of the phytoplankton community affects remineralization rates (e.g., Guidi et al., 2015), and have shown that diatom-dominated systems can lead to the export of sinking particles which are quickly respired (Guidi et al., 2015; Bach et al., 2019). In our case, the mechanistic reason for this could be that the particles contained a large fraction of easily degradable organic matter. We believe that the increasing porosities from T11 onward (**Figure 4D**) support this hypothesis. Although there are, to the best of our knowledge, no studies which found a direct positive effect of aggregate porosity on degradability, it stands to reason that higher porosities increase a particle's surface-to-volume-ratio, thus possibly enhancing its susceptibility to microbial attachment and respiration. This is in line with a hypothesis by Francois et al. (2002), who postulate that the settling of loosely packed (i.e., highly porous) aggregates leads to higher respiration rates in the mesopelagic zone. Respiration of sinking particles during this time was higher in the singular compared to the recurring treatments, likely owing to higher porosities and possibly also higher TEP concentrations. Beside the phytoplankton community structure, the zooplankton community is another factor that determines particle properties (Cavan et al., 2019). Through the packaging of phytoplankton cells into dense fecal pellets, zooplankton can make organic matter less susceptible to respiration (Steinberg and Landry, 2017). As discussed above, mesozooplankton was not abundant in our experiment, and therefore potentially not capable of repackaging the high amounts of particulate matter in the high upwelling treatments. This left the sinking biomass loosely packed for the bacterial community to feed on. We suggest that the missing repackaging of particles and the resulting high

lability of sinking organic matter was the reason for increasing remineralization with increasing upwelling intensity.

The differences in particle properties between our singular and recurring form of artificial upwelling indicate variability in the efficiency of their POC transfer to depth. Diatom spring blooms (Martin et al., 2011) and diatom communities in coastal upwelling systems (Abrantes et al., 2016) have been reported to promote efficient carbon deep export. However, the diatom blooms in our singular upwelling mode led to the export of porous, slow sinking particles, which were quickly remineralized by microbial processes. A single pulse of artificial upwelling thus resulted in a system likely to recycle the vast majority of the freshly produced organic matter in the surface ocean. Although particles in the recurring upwelling mode were respired similarly quickly, they were less porous and sank faster, which led to a slightly higher mean RLS in the recurring upwelling treatment (**Figure 5C**). This suggests a more efficient transfer of produced organic matter to depth under recurring upwelling conditions compared to a singular upwelling pulse.

Potential of Artificial Upwelling for Carbon Sequestration

As discussed above, one of the major factors that influence the potential of artificial upwelling for net carbon sequestration is how deep particles sink before they are remineralized (RLS). Another factor is the C:N ratio of the sinking organic matter (POC:PON), or, more generally speaking, the ratio of C to the limiting nutrient. The influence of both of these factors on carbon sequestration efficiency will be discussed in the following. We emphasize that the discussion is based upon a highly simplified 1-dimensional view of the water column, and neglects 3 dimensional movements of water masses, carbon, and nutrients through the ocean.

We start this discussion with the influence of the ratio of carbon to the limiting nutrient. Since the latter was nitrogen in our case, as is typical for large parts of the Atlantic (Moore et al., 2013), we will focus on the C:N ratio in the following. Let us assume that over long enough time scales all upwelled nutrients will be sequestered (i.e., exported to the sequestration depth), and that the upwelled deep water contains excess DIC (excess DIC = deep water DIC – surface water DIC) and excess DIN (excess DIN = deep water DIN – surface water DIN) compared to the surface ocean. In this case, a system will act as a net carbon sink if it sequesters organic matter with a C:N ratio higher than that of the upwelled excess DIC and nitrogen. In the Canary Island region, excess DIC and excess DIN between surface and 1,000 m depth (here assumed as sequestration depth) are approximately ∼150 and ∼20 μmol L^{-1}, respectively (Llinás et al., 1994; González-Dávila et al., 2010). This corresponds to a C:N ratio of 7.5 of upwelled excess DIC and DIN. Accordingly, for the artificial upwelling approach to generate a net carbon sink, the C:N of sequestered organic matter would need to exceed 7.5 on average, until all N added via deep water has been sequestered.

We found that artificial upwelling led to an increase in C:N ratios of sedimented matter to well above 7.5. There was a trend of increasing POC_{ST}:PON_{ST} ratios over time in all mesocosms (**Figure 3A**). The ratios in the singular treatment mesocosms correlated positively with upwelling intensity in the period of highest export (T11–T21, **Figure 3C**). It is likely that these high ratios would have either prevailed with depth or increased even further, owing to preferential N remineralization by heterotrophic microorganisms (Boyd and Trull, 2007).

It should be noted that the control mesocosm also displayed increasing C:N ratios during the experiment. This suggests that increasing C:N might have at least partly been an enclosure effect, which also occurred in absence of an artificial upwelling treatment. By enclosing a planktonic community inside a mesocosm, the vertical mixing is reduced from the depth of the mixed layer (20–120 m in the Canary Island region, see Troupin et al., 2010) to the depth of the mesocosm (15 m in our setup). This leads e.g., to an increase of depth- and time-integrated light intensity experienced by the phytoplankton community, which may affect phytoplankton photophysiology. Moreover, the community gets truncated as large grazers (>3 mm) are excluded from the food web, thus relieving lower trophic levels like microzooplankton of grazing pressure. Both effects could have caused changes in lower trophic level productivity in our mesocosm experiment, which was fueled by leftover nutrients enclosed at experiment start (see **Supplementary Figure 1**), thereby leading to an increase in POC_{WC} and POC_{ST}:PON_{ST} ratios (**Figures 2C**, **3A**). Nevertheless, the increase in sedimented matter C:N ratios was larger in those mesocosms that received deep water fertilizations, and scaled almost linearly with high upwelling rates.

Artificial upwelling can consequently enhance C:N ratios of sinking organic matter in the surface, which would favor potential carbon sequestration. This is especially the case when fertilization is carried out in single pulses. We cannot assess, however, if these ratios would have prevailed over longer time scales, i.e., until all added N had been exported with the remaining suspended particulate organic matter.

A mechanism that might counteract the positive effect of elevated C:N ratios is the observed decrease in RLS with increasing upwelling intensity in both upwelling modes. Particle sinking velocities decreased while at the same time respiration of sinking organic material accelerated with increasing nutrient input via deep water addition. Both effects resulted in a lower RLS and thus higher flux attenuation with increasing fertilization (**Figures 5A–C**). Earlier studies have shown that a higher fraction of export production makes it through the mesopelagic zone in less productive ecosystems and ends up in the deep ocean (e.g., Henson et al., 2012b). Our results match this finding, with less productive mesocosms showing a higher RLS than the very productive ones. These differences in RLS and thus particle transfer efficiency to depth, as well as the differences in C:N stoichiometries of sinking matter are illustrated in **Figure 6**.

It should be noted that our study could not assess several factors that might play an important role in determining the potential of artificial upwelling for carbon export and sequestration. First of all, our study did not account for any active biological or physical processes occurring further down the water column. Processes such as repackaging and

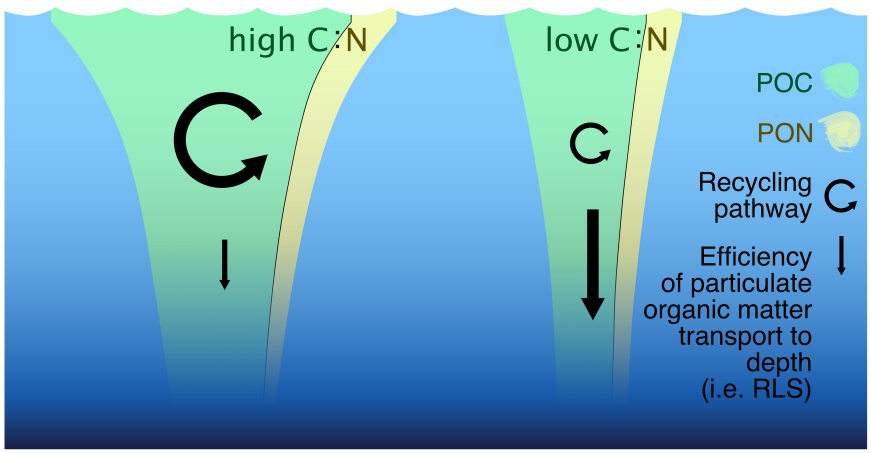

FIGURE 6 | Scheme depicting the effects that upwelling intensity had on carbon sequestration-relevant parameters in our high and low upwelling scenarios. It visualizes the strength and C:N ratio of the export flux (POC_{ST}:PON_{ST}), as well as the arrow size indicating strength of the recycling pathway and the efficiency of particle transport to depth. Note that we put more emphasis on the difference between POC:PON ratios than on the quantitative PON difference between high and low upwelling intensities. It should also be noted that the effects depicted here only reflect the initial responses to artificial upwelling in oligotrophic waters. They do not cover the ultimate fate of the upwelled inorganic nutrients and hence do not represent the long-term potential for carbon sequestration.

consumption of settling particles by zooplankton (Turner, 2015; Stukel et al., 2019) or the active diel migration of mesopelagic biota (Boyd et al., 2019 and references therein) play an important role in regulating particle transfer to depth and thus carbon sequestration (Buesseler et al., 2007; Robinson et al., 2010; Giering et al., 2014; Sanders et al., 2016; Cavan et al., 2019). Due to the limited vertical dimensions of our mesocosms, we were not able to resolve these complex processes occurring throughout the water column, and they are thus not incorporated in **Figure 6**. Secondly, due to the limited experimental duration and the decoupling between production and export of organic matter (especially in the high recurring treatments, see section "Temporal Decoupling of Biomass Production and POC Export"), we could not cover the whole export response period. We were therefore not able to draw quantitative conclusions for the carbon sequestration potential of artificial upwelling. It is likely that this potential would have increased, had the plankton communities had more time to adapt. For example, increased repackaging of suspended biomass into dense, fast-sinking fecal pellets could have favored POC deep export. Hence, we stress the need for monthly to seasonal experimental durations to validate the long-term potential of artificial upwelling for enhanced export production and carbon sequestration.

CONCLUSION AND OUTLOOK

Artificial upwelling had opposing effects on carbon export and potential transfer to the deep ocean. On the one hand, it enhanced the mass flux and C:N ratios of sinking matter. The latter is a key prerequisite for enhancing ocean carbon sequestration. Biogeochemical modeling studies examining the feasibility of artificial upwelling in terms of carbon sequestration usually assume a static stoichiometry of C and N according to the Redfield-ratio (= 6.6). An important next step would be to re-evaluate the findings of these studies with a higher than Redfield C:N ratio as we found in our experiment. On the other hand, artificial upwelling resulted in a shallower remineralization depth and a stronger temporal decoupling between POC production and its export. The grazer community was not able to capitalize on the enhanced primary production, and hence could not form the link between biomass production and vertical flux. Thus, artificial upwelling resulted in the export of relatively porous, slowly sinking particles, which were susceptible to remineralization and therefore of low potential for deep export and sequestration. Future work should thus focus on responses of the zooplankton community and allow it more time to react to phytoplankton growth. We furthermore found that the mode, with which upwelling is applied, is an important factor for particle properties and carbon export. We found that the post-bloom export event in the singular mode produced carbon-rich particles, which were, however, respired faster and sank slower than under recurring upwelling conditions. In contrast, particle properties and the resulting RLS in the recurring mode were more favorable for POC deep export. Additionally, the continuously elevated primary and export production in the recurring mode might be more advantageous for linking the primary and export production of a slow reacting oligotrophic food web. Our assessment thus suggests that a recurring fertilization mode might be more suitable for net CO_2 removal from the atmosphere than a singular upwelling pulse. However, further research will be needed to verify if either the higher C:N ratios of sinking matter

in the singular mode or the more suitable particle properties in the recurring mode are more critical for carbon dioxide removal.

DATA AVAILABILITY STATEMENT

The datasets presented in this study can be found in an online repository. The name of the repository and accession numbers are: PANGAEA, https://doi.pangaea.de/10.1594/PANGAEA.933090 and https://doi.pangaea.de/10.1594/PANGAEA.933089.

AUTHOR CONTRIBUTIONS

UR, JT, AJP, and LTB: experimental concept and design. All authors: execution of the experiment. MB, JO, MV, MH, JT, NH-H, and IB: data analysis. MB: manuscript writing with input from all co-authors.

FUNDING

This study was funded by an Advanced Grant of the European Research Council (ERC) in the framework of the Ocean Artificial Upwelling project (Ocean artUp, No. 695094). Additional Transnational Access funds were provided by the EU projects AQUACOSM (EU H2020-INFRAIA-project, No. 731065), which supported the participation of KS and MV, and TRIATLAS (EU H2020- project, No. 817578-5), which supported JA. MH received additional funding from the German Federal Ministry of Education and Research (BMBF) during this study through the PalMod Project (Nos. 01LP1505D and 01LP1919C). JA was also supported by a Helmholtz International Fellow Award, 2015 (Helmholtz Association, Germany).

ACKNOWLEDGMENTS

We would like to thank the Oceanic Platform of the Canary Islands (Plataforma Oceánica de Canarias, PLOCAN) for sharing their research facilities with us and for their enormous support throughout the experiment. We would also like to express our gratitude toward the Marine Science and Technology Park (Parque Cientìifico Tecnoloìgico Marino, PCTM), from the University of Las Palmas (Universidad de Las Palmas de Gran Canaria, ULPGC), for providing further critical research facilities. We thank the captain and crew of RV James Cook for the deployment of the mesocosms and the deep water collection, as well as the captain and crew of the vessel J.SOCAS for helping with the second deep water collection and the recovery of the mesocosms. We especially thank the KOSMOS team (GEOMAR) for taking care of the logistics and technical work necessary to conduct the mesocosm experiment. Finally, we thank Michael Sswat, Markel Gómez Letona, Carsten Spisla, Kerstin Nachtigall, Jana Meyer, Andrea Ludwig, Levka Hansen, Jannes Hoffmann, and Rokhya Bhano Kaligatla for their contribution to data analysis and data exchange.

SUPPLEMENTARY MATERIAL

The Supplementary Material for this article can be found online at: https://www.frontiersin.org/articles/10.3389/fmars.2021.742142/full#supplementary-material

REFERENCES

Abrantes, F., Cermeño, P., Lopes, C., Romero, O., Matos, L., Van Iperen, J., et al. (2016). Diatoms Si uptake capacity drives carbon export in coastal upwelling systems. *Biogeosciences* 13, 4099–4109. doi: 10.5194/bg-13-4099-2016

Azetsu-Scott, K., and Passow, U. (2004). Ascending marine particles: significance of Transparent Exopolymer Particles (TEP) in the upper ocean. *Limnol. Oceanogr.* 49, 741–748. doi: 10.4319/lo.2004.49.3.0741

Bach, L. T., Paul, A. J., Boxhammer, T., von der Esch, E., Graco, M., Schulz, K. G., et al. (2020). Factors controlling plankton community production, export flux, and particulate matter stoichiometry in the coastal upwelling system off peru. *Biogeosciences* 17, 4831–4852. doi: 10.5194/bg-17-4831-2020

Bach, L. T., Riebesell, U., Sett, S., Febiri, S., Rzepka, P., and Schulz, K. G. (2012). An approach for particle sinking velocity measurements in the 3–400 μm size range and considerations on the effect of temperature on sinking rates. *Mar. Biol.* 159, 1853–1864. doi: 10.1007/s00227-012-1945-2

Bach, L. T., Stange, P., Taucher, J., Achterberg, E. P., Algueró-Muñiz, M., Horn, H., et al. (2019). the influence of plankton community structure on sinking velocity and remineralization rate of marine aggregates. *Global Biogeochem. Cycles* 33, 971–994. doi: 10.1029/2019GB006256

Boxhammer, T., Bach, L. T., Czerny, J., and Riebesell, U. (2016). Technical note: sampling and processing of mesocosm sediment trap material for quantitative biogeochemical analysis. *Biogeosciences* 13, 2849–2858. doi: 10.5194/bg-13-2849-2016

Boyd, P. W., Claustre, H., Levy, M., Siegel, D. A., and Weber, T. (2019). Multi-faceted particle pumps drive carbon sequestration in the ocean. *Nature* 568, 327–335. doi: 10.1038/s41586-019-1098-2

Boyd, P. W., and Trull, T. W. (2007). Understanding the export of biogenic particles in oceanic waters: is there consensus? *Prog. Oceanogr.* 72, 276–312. doi: 10.1016/j.pocean.2006.10.007

Buesseler, K. O., Antia, A. N., Chen, M., Fowler, S. W., Gardner, W. D., Gustafsson, O., et al. (2007). An assessment of the use of sediment traps for estimating upper ocean particle fluxes. *J. Mar. Res.* 65, 345–416. doi: 10.1357/002224007781567621

Casareto, Beatriz, E., Niraula, M. P., and Yoshimi, S. (2017). Marine planktonic ecosystem dynamics in an artificial upwelling area of Japan: phytoplankton production and biomass fate. *J. Exp. Mar. Biol. Ecol.* 487, 1–10. doi: 10.1016/j.jembe.2016.11.002

Cavan, E. L., Laurenceau-Cornec, E. C., Bressac, M., and Boyd, P. W. (2019). Exploring the ecology of the mesopelagic biological pump. *Prog. Oceanogr.* 176:102125. doi: 10.1016/j.pocean.2019.102125

Cavan, E. L., Le Moigne, F. A. C., Poulton, A. J., Tarling, G. A., Ward, P., Daniels, C. J., et al. (2015). Attenuation of particulate organic carbon flux in the Scotia Sea, Southern Ocean, is controlled by zooplankton fecal pellets. *Geophys. Res. Lett.* 42, 821–830. doi: 10.1002/2014GL062744

Cavan, E. L., Trimmer, M., Shelley, F., and Sanders, R. (2017). Remineralization of particulate organic carbon in an ocean oxygen minimum zone. *Nat. Commun.* 8:14847. doi: 10.1038/ncomms14847

Cermeño, P., Fernández, A., and Marañón, E. (2012). *Deteminación de La Producción Primaria Por Tamaños In Expedición de Circunnavegación Malaspina 2010: Cambio Global y Exploración de La Biodiversidad Del Océano Global: Libro Blanco de Métodos y Técnicas de Trabajo Oceanográfico*, 437–42. CSIC. Available online at: http://hdl.handle.net/10508/4238 (accessed May 14, 2021).

Engel, A., Delille, B., Jacquet, S., Riebesell, U., Rochelle-Newall, E., Terbrüggen, A., et al. (2004). Transparent exopolymer particles and dissolved organic carbon production by emiliania huxleyi exposed to different CO2 concentrations: a mesocosm experiment. *Aquat. Microb. Ecol.* 34, 93–104. doi: 10.3354/ame034093

Fan, W., Pan, Y., Zhang, D., Xu, C., Qiang, Y., and Chen, Y. (2016). Experimental study on the performance of a wave pump for artificial upwelling. *Ocean Eng.* 113, 191–200.

Francois, R., Honjo, S., Krishfield, R., and Manganini, S. (2002). Factors controlling the flux of organic carbon to the bathypelagic zone of the ocean: factors controlling organic carbon flux. *Global Biogeochem. Cycles* 16, 34–1–34–20. doi: 10.1029/2001GB001722

GESAMP (2019). "High level review of a wide range of proposed marine geoengineering techniques," in *Rep. Stud. GESAMP No.98. IMO/FAO/UNESCO-IOC/UNIDO/WMO/IAEA/UN/UN Environment/ UNDP/ISA Joint Group of Experts on the Scientific Aspects of Marine Environmental Protection*, eds P. W. Boyd and C. M. G. Vivian (London: International Maritime Organization), 144.

Giering, S. L. C., Sanders, R., Lampitt, R. S., Anderson, T. R., Tamburini, C., Boutrif, M., et al. (2014). Reconciliation of the carbon budget in the ocean's twilight zone. *Nature* 507, 480–483. doi: 10.1038/nature13123

Giraud, M., Boye, M., Garçon, V., Donval, A., and de la Broise, D. (2016). Simulation of an artificial upwelling using immersed in situ phytoplankton microcosms. *J. Exp. Mar. Biol. Ecol.* 475, 80–88. doi: 10.1016/j.jembe.2015.11.006

Giraud, M., Garçon, V., De La Broise, D., L'Helguen, S., Sudre, J., and Boye, M. (2019). Potential effects of deep seawater discharge by an ocean thermal energy conversion plant on the marine microorganisms in oligotrophic waters. *Sci. Total Environt.* 693:133491. doi: 10.1016/j.scitotenv.2019.07.297

González-Dávila, M., Santana-Casiano, J. M., Rueda, M. J., and Llinás, O. (2010). The water column distribution of carbonate system variables at the ESTOC Site from 1995 to 2004. *Biogeosciences* 7, 3067–3081. doi: 10.5194/bg-7-3067-2010

Guidi, L., Legendre, L., Reygondeau, G., Uitz, J., Stemmann, L., and Henson, S. A. (2015). A new look at ocean carbon remineralization for estimating deepwater sequestration: ocean remineralization and sequestration. *Global Biogeochem. Cycles* 29, 1044–1059. doi: 10.1002/2014GB005063

Guidi, L., Stemmann, L., Jackson, G. A., Ibanez, F., Claustre, H., Legendre, L., et al. (2009). Effects of phytoplankton community on production, size, and export of large aggregates: a world-ocean analysis. *Limnol. Oceanogr.* 54, 1951–1963. doi: 10.4319/lo.2009.54.6.1951

Hansen, H. P., and Koroleff, F. (1999). *Determination of Nutrients in Methods of Seawater Analysis, Third, Completely Revised and Extended Edition*, 3rd Edn. Weinheim: WILEY-VCH, 159–228.

Henson, S. A., Sanders, R., and Madsen, E. (2012b). Global patterns in efficiency of particulate organic carbon export and transfer to the deep ocean: export and transfer efficiency. *Global Biogeochem. Cycles* 26:1028. doi: 10.1029/2011GB004099

Henson, S. A., Lampitt, R. S., and Johns, D. (2012a). Variability in phytoplankton community structure in response to the north atlantic oscillation and implications for organic carbon flux. *Limnol. Oceanogr.* 57, 1591–1601. doi: 10.4319/lo.2012.57.6.1591

Henson, S. A., Le Moigne, F., and Giering, S. L. C. (2019). Drivers of carbon export efficiency in the global ocean. *Global Biogeochem. Cycles* 33, 891–903. doi: 10.1029/2018GB006158

IPCC (2018). "Summary for policymakers global warming of 1.5°C. An IPCC special report on the impacts of global warming of 1.5°C above pre-industrial levels and related global greenhouse gas emission pathways," *in The Context of Strengthening the Global Response to the Threat of Climate Change, Sustainable Development, and Efforts to Eradicate Poverty*, eds V. Masson-Delmotte, P. Zhai, H.-O. Pörtner, D. Roberts, J. Skea, P. R. Shukla, et al. (Geneva: World Meteorological Organization)

Iversen, M. H., and Ploug, H. (2010). Ballast minerals and the sinking carbon flux in the ocean: carbon-specific respiration rates and sinking velocity of marine snow aggregates. *Biogeosciences* 7, 2613–2624. doi: 10.5194/bg-7-2613-2010

Iversen, M. H., and Ploug, H. (2013). Temperature effects on carbon-specific respiration rate and sinking velocity of diatom aggregates–potential implications for deep ocean export processes. *Biogeosciences* 10, 4073–4085. doi: 10.5194/bg-10-4073-2013

Jakobsen, H. H., Blanda, E., Staehr, P. A., Højgård, J. K., Rayner, T. A., Pedersen, M. F., et al. (2015). Development of phytoplankton communities: implications of nutrient injections on phytoplankton composition, PH and ecosystem production. *J. Exp. Mar. Biol. Ecol.* 473, 81–89. doi: 10.1016/j.jembe.2015.08.011

Keller, D. P., Feng, E. Y., and Oschlies, A. (2014). Potential climate engineering effectiveness and side effects during a high carbon dioxide-emission scenario. *Nat. Commun.* 5:3304. doi: 10.1038/ncomms4304

Kelly, T. B., Goericke, R., Kahru, M., Song, H., and Stukel, M. R. (2018). CCE II: spatial and interannual variability in export efficiency and the biological pump in an eastern boundary current upwelling system with substantial lateral advection. *Deep Sea Res. 1 Oceanogr. Res. Pap.* 140, 14–25. doi: 10.1016/j.dsr.2018.08.007

Khatiwala, S., Primeau, F., and Hall, T. (2009). Reconstruction of the history of anthropogenic CO2 concentrations in the ocean. *Nature* 462, 346–349. doi: 10.1038/nature08526

Khatiwala, S., Tanhua, T., Mikaloff Fletcher, S., Gerber, M., Doney, S. C., Graven, H. D., et al. (2013). Global ocean storage of anthropogenic carbon. *Biogeosciences* 10, 2169–2191. doi: 10.5194/bg-10-2169-2013

Kirchman, D. L., and Ducklow, H. W. (1993). "Estimating conversion factors for thymidine and leucine methods for measuring bacterial production," in *Handbook of Methods in Aquatic Microbial Ecology*, eds P. F. Kemp, B. F. Sherr, E. B. Sherr, and J. J. Cole (Boca Raton, FL: Lewis Publishers), 513–517.

Kwiatkowski, L., Ricke, K. L., and Caldeira, K. (2015). Atmospheric consequences of disruption of the ocean thermocline. *Environ. Res. Lett.* 10:034016. doi: 10.1088/1748-9326/10/3/034016

Lam, P. J., Doney, S. C., and Bishop, J. K. B. (2011). The dynamic ocean biological pump: insights from a global compilation of particulate organic carbon, $CaCO_3$, and opal concentration profiles from the mesopelagic: the dynamic ocean biological pump. *Global Biogeochem. Cycles* 25:GB3009. doi: 10.1029/2010GB003868

Laws, E. A., and Maiti, K. (2019). The relationship between primary production and export production in the ocean: effects of time lags and temporal variability. *Deep Sea Res. 1 Oceanogr. Res. Pap.* 148, 100–107. doi: 10.1016/j.dsr.2019.05.006

Le Moigne, F. A. C., Henson, S. A., Cavan, E., Georges, C., Pabortsava, K., Achterberg, E. P., et al. (2016). What causes the inverse relationship between primary production and export efficiency in the southern ocean: PP and *e* ratio in the southern ocean. *Geophys. Res. Lett.* 43, 4457–4466. doi: 10.1002/2016GL068480

Legendre, L., and Le Fèvre, J. (1995). Microbial food webs and the export of biogenic carbon in oceans. *Aquat. Microb. Ecol.* 9, 69–77. doi: 10.3354/ame009069

Legendre, L., and Rivkin, R. B. (2002). Fluxes of carbon in the upper ocean: regulation by food-web control nodes. *Mar. Ecol. Prog. Ser.* 242, 95–109. doi: 10.3354/meps242095

Leibold, M. A., Chase, J. M., Shurin, J. B., and Downing, A. L. (1997). *Species Turnover and the Regulation of Trophic Structure*, Palo Alto: CA Annual Reviews, 29.

Liu, C. C. K., Dai, J. J., Lin, H., and Guo, F. (1999). Hydrodynamic performance of wave-driven artificial upwelling device. *J. Eng. Mech.* 125, 728–732.

Llinás, O., Rodríguez de León, A., Siedler, G., and Wefer, G. (1994). *ESTOC Data Report 1994*, Las Palmas de Gran Canaria: lCCM, Dirección General de Universidades e Investigación, Consejería de Educación, Cultura y Deportes del Gobierno de Canarias, 77.

Maiti, K., Charette, M. A., Buesseler, K. O., and Kahru, M. (2013). An inverse relationship between production and export efficiency in the southern ocean: export efficiency in the southern ocean. *Geophys. Res. Lett.* 40, 1557–1561. doi: 10.1002/grl.50219

Mari, X., Passow, U., Migon, C., Burd, A. B., and Legendre, L. (2017). Transparent exopolymer particles: effects on carbon cycling in the ocean. *Prog. Oceanogr.* 151, 13–37. doi: 10.1016/j.pocean.2016.11.002

Martin, P., Lampitt, R. S., Jane Perry, M., Sanders, R., Lee, C., and D'Asaro, E. (2011). Export and mesopelagic particle flux during a North Atlantic spring diatom bloom. *Deep Sea Res. 1 Oceanogr. Res. Pap.* 58, 338–349. doi: 10.1016/j.dsr.2011.01.006

McAndrew, P. M., Björkman, K. M., Church, M. J., Morris, P. J., Jachowski, N., Williams, P. J. L. B., et al. (2007). Metabolic response of oligotrophic plankton communities to deep water nutrient enrichment. *Mar. Ecol. Prog. Ser.* 332, 63–75. doi: 10.3354/meps332063

Moore, C. M., Mills, M. M., Arrigo, K. R., Berman-Frank, I., Bopp, L., Boyd, P. W., et al. (2013). Processes and patterns of oceanic nutrient limitation. *Nat. Geosci.* 6, 701–710. doi: 10.1038/ngeo1765

Nielsen, E. S. (1952). The use of radio-active carbon (C14) for measuring organic production in the sea. *ICES J. Mar. Sci.* 18, 117–140. doi: 10.1093/icesjms/18.2.117

Obernosterer, I., and Herndl, G. J. (1995). Phytoplankton extracellular release and bacterial growth: dependence on the inorganic N: P ratio. *Mar. Ecol. Prog. Ser.* 116, 247–257. doi: 10.3354/meps116247

Oschlies, A., Pahlow, M., Yool, A., and Matear, R. J. (2010). Climate engineering by artificial ocean upwelling: channelling the Sorcerer's apprentice: ocean pipe impacts. *Geophys. Res. Lett.* 37:961. doi: 10.1029/2009GL041961

Pan, Y., Fan, W., Huang, T.-H., Wang, S.-L., and Chen, C.-T. A. (2015). Evaluation of the sinks and sources of atmospheric CO2 by artificial upwelling. *Sci. Total Environ.* 511, 692–702. doi: 10.1016/j.scitotenv.2014.11.060

Pan, Y., Fan, W., Zhang, D., Chen, J. W., Huang, H., Liu, S., et al. (2016). Research progress in artificial upwelling and its potential environmental effects. *Sci. China Earth Sci.* 59, 236–248. doi: 10.1007/s11430-015-5195-2

Passow, U. (2002). Transparent Exopolymer Particles (TEP) in aquatic environments. *Prog. Oceanogr.* 55, 287–333. doi: 10.1016/S0079-6611(02)00138-6

Pedrosa-Pàmies, R., Conte, M. H., Weber, J. C., and Johnson, R. (2019). Hurricanes enhance labile carbon export to the deep ocean. *Geophys. Res. Lett.* 46:11. doi: 10.1029/2019GL083719

Ploug, H., and Grossart, H.-P. (2000). Bacterial growth and grazing on diatom aggregates: respiratory carbon turnover as a function of aggregate size and sinking velocity. *Limnol. Oceanogr.* 45, 1467–1475. doi: 10.4319/lo.2000.45.7.1467

Puigcorbé, V., Benitez-Nelson, C. R., Masqué, P., Verdeny, E., White, A. E., Popp, B. N., et al. (2015). Small phytoplankton drive high summertime carbon and nutrient export in the Gulf of California and Eastern Tropical North Pacific. *Global Biogeochem. Cycles* 29, 1309–1332. doi: 10.1002/2015GB005134

R Core Team (2017). *R: A Language and Environment for Statistical Computing*. Vienna: R Foundation for Statistical Computing.

Riebesell, U., Czerny, J., von Bröckel, K., Boxhammer, T., Büdenbender, J., Deckelnick, M., et al. (2013). Technical note: a mobile sea-going mesocosm system–new opportunities for ocean change research. *Biogeosciences* 10, 1835–1847. doi: 10.5194/bg-10-1835-2013

Ristow, G. H. (1997). Wall correction factor for sinking cylinders in fluids. *Phys. Rev. E* 55, 2808–2813. doi: 10.1103/PhysRevE.55.2808

Robinson, C., Steinberg, D. K., Anderson, T. R., Arístegui, J., Carlson, C. A., Frost, J. R., et al. (2010). Mesopelagic zone ecology and biogeochemistry–a synthesis. *Deep Sea Res. 2 Top. Stud. Oceanogr.* 57, 1504–1518. doi: 10.1016/j.dsr2.2010.02.018

Sabine, C. L., Feely, R. A., Gruber, N., Key, R. M., Lee, K., Bullister, J. L., et al. (2004). The oceanic sink for anthropogenic CO2. *Science* 305, 367–371.

Sanders, R. J., Henson, S. A., Martin, A. P., Anderson, T. R., Bernardello, R., Enderlein, P., et al. (2016). Controls over Ocean Mesopelagic Interior Carbon Storage (COMICS): fieldwork, synthesis, and modeling efforts. *Front. Mar. Sci.* 3:136. doi: 10.3389/fmars.2016.00136

Sharp, J. H. (1974). Improved analysis for 'particulate' organic carbon and nitrogen from seawater. *Limnol. Oceanogr.* 19, 984–989. doi: 10.4319/lo.1974.19.6.0984

Smith, D. C., and Azam, F. (1992). A simple, economical method for measuring bacterial protein synthesis rates in seawater using 3H-leucine. *Marine Microbial. Food Webs* 6, 107–114.

Stange, P., Bach, L. T., Le Moigne, F. A. C., Taucher, J., Boxhammer, T., and Riebesell, U. (2017). Quantifying the time lag between organic matter production and export in the surface ocean: implications for estimates of export efficiency: time lag and export efficiency. *Geophys. Res. Lett.* 44, 268–276. doi: 10.1002/2016GL070875

Steinberg, D. K., and Landry, M. R. (2017). Zooplankton and the ocean carbon cycle. *Ann. Rev. Mar. Sci.* 9, 413–444. doi: 10.1146/annurev-marine-010814-015924

Strohmeier, T., Strand, Ø, Alunno-Bruscia, M., Duinker, A., Rosland, R., Aure, J., et al. (2015). Response of *Mytilus edulis* to enhanced phytoplankton availability by controlled upwelling in an oligotrophic fjord. *Mar. Ecol. Prog. Ser.* 518, 139–152. doi: 10.3354/meps11036

Stukel, M. R., Landry, M. R., Benitez-Nelson, C. R., and Goericke, R. (2011). Trophic cycling and carbon export relationships in the California current ecosystem. *Limnol. Oceanogr.* 56, 1866–1878. doi: 10.4319/lo.2011.56.5.1866

Stukel, M. R., Ohman, M. D., Kelly, T. B., and Biard, T. (2019). The roles of suspension-feeding and flux-feeding zooplankton as gatekeepers of particle flux into the Mesopelagic Ocean in the Northeast Pacific. *Front. Mar. Sci.* 6:397. doi: 10.3389/fmars.2019.00397

Svensen, C., Nejstgaard, J. C., Egge, J. K., and Wassmann, P. (2002). Pulsing versus constant supply of nutrients (N, P and Si): effect on phytoplankton, mesozooplankton and vertical flux of biogenic matter. *Sci. Mar.* 66, 189–203. doi: 10.3989/scimar.2002.66n3189

Taucher, J., Bach, L. T., Boxhammer, T., Nauendorf, A., Achterberg, E. P., Algueró-Muñiz, M., et al. (2017). Influence of ocean acidification and deep water upwelling on oligotrophic plankton communities in the subtropical North Atlantic: insights from an in situ mesocosm study. *Front. Mar. Sci.* 4:85. doi: 10.3389/fmars.2017.00085

Taucher, J., Boxhammer, T., Bach, L. T., Paul, A. J., Schartau, M., Stange, P., et al. (2021). changing carbon-to-nitrogen ratios of organic-matter export under ocean acidification. *Nat. Clim. Chang.* 11, 52–57. doi: 10.1038/s41558-020-00915-5

Taucher, J., Stange, P., Algueró-Muñiz, M., Bach, L. T., Nauendorf, A., Kolzenburg, R., et al. (2018). In situ camera observations reveal major role of zooplankton in modulating marine snow formation during an upwelling-induced plankton bloom. *Prog. Oceanogr.* 164, 75–88. doi: 10.1016/j.pocean.2018.01.004

Troupin, C., Sangrà, P., and Arístegui, J. (2010). Seasonal variability of the oceanic upper layer and its modulation of biological cycles in the canary island region. *J. Mar. Syst.* 80, 172–183. doi: 10.1016/j.jmarsys.2009.10.007

Turner, J. T. (2015). Zooplankton fecal pellets, marine snow, phytodetritus and the ocean's biological pump. *Prog. Oceanogr.* 130, 205–248. doi: 10.1016/j.pocean.2014.08.005

Wickham, H., Averick, M., Bryan, J., Chang, W., D'Agostino McGowan, L., François, R., et al. (2019). Welcome to the tidyverse. *J. Open Source Softw.* 4:1686. doi: 10.21105/joss.01686

Yool, A., Shepherd, J. G., Bryden, H. L., and Oschlies, A. (2009). Low efficiency of nutrient translocation for enhancing oceanic uptake of carbon dioxide. *J. Geophys. Res.* 114:C08009. doi: 10.1029/2008JC004792

Conflict of Interest: The authors declare that the research was conducted in the absence of any commercial or financial relationships that could be construed as a potential conflict of interest.

Publisher's Note: All claims expressed in this article are solely those of the authors and do not necessarily represent those of their affiliated organizations, or those of the publisher, the editors and the reviewers. Any product that may be evaluated in this article, or claim that may be made by its manufacturer, is not guaranteed or endorsed by the publisher.

frontiers in Marine Science

ORIGINAL RESEARCH
published: 03 January 2022
doi: 10.3389/fmars.2021.804875

Numerical Flow Modeling of Artificial Ocean Upwelling

Jost Kemper[1]*, *Ulf Riebesell*[2] and *Kai Graf*[1]

[1] *Naval Architecture and Maritime Technology, Faculty of Mechanical Engineering, University of Applied Sciences, Kiel, Germany,* [2] *Marine Biogeochemistry, Biological Oceanography, GEOMAR Helmholtz Centre for Ocean Research, Kiel, Germany*

Artificial Upwelling (AU) of nutrient-rich Deep Ocean Water (DOW) to the ocean's sunlit surface layer has recently been put forward as a means of increasing marine CO_2 sequestration and fish production. AU and its possible benefits have been studied in the context of climate change mitigation as well as food security for a growing human population. However, extensive research still needs to be done into the feasibility, effectiveness and potential risks, and side effects associated with AU to be able to better predict its potential. Fluid dynamic modeling of the AU process and the corresponding inorganic nutrient transport can provide necessary information for a better quantification of the environmental impacts of specific AU devices and represents a valuable tool for their optimization. Yet, appropriate capture of all flow phenomena relevant to the AU process remains a challenging task that only few models are able to accomplish. In this paper, simulation results obtained with a newly developed numerical solution method are presented. The method is based on the open-source modeling environment *OpenFOAM*. It solves the unsteady Reynolds-Averaged Navier-Stokes (RANS) equations with additional transport equations for energy, salinity, and inorganic nutrients. The method aims to be widely applicable to oceanic flow problems including temperature- and salinity-induced density stratification and passive scalar transport. The studies presented in this paper concentrate on the direct effects of the AU process on nutrient spread and concentration in the ocean's mixed surface layer. Expected flow phenomena are found to be captured well by the new method. While it is a known problem that cold DOW that is upwelled to the surface tends to sink down again due to its high density, the simulations presented in this paper show that the upwelled DOW settles at the lower boundary of the oceans mixed surface layer, thus keeping a considerable portion of the upwelled nutrients available for primary production. Comparative studies of several design variants, with the aim of maximizing the amount of nutrients that is retained inside the mixed surface layer, are also presented and analyzed.

Keywords: artificial upwelling, computational fluid dynamics (CFD), RANS, *OpenFOAM*, oceanic flow, scalar transport, buoyancy-affected flow, stratified flow

OPEN ACCESS

Edited by:
Eugen Victor Cristian Rusu, Dunarea de Jos University, Romania

Reviewed by:
Haocai Huang, Zhejiang University, China
Weiwen Zhao, Shanghai Jiao Tong University, China

***Correspondence:**
Jost Kemper
jost.kemper@fh-kiel.de

Specialty section:
This article was submitted to Ocean Solutions, a section of the journal Frontiers in Marine Science

Received: *29 October 2021*
Accepted: *29 November 2021*
Published: *03 January 2022*

Citation:
Kemper J, Riebesell U and Graf K (2022) Numerical Flow Modeling of Artificial Ocean Upwelling. Front. Mar. Sci. 8:804875. doi: 10.3389/fmars.2021.804875

1. INTRODUCTION

In view of a continuing growth in human population, compliance with planetary boundaries is increasingly becoming the central challenge of our time. Past human resource consumption has lead to a state, where marine fish stocks are largely overexploited (FAO, 2018) and mere reduction of greenhouse gas emissions is no longer sufficient to meet international climate goals (Lawrence et al., 2018). In the search for ways to mitigate these consequences of resource overconsumption, Artificial Upwelling (AU) of nutrient-rich Deep Ocean Water (DOW) to the ocean's sunlit surface layer has recently been proposed (Kirke, 2003; Lovelock and Rapley, 2007).

By bringing DOW to the ocean's surface, AU aims to replicate processes that occur in natural upwelling systems. Here, the supply of inorganic nutrients stimulates a high primary production, thereby providing the basis for highly efficient food chains, which make natural upwelling systems some of the world's richest fishing grounds (Roels et al., 1977). So far, it has not been shown whether AU can effectively replicate important features of natural upwelling systems. Nevertheless, AU is seen as a possible way of increasing fishery yields in less productive oceanic regions. As such, AU could promote food security for a growing human population (Kirke, 2003) and reduce pressure on natural fish stocks. Further, it has been pointed out that an increased primary production induced by AU could act as a driver for the biologic carbon pump, a process that naturally extracts CO_2 from the atmosphere (Lovelock and Rapley, 2007). This has led to a discussion on whether AU can contribute to future climate change mitigation efforts (Lovelock and Rapley, 2007; Oschlies et al., 2010; Williamson et al., 2012; Bauman et al., 2014; Pan et al., 2015; GESAMP, 2019). Despite its potential, a wide range of ecological responses and biogeochemical consequences of AU remain largely unstudied to date. Responsible use of AU on a large scale demands thorough understanding and accurate quantification of all environmental and ecological impacts associated with this process.

Numerical modeling of the involved fluid dynamic processes plays an important role in this context. Numerical models provide information for the technical design and optimization of AU systems. Additionally, the detailed information on the associated spread and concentration levels of nutrient-rich DOW can be used as a basis for biological model calculations and thus contribute to the quantification of environmental and ecological impacts of specific AU devices. Numerical methods based on the Reynolds-Averaged Navier-Stokes (RANS) equations are capable of accurately predicting both small-scale flow phenomena inside the AU device and large-scale far-field phenomena. They thus represent a valuable tool for assessing the AU processes with high accuracy.

A number of hydrodynamic studies on AU are reported in literature. Several publications deal with artificial upwelling by utilizing the energy of ocean waves. A first overview of the topic was given by Kirke (2003). Beyond pointing out the potential of the use of DOW for increasing fish stocks, Kirke also mentions the problem that the cold DOW, when artificially upwelled, generally tends to sink back down due to its high density and thus does not remain available for primary production. Liu and Jin (1995) apply a simple mathematical model to calculate upwelling volumes of a wave-driven device. They find that a flow rate of 0.95 $[m^3/s]$ could be obtained with their device in a typical sea state off the Hawaiian islands. Similar calculations are presented by Soloviev (2016), who additionally applied a numerical model that is not specified in detail. Both of these studies do not model nutrient transport.

The *air lift* method proposed by Liang and Peng (2005) has also been studied. Here, artificial upwelling is achieved by pumping air into the ocean at a certain depth. Thereby a flow of air bubbles is created which transports DOW to the surface. A RANS-based numerical model for this type of upwelling was presented by Meng et al. (2013). Here, it is found that the applied, simplified model was able to accurately predict the dispersed flow and achieve a satisfactory agreement with experimental data. Some authors have reported results of sea trials with air lift AU systems (Fan et al., 2013; Pan et al., 2019).

Other publications deal with a device referred to as *perpetual salt fountain*, which was initially proposed by Stommel et al. (1956). Here, the opposing effect which a decrease in temperature and salinity with depth (i.e., a typical open ocean depth profile) has on water density are used to drive a self-sustaining upwelling process in a long ocean pipe. Once the pipe is filled with DOW, temperature differences between the pipe- and surrounding water diminish over time while salinity differences remain and account for a positive buoyancy of the DOW in the pipe. Results of sea trials with this device are reported in Maruyama et al. (2004) and Tsubaki et al. (2007). Maruyama et al. (2004) also apply a RANS-based numerical model to predict the flow inside their device. However, they do not apply any turbulence model but use turbulent diffusion data from their experiment in the calculations. Williamson et al. (2009) extend this work to studies of near-field mixing in crossflow at the device outlet, using a commercial RANS code. Williamson et al. find that the flow can be characterized into a region with high turbulent diffusion local to the pipe outlet and a second region further downstream with very little diffusion. They further point out the problem of turbulence anisotropy in buoyancy-affected flows, which also plays a role in the present paper. Finally, Williamson et al. find that, given the small observed diffusion, the outlet depth of their device is too large for the pumped DOW to be mixed into the ocean's surface layer.

Fan et al. (2015) propose a simple mathematical model for the optimization of forced upwelling in a pipe. To maintain high nutrient concentrations for mariculture inside a confined DOW plume, Fan et al. aim to minimize dilution of the plume. They find that the plume trajectory and the DOW concentration inside the plume are highly dependent on several technical parameters, like flow rate, pipe diameter, and outlet depth as well as environmental influences, like current speed and stratification strength. A validation of their mathematical model against steady-state RANS CFD data is also provided in Fan et al. (2015) along with some validation of the CFD model.

The present paper reports of AU simulations with a new RANS solution method. The development of the new method is based on Computational Fluid Dynamics (CFD) methods

available within the open-source framework *OpenFOAM*, namely the *buoyantPimpleFoam* solver and the thermophysical and turbulence modeling libraries. A transport equation for salinity is added to the *buoyantPimpleFoam* solver, the thermophysical modeling library is extended to correctly reproduce the physical properties of seawater, and a simple modification is introduced into the k-ωSST turbulence model to better capture turbulence effects for buoyancy-affected flows. Thus, a numerical method for small-scale oceanic flow is created which, due to its open-source basis, allows for flexible adjustment and extension to specific modeling problems, like AU. For the simulations presented in this paper the method is further extended with a transport equation for nutrient concentration, which enables a direct quantification of the nutrient transport introduced by the AU device.

The remainder of this paper is structured as follows. First, the applied method and the underlying equations will be described. Then, the results of some studies carried out with the new method will be presented and discussed. Finally, conclusions from the presented work will be drawn before finishing with recommendations for necessary future extensions.

2. NUMERICAL METHOD

The method presented in this paper solves the RANS modeling problem for buoyancy-affected oceanic flow. The mathematical model and its numerical solution will be outlined briefly in this section.

At present, the method incorporates a single-phase (i.e., water) only and does not model influences of deformation of the water surface. This approach was chosen because early studies indicated that the influences of the water surface on the general flow were very small, while accurate modeling of free surface motion would have been associated with high computational cost. Also, this approach enabled a more direct control over the heat transfer processes at the surface than a multiphase simulation using the volume of fluid method.

2.1. Momentum and Mass Equations

A flow of a Newtonian fluid in an Eulerian reference frame is considered. To account for density fluctuations, Favre averaging is used instead of the more common Reynolds averaging. In the following, Favre-averaged quantities are marked by an overtilde, while Reynolds averaging is indicated by an overscore. The conservation equations for momentum and mass, in their conservative form, can thus be written as

$$\begin{aligned}\frac{\partial\left(\overline{\rho}\widetilde{\boldsymbol{u}}\right)}{\partial t}+\nabla\cdot\left(\overline{\rho}\widetilde{\boldsymbol{u}}\widetilde{\boldsymbol{u}}\right)=&\nabla\cdot\left(2\mu_e\widetilde{\boldsymbol{S}}-\frac{2}{3}\mu_e\left(\nabla\cdot\widetilde{\boldsymbol{u}}\right)\boldsymbol{I}\right)\\&-\frac{2}{3}\nabla\left(\overline{\rho}k\right)-\nabla\overline{p}+\overline{\rho}\boldsymbol{g}\end{aligned}\tag{1}$$

and

$$\frac{\partial\overline{\rho}}{\partial t}+\nabla\cdot\left(\overline{\rho}\widetilde{\boldsymbol{u}}\right)=0\,.\tag{2}$$

In Equations (1) and (2), $\widetilde{\boldsymbol{u}}$ is the Favre-averaged velocity, $\overline{p}$ is Reynolds-averaged pressure and $\overline{\rho}$, μ_e and $\boldsymbol{g}$ are Reynolds-averaged density, effective dynamic viscosity and the gravitational acceleration vector, respectively. The tensor $\boldsymbol{I}$ represents the unit matrix, and $\widetilde{\boldsymbol{S}}$ is the mean strain rate tensor, which is defined as

$$\widetilde{\boldsymbol{S}}=\frac{1}{2}\left(\nabla\widetilde{\boldsymbol{u}}+\left(\nabla\widetilde{\boldsymbol{u}}\right)^T\right)\,.\tag{3}$$

Boussinesq's linear eddy viscosity theory is applied in Equation (1) to model the effect of turbulence. The effective dynamic viscosity consist of the molecular and eddy viscosities as follows

$$\mu_e=\mu+\mu_t\,.\tag{4}$$

The eddy viscosity μ_t and the turbulent kinetic energy k have to be modeled by turbulence closure models as discussed in section 2.4. For convenience, a modified pressure $\overline{p}^*=\overline{p}+\frac{2}{3}\overline{\rho}k$ is introduced. Also, in Equation (1) the main hydrostatic impact is subtracted from $\overline{p}^*$ yielding

$$\overline{p}^*_{rgh}=\overline{p}^*-\overline{\rho}\boldsymbol{g}\cdot\boldsymbol{r},\tag{5}$$

where $\boldsymbol{r}$ is the position vector with respect to a reference position. The pressure and buoyancy terms in Equation (1) can then be restructured as follows

$$-\nabla\overline{p}^*+\overline{\rho}\boldsymbol{g}=-\nabla\overline{p}^*_{rgh}-\left(\boldsymbol{g}\cdot\boldsymbol{r}\right)\nabla\overline{\rho}\,.\tag{6}$$

With these changes, the implemented momentum equation reads

$$\begin{aligned}\frac{\partial\left(\overline{\rho}\widetilde{\boldsymbol{u}}\right)}{\partial t}+\nabla\cdot\left(\overline{\rho}\widetilde{\boldsymbol{u}}\widetilde{\boldsymbol{u}}\right)=&\nabla\cdot\left(2\mu_e\widetilde{\boldsymbol{S}}-\frac{2}{3}\mu_e\left(\nabla\cdot\widetilde{\boldsymbol{u}}\right)\boldsymbol{I}\right)\\&-\nabla\overline{p}^*_{rgh}-\left(\boldsymbol{g}\cdot\boldsymbol{r}\right)\nabla\overline{\rho}\,.\end{aligned}\tag{7}$$

2.2. Energy Equation

A conservation equation for energy needs to be solved to account for buoyancy effects. Here, potential enthalpy, i.e., the enthalpy that a parcel of water would have if adiabatically and without salt exchange raised to the sea surface, is used as energy variable. As pointed out by McDougall (2003), a simple conservation equation for potential enthalpy is, to a high degree of accuracy, equivalent to the first law of thermodynamics in the ocean. The conservation equation for potential enthalpy per unit mass $\widetilde{h}$ reads

$$\frac{\partial\left(\overline{\rho}\widetilde{h}\right)}{\partial t}+\nabla\cdot\left(\overline{\rho}\widetilde{\boldsymbol{u}}\widetilde{h}\right)=\nabla\cdot\left(\alpha_e\nabla\widetilde{h}\right)\,.\tag{8}$$

Here, α_e is the effective thermal diffusivity

$$\alpha_e=\frac{\mu_t}{Pr_t}+\frac{\mu}{Pr}=\frac{\mu_t}{Pr_t}+\frac{\kappa}{c_p}\,.\tag{9}$$

As for the momentum equation, the turbulent fluctuations are modeled as additional diffusion by applying the gradient diffusion hypothesis. In Equation (9) κ is thermal conductivity, c_p is specific heat capacity and Pr and Pr_t are Prandtl number and turbulent Prandtl number, respectively. Throughout this study a value of 1 was used for Pr_t. For c_p a constant value of 3991.867 957 119 63 [J/kgK] was used, as suggested by IOC et al. (2010). κ is calculated from the thermophysical model (see section 2.4).

2.3. Scalar Transport Equation

Scalar transport equations have to be solved for salinity and nutrient concentration. By again applying the gradient diffusion hypothesis, the conservation equation for these quantities reads

$$\frac{\partial\left(\overline{\rho}\widetilde{\phi}\right)}{\partial t}+\nabla\cdot\left(\overline{\rho}\widetilde{\boldsymbol{u}}\widetilde{\phi}\right)=\nabla\cdot\left(\overline{\rho}D_e\nabla\widetilde{\phi}\right), \tag{10}$$

where $\widetilde{\phi}$ is salinity or nutrient concentration. The effective diffusion coefficient D_e is defined as

$$D_e=\frac{\mu_t}{\overline{\rho}Sn_t}+D, \tag{11}$$

where D is the molecular diffusivity in $[m^2/s]$ and Sn_t is the turbulent Schmidt number. For Sn_t, a value of 1 was used throughout this study. D was set to 1×10^{-9} $[m^2/s]$ for both, salinity and nutrients. This represents a typical value for mass diffusion in water (see e.g., Zhang et al., 2004; Thorpe, 2007).

2.4. Thermophysical Model for Seawater

The flow behavior of any fluid is tightly coupled to its physical properties, which in turn depend on the state of the fluid and its composition. In the *OpenFOAM* framework this relation is replicated by a thermophysical model. In its standard version, the thermophysical model calculates fluid properties based on pressure and temperature. This functionality was extended here, to include the influence of salinity. For the present study, the modeled fluid properties are:

- Viscosity μ
- Thermal conductivity κ
- Density ρ.

To model ρ based on temperature, salinity, and pressure, the 75term polynomial of McDougall et al. (2003) was used. This is part of the widely used *TEOS-10* (IOC et al., 2010) standard. By including pressure dependence in the calculation, the full compressibility is captured in the system of equations. Since the time steps for the applications considered here are small (about 1×10^{-1} $[s]$), acoustic modes do not need to be filtered from the system, as often done in ocean models (Griffies and Adcroft, 2008). For μ and κ, the pressure-independent polynomials of Sharqawy et al. (2010) and Nayar et al. (2016) were implemented.

2.5. Turbulence Model for Buoyancy-Affected Flow

In Equations (7), (8), and (10) the turbulent fluxes are expressed in terms of the turbulent viscosity μ_t, by means of the eddy viscosity and gradient diffusion hypotheses. Eddy viscosity turbulence models are concerned with determining μ_t. This is usually achieved by solving one or more transport equations for different turbulence variables. Numerous approaches have been presented in the past, of which the standard k-ϵ model (Launder and Spalding, 1974) and the k-ωSST model (Menter, 1994) are the ones most widely used for industrial applications. For the present study, the k-ωSST model was chosen with a simple modification. This model is known to provide a more realistic approximation of the turbulence level in stagnation regions. Within this study, it also proved preferable for cases where a jet of DOW meets the water surface. The k-ωSST model and its application for buoyancy-affected flow will be presented here briefly.

The k-ωSST model describes μ_t as a function of turbulent kinetic energy k and its specific dissipation rate ω. The transport equations for these two quantities, as implemented in *OpenFOAM*, read

$$\begin{aligned}&\frac{\partial\overline{\rho}k}{\partial t}+\nabla\cdot\left(\overline{\rho}\widetilde{\boldsymbol{u}}k\right)-\nabla\cdot\left(\left(\mu+\sigma_k\mu_t\right)\nabla k\right)\\&=P_k-\overline{\rho}\beta^*k\omega\end{aligned} \tag{12}$$

and

$$\begin{aligned}&\frac{\partial\overline{\rho}\omega}{\partial t}+\nabla\cdot\left(\overline{\rho}\widetilde{\boldsymbol{u}}\omega\right)-\nabla\cdot\left(\left(\mu+\sigma_\omega\mu_t\right)\nabla\omega\right)\\&=\overline{\rho}\gamma\frac{P_k}{\mu_t}-\overline{\rho}\beta\omega^2+2\left(1-F_1\right)\overline{\rho}\frac{\sigma_{\omega2}}{\omega}\left(\nabla k\cdot\nabla\omega\right).\end{aligned} \tag{13}$$

Here, P_k is the shear production term, β^* is a model constant, and σ_k, σ_ω, β and γ are blended between values reproducing k-ω (Wilcox, 1988) (subscript 1) and k-ϵ (Launder and Spalding, 1974) (subscript 2) model behavior, using the wall distance dependent blending factor F_1. The turbulent dynamic viscosity is calculated by

$$\mu_t=\frac{\overline{\rho}a_1k}{\max\left(a_1\omega,\sqrt{S_2}F_2\right)}, \tag{14}$$

where a_1 is a model constant, $\sqrt{S_2}$ is the vorticity magnitude and F_2 is an additional blending function based on the wall distance.

Within the present study a considerable overprediction of vertical diffusion was observed for the standard *OpenFOAM* implementation of the k-ωSST model. This problem can be accounted to the inadequate representation of buoyancy effects on turbulence and is often treated by adding additional terms to Equations (12) and (13) (Van Maele and Merci, 2006). A simple approach was recently presented by Devolder et al. (2017) following the work of Van Maele and Merci (2006). This approach was adopted for the present work. The formulation of the buoyancy term, which is added to Equation (12), reads

$$-\frac{\mu_t}{\overline{\rho}Sn_t}\boldsymbol{g}\cdot\left(\nabla\overline{\rho}\right). \tag{15}$$

Here, the turbulent Schmidt number Sn_t is set to 0.85, to be in line with Van Maele and Merci (2006) and Devolder et al. (2017).

As stated by Van Maele and Merci (2006), the simple approach implemented here cannot be expected to provide a fully realistic capture of turbulence effects in buoyancy-affected flow. Namely, an overprediction of vertical turbulent diffusion in stably stratified flow must still be expected as shown by several authors (Stankov et al., 2001; Worthy et al., 2001; Van Maele and Merci, 2006). However, the implemented approach was seen to provide a much-needed improvement over the standard *OpenFOAM* implementation of the k-ωSST model. Since the implementation of a more sophisticated buoyancy treatment method was outside the scope of this study, the shortcomings of the present approach were accepted.

2.6. Solution Method

The set of equations described above has to be solved by a numerical solution method. To do so, the partial differential equations have to be approximated by algebraic equations at a finite number of locations in space and time. The flow domain (i.e., the fluid volume for which the equations are to be solved) is discretized by a large number of small volumes (cells) and the equations are solved for each of these volumes. Using Gauss's theorem, the divergence in the conservation equations can be calculated by considering the flux across the boundaries of each volume. This discretization method is known as the finite volume method. By further applying suitable discretization methods for the remaining differentials and integrals, a system of algebraic equations, containing the contributions from all cells, is created for each of the governing equations. These algebraic systems of equations are still both coupled and non-linear. For example, the momentum (Equation 7) contains the unknown eddy viscosity, pressure, and density. By taking these values from a previous solution (e.g., a previous iteration or a previous time step) and treating non-linearities in a similar manner, the coupled system of non-linear equations can be solved by iteratively solving linear systems of equations until the difference between the current and previous solution becomes small, and with it the error of the previously explained approximation.

Here, *OpenFOAM*s PIMPLE algorithm is employed for the iterative solution process. The PIMPLE algorithm represents a combination of the well-known SIMPLE (Patankar and Spalding, 1972) and PISO (Issa, 1986) algorithms. A pressure equation is formulated based on the continuity equation (Equation 2)[1]. Including the necessary additional equations for salinity and nutrients, the implemented PIMPLE algorithm can be summarized by the following steps:

1. Solve momentum equation
2. Solve salinity equation
3. Solve potential enthalpy equation
4. Calculate density based on new salinity and temperature
5. Solve pressure equation
6. Correct velocity and density based on new pressure
7. Solve turbulence equations
8. Solve nutrient transport equation
9. Advance to next time step.

(Steps 5 and 6: PISO loop; Steps 1–6: PIMPLE loop)

The steps of the PIMPLE loop (1–6) are repeated for a set number of times, or until a converged solution for the time step is reached. Also, one or two additional PISO loops (Steps 5 and 6) are usually included.

The following schemes are used for the discretization of the equation system. Linear interpolation is used to obtain cell face values from the cell centered data. Likewise, all gradients occurring in the equations are calculated by linear interpolation. For the divergence terms, the *limittedLinear* scheme is applied, which generally uses linear interpolation but limits toward upwind interpolation in regions with strong gradient changes. For the temporal derivative, the second-order *backward* scheme is used for all equations except for the nutrient and salinity transport equations, where the implicit *Euler* scheme is used to ensure boundedness.

[1]The derivation of the pressure equation is not discussed here for brevity. For more information please refer to standard literature (e.g., Ferziger et al., 2020).

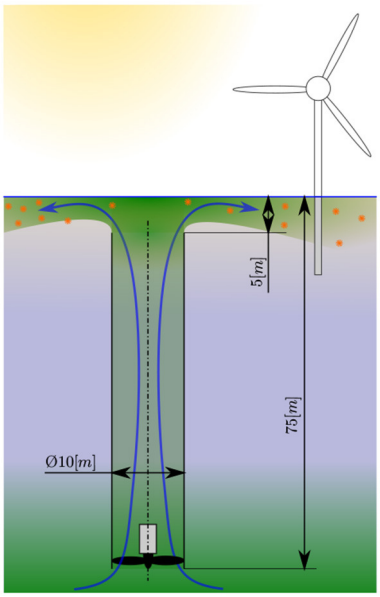

FIGURE 1 | AU system concept and main dimensions.

3. RESULTS

3.1. AU Application

The simulations presented in this paper concentrate on forced upwelling in a pipe, powered by a large propeller at the pipe inlet. Prior to the present project, the main dimensions of a prototype system had been optimized in a dedicated study. It was found that a large-diameter pipe in combination with a single propeller ensures a maximum energy efficiency of the system. A diameter of 10 $[m]$ was recommended as a compromise between efficiency and technical feasibility. The prototype simulated in this paper is designed for field studies in the center of the Guinea Dome region, close to $10°N$, $22°W$. In this region, with a water depth of 4,000–5,000 $[m]$, nutrient-rich DOW naturally rises to depths above 100 $[m]$. A depth of 75 $[m]$ is thus sufficient for the DOW inlet of this specific device. The device is intended to be deployed free-floating and powered by a renewable energy source, providing 500 $[kW]$ of electric power. The estimated volume flow rate is 155 $[m^3/s]$. Since the pipe will be made from an elastic material, a positive pressure inside the pipe is desirable to prevent it from collapsing. Thus, the propeller is installed at the device inlet. A schematic of the device is shown in **Figure 1** along with its main dimensions. With larger inlet depths the same type of device can be deployed in other ocean regions, however, in this paper, the results concentrate solely on the Guinea Dome region.

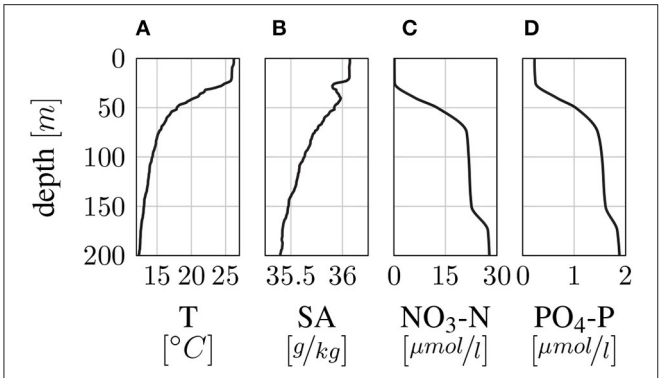

FIGURE 2 | Depth profiles for *in situ* temperature **(A)**, absolute salinity **(B)**, NO_3-N **(C)** and PO_4-P **(D)** in the deployment region. Data taken from Krahmann (2016).

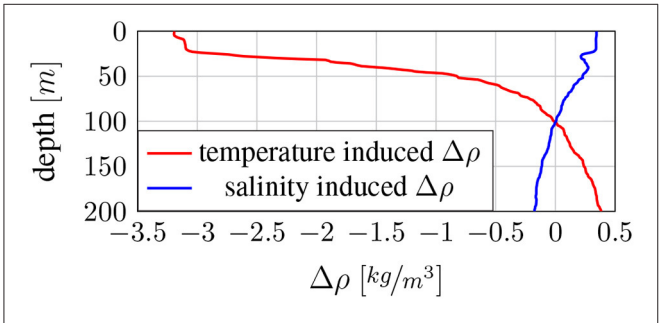

FIGURE 3 | Density change $\Delta\rho$ introduced by the temperature (red) and salinity (blue) profiles in **Figure 2**.

Figure 2 shows depth profiles of *in situ* temperature, absolute salinity, PO_4-P and NO_3-N for the deployment region. The data was taken from Krahmann (2016). As can be seen in **Figure 2**, high nutrient concentrations are already found at depths smaller than 100 $[m]$ in the example region. The water column in this region is stably stratified due to large temperature and salinity-induced changes in water density. The mixed layer depth (MLD) is 21.8 $[m]$[2]. **Figure 3** depicts the counteracting effects of salinity and temperature on density in the modeled region. Here, profiles of the absolute density change $\Delta\rho$ introduced by temperature and salinity are shown for depths up to 200 $[m]$. $\Delta\rho$ is calculated with respect to a standard potential density of 1026.49 $[kg/m^3]$. It can be seen from **Figure 3** that, especially in the surface region, temperature has a much stronger influence on density than salinity.

Expected Flow Phenomena

The vertical density gradient has important impacts on the general flow field created by the AU device. Stratified flow exhibits the tendency to return to a stable stratification once disturbed. This will generally dampen out vertical velocities that are not driven by buoyancy forces. Thus, when artificially pumped to the surface, the cold DOW, after having dissipated its upwards directed momentum, starts sinking downwards again due to its high density. Williamson *et al.* therefore characterize the flow as a weak fountain (Williamson et al., 2009). During the process, the density difference between the pumped DOW and the surrounding surface water is decreased by mixing as well as water surface heat transfer. Thus, the DOW does not sink to its original depth but creates a layer in the upper region of the water column, which spreads horizontally as more water is pumped up by the AU system. Consequently, the flow close to the AU system can be characterized as buoyant flow (i.e., the main flow direction is aligned with the direction of gravity) with forced convection, while in the far field the flow fulfills the characteristics of stratified flow (i.e., the main flow direction is normal to the direction of gravity).

Simulation Setup

The geometry of the AU system is idealized to a cylindrical shape for the simulations. All structural elements or construction details are thereby neglected, which is appropriate considering the early development stage of the system. A cylindrical shape was also chosen for the flow domain (i.e., the water volume which is modeled in the simulations). Use was made of the symmetry effects in the sense that only a quarter of the cylindrical flow domain was modeled. This allows for a significant reduction of the overall count of computational cells without compromising the three-dimensional resolution of the flow. The necessary radius of the cylindrical flow domain was actively studied. Since the influence of the AU system spreads over time, the size of the flow domain critically influences how long the simulation can run before an unwanted interaction of the flow with the outer boundary can occur. Eventually, a radius of 480 $[m]$ was chosen, which kept the computational burden acceptable and enabled simulated times of 10,000 $[s]$ with no visible outer-boundary effects. Equally, a depth of 200 $[m]$ was chosen for the flow domain. A heat transfer boundary condition is used at the top boundary of the flow domain to model sensible heat flux through the water surface. The air temperature is assumed to be the same as the initial water temperature at the water surface. A sensible heat transfer coefficient of 13.5 $[W/m^2K]$ was derived from work of Komori et al. (2011). The propeller, which is driving the AU device, is modeled as a momentum source inside the lower part of the pipe. Here, the desired flow velocity of 1.969 $[m/s]$ is uniformly prescribed. It has to be noted that this approach does not realistically model the complex flow field behind a propeller. However, since full modeling of the propeller and its influences was not feasible within this study, it was decided that this approach was most general and sufficiently accurate to not have an influence on the general behavior of the AU system. All simulations were started from an initial state of zero velocity with temperature and salinity profiles as depicted in **Figure 2**. To represent the nutrient concentration, a Nutrient Index (NI) was defined. Its initial value is calculated based on the NO_3-N profile (see **Figure 2**) divided by its value at the device inlet depth (i.e., 75 $[m]$). The initial NI value (i.e., before the start of the AU operation) is thus close to zero at the water surface and

[2]The MLD was established using a 0.03 $[kg/m^3]$ potential density criterion with a reference depth of 10 $[m]$.

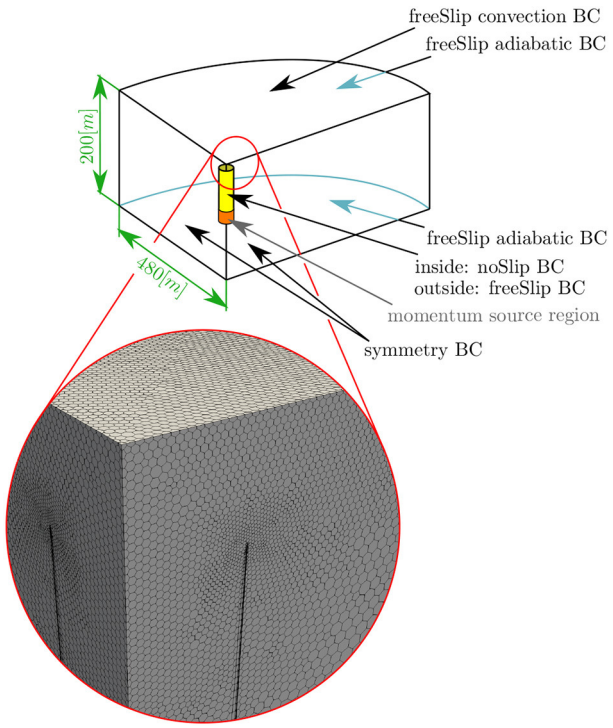

FIGURE 4 | Schematic of the simulation setup with Boundary Conditions (BC) and mesh details.

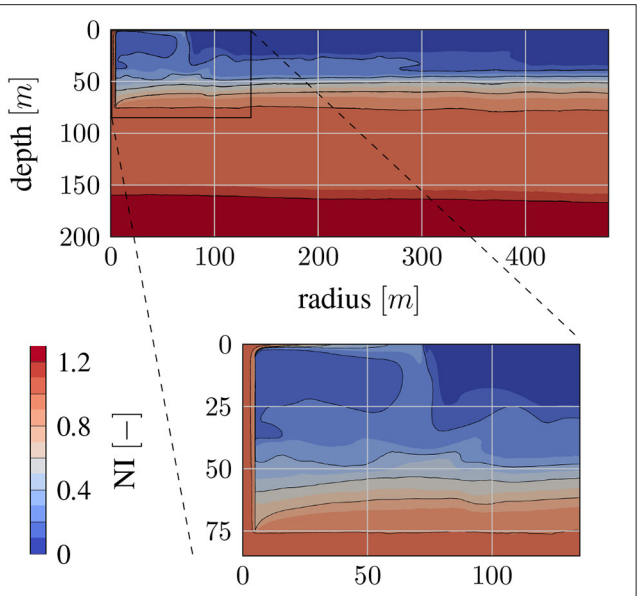

FIGURE 5 | NI on a vertical slice through the flow domain after 5.000 [s] (ST).

reaches one at 75 [m] depth[3]. The simulation setup is depicted in **Figure 4** along with the applied boundary conditions and the computational mesh.

Discretization

The flow domain was discretized using an unstructured, polyhedral mesh. The mesh was gradually refined toward the water surface region as well as the pipe inlet and outlet. The boundary layer region inside the pipe was refined with prism layers to maintain a dimensionless wall distance (y^+) between 30 and 100. An average grid edge size[4] of about 1.5 [m] and a time step size of 0.125 [s] were used for all studies presented in this paper. The described geometry is thus discretized by 9.3 million cells. This discretization was chosen based on experience and sensitivity studies carried out for similar problems. On a dedicated cluster[5] about 100 [s] of Computation Time (CT) were needed per second of Simulated Time (ST).

3.2. Basic Study

The aim of this first study is to establish whether the described numerical method is able to plausibly capture and quantify the expected flow effects corresponding to the AU process and the mixing of DOW and surface waters. This is studied here, using the previously described case setup. **Figure 5** shows typical, graphical results for NI on a vertical slice through the flow domain after 5,000 [s] of simulated time (i.e., 1.39 [hrs]).

The expected fountain-like flow close to the pipe outlet can be observed in **Figure 5**. The jet of DOW spreads on the free surface to a patch of about 130 [m] diameter before the cold DOW starts to sink due to its high density. Once the DOW has sunk to its depth of neutral buoyancy, the flow becomes almost purely horizontal and a layer with increased NI values is created, which can also be observed in **Figure 5**. Since the fountain-like flow feature close to the device is comparably small, changes in the NI-depth profiles need to be analyzed to be able to quantify the large-scale effect of the AU device. For this analysis a region of study between a 150 and 330 [m] radius around the AU system is defined, thus excluding the fountain-like flow feature local to the device as well as the outer part of the domain, where the nutrient-rich layer does not fully develop within the simulated time span. **Figure 6** shows average NI depth profiles for this region of study. Depth profiles for multiple points in time, after the start of the AU process, are depicted. The previously described layer creation process can be observed in **Figure 6**. The strongest changes in the depth profile due to the AU operation take place within a confined depth range of 10–40 [m]. In this region, the nutrient concentration is increased due to the influence of the nutrient-rich layer, which is initially created at a depth of about 30 [m] and expands in height over time. Between 40 and 70 [m] depth the initial nutricline is lowered slightly due to the extraction of the DOW below. After 7500 [s] the depth profile becomes temporally

[3]Since the nutrient concentration is still increasing with depth below the device inlet, NI values greater than one are common at depths greater than 75 [m], indicating that the nutrient concentration here is higher than the initial concentration at the device inlet.

[4]The basic grid edge size is calculated as $\sqrt[3]{\frac{TotalVolume}{CellCount}}$.

[5]Two dual CPU nodes were used for most of the studies presented. The nodes were based on AMD EPYC 7302, 16 Core Processors. FDR InfiniBand was used for distributed computations.

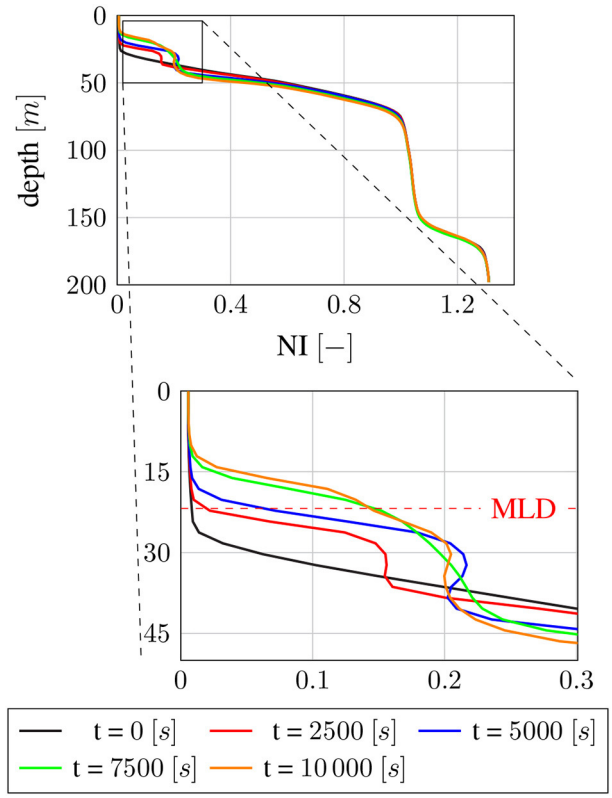

FIGURE 6 | NI depth profiles for different points in time (ST). Profiles are averaged over a radius of 150–330 [*m*] around the AU system.

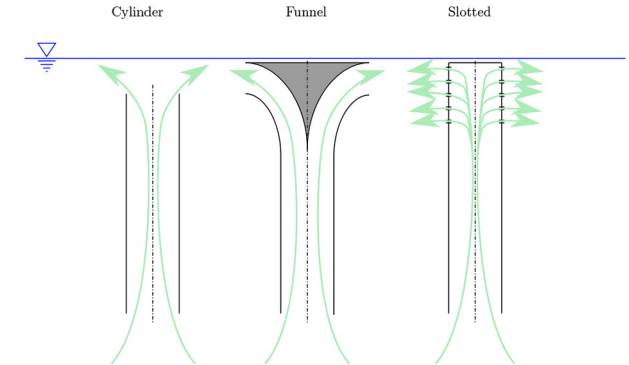

FIGURE 7 | Tested design variants for the AU system.

stable, indicating that by this point the nutrient-rich layer is fully developed throughout the region of study.

It is not within the scope of this study to establish to which extent the upwelled nutrients in the nutrient-rich layer can be utilized for primary production. The change of the average NI value inside the mixed layer of the studied region is thus taken as measure for the upwelling efficiency of the AU device. From the depth profiles shown in **Figure 6** it can be calculated that the average NI inside the mixed surface layer is raised from an initial value of 0.0064 to 0.0402 after 10 000 [*s*]. This corresponds to NO_3-N values of 0.14 and 0.85 [$\mu mol/l$], respectively.

3.3. Variant Studies

Having shown the general ability of the described model to capture and quantify the flow effects relevant to the AU process, comparative studies between device variations are possible. In a first study, three design variants were chosen, which were expected to exhibit different flow characteristics at the outlet of the AU system. The investigated variants are depicted in **Figure 7**. The first variant, referred to as *Cylinder*, represents the basic cylindrical geometry as described in the previous sections. Here the flow at the outlet of the AU system is characterized by its impingement on the surface. The second variant, referred to as *Funnel*, features a funnel-shaped outlet with a maximum diameter of 30 [*m*]. Also, a body (gray shaded area in **Figure 7**) is installed inside the Funnel to make sure the flow follows the funnel surface (i.e., avoid flow separation). The flow for this variant is characterized by the horizontal decay of the momentum introduced by the AU system. The third variant, referred to as *Slotted*, represents a pipe that is closed at the top, such that the outflow occurs through multiple horizontal slots on the upper part of the pipe. Five slots are arranged over the top 10 [*m*] of the pipe. A width of 0.125 [*m*] was chosen for the slots such that the total area of all slots equals 1/4 of the pipes cross-sectional area. The outflow for this variant is characterized by five planar jets. For all three variants a flow velocity of 1.969 [m/s] inside the pipe was specified.

Figure 8 shows the results of the variant study after 10 000 [*s*] (ST). Averaged NI depth profiles are shown in **Figure 8A**. Again only the region between a radius of 150 and 330 [*m*] around the AU system is analyzed. As can be seen from this figure, a similar nutrient-rich layer is created by all device variants. It can further be seen from **Figure 8A** that, between 20 and 40 [*m*] depth, the *Funnel* variant reaches higher NI values than the other variants, while inside the mixed surface layer (i.e., above the MLD) the *Cylinder* variant reaches slightly higher values. For the *Slotted* variant, the nutrient-rich layer seems to be slightly narrower, which leads to smaller NI values inside the mixed surface layer.

Again, the increase of the Average NI inside the mixed layer of the studied region is taken as measure for upwelling efficiency. **Figure 8C** shows the average mixed layer NI in the analyzed region for all device variants. Here, the superiority of the *Cylinder* variant becomes clearly visible.

To understand the origin of the different performances of the device variants, the amount of turbulent mixing created by these variants must be considered. **Figure 8B** shows the Average mixed layer eddy viscosity ratio ν_t/ν over the radial distance from the device center. This figure shows that turbulence is created near the device outlet and decays with larger distances to the device. The strongest turbulent mixing is found at some distance from the device outlet, where the DOW starts to sink down due to its high density. It becomes evident from **Figure 8B** that, while the *Slotted* variant reaches the highest eddy viscosity ratios, the *Cylinder* variant creates overall more turbulence, by maintaining higher values at greater radii. The *Funnel* variant

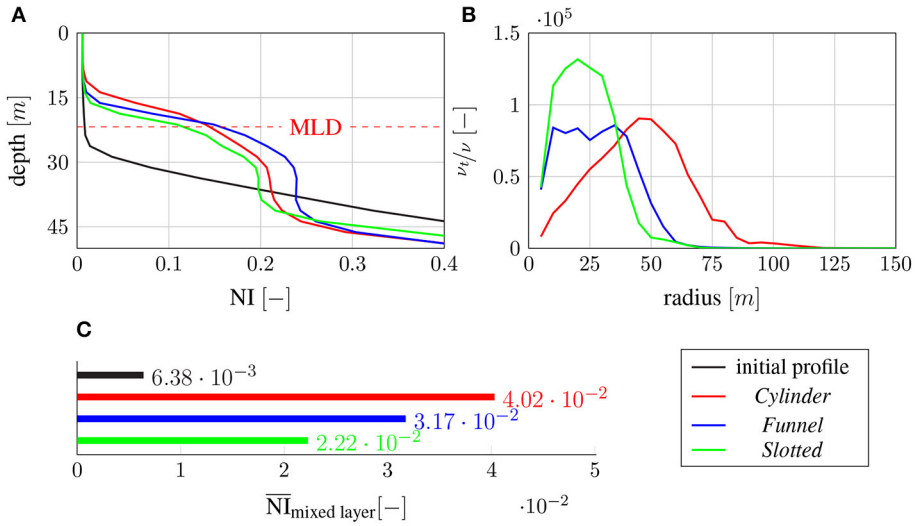

FIGURE 8 | Results of first variant study after 10 000 [*s*] (ST): **(A)** NI depth profiles averaged over a radius of 150–330 [*m*] around the AU system. The upper 50 [*m*] of the water column are shown. **(B)** Radial profiles of eddy viscosity ratio ν_t/ν averaged over the mixed layer. The inner 150 [*m*] of the domain are shown. **(C)** Average mixed layer NI values based on depth profiles in **(A)**.

produces generally lower eddy viscosity ratios, when compared to the *Cylinder* and *Slotted* variants, but maintains its maximum values over a relatively large range of radii.

For the *Cylinder* variant, the widest spread of DOW along the surface is achieved before the sinking occurs. This is reflected in **Figure 8B** in high eddy viscosity ratios further away from the AU system. For the *Slotted* variant, the horizontal momentum decays close to the device due to the high turbulence levels. Here, the sinking of the DOW occurs over a smaller region, close to the device. Finally, the *Funnel* variant produces a more confined jet of DOW with an intermediate spread along the water surface. Here, the peak in the eddy viscosity ratio at the maximum spreading radius along the free surface is less pronounced.

In a second variant study, different depths of the device outlet were tested for the *Cylinder* shape, and the influences on the DOW layer formation and nutrient enrichment in the mixed surface layer were studied. In addition to the standard version, with an outlet depth of 5 [*m*], two versions with outlet depths of 2.5 and 7.5 [*m*] were studied. Again, depth profiles and mixed surface layer average values after 10 000 [*s*] (ST) are analyzed to establish the influence of the device outlet depth on the nutrient-rich layer.

In **Figure 9**, the differences between the studied versions, in terms of nutrient enrichment, are much smaller than the ones observed in the previous variant study. As can be seen from **Figure 9A**, slightly higher NI values in the mixed surface layer are reached by the 2.5 [*m*] outlet depth variant. This is reflected in higher average values in **Figure 9C**, respectively. **Figure 9B** again shows the radial profile of the average mixed layer eddy viscosity ratio ν_t/ν. Here, much larger differences than for the NI depth profiles (**Figure 9A**) are observed. When compared to the other variants, the 2.5 [*m*] outlet depth variant reaches a slightly greater spreading radius of the DOW along the water surface and much larger eddy viscosity ratios during the sinking phase of the upwelled DOW. The 7.5 [*m*] outlet depth variant shows the lowest eddy viscosity ratios.

4. DISCUSSION

The results presented in this paper show that RANS-based flow simulations with the newly developed numerical method provide valuable insight into the AU process. The numerical method has been successfully applied to studies of an AU device, including general flow phenomena and the relative performance of several design variants.

4.1. Basic Study

The expected flow behavior can clearly be observed in the results of the first study. In the device near field, the flow that Williamson et al. (2009) describe as a weak fountain is reproduced. At larger distances from the device, the flow becomes purely horizontal and a distinct layer containing the upwelled DOW is created. This was expected based on the stable stratification of the water column and has been described by Fan et al. (2015), who conducted flow simulations for a similar device in crossflow. The fact that, in all cases presented here, the nutrient-rich layer extended into the mixed surface layer can be seen as an unexpected result of this study. While Kirke (2003) states that DOW, when pumped to the surface, tends to sink below the mixed layer and thus becomes unavailable for primary production, the results of this study suggest that the horizontal spreading of the nutrient-rich layer still leads to a considerable increase in the mixed layer nutrient concentration despite the initial re-sinking of the DOW. In fact, the horizontal spreading of the nutrient-rich layer appears to be the main process by which the mixed layer is fertilized through the proposed AU system.

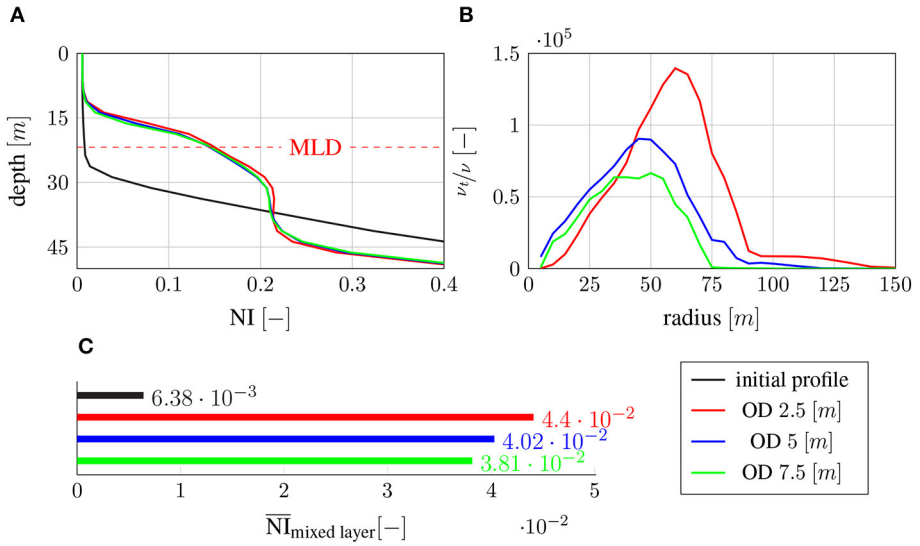

FIGURE 9 | Results of second variant study after 10.000 [s] (ST): **(A)** NI depth profiles averaged over a radius of 150–330 [*m*] around the AU system. The upper 50 [*m*] of the water column are shown. **(B)** Radial profiles of eddy viscosity ratio ν_t/ν averaged over the mixed layer. The inner 150 [*m*] of the domain are shown. **(C)** Average mixed layer NI values based on depth profiles in **(A)**.

Since the horizontal spreading process is associated with very little vertical mixing, it can be assumed that the nutrient-rich layer can spread over large horizontal distances.

Within the region where the nutrient rich layer fully developed during the simulated time (i.e., between a radius of 150 and 330 [*m*] around the AU system) the average mixed layer NO_3-N concentration was increased ba a factor of 6.3, from an initial value of 0.14 to 0.85 [$\mu mol/l$]. These values in the same order of magnitude as those observed in natural eastern boundary upwelling regions (Chavez and Messié, 2009). The results thus seem encouraging enough to motivate further research on the concept of forced upwelling.

4.2. Variant Studies

The presented variant studies show the effect of different device outlet configurations on the local and global flow characteristics and the intended mixed layer nutrient enrichment. Generally, the importance of turbulent mixing for nutrient enrichment in the mixed surface layer is highlighted by the results. All variants show the same general flow features which have already been described for the basic study. It was expected that strong turbulence introduced by the device as high up in the water column as possible would enhance mixing between the upwelled DOW and surface waters, and thus lead to a higher efficiency of the AU system. However, the strongest turbulent mixing was generally observed at some distance to the device, during the sinking phase, which follows the initial upwelling and spreading of the DOW along the water surface. This suggests that shear-based turbulence production at the device outlet is less important than expected. The results of both variant studies show that a greater spread of the DOW jet along the surface leads to more effective mixing during the sinking phase. High turbulence levels near the device outlet, on the other hand, decrease the spread of the DOW jet, and thus the device efficiency, as observed for the *Slotted* variant. While the importance of turbulent mixing is confirmed by these results, they reveal that the design should be optimized for convective spreading of the nutrients along the water surface rather than for shear-based turbulent mixing local to the device outlet.

Throughout the studies presented here, the standard *Cylinder* variant with an outlet depth of 2.5 [*m*] achieved the strongest mixed layer nutrient enrichment with about 7 times the initial nutrient concentration.

It is noteworthy that the idea to maximize the dilution of the upwelled DOW contrasts with the approach of Fan et al. (2015), who aim to minimize dilution and thus maximize the nutrient concentration in the DOW plume. This is explained by the fact that Fan *et al.* aim to increase nutrient concentrations only local to a mariculture project within the DOW plume, whereas here the intention is to fertilize the mixed surface layer over a large area.

4.3. Limitations

While the results presented in this paper show the applicability of the newly developed method for AU simulations as well as its ability to provide insight into function principles and the effectiveness of AU devices, the significance of the results, in absolute terms, is still limited by simplifications made during both model development and experiment design.

It has to be noted that the eddy viscosity ratios observed in **Figures 8B**, **9B** are significantly higher than the values typically obtained in engineering simulations. The high values mainly result from the coexistence of shear- and buoyancy-based turbulence production in the sinking region. While strong turbulence is a typical feature of the Raleigh-Taylor instability

observed in this region, it yet has to be established whether the magnitude of the effect is realistically captured by the turbulence model.

Based on the second variant study, it may be assumed that a variant with an even smaller outlet depth than the ones studied here might perform even more desirable. It has to be noted, however, that the water surface is fixed in the simulations presented here. Thus, any water surface deformation due to the operation of the AU system is neglected. This simplification is expected to have an increasing influence as the outlet depth of the device decreases. It may thus impair the validity of simulations with very shallow outlet depths.

It also has to be noted that, since the same flow rate was taken for all variant studies, these studies do not consider the implications of the different variants on the necessary propeller shaft power to obtain the specified flow rate, which would be the limiting factor for upwelling volume in a realistic setting. This was chosen with the intention to first obtain an understanding of the implications of local design changes on the flow, before optimizing the AU system as a whole.

The results presented in this paper rely on a single set of depth profile data for a very specific ocean region. Since the efficiency in bringing nutrients to the ocean's mixed layer might depend strongly on the stratification in the deployment region, the presented results can not be generalized.

Further, in this paper the amount of permanent nutrient enrichment in the mixed surface layer was estimated by calculating the mean NI value above the initial MLD inside a region where the nutrient-rich layer was fully established within the simulated time (i.e., between a radius of 150 [m] to 330 [m] from the device center). It has to be noted that this method of estimating the amount of permanent mixed surface layer nutrient enrichment is based on simplification. It is assumed that all nutrients which permanently settle above the initial MLD can be further spread throughout the mixed surface layer by natural processes and thus remain available for primary production, while all nutrients which settle below the MLD are lost. While this assumption enables a simple comparison of device variants, it does not adequately reflect the physical processes in the ocean's surface region. In particular, this calculation method does not take into account any changes to the MLD due to AU. These changes cannot be evaluated without considering natural forcing effects which balance the perturbation in the water column caused by the AU device over time.

Finally, the total spatial extend and timescales of the device influence are not captured by the simulations presented here due to the limited availability of computational resources.

4.4. Conclusions

Flow simulations of AU have been carried out with a newly developed numerical method. The method is based on numerous modifications to the open-source framework *OpenFOAM*, which have been described in this paper. The capabilities of the new model have been demonstrated in several studies. The newly developed numerical method was able to reproduce expected flow phenomena and allow a first quantification of the local nutrient enrichment potential in the affected region, as well as comparative studies for device optimization. The spreading of the nutrient-rich layer, which is created by the device, was identified as the main large-scale nutrient enrichment effect. The results suggest that device variants should be optimized for a large convective spread of the DOW jet along the water surface to achieve more permanent mixed layer nutrient enrichment. With a growing interest in ocean-based solutions to the emerging challenges of our time, the role of efficient modeling of these solutions is becoming increasingly important. The presented results should provide the reasoning for continued modeling efforts to improve the understanding of AU.

4.5. Future Work

To be able to obtain more general results from the proposed numerical method, some improvements have to be made:

1. The implemented buoyancy modification for the k-ωSST turbulence marks a simplified turbulence modeling approach for the AU flow problem. A separate study should be carried out on the applicability of different turbulence modeling approaches to stratified, oceanic flow. Different formulations of the buoyancy terms for the k-ωSST turbulence model and other approaches should be taken into account.
2. The simulations presented in this paper were stopped after 10 000 [s] (ST) to avoid boundary effects due to the spatial limitation of the flow domain. A boundary condition that allows free in- and outflow through the boundary would enable longer simulated times with spatially confined flow domains and should therefore be implemented.
3. Throughout this study, a value of 1 was invariably used for the turbulent Prandtl and Schmidt numbers. The use of the gradient diffusion hypothesis with global constant Pr_t and Sn_t values is generally criticized by Combest et al. (2011). Different constant values and other alternatives should be evaluated and compared against data.
4. The numerical model should further be extended with realistic modeling approaches for natural mixing in the mixed surface layer to be able to model the effect of these processes on mixed surface layer nutrient enrichment.

Finally, after careful verification and validation of the improved numerical method, studies on greater spatial and temporal scales should be undertaken to fully determine the influence of the proposed AU device on its environment. In particular, the horizontal extent of the nutrient-rich layer and its spreading rate should be studied, along with the question what fraction of the nutrients in the nutrient-rich layer can eventually be utilized for primary production.

DATA AVAILABILITY STATEMENT

The raw data supporting the conclusions of this article will be made available by the authors, without undue reservation.

AUTHOR CONTRIBUTIONS

JK developed and implemented the numerical method, performed the calculations, and analyzed the results under the scientific and technical supervision of UR and KG. JK wrote the manuscript with input from all authors.

FUNDING

This study was funded by an Advanced Grant of the European Research Council (ERC) in the framework of the Ocean Artificial Upwelling project (Ocean artUp, No. 695094). Additional support was obtained by the Test-ArtUp project, which is funded by the German Federal Ministry of Education and Research (Bundesministerium für Bildung und Forschung, BMBF) as part of the *CDRmare* research mission of the German Marine Research Alliance (Deutsche Allianz Meeresforschung, DAM) under Grant Agreement No. 03F0897B. The publication was financially supported by *Land Schleswig-Holstein* within the funding programme *Open Access Publikationsfonds*.

REFERENCES

Bauman, S., Costa, M., Fong, M., House, B., Perez, E., Tan, M., et al. (2014). Augmenting the biological pump: the shortcomings of geoengineered upwelling. *Oceanography* 27, 17–23. doi: 10.5670/oceanog.2014.79

Chavez, F. P., and Messié, M. (2009). A comparison of eastern boundary upwelling ecosystems. *Prog. Oceanogr.* 83, 80–96. doi: 10.1016/j.pocean.2009.07.032

Combest, D. P., Ramachandran, P. A., and Dudukovic, M. P. (2011). On the gradient diffusion hypothesis and passive scalar transport in turbulent flows. *Ind. Eng. Chem. Res.* 50, 8817–8823. doi: 10.1021/ie200055s

Devolder, B., Rauwoens, P., and Troch, P. (2017). Application of a buoyancy-modified k-ω SST turbulence model to simulate wave run-up around a monopile subjected to regular waves using OpenFOAM ®. *Coastal Eng.* 125, 81–94. doi: 10.1016/j.coastaleng.2017.04.004

Fan, W., Chen, J., Pan, Y., Huang, H., Chen, C.-T. A., and Chen, Y. (2013). Experimental study on the performance of an air-lift pump for artificial upwelling. *Ocean Eng.* 59, 47–57. doi: 10.1016/j.oceaneng.2012.11.014

Fan, W., Pan, Y., Liu, C. C., Wiltshire, J. C., Chen-Tung, A. C., and Chen, Y. (2015). Hydrodynamic design of deep ocean water discharge for the creation of a nutrient-rich plume in the south china sea. *Ocean Eng.* 108, 356–368. doi: 10.1016/j.oceaneng.2015.08.006

FAO (2018). *The State of World Fisheries and Aquaculture 2018 - Meeting the Sustainable Development Goals*. Rome. Licence: CC BY-NC-SA 3.0 IGO.

Ferziger, J. H., Perić, M., and Street, R. L. (2020). *Computational Methods for Fluid Dynamics*. Cham: Springer International Publishing.

GESAMP (2019). "High level review of a wide range of proposed marine geoengineering techniques," in *Rep. Stud. GESAMP No. 98, (IMO/FAO/UNESCO-IOC/UNIDO/WMO/IAEA/UN/UN Environment/ UNDP/ISA Joint Group of Experts on the Scientific Aspects of Marine Environmental Protection),* eds P. W. Boyd and C. M. G. Vivian (London: International Maritime Organization), 144p.

Griffies, S. M., and Adcroft, A. J. (2008). Formulating the equations of ocean models. *Ocean Model. Eddying Regime* 177, 281–317. doi: 10.1029/177GM18

IOC, SCOR, and IAPSO (2010). *The International Thermodynamic Equation of Seawater-2010: Calculation and Use of Thermodynamic Properties*. Paris: Intergovernmental Oceanographic Commission, Manuals and Guides.

Issa, R. (1986). Solution of the implicitly discretised fluid flow equations by operator-splitting. *J. Comput. Phys.* 62, 40–65. doi: 10.1016/0021-9991(86)90099-9

Kirke, B. (2003). Enhancing fish stocks with wave-powered artificial upwelling. *Ocean Coastal Manag.* 46, 901–915. doi: 10.1016/S0964-5691(03)00067-X

Komori, S., Kurose, R., Takagaki, N., Ohtsubo, S., Iwano, K., Handa, K., et al. (2011). *Gas Transfer at Water Surfaces, Chapter Sensible and Latent Heat Transfer Across the Air-Water Interface in Wind-Driven Turbulence*. Kyoto: Kyoto University Press.

Krahmann, G. (2016). Property changes of deep and bottom waters in the western tropical atlantic. *Deep Sea Res. I Oceanogr. Res. Pap.* 124, 103–125. doi: 10.1016/j.dsr.2017.04.007

Launder, B., and Spalding, D. (1974). The numerical computation of turbulent flows. *Comput. Methods Appl. Mech. Eng.* 3, 269–289. doi: 10.1016/0045-7825(74)90029-2

Lawrence, M. G., Schäfer, S., Muri, H., Scott, V., Oschlies, A., Vaughan, N. E., et al. (2018). Evaluating climate geoengineering proposals in the context of the paris agreement temperature goals. *Nat. Commun.* 9:3734. doi: 10.1038/s41467-018-05938-3

Liang, N.-K., and Peng, H.-K. (2005). A study of air-lift artificial upwelling. *Ocean Eng.* 32, 731–745. doi: 10.1016/j.oceaneng.2004.10.011

Liu, C. C., and Jin, Q. (1995). Artificial upwelling in regular and random waves. *Ocean Eng.* 22, 337–350. doi: 10.1016/0029-8018(94)00019-4

Lovelock, J. E., and Rapley, C. G. (2007). Ocean pipes could help the earth to cure itself. *Nature* 449, 403–403. doi: 10.1038/449403a

Maruyama, S., Tsubaki, K., Taira, K., and Sakai, S. (2004). Artificial upwelling of deep seawater using the perpetual salt fountain for cultivation of ocean desert. *J. Oceanogr.* 60, 563–568. doi: 10.1023/B:JOCE.0000038349.56399.09

McDougall, T. J. (2003). Potential enthalpy: a conservative oceanic variable for evaluating heat content and heat fluxes. *J. Phys. Oceanogr.* 33, 945–963. doi: 10.1175/1520-0485(2003)033andlt;0945:PEACOVandgt;2.0.CO;2

McDougall, T. J., Jackett, D. R., Wright, D. G., and Feistel, R. (2003). Accurate and computationally efficient algorithms for potential temperature and density of seawater. *J. Atmos. Oceanic Technol.* 20, 730–741. doi: 10.1175/1520-0426(2003)20andlt;730:AACEAFandgt;2.0.CO;2

Meng, Q., Wang, C., Chen, Y., and Chen, J. (2013). A simplified CFD model for air-lift artificial upwelling. *Ocean Eng.* 72, 267–276. doi: 10.1016/j.oceaneng.2013.07.006

Menter, F. R. (1994). Two-equation eddy-viscosity turbulence models for engineering applications. *AIAA J.* 32, 1598–1605. doi: 10.2514/3.12149

Nayar, K. G., Sharqawy, M. H., Banchik, L. D., and Lienhard, V., J. H. (2016). Thermophysical properties of seawater: a review and new correlations that include pressure dependence. *Desalination* 387, 1–24. doi: 10.1016/j.desal.2016.02.024

Oschlies, A., Pahlow, M., Yool, A., and Matear, R. J. (2010). Climate engineering by artificial ocean upwelling: channelling the sorcerer's apprentice. *Geophys. Res. Lett.* 37:L04701. doi: 10.1029/2009GL041961

Pan, Y., Fan, W., Huang, T.-H., Wang, S.-L., and Chen, C.-T. A. (2015). Evaluation of the sinks and sources of atmospheric CO_2 by artificial upwelling. *Sci. Total Environ.* 511, 692–702. doi: 10.1016/j.scitotenv.2014.11.060

Pan, Y., Li, Y., Fan, W., Zhang, D., Qiang, Y., Jiang, Z.-P., et al. (2019). A sea trial of air-lift concept artificial upwelling in the east china sea. *J. Atmos. Oceanic Technol.* 36, 2191–2204. doi: 10.1175/JTECH-D-18-0238.1

Patankar, S., and Spalding, D. (1972). A calculation procedure for heat, mass and momentum transfer in three-dimensional parabolic flows. *Int. J. Heat Mass. Transf.* 15, 1787–1806. doi: 10.1016/0017-9310(72)90054-3

Roels, O. A., Laurence, S., Farmer, M. W., and Hemelryck, L. V. (1977). "Organic production potential of artificial upwelling marine culture," in *Microbial Energy Conversion* (Pergamon: Elsevier), 69–81.

Sharqawy, M. H., Lienhard, V., J. H., and Zubair, S. M. (2010). Thermophysical properties of seawater: a review of existing correlations and data. *Desalination Water Treat.* 16, 354–380. doi: 10.5004/dwt.2010.1079

Soloviev, A. V. (2016). "Ocean upwelling system utilizing energy of surface waves," in *Proceedings of the 2016 Techno-Ocean Conefrence* (Kobe: IEEE), 221–224.

Stankov, P., Denev, J., Barták, M. M., Drkal, F., Lain, M. M., Schwarzer, J., et al. (2001). "Experimental and numerical investigation of temperature distribution in room with displacement ventilation," in *Proceedings of the 7th World Congress Clima 2000* (Naples).

Stommel, H., Arons, A. B., and Blanchard, D. (1956). An oceanographical curiosity: the perpetual salt fountain.

Deep Sea Res. 3, 152–153. doi: 10.1016/0146-6313(56)90095-8

Thorpe, S. A. (2007). *An Introduction to Ocean Turbulence*. Cambridge: Cambridge University Press.

Tsubaki, K., Maruyama, S., Komiya, A., and Mitsugashira, H. (2007). Continuous measurement of an artificial upwelling of deep sea water induced by the perpetual salt fountain. *Deep Sea Res. I Oceanogr. Res. Pap*. 54, 75–84. doi: 10.1016/j.dsr.2006.10.002

Van Maele, K., and Merci, B. (2006). Application of two buoyancy-modified –turbulence models to different types of buoyant plumes. *Fire Safety J*. 41, 122–138. doi: 10.1016/j.firesaf.2005.11.003

Wilcox, D. C. (1988). Reassessment of the scale-determining equation for advanced turbulence models. *AIAA J*. 26, 1299–1310. doi: 10.2514/3.10041

Williamson, N., Komiya, A., Maruyama, S., Behnia, M., and Armfield, S. W. (2009). Nutrient transport from an artificial upwelling of deep sea water. *J. Oceanogr*. 65, 349–359. doi: 10.1007/s10872-009-0032-x

Williamson, P., Wallace, D. W., Law, C. S., Boyd, P. W., Collos, Y., Croot, P., et al. (2012). Ocean fertilization for geoengineering: a review of effectiveness, environmental impacts and emerging governance. *Process Safety Environ. Protect*. 90, 475–488. doi: 10.1016/j.psep.2012.10.007

Worthy, J., Sanderson, V., and Rubini, P. (2001). A comparison of modified k-ϵ turbulence models for and buoyant plumes. *Numer. Heat Transfer B* 39, 151–165. doi: 10.1080/10407790150503486

Zhang, X., Maruyama, S., Sakai, S., Tsubaki, K., and Behnia, M. (2004). Flow prediction in upwelling deep seawater—the perpetual salt fountain. *Deep Sea Res. I Oceanogr. Res. Pap*. 51, 1145–1157. doi: 10.1016/j.dsr.2004.03.010

Conflict of Interest: The authors declare that the research was conducted in the absence of any commercial or financial relationships that could be construed as a potential conflict of interest.

Publisher's Note: All claims expressed in this article are solely those of the authors and do not necessarily represent those of their affiliated organizations, or those of the publisher, the editors and the reviewers. Any product that may be evaluated in this article, or claim that may be made by its manufacturer, is not guaranteed or endorsed by the publisher.

frontiers in Marine Science

ORIGINAL RESEARCH
published: 12 January 2022
doi: 10.3389/fmars.2021.743105

Artificial Upwelling in Singular and Recurring Mode: Consequences for Net Community Production and Metabolic Balance

Joaquin Ortiz[1], Javier Arístegui[2], Jan Taucher[1] and Ulf Riebesell[1]*

[1] *Marine Biogeochemistry, Biological Oceanography, GEOMAR Helmholtz Center for Ocean Research, Kiel, Germany,*
[2] *Oceanografía Biológica, Instituto de Oceanografía y Cambio Global (IOCAG), Universidad de Las Palmas de Gran Canaria, Las Palmas de Gran Canaria, Spain*

OPEN ACCESS

Edited by:
Jun Sun,
China University of Geosciences Wuhan, China

Reviewed by:
Alfonso Corzo,
University of Cadiz, Spain
Camila Fernandez,
UMR7621 Laboratoire d'Océanographie Microbienne (LOMIC), France

***Correspondence:**
Joaquin Ortiz
jortiz@geomar.de

Specialty section:
This article was submitted to Marine Biogeochemistry, a section of the journal Frontiers in Marine Science

Received: *17 July 2021*
Accepted: *07 December 2021*
Published: *12 January 2022*

Citation:
Ortiz J, Arístegui J, Taucher J and Riebesell U (2022) Artificial Upwelling in Singular and Recurring Mode: Consequences for Net Community Production and Metabolic Balance. Front. Mar. Sci. 8:743105. doi: 10.3389/fmars.2021.743105

Artificial upwelling of nutrient-rich waters and the corresponding boost in primary productivity harbor the potential to enhance marine fishery yields and strengthen the biological pump for sequestration of atmospheric CO_2. There is increasing urgency to understand this technology as a "ocean-based solution" for counteracting two major challenges of the 21st century—climate change and overfishing. Yet, little is known about the actual efficacy and/or possible side effects of artificial upwelling. We conducted a large-scale off-shore mesocosm study (~44 m^3) in the oligotrophic waters of the Canary Islands to identify the community-level effects of artificial upwelling on a natural oligotrophic plankton community. Four upwelling intensities were simulated (approx. 1.5/3/5.7/10 μmol L^{-1} of nitrate plus phosphate and silicate) *via* two different upwelling modes (a singular deep-water pulse vs. recurring supply every 4 days) for 37 days. Here we present results on the response of net community production (NCP), metabolic balance and phytoplankton community composition (<250 μm). Higher upwelling intensities yielded higher cumulative NCP. Following upwelling onset, the phytoplankton community became dominated by diatoms in all treatments, but other taxa such as Coccolithophores increased later in the experiment. The magnitude of effects on the metabolic balance scaled with the amount of added deep water, leading to (i) a balanced to net-heterotrophic system in the singular and (ii) a net-autotrophic system in the recurring upwelling treatments. Accordingly, the mode in which nutrients are supplied to an oligotrophic system plays a crucial role in the ecosystem response, with recurring upwelling leading to higher long-term positive NCP than singular upwelling. These results highlight the importance of empirically measured local responses to upwelling such as community structure and metabolism, with major implications for the potential employment of artificial upwelling as an ocean-based solution to generate (primary) production.

Keywords: artificial upwelling, metabolic balance, primary production, net community production, mesocosm, CHEMTAX

INTRODUCTION

Food security for a growing human population and climate change are two main global challenges of our time. The world population is projected to keep growing at least until the end of this century and the ensuing demand for food needs to be covered (United Nations, 2019). While food production on land shows some potential for sustainable improvement (Godfray et al., 2010), the oceans are already being exploited at, or even past, the limit of sustainability (Garcia and Rosenberg, 2010). Meanwhile, global agreements to mitigate the effects of anthropogenic climate change have been reached (UNFCC, 2015; Schellnhuber et al., 2016). But palpable actions still need to follow and it is clear that a mere reduction of emissions will not suffice (Lawrence et al., 2018). Yet most of the urgently needed technologies to actively remove CO_2 from the atmosphere remain largely unexplored.

One approach that has been suggested to tackle both of these challenges at the same time is artificial upwelling. It has been proposed as a method to sustainably increase fisheries yield in unproductive areas of the ocean and potentially enhance carbon sequestration (Kirke, 2003; Lovelock and Rapley, 2007; GESAMP, 2019). However, the most essential prerequisite to achieve these goals is that the nutrients introduced *via* artificial upwelling fuel the growth of primary producers that subsequently increase productivity on higher trophic levels up to harvestable fish. Experimental data focusing on the effects of artificial upwelling are scarce. Several authors have found that artificial upwelling in oligotrophic waters can lead to (i) increased primary productivity (PP) and phytoplankton biomass, (ii) higher abundance of diatoms, (iii) a community succession from picophytoplankton to larger nano- and microphytoplankton as well as a (iv) shift from a balanced or net heterotrophic ecosystem to a net autotrophic one (McAndrew et al., 2007; Giraud et al., 2016; Casareto et al., 2017). But most of these data stem from small scale bottle fertilization experiments, making it difficult to extrapolate these finding to the community and ecosystem level. Maruyama et al. (2011) induced artificial upwelling in the open water through a perpetual salt fountain but only provided data on Chl*a*, which increased significantly. The only open water study that included effects on the phytoplankton community was conducted by Masuda et al. (2010), who pumped up water from 205 m depth, discharged it at 20 m mixed with water from 5 m and tracked changes in nutrient concentrations, phytoplankton composition and growth for 63.9 h. Other previous mesocosm studies included the addition of inorganic nutrients or nutrient rich deep water, but also further manipulations like artificially elevated CO2 concentration (Riebesell et al., 2013b; Taucher et al., 2017). This made it difficult to study exclusively the effects of the deep-water addition on the community.

Here we present results from an *in situ* mesocosm experiment in which we examined how a natural plankton community responds to artificial upwelling applied on a much larger, unprecedented scale under close to natural conditions. The main objective of the entire experiment was to assess the effectiveness and potential side effects of artificial upwelling as a technology to enhance marine food production and/or CO_2 sequestration, so that better judgments can be made regarding its applicability on a larger spatial and temporal scale. This was achieved comparing different temporal frequencies and intensities of artificial upwelling through a multitude of parameters. The specific objective of this study was to evaluate its effects on net community production (NCP) and metabolic state of an oligotrophic community that is not adapted to more than occasional nutrient inputs. Based on this, we explore whether the response of the phytoplankton community could lead to the establishment of a solid foundation of primary producers needed to fuel a productive food web.

MATERIALS AND METHODS

Experimental Setup

The Canary Islands are a suitable place to test artificial upwelling: the subtropical oligotrophic waters display an overall year-round rather low PP (∼100–400 mg C m^{-2} d^{-1}, Arístegui et al., 2001). A bay located on the east coast of the island of Gran Canaria was chosen as the deployment site for the nine KOSMOS (Kiel Offshore Mesocosms for Ocean Simulations) units, laying protected from the most common swell and wind patterns (Gando Bay, 27.9279°N, 15.3654°W). Transparent plastic roofs served as protection from precipitation and bird droppings. Technical details of the infrastructure are specified in Riebesell et al. (2013a). After a 7-day period of open water exchange the mesocosms were closed by lifting the top end out of the water and attaching the sediment traps to the bottom. A net (3 mm mesh size) was pulled from bottom to top right after closure to exclude unevenly distributed large organisms from the enclosures. Total length of the mesocosm bags was 13 m plus an additional 2.7 m for the sediment trap, hereby enclosing a mean water volume of 43.78 ± 1.35 m^3 (**Table 1**).

To obtain suitable deep water (DW) an electric pump was deployed from a ship (RRS James Cook (United Kingdom) and J Socas (ES); between 28°00′N, 15°18′E and 27°57′N, 15°10′E) to 330 m depth. The water was pumped into a custom built DW collector bag (∼100 m^3 capacity) and towed to the mesocosm site (for technical specifications see Taucher et al., 2017). Due to technical constraints the intended pumping depth of ∼600 m could not be reached. Therefore, collected DW was spiked with additional nutrients (NO_3, PO_4 and Si as sodium nitrate, disodium phosphate and sodium silicate) to adjust the stoichiometry to the intended pumping depth. Nutrient concentrations were measured and adjusted routinely before each addition to the mesocosms. During the 39 days of the experiment, mesocosms were cleaned regularly on the inside and outside (for details on all activities see **Supplementary Figure 1**). Depth-integrated water samplers (IWS, Hydro-Bios, Kiel) were used to sample the entire water column (0–13 m) of each mesocosm every other day. The water column outside of the mesocosms at the mooring site was also sampled ("Atlantic") as an additional comparison for inorganic nutrients and photosynthetic pigments. In this paper we focus on PP measured through oxygen incubations. Inorganic nutrient concentrations are also provided and photosynthetic pigments were analyzed to

TABLE 1 | Treatment overview with mesocosm volumes, total nutrients added and mean CR/GP/NCP rates with standard deviations for the duration of the study.

Mesocosm	Treatment	Total inorg. N added [μmol L^{-1}]*	Mean CR** [μmol O_2 L^{-1} d^{-1}]	Mean GP** [μmol O_2 L^{-1} d^{-1}]	Mean NCP** [μmol O_2 L^{-1} d^{-1}]
3	Low singular	1.61	3.24 ± 0.44	3.56 ± 1.23	0.31 ± 0.98
2	Low recurring	1.54	3.48 ± 0.82	3.27 ± 1.42	−0.21 ± 1.67
7	Medium singular	3.01	3.90 ± 1.35	5.57 ± 5.04	1.67 ± 4.82
4	Medium recurring	3.06	4.38 ± 0.84	6.21 ± 1.89	1.84 ± 1.6
6	High recurring	6.15	5.47 ± 1.54	9.57 ± 4.14	4.10 ± 3.5
1	Extreme singular	9.82	8.92 ± 4.05	12.31 ± 16.01	3.39 ± 15.33
8	Extreme recurring	12.26	9.50 ± 3.24	19.47 ± 7.21	9.97 ± 5.8
5	Control	0.00	2.58 ± 0.49	3.09 ± 0.58	0.51 ± 0.63

**For recurring treatments, the total amount of N added represents the sum of all DW additions. **The pre-treatment phase (d1–3) was excluded from the calculation of mean rates to better reflect treatment effects.*

contribute additional information on the relative abundance of specific phytoplankton taxa.

Treatment Details

The experimental treatment consisted of one control mesocosm and two groups of four mesocosms subjected to either a singular (M1, M3, M7, M9; "singular") DW addition on day four (d4) or a total of eight DW additions every 4 days (M2, M4, M6, M8; "recurring") from d4 onward. An exception was d21, when DW addition was delayed by 1 day due to bad weather conditions. Within each group a gradient in upwelling intensity was established from "low" to "extreme" treatments, referring to the total amount of water volume replaced by DW (see **Table 1**). In accordance with upwelling intensity, respective singular and recurring upwelling treatments were intended to receive an equal total amount of inorganic nutrients e.g., low treatments should ideally receive the same total amount either at once (low singular) or throughout all eight additions (low recurring). The technical concept of the upwelling modes applied in this experiment roots in the design of potentially applicable pump types: stationary (moored) pumps would provide singular upwelling, as the fertilized water mass moves away with currents and winds; while free drifting pumps would provide continuous upwelling as they would move along with the water mass.

Inorganic Nutrients

Between 250–500 mL of water from the IWS, as well as from the DW bag, were subsampled into polypropylene bottles for analysis of inorganic nutrient concentrations [NO_3^-, NO_2^-, NH_4^+, PO_4^{3-}, $Si(OH)_4$]. In the laboratories all nutrient samples were measured spectrophotometrically on a five channel Quaatro Autoanalyzer (Seal Analytical, Mequon, WI, United States) after being filtered through 0.45 μm pore size glass fiber filters (Sterivex, Merck, Darmstadt, Germany).

Thanks to the intense monitoring of inorganic nutrients as well as dissolved and particulate organic N and P of both the water column and DW bag, it was possible to correct the inorganic nutrient concentrations in the water column to account for any N shifting to the dissolved and particulate organic nitrogen pool and inorganic nutrients lost in the removal of water before DW pumping. i.e., it was possible to factor in inorganic N previously added through the spiking of the DW that might have shifted to the organic N pool in the time elapsed until the actual addition. This allowed for accurate assessment of how much inorganic N was actually added. Since suspended particulate and dissolved organic nitrogen are not relevant nutrient sources for phytoplankton, henceforth "μmol of nutrients" refers to total added inorganic nitrogen.

Oxygen Production Rates

Oxygen production as well as respiration rates were measured through 24-h incubations and the Winkler method, following recommendations from Carritt and Carpenter (1966), Bryan et al. (1976) and Grasshoff et al. (1999). Five liters of water were sampled from each treatment every second day and transported back to land in a cool box. Using a silicone tube with an attached 250 μm mesh for pre-filtering of the samples, Winkler-suitable, precisely calibrated borosilicate glass bottles of 125 mL nominal volume (Afora) were first rinsed with water from the corresponding treatment and then filled past the point of overflowing for a few seconds. The lids were carefully placed and each bottle was checked to be bubble free or otherwise be subsampled again. Due to a logistical issue in the supply of the glass bottles, only eight out of nine mesocosms were sampled.

For each treatment/mesocosm a total of 12 measurements were made consisting of fourfold measurements for initial oxygen values fixed with the reagents immediately after subsampling ("Initial"), fourfold 24-h dark incubations ("Dark") and fourfold 24-h light incubations ("Light"), respectively. All samples were stored together in an outdoor pool with constant flow of seawater to keep the incubations at seawater temperature (∼20.7–21.5°C) and exposed to ambient day and night cycles. Initials were stored in the same pool too and covered with opaque material to block sunlight. Dark samples were incubated in light proof bags inside opaque boxes. Light samples were randomly distributed inside clear Plexiglas boxes and covered with one layer of blue foil to better mimic the light spectrum of the water column inside the mesocosms (172 Lagoon Blue foil, Lee filters, Burbank, CA, United States). The mean daily light irradiance received by the light incubations was approx. 22.4 ± 8.8 μmol photons m^{-2} s^{-1} during the duration of the experiment as measured by data loggers inside the incubators (HOBO UA-002-64, Australia/New Zealand).

Dark samples were incubated for at least 20 h and light samples for 24 h before being fixed and titrated during ∼3 min by means of an automated, precise titration system with colorimetric end-point detection along with the initials (Williams and Jenkinson, 1982). The precision achieved in replicates was %CV < 0.07. The mean of each fourfold measurement was calculated and used for determining the rates for community respiration (CR), net community production (NCP) and gross production (GP) as follows:

$$\mathrm{CR}\left[\mu\mathrm{mol\,L^{-1}h^{-1}}\right] = \frac{\mathrm{Conc_I} - \mathrm{Conc_D}}{\mathrm{h_D}} \quad (1)$$

$$\mathrm{NCP}\left[\mu\mathrm{mol\,L^{-1}h^{-1}}\right] = \frac{\mathrm{Conc_L} - \mathrm{Conc_I}}{\mathrm{h_L}} \quad (2)$$

$$\mathrm{GP}\left[\mu\mathrm{mol\,L^{-1}h^{-1}}\right] = \mathrm{CR} + \mathrm{NCP} \quad (3)$$

$\mathrm{Conc_I}$ / $\mathrm{Conc_D}$ / $\mathrm{Conc_L}$ = mean oxygen concentration of the Initial / Dark / Light samples;

$\mathrm{h_D}$ / $\mathrm{h_L}$ = hours of incubation of Dark / Light samples; CR, NCP and GP in [μmol $\mathrm{L^{-1}\,h^{-1}}$].

Hourly rates were then multiplied by 24 to yield daily rates. Assessment of accumulated NCP ($\mathrm{NCP_{cum}}$) over all 37 days required estimates of oxygen production rates for non-sampling days. The mean NCP of the day before and after each non-sampling day was calculated according to Equation 4 to account for this (e.g., estimated NCP for d22 was the mean NCP from d21 and d23).

$$\mathrm{NCP_{nsd}} = \frac{\mathrm{NCP_{nsd-1}} + \mathrm{NCP_{nsd+1}}}{2} \quad (4)$$

where $\mathrm{NCP_{nsd}}$ = NCP of the non-sampling day and $\mathrm{NCP_{nsd-1/+1}}$ = NCP of the sampling day before / after the non-sampling day. With non-sampling days accounted for, $\mathrm{NCP_{cum}}$ for a given day could be calculated by summing up the NCP of all previous days (using d3 as an example):

$$\mathrm{NCP_{cum\ d3}} = \mathrm{NCP_{d3}} + \mathrm{NCP_{d2}} + \mathrm{NCP_{d1}} \quad (5)$$

NCP of all 37 days was then consecutively summed up to estimate $\mathrm{NCP_{cum}}$ throughout the entire experimental period. This served to better visualize the contrasting developments of the parameter among the treatments (as done similarly by e.g., Engel et al., 2013).

Phytoplankton Community Composition

Water samples from the IWS were gently filtered on 0.7 μm pore size glass fiber filters (200 mbar, Whatman GF/F, Maidstone, United Kingdom) on custom-built filtration manifolds. The filtered volume varied between 0.3 and 1 liter since it had to be adapted to the abundance of plankton in the mesocosms every sampling day to avoid clogging and long filtration times that could affect sample quality. Precautions were also taken to minimize the exposure of the samples to light (e.g., covering filtration manifolds). Afterward filters were shock frozen in liquid nitrogen before being stored in a −80°C freezer until the end of the experiment.

Before analysis samples were mixed with 0.5 mm glass beads and 1.3 ml of 100% HPLC grade acetone (Baker 8142, Avantor, Radnor, PA, United States) and extracted in a homogenizer (Precellys, Montigny-le-Bretonneux, France). They were then centrifuged (10 min, 4°C, 10,000 rpm), the supernatant removed with a syringe and filtered through a PTFE filter (0.2 μm pore size). All relevant photosynthetic pigments were analyzed through reverse-phase high-performance liquid chromatography (HPLC, according to Van Heukelem and Thomas, 2001) on a Thermo Scientific HPLC Ultimate 3000.

Determination of the relative abundance of different phytoplankton classes was conducted with the CHEMTAX software developed by Mackey et al. (1996) and applying pigment ratios typically found in the waters off Gran Canaria (Taucher et al., 2018). By calculating the ratios between class-specific pigments and total Chl*a* [ng/l] the software determines the individual contribution of *Prasinophyceae*, *Chlorophyceae*, *Dinophyceae*, *Cryptophyceae*, *Chrysophyceae*, *Prymnesiophyceae*, *Prochlorophyceae*, *Cyanophyceae* and *Diatomea* to total Chl*a*. Additional identification of diatom species and abundances was carried out through microscopy counts and size measurements, followed by biovolume calculations and conversion to biomass using the conversion factor from Menden-Deuer and Lessard (2000).

Data Analysis

Simple linear regressions were performed on the mean NCP/GP/CR datasets to assess the relationship between increasing UI and increasing NCP/GP/CR, and to check for differences between both upwelling modes. The control treatment was used twice in the linear regression model analysis of singular and recurring treatments respectively. Statistical comparison of both upwelling modes required the control to be removed, since using the same control for both groups would create a paired data-point in otherwise unpaired data. Data analysis was performed with R (Version 4.0.3, packages stats, ggplot2; The R Foundation). Assumptions of normality and homoscedasticity were tested using q-q and residual vs. fitted variable plots.

RESULTS

Inorganic Nutrients

Nutrient concentration peaks were visible in all treatments in proportion to simulated upwelling intensity after the first DW addition (**Figure 1**). In singular treatments, all nutrients were almost entirely consumed within 5 days (by d9), while recurring treatments exhausted most nutrients within 2 days after each addition. The only exceptions were silicate, which was no longer fully taken up after d27 in extreme recurring, and ammonia, which fluctuated around relatively constant levels in most treatments throughout the experiment.

Oxygen Production and Metabolic Balance

Following the first DW addition, NCP rates increased in all treatments according to upwelling intensity, though duration

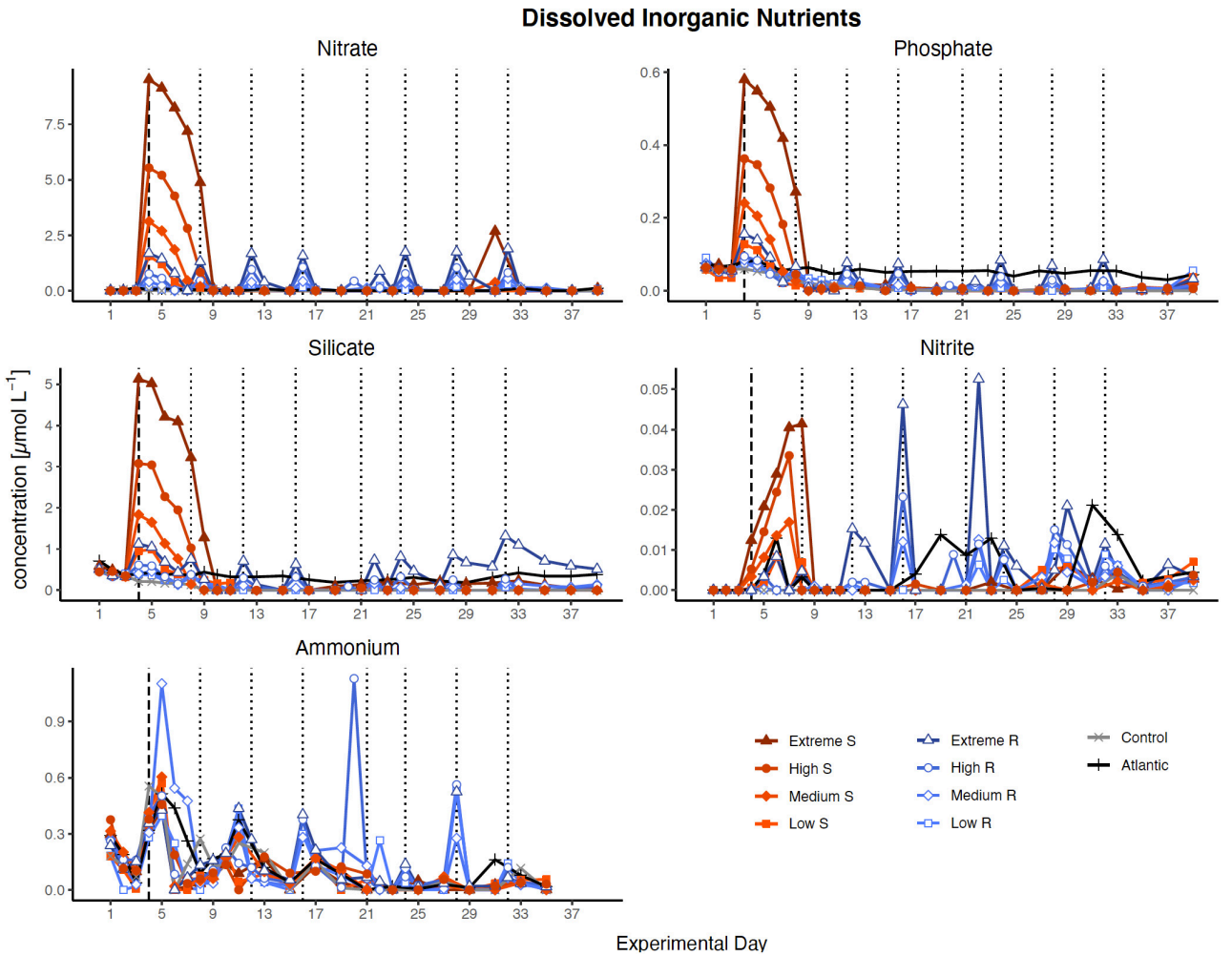

FIGURE 1 | Inorganic nutrient concentration over the course of the study. Dotted lines represent DW additions, dashed line marks the single DW addition to singular treatments. S, singular; R, recurring treatment. Atlantic refers to samples taken from the water surrounding the mesocosm field.

of the increase and peak rates varied substantially (**Figure 2A**). Singular treatment NCP increased up to 61.52 O_2 L^{-1} d^{-1} (extreme) before dropping to levels close to the control. Following nutrient depletion, NCP in all singular treatments dropped to control values close to 0, and the extreme singular even maintained negative (i.e., net heterotrophic) NCP rates until the end of the experiment. Recurring treatments on the other hand retained entirely positive (i.e., net autotrophic) NCP rates after treatment initiation with the exception of the low recurring. Accumulated NCP rates highlighted this particular difference between both treatment groups (**Figure 2D**). Recurring treatments exhibited a steady increase (except low) while the singular treatments stagnated or even began dropping, to the point that extreme recurring surpassed the NCP_{cum} of extreme singular on d24. Ultimately, it outperformed extreme singular by a factor of 2.7. Gross production was similarly enhanced, with extreme recurring outperforming extreme singular by a factor of 1.6 (**Figure 2B**). The temporal development of the ratio of GP and respiration was also akin to that of NCP (**Figure 2C**). Extreme recurring in particular displayed an increase in all productivity measures toward the end of the experiment, even reaching the highest overall GP at 31.94 µmol O_2 L^{-1} d^{-1} on d35. Mean NCP rates calculated for the duration of the experiment showed that recurring upwelling led to higher mean NCP than singular, with the extreme recurring reaching a three times higher mean NCP despite receiving only 1.2 times as many nutrients as the extreme singular (**Figure 3** and **Table 1**). Mean NCP, GP and CR all strongly correlated with upwelling intensity under both upwelling modes (**Table 2**). However, recurring upwelling led to significantly higher mean NCP and GP than singular. Chl*a* normalized NCP rates were not influenced much by upwelling intensity, but rather by upwelling mode (**Supplementary Figure 2**): following an initial peak (2.19–8.68 µmol O_2 (µg Chl*a*) d^{-1}) in all treatments after upwelling onset, singular treatments dropped to rates between −3 and 1.1 µmol O_2 (µg Chl*a*) d^{-1} under low and medium intensity, while the extreme upwelling intensity oscillated as far as −9 µmol O_2 (µg Chl*a*) d^{-1} on d31. Contrary to this, recurring treatments

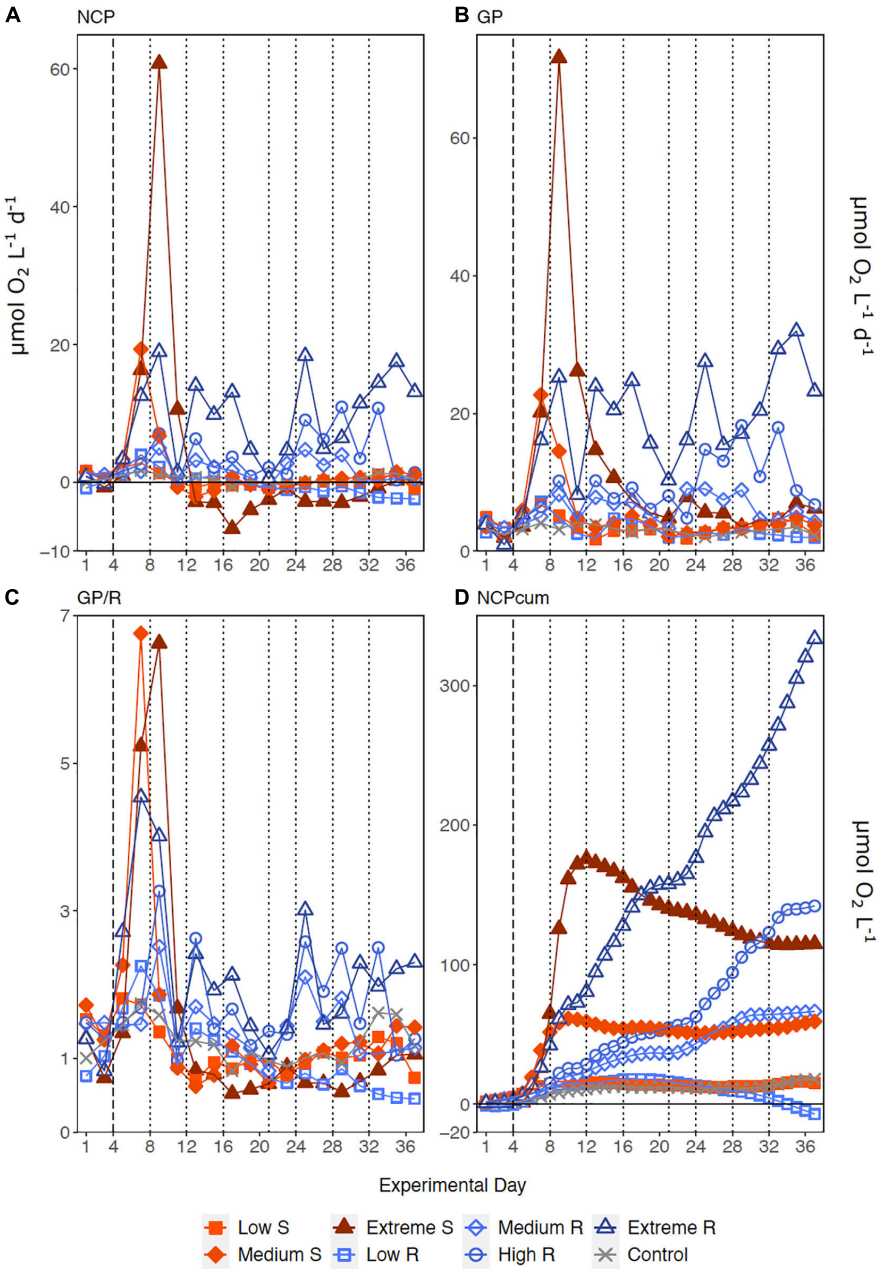

FIGURE 2 | Temporal development of **(A)** Net Community Production, **(B)** Gross Production, **(C)** the ratio of GP to respiration (GP/R) and **(D)** accumulated NCP. Dotted lines represent DW additions, dashed line marks the single DW addition to singular treatments. S, singular; R, recurring treatment.

of medium, high and extreme intensity mostly retained rates between 0 and 4.7 µmol O_2 (µg Chl*a*) d^{-1}. With the low recurring treatment again representing the exception, dropping down as far as −11 µmol O_2 (µg Chl*a*) d^{-1} toward the end of the experiment.

Phytoplankton Community Composition

Low treatments developed similarly to the control throughout the experiment, showing constant shifts in relative class abundances though diatoms mostly represented the largest proportion (**Figure 4**). But strong differences were present regarding the timing and magnitude of diatom prevalence: after the DW addition, all singular treatments developed strong initial Chl*a* peaks dominated by diatoms and, to a lesser extent by prymnesiophytes. In general, diatoms remained the class with the highest contribution to total Chl*a* in singular treatments, also following the overall decrease in Chl*a* and productivity during the course of the experiment. Recurring treatments were highly dominated by diatoms throughout the experiment albeit the magnitude of Chl*a* increase was smaller. Prymnesiophyte

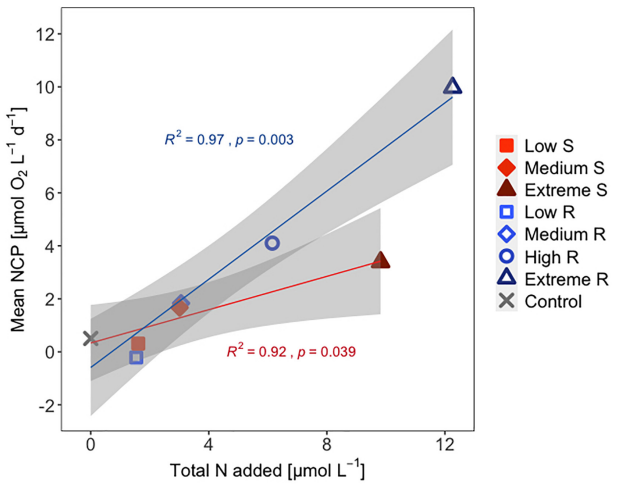

FIGURE 3 | Mean NCP [µmol O_2 L^{-1} d^{-1}] of each treatment vs. amount of inorganic N added [µmol L^{-1}]. S, singular; R, recurring treatment. Shaded area shows the 95% confidence interval. R^2- and *p*-values shown for the linear regression line of each upwelling mode + control.

TABLE 2 | Linear regressions statistics of the relationship between productivity parameters (NCP, GP, CR, Chla) vs. upwelling intensity and for differences between upwelling modes.

Parameter	*F* statistic	R^2	*p*-value
Singular mean NCP vs. µmol N L^{-1}	23.79	0.92	**0.039**
Singular mean GP vs. µmol N L^{-1}	170.7	0.99	**0.006**
Singular mean CR vs. µmol N L^{-1}	192.2	0.99	**0.005**
Singular mean Chl*a* vs. µmol N L^{-1}	300.8	0.99	**0.003**
Recurring mean NCP vs. µmol N L^{-1}	83.08	0.97	**0.003**
Recurring mean GP vs. µmol N L^{-1}	176.7	0.98	**<0.001**
Recurring mean CR vs. µmol N L^{-1}	301.6	0.99	**<0.001**
Recurring mean Chl*a* vs. µmol N L^{-1}	140.4	0.98	**0.001**
mean $NCP^{singular}$ vs. mean $NCP^{recurring}$	105.2	0.99	**0.008**
mean $GP^{singular}$ vs. mean $GP^{recurring}$	210.1	0.99	**0.03**
mean $CR^{singular}$ vs. mean $CR^{recurring}$	119.4	0.99	0.114
mean $Chla^{singular}$ vs. mean $Chla^{recurring}$	318.1	0.99	0.175

Statistically significant correlations / differences are highlighted in bold.

relative abundance increased slightly with upwelling intensity toward the end, particularly in the extreme recurring. Overall, there was a visible reaction pattern to DW additions in all recurring treatments except the low. Under both upwelling modes, Chl*a* showed a strong positive correlation with upwelling intensity (**Table 2**).

In contrast to all treated mesocosms, the Atlantic maintained an overall low concentration of Chl*a*, rarely rising above 0.3 µg L^{-1}, and displayed a variable phytoplankton community composition with a very low contribution of diatoms. Additional diatom biomass calculations based on taxonomic identification and size measurements through microscopy revealed no pronounced species composition differences between treatments. Relative Biomass contribution in all treatments and the control was at least ∼25% from *Leptocylindrus danicus* followed by *Guinardia striata* in the singular and *G. striata* and *Leptocylindrus minimus* in the recurring treatments. *Chaetoceros sp.* contributed approx. 10–15% biomass in all mesocosms (**Supplementary Figure 3** and **Table 1**).

DISCUSSION

Phytoplankton Community Responses to Artificial Upwelling

The results presented require an interpretation of singular and recurring upwelling modes by themselves as well as a comparison of both. Regarding the former, i.e., within each upwelling mode, the results are in line with what we expected from an oligotrophic system reacting to nutrient input: GP, NCP and Chl*a* peaks scaled with upwelling intensity (**Figures 2**, **4**). While singular treatments only displayed one peak after the DW addition, an increase in GP and NCP was visible after each addition in the high and extreme recurring treatments. The same pattern was visible in the Chl*a* concentration of medium recurring as well. The strong positive response of all variables to increasing upwelling intensity was corroborated by the linear regression analysis for both upwelling modes (**Table 2**). The observed shift to a dominance of diatoms in all treatments (**Figure 4**) is also coherent with earlier studies: Phytoplankton community analysis from mesocosms, upwelling filaments, eddies and oligotrophic areas within the Canary Islands region have consistently shown the same succession patterns. There is a consistent shift from small picophytoplankton under nutrient depleted to larger microphytoplankton, and predominantly diatoms, under nutrient replete conditions. This is valid for both, nutrient-enriched water bodies (e.g., eddies or mesocosm experiments) (Mann, 1993; Arístegui and Montero, 2005; Fawcett and Ward, 2011; Taucher et al., 2017) as well as for transects following filaments from (oligotrophic) offshore to (eutrophic) coastal upwelling areas (Arístegui et al., 2004). Additionally, Ferreira et al. (2020) found that nutrient pulses in a microcosm experiment led to similar community composition changes. Interestingly, from the three largest contributors to diatom biomass, *Leptocylindrus danicus* and *L. minimus* were also found to be by far the most abundant in a previous mesocosm study with nutrient fertilization at the same geographical location (Taucher et al., 2018). The development of phytoplankton size and composition is somewhat contrary to what Masuda et al. (2010) found in their study: Despite Nitrate concentrations of 4.6 µM in the discharged water, they reported active growth of pico- and nanophytoplankton (particularly Cryptophytes and Synechococcus), but not diatoms. They attributed this to low light availability at discharge depth (6 ± 3%) compared to the surface layer combined with poor shade adaptation of surface populations (5 m) mixed into the discharge depth (20 m), visible as a lack of photosynthetic pigment increase. Low light availability was not an issue in our experiment that hence provided better growing conditions for diatoms. Similarly, Maruyama et al. (2011) measured far higher peak Chl*a* concentrations than we found (up to ∼30 µg L^{-1}),

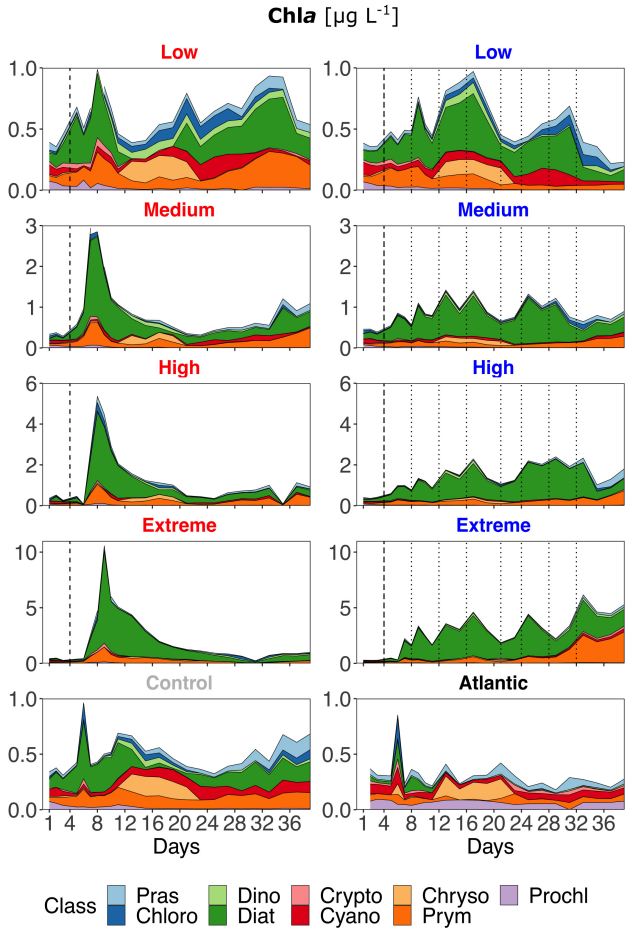

FIGURE 4 | Contribution of each phytoplankton class to total Chla based on Chemtax analysis of photosynthetic pigments (HPLC). Note the different y-axis scales. Abbreviations stand for: *Prasinophyceae*, *Chlorophyceae*, *Dinophyceae*, *Cryptophyceae*, *Chrysophyceae*, *Prymnesiophyceae*, *Prochlorophyceae*, *Cyanophyceae*, and *Diatomea*. Atlantic refers to samples taken from the water surrounding the mesocosm field. Dotted lines represent DW additions, dashed line marks the single DW addition to singular treatments. Red labels represent singular and blue labels recurring treatments.

the explanation for this being that they measured Chl*a* concentrations in the top surface layer close to the output of the upwelling pump. Our samples were integrated over 15 m of water column and still showed peak Chl*a* concentrations of up to ∼10 µg L^{-1}, with the high and extreme recurring treatments constantly maintaining concentrations between 1 and 5 µg L^{-1}.

Inorganic nutrients were generally consumed entirely and quickly. It took the phytoplankton in the singular treatments a few days after the initial DW addition and once the phytoplankton community in the recurring treatments adapted to the input, consumption was immediate and almost absolute (**Figure 1**). This pattern of fast and complete nutrient uptake is comparable to what has been observed in other studies with simulated upwelling in the same geographical location (Hernández-Hernández et al., 2018; Taucher et al., 2018).

Since these results do not offer a straightforward explanation as to why recurring upwelling significantly outperformed singular upwelling in terms of NCP_{cum} and mean NCP we discuss two points that might have contributed to this disparity and that also make the comparison of both upwelling modes more complex.

Underestimation of Singular Treatment Peaks

The workload produced by the oxygen measurements only allowed for sampling every second day. Meanwhile, almost the entire period of autotrophy (positive NCP values) in this treatment took place between d7-d11 (**Figure 2A**). Considering the swiftness and strength of the response in the extreme singular treatment, this might have led to an underestimation of the initial productivity peak. Given that the NCP_{cum} of this treatment differed most from its recurring counterpart this is relevant for the interpretation of the data. If NCP peaked on a non-sampling day, the real magnitude of the initial peak might have been higher than we measured. This in turn would affect the temporal development of NCP_{cum}. To some extent, the high and sudden nutrient input might have led to so called luxury consumption (Droop, 1974) rather than immediate production. But judging by the swiftness of both nutrient consumption and the following GP decrease (**Figure 2B**), luxury consumption could only have taken place during a short period of time and it does not bar an underestimation of the initial peak. Hence in terms of NCP_{cum}, there is a chance that particularly the extreme treatments differed less than observed. The stark difference in mean NCP per µmol N visible in **Figure 3** should therefore be interpreted with some caution, not least because it represents a regression run through 4–5 data points. This is also the case for the other linear regression statistics displayed in **Table 2**. An underestimation of peak values would also provide an explanation to why mean NCP and GP was significantly higher under recurring upwelling compared to singular whereas Chl*a* was not (**Table 2**), although at least GP and Chl*a* should be closely related.

Different Temporal Evolution of Production and Respiration

Productivity and respiration happened on different timeframes and magnitudes in each upwelling mode: Singular treatments went through a brief productive phase (d5-d11) followed by an extended period of low productivity and higher respiration (d12-d37), visible in the consistently low GP/R or negative NCP from day 12 onward (**Figures 2A,C**). Recurring treatments on the other hand consistently retained a net-autotrophic state after treatment onset. The same trend persisted when normalizing NCP rates to Chl*a* (**Supplementary Figure 2**). In the singular treatments, this extended phase of a balanced to net-heterotrophic state might also have opened a niche for mixotrophic organisms that could further influence the metabolic balance: microscopic cell counts and flow cytometry showed an increase in dinoflagellate abundance, that followed the singular DW addition and coincided temporally with the ensuing decrease in GP/R

(Schulz et al., unpublished data). Many of the dinoflagellate genera identified in this experiment are potentially mixotrophic (**Supplementary Table 2**), a very common physiological trait among dinoflagellates in general (Stoecker, 1999). On the other hand, the constant net autotrophy of the recurring treatments implies that the phytoplankton that capitalized first on nutrient availability succeeded in doing so throughout the experiment (mainly diatoms, followed by Prymnesiophytes toward the end in high and extreme recurring). This is corroborated by a recent modeling study on competition between diatoms and mixotrophic protists that found key diatom traits (phototrophy and vacuolation) to be more advantageous under high nutrient concentration, while mixotroph traits (phototrophy and phagotrophy) succeeded under nutrient limitation (Cadier et al., 2020). The increase in dinoflagellate abundance might also offer an explanation for the overall lower Chla-normalized NCP rates in the singular treatments compared to the recurring.

CONCLUSION

In summary, our results show that artificial upwelling led to the establishment of a productive, diatom dominated community of primary producers. However, differences in NCP became more pronounced with increasing upwelling intensity. We conclude that the mode in which nutrients are supplied to an oligotrophic system plays a crucial role in how it responds to artificial upwelling.

The results imply that high intensity recurring upwelling might be better suited to increase overall food web productivity (and therefore fishery yields) than singular, as it managed to sustain a net autotrophic community of primary producers that could nurture the rest of the food web. The highest recurring upwelling intensity yielded a three times higher mean NCP compared to the singular despite receiving only 1.25 times as many nutrients, and overall, recurring upwelling led to significantly higher mean NCP and GP compared to singular. This needs to be put into context with higher trophic levels, as well as factors that influence productivity (biomass, grazing, export) to evaluate if high trophic transfer efficiency and/or carbon export was actually achieved. If artificial upwelling is to be applied with a specific purpose (increase of carbon sequestration or food web productivity) we also need to understand why the observed "autotrophic recurring" vs. "heterotrophic singular" scenario developed.

These results highlight the need to consider empirically measured local effects like community structure and metabolism under artificial upwelling. They have major implications not only for future assessments of upwelling impacts, but specifically for imminent policymaker decisions on the potential employment of artificial upwelling as an ocean-based solution.

DATA AVAILABILITY STATEMENT

The raw data supporting the conclusions of this article will be made available by the authors, without undue reservation. The data will be submitted to Pangaea, https://www.pangaea.de/.

AUTHOR CONTRIBUTIONS

UR, JA, and JT contributed to experimental concept and design. JO and JA contributed to data analysis. JO wrote the manuscript with input from all co-authors. All authors contributed to the execution of the experiment.

FUNDING

This project was conducted in the framework of the project *Ocean Artificial Upwelling* (*Ocean artUp*) funded by an Advanced Grant of the European Research Council. Additional support was provided through Transnational Access funds by the EU project AQUACOSM, EU H2020-INFRAIA-project No. 731065, and by project TRIATLAS (AMD-817578-5) from the European Union's Horizon 2020 to JA. JA was also supported by a Helmholtz International Fellow Award, 2015 (Helmholtz Association, Germany) as well as Project FONIAC 2019 (Fundación Caja Canarias and Fundación Bancaria La Caixa).

ACKNOWLEDGMENTS

The authors are grateful to the Oceanic Platform of the Canary Islands (PLOCAN) and its staff for the use of their facilities, and for their hospitality and help with the logistics and organization of this research campaign. The authors would also like to thank the biological oceanography group of the University of Las Palmas de Gran Canaria (GOB-ULPGC) for providing additional lab facilities. Particular thanks go to Minerva Espino and Acorayda González for their valuable contribution to the measurements of primary productivity. The captain and crew of RV James Cook are thanked for deploying the mesocosms and collecting the deep water. Special thanks go to the KOSMOS team of GEOMAR for taking care of all logistical and technical aspects of this mesocosm campaign and for coordinating the research activities on site as well as the data management and exchange.

SUPPLEMENTARY MATERIAL

The Supplementary Material for this article can be found online at: https://www.frontiersin.org/articles/10.3389/fmars.2021.743105/full#supplementary-material

REFERENCES

Arístegui, J., and Montero, M. F. (2005). Temporal and spatial changes in plankton respiration and biomass in the Canary Islands region: the effect of mesoscale variability. *J. Mar. Syst.* 54, 65–82. doi: 10.1016/j.jmarsys.2004.07.004

Arístegui, J., Barton, E. D., Tett, P., Montero, M. F., García-Muñoz, M., Basterretxea, G., et al. (2004). Variability in plankton community structure, metabolism, and vertical carbon fluxes along an upwelling filament (Cape Juby, NW Africa). *Prog. Oceanogr.* 62, 95–113. doi: 10.1016/j.pocean.2004.07.004

Arístegui, J., Hernández-León, S., Montero, M. F., and Gómez, M. (2001). The seasonal planktonic cycle in coastal waters of the Canary Islands. *Sci. Mar.* 65, 51–58. doi: 10.3989/scimar.2001.65s151

Bryan, J. R., Rlley, J. P., and Williams, P. J. L. (1976). A winkler procedure for making precise measurements of oxygen concentration for productivity and related studies. *J. Exp. Mar. Bio. Ecol.* 21, 191–197. doi: 10.1016/0022-0981(76)90114-3

Cadier, M., Hansen, A. N., Andersen, K. H., and Visser, A. W. (2020). Competition between vacuolated and mixotrophic unicellular plankton. *J. Plankton Res.* 42, 425–439. doi: 10.1093/plankt/fbaa025

Carritt, D. E., and Carpenter, J. H. (1966). Comparison and evaluation of currently employed modifications of the Winkler method for determining dissolved oxygen in seawater; a NASCO report. *J. Mar. Res.* 24, 286–318.

Casareto, B. E., Niraula, M. P., and Suzuki, Y. (2017). Marine planktonic ecosystem dynamics in an artificial upwelling area of Japan: phytoplankton production and biomass fate. *J. Exp. Mar. Bio. Ecol.* 487, 1–10. doi: 10.1016/j.jembe.2016.11.002

Droop, M. R. (1974). The nutrient status of algal cells in continuous culture. *J. Mar. Biol. Assoc. U. K.* 54, 825–855. doi: 10.1017/S002531540005760X

Engel, A., Borchard, C., Piontek, J., Schulz, K. G., Riebesell, U., and Bellerby, R. (2013). CO2 increases 14C primary production in an Arctic plankton community. *Biogeosciences* 10, 1291–1308. doi: 10.5194/bg-10-1291-2013

Fawcett, S. E., and Ward, B. B. (2011). Phytoplankton succession and nitrogen utilization during the development of an upwelling bloom. *Mar. Ecol. Prog. Ser.* 428, 13–31. doi: 10.3354/meps09070

Ferreira, A., Sá, C., Silva, N., Beltrán, C., Dias, A. M., and Brito, A. C. (2020). Phytoplankton response to nutrient pulses in an upwelling system assessed through a microcosm experiment (Algarrobo Bay, Chile). *Ocean Coast. Manag.* 190:105167. doi: 10.1016/j.ocecoaman.2020.105167

Garcia, S. M., and Rosenberg, A. A. (2010). Food security and marine capture fisheries: Characteristics, trends, drivers and future perspectives. *Philos. Trans. R. Soc. B Biol. Sci.* 365, 2869–2880. doi: 10.1098/rstb.2010.0171

GESAMP (2019). High level review of a wide range of proposed marine geoengineering techniques. *GESAMP Rep. Stud.* 144. Available online at: http://www.gesamp.org/publications/high-level-review-of-a-wide-range-of-proposed-marine-geoengineering-techniques (accessed December 6, 2021).

Giraud, M., Boye, M., Garçon, V., Donval, A., and de la Broise, D. (2016). Simulation of an artificial upwelling using immersed in situ phytoplankton microcosms. *J. Exp. Mar. Bio. Ecol.* 475, 80–88. doi: 10.1016/j.jembe.2015.11.006

Godfray, H. C. J., Crute, I. R., Haddad, L., Muir, J. F., Nisbett, N., Lawrence, D., et al. (2010). The future of the global food system. *Philos. Trans. R. Soc. B Biol. Sci.* 365, 2769–2777. doi: 10.1098/rstb.2010.0180

Grasshoff, K., Kremling, K., and Ehrhardt, M. (1999). *Methods of Seawater Analysis. Chapter 4: Determination of Oxygen*, Vol. 3. Weinheim: Wiley-VCH.

Hernández-Hernández, N., Bach, L. T., Montero, M. F., Taucher, J., Baños, I., Guan, W., et al. (2018). High CO 2 under nutrient fertilization increases primary production and biomass in subtropical phytoplankton communities: a mesocosm approach. *Front. Mar. Sci.* 5:213. doi: 10.3389/fmars.2018.00213

Kirke, B. (2003). Enhancing fish stocks with wave-powered artificial upwelling. *Ocean Coast. Manag.* 46, 901–915. doi: 10.1016/S0964-5691(03)00067-X

Lawrence, M. G., Schäfer, S., Muri, H., Scott, V., Oschlies, A., Vaughan, N. E., et al. (2018). Evaluating climate geoengineering proposals in the context of the Paris Agreement temperature goals. *Nat. Commun.* 9:5938. doi: 10.1038/s41467-018-05938-3

Lovelock, J. E., and Rapley, C. G. (2007). Ocean pipes could help the Earth to cure itself. *Nature* 449:2007.

Mackey, M. D., Mackey, D. J., Higgins, H. W., and Wright, S. W. (1996). CHEMTAX - A program for estimating class abundances from chemical markers: application to HPLC measurements of phytoplankton. *Mar. Ecol. Prog. Ser.* 144, 265–283. doi: 10.3354/meps144265

Mann, K. H. (1993). Physical oceanography, food chains, and fish stocks: a review. *ICES J. Mar. Sci.* 50, 105–119. doi: 10.1006/jmsc.1993.1013

Maruyama, S., Yabuki, T., Sato, T., Tsubaki, K., Komiya, A., Watanabe, M., et al. (2011). Evidences of increasing primary production in the ocean by Stommel's perpetual salt fountain. *Deep. Res. Part I Oceanogr. Res. Pap.* 58, 567–574. doi: 10.1016/j.dsr.2011.02.012

Masuda, T., Furuya, K., Kohashi, N., Sato, M., Takeda, S., Uchiyama, M., et al. (2010). Lagrangian observation of phytoplankton dynamics at an artificially enriched subsurface water in Sagami Bay. *Japan. J. Oceanogr.* 66, 801–813. doi: 10.1007/s10872-010-0065-1

McAndrew, P. M., Björkman, K. M., Church, M. J., Morris, P. J., Jachowski, N., Williams, P. J. L. B., et al. (2007). Metabolic response of oligotrophic plankton communities to deep water nutrient enrichment. *Mar. Ecol. Prog. Ser.* 332, 63–75. doi: 10.3354/meps332063

Menden-Deuer, S., and Lessard, E. J. (2000). Carbon to volume relationships for dinoflagellates, diatoms, and other protist plankton. *Limnol. Oceanogr.* 45, 569–579. doi: 10.4319/lo.2000.45.3.0569

Riebesell, U., Gattuso, J. P., Thingstad, T. F., and Middelburg, J. J. (2013b). Arctic ocean acidification: Pelagic ecosystem and biogeochemical responses during a mesocosm study. *Biogeosciences* 10, 5619–5626. doi: 10.5194/bg-10-5619-2013

Riebesell, U., Czerny, J., Von Bröckel, K., Boxhammer, T., Büdenbender, J., Deckelnick, M., et al. (2013a). Technical note: a mobile sea-going mesocosm system – new opportunities for ocean change research. *Biogeosciences* 10, 1835–1847. doi: 10.5194/bg-10-1835-2013

Schellnhuber, H. J., Rahmstorf, S., and Winkelmann, R. (2016). Why the right climate target was agreed in Paris. *Nat. Clim. Chang.* 6, 649–653. doi: 10.1038/nclimate3013

Stoecker, D. K. (1999). Mixotrophy among dinoflagellates. *J. Eukaryot. Microbiol.* 46, 397–401. doi: 10.1111/j.1550-7408.1999.tb04619.x

Taucher, J., Arístegui, J., Bach, L. T., Guan, W., Montero, M. F., Nauendorf, A., et al. (2018). Response of subtropical phytoplankton communities to ocean acidification under oligotrophic conditions and during nutrient fertilization. *Front. Mar. Sci.* 5:330. doi: 10.3389/fmars.2018.00330

Taucher, J., Bach, L. T., Boxhammer, T., Nauendorf, A., Achterberg, E. P., Algueró-Muñiz, M., et al. (2017). Influence of ocean acidification and deep water upwelling on oligotrophic plankton communities in the subtropical North Atlantic: insights from an in situ mesocosm study. *Front. Mar. Sci.* 4:85. doi: 10.3389/fmars.2017.00085

UNFCC (2015). *Adoption of the Paris Agreement*. Available online at: https://unfccc.int/documents/9064 (accessed December 6, 2021).

United Nations (2019). *World Population Prospects 2019: Highlights (ST/ESA/SER.A/423)*. Available online at: https://population.un.org/wpp/Publications/Files/WPP2019_Highlights.pdf (accessed December 6, 2021).

Van Heukelem, L., and Thomas, C. S. (2001). Computer-assisted high-performance liquid chromatography method development with applications to the isolation and analysis of phytoplankton pigments. *J. Chromatogr. A* 910, 31–49.

Williams, P. J., and Jenkinson, N. W. (1982). A transportable microprocessor-controlled precise Winkler titration suitable for field station and shipboard use. *Limnol. Oceanogr.* 27, 576–584. doi: 10.4319/lo.1982.27.3.0576

Conflict of Interest: The authors declare that the research was conducted in the absence of any commercial or financial relationships that could be construed as a potential conflict of interest.

Publisher's Note: All claims expressed in this article are solely those of the authors and do not necessarily represent those of their affiliated organizations, or those of the publisher, the editors and the reviewers. Any product that may be evaluated in this article, or claim that may be made by its manufacturer, is not guaranteed or endorsed by the publisher.

frontiers | Frontiers in Marine Science

ORIGINAL RESEARCH
published: 20 June 2022
doi: 10.3389/fmars.2022.880550

Oligotrophic Phytoplankton Community Effectively Adjusts to Artificial Upwelling Regardless of Intensity, but Differently Among Upwelling Modes

Joaquin Ortiz[1], Javier Arístegui[2], Nauzet Hernández-Hernández[2], Mar Fernández-Méndez[1,3] and Ulf Riebesell[1]*

[1] Marine Biogeochemistry, Biological Oceanography, Geomar Helmholtz Centre for Ocean Research Kiel, Kiel, Germany, [2] Oceanografía Biológica, Instituto de Oceanografía y Cambio Global, IOCAG, Universidad de Las Palmas de Gran Canaria, Las Palmas de Gran Canaria, Spain, [3] Polar Biological Oceanography Section, Alfred Wegener Institute Helmholtz Centre for Polar and Marine Research, Bremerhaven, Germany

OPEN ACCESS

Edited by:
Monique Messié,
Monterey Bay Aquarium Research Institute (MBARI), United States

Reviewed by:
Adrian Marchetti,
University of North Carolina at Chapel Hill, United States
France Van Wambeke,
UMR7294 Institut Méditerranéen d'océanographie (MIO), France
Renate Scharek,
Gijón Oceanographic Center, Spain

***Correspondence:**
Joaquin Ortiz
jortiz@geomar.de

Specialty section:
This article was submitted to Marine Biogeochemistry, a section of the journal Frontiers in Marine Science

Received: 21 February 2022
Accepted: 24 May 2022
Published: 20 June 2022

Citation:
Ortiz J, Arístegui J, Hernández-Hernández N, Fernández-Méndez M and Riebesell U (2022) Oligotrophic Phytoplankton Community Effectively Adjusts to Artificial Upwelling Regardless of Intensity, but Differently Among Upwelling Modes. Front. Mar. Sci. 9:880550. doi: 10.3389/fmars.2022.880550

Artificial upwelling has been proposed as a means of enhancing oceanic CO_2 sequestration and/or raising fishery yields through an increase in primary production in unproductive parts of the ocean. However, evidence of its efficacy, applicability and side effects is scarce. Here we present part of the results of a 37-day mesocosm study conducted in oligotrophic waters off the coast of Gran Canaria. The goal was to assess *in situ* the effects of artificial upwelling on the pelagic community. Upwelling was simulated *via* two modes: i) a singular deep-water pulse and ii) a recurring supply every 4 days; each mode at four different intensities defined by the total amount of nitrate added: approx. 1.5, 3, 5.7, and 11 µmol L^{-1}. In this study we focus on the phytoplankton response through size-fractionated ^{14}C primary production rates (PP), Chlorophyll *a* and biomass. We observed increases in PP, accumulated PP, Chlorophyll *a* and biomass that scaled linearly with upwelling intensity. Upwelling primarily benefitted larger phytoplankton size fractions, causing a shift from pico- and nano- to nano- and microphytoplankton. Recurring deep-water addition produced more biomass under higher upwelling intensities than a single pulse addition. It also reached significantly higher accumulated PP per unit of added nutrients and showed a stronger reduction in percentage extracellular release with increasing upwelling intensity. These results demonstrate that oligotrophic phytoplankton communities can effectively adjust to artificial upwelling regardless of upwelling intensity, but differently depending on the upwelling mode. Recurring supply of upwelled waters generated higher efficiencies in primary production and biomass build-up than a single pulse of the same volume and nutrient load.

Keywords: artificial upwelling, primary production, mesocosm, biomass, phytoplankton, oligotrophic

1 INTRODUCTION

Marine primary production is a key process in the ocean that directly and indirectly supports all trophic levels of the pelagic ecosystem. However, unabated climate change is negatively impacting this ecosystem by enhancing ocean stratification and reducing nutrient mixing, which lead to a decline of marine production particularly in low latitude regions (Frölicher et al., 2016; Li et al., 2020). Artificial upwelling has been suggested as a nature-based technology to supply nutrient-rich deep water to the sunlit surface layers. This would not only, at least locally, counteract the increasing stratification thereby restoring marine productivity. It could also lead to increased fishery yields through enhanced food web productivity and carbon sequestration *via* the biological carbon pump, especially if applied in presently oligotrophic waters. Consequently, it could provide a sustainable food source and potentially reduce atmospheric CO_2 concentrations (Kirke, 2003; Lovelock and Rapley, 2007; GESAMP, 2019). Mechanisms tested so far to power the upwelling process include (i) pumps (Miyabe et al., 2004; White et al., 2010), (ii) release of air-bubbles at depth to create an upward flow (McClimans et al., 2010; Handå et al., 2014), (iii) pumping of brackish water to depth that then rises to the surface (Aure et al., 2007), (iv) a perpetual salt fountain (Maruyama et al., 2004) and (v) the creation of an artificial sea mount (Jeong et al., 2013).

Empirical evidence on the effects of artificial upwelling is mostly limited to either small-scale lab experiments or model simulations. Some experimental studies have shown promising results though: McAndrew et al. (2007) conducted 25 L bottle incubation experiments in oligotrophic waters adding nutrient-rich deep water (DW) from 700 m depth. Following fertilization, the phytoplankton community shifted from a picoplankton-dominated net heterotrophic to a highly autotrophic community in the course of 5 days with up to 60-fold increases in gross PP and 13-fold increases in respiration. Giraud et al. (2016) found a community shift towards diatoms in oligotrophic waters after DW (1100 m depth) addition to 2.3 L incubators. And Casareto et al. (2017) reported increased PP and phytoplankton biomass after very mild natural upwelling in oligotrophic waters close to Japan. Previous mesocosm studies have included simulated upwelling among other manipulations (such as elevated CO_2 concentration), but never focused exclusively on artificial upwelling effects (Riebesell et al., 2013b; Hernández-Hernández et al., 2018). Among the only field studies, Jeong et al. (2013) studied the effects on several trophic levels around an artificial seamount created to induce upwelling over 5 years. They found a 50- and 2.3-fold increase in standing stock of phyto- and zooplankton, respectively and a significant increase in both phytoplankton diversity and richness index. A first attempt at *in situ* implementation of artificial upwelling wave pumps in the open ocean was made by White et al. (2010), but had to be aborted due to technical problems with the pipes before sufficient data could be gathered. Masuda et al. (2010) succeeded in pumping up water from 205 m depths, leading to increases in phytoplankton growth, but only monitored the upwelling plume for approx. 3 days. Meanwhile Maruyama et al. (2011) reported strongly elevated surface layer Chl*a* concentrations (but no further parameters) in the water body around their upwelling pump using the perpetual salt fountain technique.

All this points out the urgent need for more extensive *in situ* studies to assess the effects of artificial upwelling on natural communities. To expand our knowledge on the potential of artificial upwelling to increase ecosystem productivity, in this study we evaluated the response of the phytoplankton community of the Gran Canaria oligotrophic waters to different intensities and modes of artificial upwelling. The technical concept of the upwelling modes applied in this experiment (a single pulse of upwelled water vs recurring i.e., multiple upwelling events) roots in the design of potentially applicable pump types: stationary (moored) pumps would provide singular upwelling, as the fertilized water mass moves away with currents and winds; while free drifting pumps would provide recurring upwelling as they would move along with the water mass. Using large off-shore mesocosms we added different amounts of nutrient-rich deep-sea water to a natural community adapted to oligotrophic conditions. During 37 days, we examined the effects of artificial upwelling on PP, Chlorophyll a (Chl*a*) and phytoplankton biomass (B) of micro-, nano- and picophytoplankton through a comprehensive set of size-fractionated ^{14}C uptake measurements, fluorometry, flow cytometry and microscopy. Our aim was to understand how the phytoplankton community adapts to the treatments and how upwelling intensity and mode impact PP distribution among primary producers of different size classes. And whether the adaptations create the conditions needed to sustain a productive food web.

2 MATERIALS AND METHODS

2.1 Experimental Setup

Nine KOSMOS (Kiel Offshore Mesocosms for Ocean Simulations; Riebesell et al., 2013a) units of 43.78 m^3 each were set up in Gando Bay on the east coast of the island of Gran Canaria (27.9279°N, 15.3654°W) from November to December 2018. This location provided protection against common swells and winds. The mesocosm bags were deployed and left open for a seven-day period of open water exchange in order to enclose a homogeneous as possible natural phytoplankton community. To close the mesocosms the sediment traps were attached and the top ends of the bags were pulled above the water surface. A net (3 mm mesh size) was pulled from bottom to top right after closure to exclude unevenly distributed large organisms. Transparent plastic roofs were attached on top of the mesocosms to prevent contamination by precipitation and bird droppings. Total length of the mesocosm bags was 13 m plus an additional 2.7 m for the sediment trap, hereby enclosing a mean water volume of 43.78 m^3.

The DW was pumped into a custom-built 100 m^3 collector bag by means of an electric pump with the support of RRS James

Cook (UK) and J Socas (ES). It was collected between 28°00'N, 15°18'E and 27°57'N, 15°10'E at 330 m depth. The water was then towed to the mesocosm site and stored in the same bag collector. Mesocosm water was removed evenly along the entire water column with the help of a pump-powered dispersion device before adding the DW through the same procedure (Riebesell et al., 2013a). For technical specifications about the pumping procedure see Taucher et al. (2017). It was calculated based on vertical nutrient distribution of the region (Perez et al., 2001; Schlitzer and Mieruch-Schnülle, 2021) that the nutrient-rich DW suitable for our experimental design should be at about 600 m depth (~25/~1.5/~10 µmol L^{-1} NO_3^- /PO_4^- /$Si(OH)_4$). However, due to technical constraints the intended pumping depth could not be reached. Therefore, collected DW was spiked with additional inorganic nutrients (N, P & Si as sodium nitrate, disodium phosphate and sodium silicate) to adjust the concentrations and stoichiometry to that at the intended pumping depth. Deep water nutrient concentrations after amendment were 25 µmol L^{-1}, 1.38 µmol L^{-1} and 12.1 µmol L^{-1} for NO_3^- , PO_4^- and $Si(OH)_4$, respectively. Nutrient concentrations inside the collector bag were measured routinely and adjusted, when necessary, before each addition to the mesocosms. During the 39 days of the experiment, mesocosms were cleaned regularly on the inside with a large rubber ring pulled along the entire mesocosm length and outside by divers to remove biofouling. Potential stratification of the enclosed water column was monitored through CTD casts measuring temperature, salinity and pH, but no indications were found.

Integrated water column samples (0-13 m) for PP, Chl*a*, phytoplankton abundances and inorganic nutrients were collected by means of depth-Integrated Water Samplers (IWS, Hydro-Bios, Kiel) every second day, starting from d1 (for details on all activities see **Supplementary Figure 1**). IWS are pre-set to the mesocosm length and evenly sample the entire column in one draft through constant automated water intake. The water samples were transferred to 10 L canisters, transported in the dark from the field to the laboratory on land and then sub-sampled for every parameter. Samples labeled "Atlantic" were taken from the water surrounding the mesocosm field.

2.2 Artificial Upwelling Treatments

The experimental treatments consisted of one control mesocosm (M5) and two groups of four mesocosms subjected to: i) a one-off ("singular"; M1, M3, M7, M9) DW addition on day four (d4) or ii) a total of eight DW additions every four days ("recurring"; M2, M4, M6, M8) from d4 onwards. With the exception of d20, where the recurring DW addition was delayed by one day (d21). Within each upwelling mode, a 4-step gradient in simulated upwelling intensity was established from "low" to "extreme" treatments. See **Table 1** for the upwelling intensity corresponding to each mesocosm. This refers to the total amount of nutrients added through replacement of mesocosm water by DW. In accordance with upwelling intensity, respective singular and recurring upwelling treatments were intended to receive an equal total amount of DW, and therefore nutrients. I.e., low treatments should ideally receive the same total amount either at once (singular) or as a sum of all eight additions (recurring; **Table 1**). For the sake of simplicity "µmol of nutrients" henceforth refers to total added inorganic nitrogen (only NO_3^-). For details on the methodology of nutrient concentration measurements see Ortiz et al. (2022).

2.3 Primary Production

Primary production was measured using a modification of the method described by Cermeño et al. (2012) for size-fractionated ^{14}C uptake. A 5 mL ampoule of ^{14}C-labeled sodium bicarbonate [$NaH^{14}CO_3$] (Perkin Elmer, Waltham, USA) with a specific activity of 37 MBq mL^{-1} was diluted with 45 mL of Milli-Q water to obtain a stock solution with an activity of 3.7 MBq mL^{-1}. Four culture flasks (Sarstedt TC Flask d15, Nümbrecht, Germany) per mesocosm were first filled to the bottleneck (70 mL) with water from the 10 L canisters. Samples were pre-filtered through a 250 µm mesh to preclude large organisms. 80 µl of ^{14}C stock solution (i.e., 0.296 MBq) were added, the flask closed and then mixed gently. All bottles were incubated in a climate

TABLE 1 | Treatment overview, total inorganic nutrients added and mean values for particulate primary production (PP_{POC}), Biomass (B) and Chlorophyll a (Chla).

#	Treatment	Deep water addition [m^3]	Total inorganic N added [µmol L^{-1}]*	Mean PP_{POC} [µmol C L^{-1} d^{-1}]	Mean B [µg C L^{-1}]	Mean Chl*a* [µg L^{-1}]
3	Low Singular	1 x 2.8	1.61	1.09 ± 0.58	42.59 ± 45.88	0.61 ± 0.32
2	Low Recurring	8 x 0.35	1.54	1.16 ± 0.55	36.32 ± 20.06	0.45 ± 0.2
7	Medium Singular	1 x 5.25	3.01	1.86 ± 2.5	115.72 ± 118.94	0.63 ± 0.56
4	Medium Recurring	8 x 0.7	3.06	1.78 ± 0.94	137.14 ± 85.45	0.90 ± 0.35
9	High Singular	1 x 9.8	5.61	2.92 ± 3.23	155.74 ± 129.51	1.05 ± 0.85
6	High Recurring	8 x 1.4	6.15	3.45 ± 2.58	447.83 ± 405.21	1.44 ± 0.79
1	Extreme Singular	1 x 17.15	9.82	4.98 ± 6.91	433.64 ± 471.33	1.46 ± 1.28
8	Extreme Recurring	8 x 2.81	12.26	7.59 ± 4.82	494.43 ± 352.93	2.99 ± 2.18
5	Control	–	0.00	0.83 ± 0.32	24.45 ± 7.28	0.48 ± 0.38
10	Atlantic	–	0.00	0.56 ± 0.22	–	0.25 ± 0.09

**For recurring treatments, the total amount of N added represents the sum of all DW additions.*

chamber (Pol-Eko KK350, Loslau, Poland) for 24 hours simulating mesocosm water temperature and light conditions of the area and season (12 h light-dark cycle with a mean daily light intensity of ~500 µmol photons m^{-2} s^{-1}). Mesocosm light intensities as assessed by CTD casts ranged from roughly 1000-50 µmol photons m^{-2} s^{-1} between the surface and bottom of the enclosure. Three out of four flasks were incubated directly in the chamber (light triplicates) while the fourth was incubated inside a light-proof bag within the chamber to prevent photosynthesis (dark/control).

After incubation, all samples were sequentially filtered on a circular filtration manifold (Oceomic, Fuerteventura, Spain) under low vacuum pressure (<200 mbar) through superimposed polycarbonate membrane filters with pore sizes of 20 µm (PP_{micro}), 2 µm (PP_{nano}) and 0.2 µm (PP_{pico}) (DHI GVS 20 µm, Hørsholm, Denmark, Whatman Nuclepore 2 µm & 0.2 µm, Maidstone, UK). Filters were then placed into 5 mL scintillation vials (Sarstedt HD-PE Mini-vial, Nümbrecht, Germany) and left in a desiccator with fuming hydrochloric acid (HCl 37%) for 24 hours. For quantification of dissolved organic carbon production (PP_{DOC}) 5 mL of the filtrate (i.e., <0.2 µm) were placed in 20 mL scintillation vials (Sarstedt HD-PE Scintillation vial, Nümbrecht, Germany), acidified with 100 µL of hydrochloric acid (HCl, 37%) and placed on an orbital oscillator for 24 hours at 60 rpm. Acidifying of all samples was done to remove any remaining inorganic ^{14}C. On the following day, 10 mL of scintillation cocktail (Ultima Gold XR, Perkin Elmer, Waltham, USA) were added to all liquid samples. Filters were pushed into the vials taking care not to touch the side with the retained material and 3.5 mL of scintillation cocktail were added. All samples were shaken vigorously and left in darkness overnight before being measured on the scintillation counter (Beckman LS-6500, Brea, USA). To obtain primary production rates [µg C L^{-1} h^{-1}] from the counted disintegrations per minute the following equation was used:

$$PP = \left[\frac{V_S}{V_F}\right] \cdot \frac{DIC \cdot (DPM_S - DPM_D)}{DPM_A \cdot t_i}$$

V_S = sample volume [L]; V_F = filtered volume [L]; DPM_S = sample disintegrations per minute; DPM_D = dark/control disintegrations per minute; DIC = dissolved inorganic carbon [µg C L^{-1}]; DPM_A = added ^{14}C in disintegrations per minute; t_i = incubation time [h]

The final PP rate was calculated from the mean of the triplicates. To detect outliers, a deviation coefficient consisting of the percentage deviation of each triplicate from the standard deviation (SD) of the sample was calculated and the cutoff set at 20%. Each triplicate was checked for values that increased the cutoff to >20% and these were excluded as outliers. All resulting values were transformed to molar units before further analysis (µmol C = µg C·12.01 µg $µmol^{-1}$). Total particulate organic carbon production (PP_{POC}) was calculated from the sum of all three size fractions. To estimate cumulated PP (PP_{cum}) over the course of the experiment PP_{POC} of all days was added together for each mesocosm. Production on non-sampling days was calculated as the mean PP_{POC} of the day before and after (e.g., PP for d10 was the mean of PP_{POC} from d9 & d11). Percentage of Extracellular Release (PER) was calculated through [PP_{DOC}/(PP_{POC} + PP_{DOC})] * 100. If a sample was lost, an estimate of the PP rate was calculated through the mean PP rate of the sampling day before and after (only the case on d13 for PP_{micro} samples of the control, medium & high singular and high & extreme recurring).

Dissolved Inorganic Carbon (DIC) samples were taken from a separate IWS and directly subsampled with special precaution to avoid contamination (bubble-free, generous overflowing of the bottle and no headspace). Samples were sterile filtered (0.2 µm pore size) under low pressure with a peristaltic pump and poisoned with $HgCl_2$ before storing them until analysis. Measurements were carried out through infrared absorption on an AIRICA system (Marianda, Kiel, Germany) with a LI-COR LI-7000.

2.4 Phytoplankton Abundances and Biomass

Picophytoplankton (0.2-2 µm) and nanophytoplankton (2-20 µm) cells were counted using a FACScalibur (Becton and Dickinson, USA) flow cytometer. Duplicate samples were collected in sterile cryovials (2 mL and 5 mL for pico- and nanoplankton, respectively), immediately fixed with paraformaldehyde (2% final concentration), refrigerated at 4°C for half an hour, and quickly frozen in liquid nitrogen (-196°C). Until their analysis, samples were stored at -80°C. For picoplankton, a yellow-green 1µm latex bead (Polysciences Inc., Warrington, USA) suspension (~10^5 beads mL^{-1}) was added to every sample as an internal standard before being run at an average flowrate of 66.4 ± 2.6 µL·m^{-1} during 150 seconds. Red latex beads of 2 µm diameter (~10^5 beads mL^{-1}, Polysciences Inc.) were used as internal standard in nanoplankton samples, which were run at 165.1 ± 3.0 µL·m^{-1} during 300 seconds. Picoplankton (*Prochlorococcus*, *Synechococcus* and picoeukaryotes) and nanoplankton groups were identified by their signatures in side scatter (SSC) versus red (FL3) and orange (FL2) fluorescence bivariate plots.

In order to estimate pico- and nanoplankton cell-sizes, the flow cytometer was calibrated with nonfluorescent latex beads of 1, 2, 4, 6, 10 and 15 µm diameter (Molecular Probes). SSC's from calibration beads were normalized to the SSC measured for the fluorescent standard beads added to every sample (1 and 2 µm for pico- and nanoplankton settings, respectively). Linear regression between bead diameters and normalized SSC were conducted for picoplankton (ø = 9.914 log (SSC) - 0.219; R^2 = 0.92) and nanoplankton settings (ø = 4.753 log (SSC) + 0.008; R^2 = 0.93). Cell diameters (µm) were inferred from relative SSC for every group and then used to calculate cell biovolume ($µm^3$) assuming a spherical shape. Cell carbon content was estimated using conversion factors obtained from phytoplankton of the Canary waters by Maria F. Montero (unpublished data): 230 fg C $µm^{-3}$ for *Synechococcus*; 237 fg C $µm^{-3}$ for picoeukaryotes; and 220 fg C $µm^{-3}$ for nanoeukaryotes.

Microphytoplankton (20-250 µm cell size) biovolume and biomass (B) were calculated based on microscopy counts of diatoms (Utermöhl, 1931; on a Zeiss Axiovert 100, Carl Zeiss, Germany).

On-site size measurements were performed on all identified diatom species and used to calculate species-specific biovolumes (V) following Hillebrand et al. (1999) and Olenina et al. (2006). Biovolumes were then converted to B using the conversion factor from Menden-Deuer and Lessard (2000) (C [pg $Cell^{-1}$] = 0.288 $V^{0.811}$). Almost all diatom species identified were >20 µm in size, so that we assume no relevant number of organisms <20 µm were falsely categorized as microphytoplankton. Dinoflagellates in this size range were quantified as well, with almost all genera being potentially mixotrophic, heterotrophic or inaccurately categorized (Ortiz et al., 2022). Because the ^{14}C uptake method only measures photosynthetic PP however, dinoflagellates were excluded for better comparability of both datasets.

2.5 Chlorophyll *a*

500 mL subsamples were collected in dark bottles for Chl*a* concentration measurements and sequentially filtered through superimposed Polycarbonate filters of 20 µm, 2 µm and 0.2 µm ø pore size (DHI GVS 20 µm, Hørsholm, Denmark, Whatman Nuclepore 2 µm and 0.2 µm, Maidstone, UK) to obtain Chl*a* concentrations for micro-, nano-, and picophytoplankton, respectively. Filters were then frozen at -20°C until analysis. For pigment extraction the filters were left submerged in 10 ml of acetone (90%) for 24 hours and at 4°C. The extract was subsequently analyzed on a fluorometer (Turner Design AU-10, San Jose, USA) according to Welschmeyer (1994). The sum of all size fractions was taken as total Chl*a*.

2.6 Data Analysis

Simple linear regressions were performed on PP_{cum} and mean PER per unit of nutrients (**Figures 1B**, **2A**) to examine the relationship between upwelling intensity and PP, and to check for differences between both upwelling modes. The control treatment was used twice in the linear regression model analysis of singular and recurring treatments. Statistical comparison of the regression lines of both upwelling modes required the control to be removed, since using the same control for both groups would create a paired data-point in otherwise unpaired data. Data analysis was performed with R (Version 4.0.3, packages stats, ggplot2; The R Foundation, Wickham, 2016). Assumptions of normality and homoscedasticity were tested using q-q and residual versus fitted variable plots.

Due to the strong variability encountered among carbon to Chl*a* ratios (C:Chl*a*) compared to values reported in the literature by e.g., Sathyendranath et al. (2009); Wang et al. (2009) and Jakobsen and Markager (2016), this dataset was additionally checked for outliers using the "outlier_check" function of the performance package in R on each mesocosm (Lüdecke et al., 2021). This function runs a set of 14 outlier detection methods and creates a composite score, based on which it classifies a data point as an outlier. Identified outliers were excluded from **Figure 5**. Carbon assimilation numbers (µg C µg $Chla^{-1}$ h^{-1}) were based on hourly PP rates of the entire incubation period (24h).

3 RESULTS

3.1 Temporal Development of PP, Chl*a*, B and Nutrients

Total PP rates increased between 6.5- and 53-fold in all singular treatments after DW addition and reached their maximum rate either three (low & medium) or five (high & extreme) days after it (**Figure 1A**). Afterwards, PP rates decreased in all singular treatments to <4.5 µmol C L^{-1} d^{-1}, which was still above pre-treatment levels (<0.8 µmol C L^{-1} d^{-1}). Recurring low and medium treatments did not surpass rates of ~3.7 µmol C L^{-1} d^{-1} throughout the experiment (**Figure 1A**). The most variable progression was displayed by the extreme recurring treatment. A pronounced peak with a 38-fold increase in PP on d9 was followed by an immediate drop before steadily increasing until d17. Considering the amount of nutrients added to this treatment in the first addition (1.53 µmol N L^{-1} e.g., comparable to the single addition to low singular), this peak was disproportionately high. Afterwards, extreme recurring PP rates steadily increased until the end of the experiment. Control and Atlantic maintained overall low PP rates (maxima of 1.47 and 1.14 µmol C L^{-1} d^{-1}, respectively).

All treatments showed an increased PP_{cum} compared to the untreated control and the Atlantic. But there was a visible difference in the pattern of increase between upwelling modes: singular upwelling led to a strong PP_{cum} increase after DW addition which then flattened quickly between d11 and d15, while recurring upwelling led to a more stable and steady increase in PP_{cum} until the end of the experiment (**Figure 1C**). Within the low, medium and high upwelling intensities upwelling mode did not lead to large absolute differences in PP_{cum}. Extreme treatments showed by far the highest PP_{cum}, with extreme recurring outperforming singular by a factor of 1.47. Normalized to the amount of nutrients added, the extreme recurring treatment still led to 20% higher PP_{cum}.

An overview on the amount of organic carbon produced (based on PP_{cum}) in each treatment per unit of nutrients added throughout the experiment is shown in **Figure 1B**. Total nutrient supply and cumulative PP were significantly correlated in both treatment groups (R^2 = 0.98/0.99 and $p < 0.001$ for both upwelling modes). The statistical comparison of both groups with each other confirmed that the recurring treatments reached significantly higher PP_{cum} per µmol of nutrients than the singular treatments ($p = 0.029$).

The development of total Chl*a* concentrations exhibited similar trends to those of PP_{POC} (**Figure 1D**): Singular treatments showed initial peaks corresponding to upwelling intensity after the DW addition (i.e., low & medium peaked on d7, high & extreme on d9), while recurring treatments differed more in their development. Responses in Chl*a* concentration to the first addition ranged from a roughly 1.3-fold increase in low

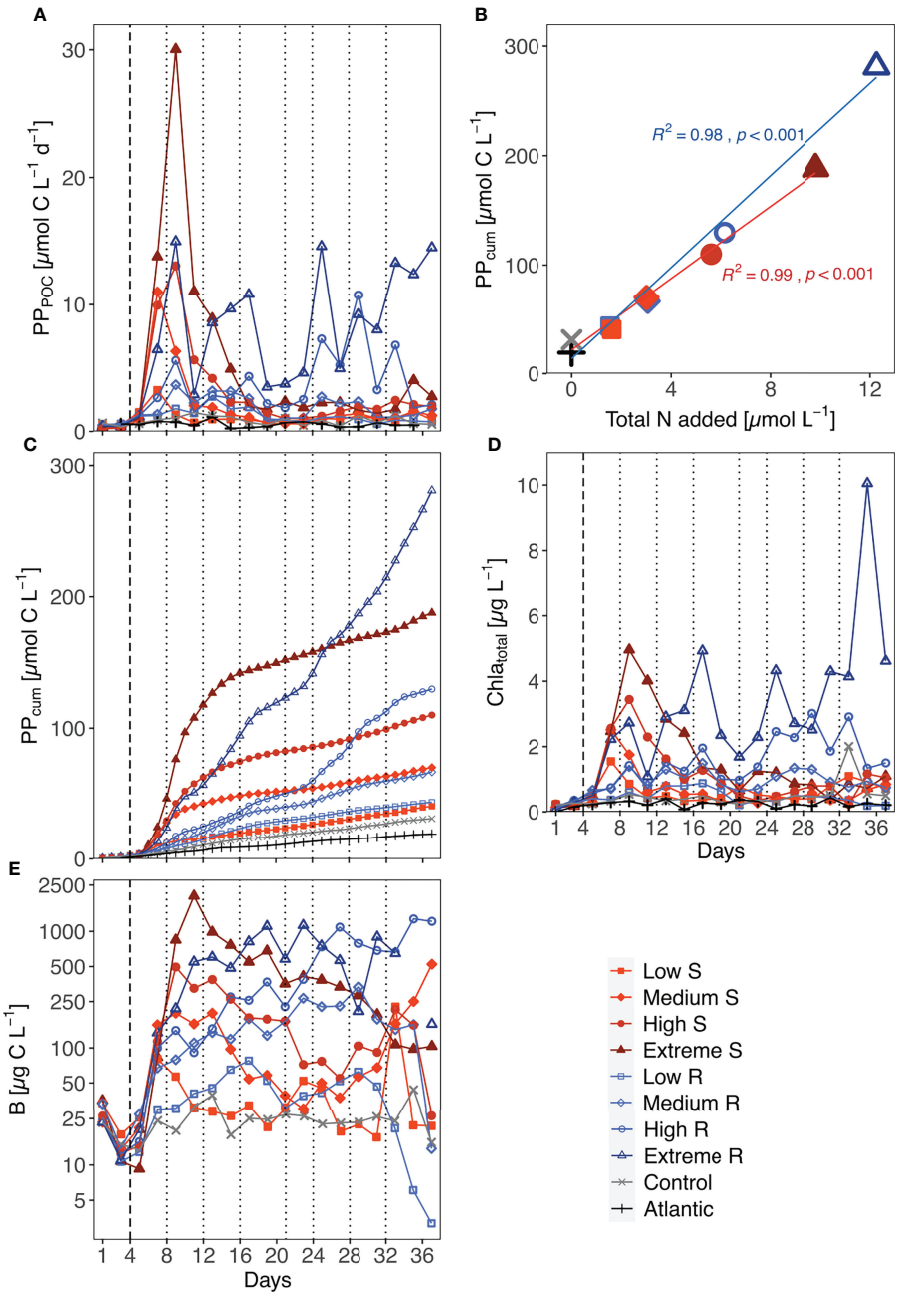

FIGURE 1 | Temporal development of **(A)** total primary production (PP_{POC}), **(C)** accumulated primary production (PP_{cum}, even day data points calculated as described in 2.3), **(D)** total Chla concentration and **(E)** total phytoplankton biomass (mind the logarithmic y-axis scale). Biomass values of the Atlantic were not measured. S, Singular; R, Recurring. **(B)** shows the accumulated organic carbon production per µmol of nutrients added at the end of the experiment. Linear regression shown for singular (n = 5) and recurring (n = 5) treatments; Difference between both upwelling modes as a whole was significant (p=0.029). Dotted lines represent DW additions, dashed line marks the single DW addition to singular treatments.

recurring up to a 28-fold increase in extreme singular. Further DW additions also mostly led to immediate increases in Chl*a* concentrations on the following day. Unexpectedly, Chl*a* concentration decreased in the high recurring after the last DW addition, while it peaked at 10.1 µg L^{-1} in the extreme recurring on d35 before decreasing.

Overall, phytoplankton biomass (B) decreased between closure of the mesocosms and treatment onset. After treatment onset, singular treatment B rose in accordance with upwelling intensity, reaching peak values between 80.26 µg C L^{-1} in the low and 2013.18 µg C L^{-1} in the extreme treatment, before shifting into a steady decrease until the end of the experiment

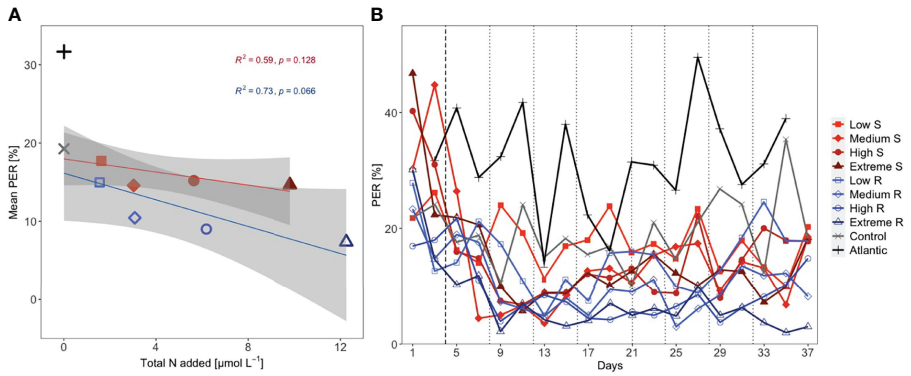

FIGURE 2 | **(A)** Mean percentage extracellular release (PER) per total amount of added nutrients (shaded area: 95% CI) and **(B)** temporal development of PER. Linear regression analysis shown for Singular (S; n = 5) and Recurring (R; n = 5) treatments. Dotted lines represent DW additions, dashed line marks the single DW addition to singular treatments.

(**Figure 1E**). An exception was the medium singular, where B increased during d27-d37. Recurring treatments on the other hand displayed a steady increase in B throughout the treatment period. After the last addition, B in the low and medium recurring treatment decreased substantially, while the high and extreme maintained high B concentrations or even increased until the end in the former.

Singular treatments displayed mean PER values close to the control (14.6-17.7%) and were negatively correlated with increasing upwelling intensity (**Figure 2A**). This pattern was more pronounced in the recurring treatments, with mean PER being highest in the low (15.0%) and lowest in the extreme recurring (7.4%). Mean PER in the control was reduced compared to the Atlantic, amounting to 19.3% and 31.7%, respectively. There was a fairly good correlation between mean PER and nutrient input ($R^2 = 0.59$ for singular and $R^2 = 0.73$ for recurring) although p-values were not significant. The temporal development of PER conveys the same message, with the singular treatments mostly maintaining values above the respective recurring (**Figure 2B**).

Nutrient concentrations peaked in all treatments according to the amounts of DW introduced after the first addition (**Figure 3**). Despite the high nutrient load of the DW (25 µmol L^{-1} NO_3^- , 1.38 µmol L^{-1} PO_4^- and 12.1 µmol L^{-1} $Si(OH)_4$), all nutrients were entirely consumed within five days (by d9) in the singular treatments, while recurring treatments exhausted most nutrients within two days after each addition. Silicate was no longer fully taken up after d27 in the extreme recurring, and ammonium displayed some variability around very low concentrations in most treatments throughout the experiment.

3.2 Size Class Contributions to PP, Chl*a* and B

The initial peaks in PP and Chl*a* in the singular treatments (**Figure 4**, red labels) were increasingly dominated by microphytoplankton with rising upwelling intensity. Overall, the main contribution to PP and Chl*a* came from microphytoplankton, followed towards the end by nanophytoplankton. However, B was composed almost exclusively of microphytoplankton even at the end of the experiment. A shift from micro- to nanophytoplankton as main contributor to B occurred in the low, medium and high singular treatments during the last five days.

The recurring treatments (**Figure 4**, blue labels) displayed a shift away from a more even distribution among all sizes before treatment onset towards a strong dominance of microphytoplankton in PP. Contribution to Chl*a* in the medium, high and extreme recurring treatments came almost exclusively from micro- and nanophytoplankton throughout most of the experiment. Picophytoplankton B was wholly negligible, whereas nanophytoplankton B increased exceptionally in all recurring treatments except low from d33-d35 on, similar to the aforementioned shift in the low, medium and high singular treatment. Simultaneously, microphytoplankton B plummeted during these days until the end of the experiment.

Across all treatments PP_{DOC} did not increase as a consequence of artificial upwelling (**Figure 4** left column). Under singular upwelling, PP_{DOC} increased slightly after the addition, but then receded to pre-treatment levels.

The control and Atlantic (**Figure 4**, bottom plots) displayed mixed size class contributions in all parameters, but with generally higher presence of picophytoplankton, as well as higher DOC contributions to PP than in all the treatments.

3.3 Carbon to Chlorophyll Ratios and Assimilation Numbers

The temporal development of total C:Chl*a* ratios was characterized by strong oscillations, ranging from 1 up to 1708 (**Figure 5**). Looking at the different size fractions it becomes evident that most of the variability was driven by the temporal B changes described in 3.2 and hence by microphytoplankton overall and nanophytoplankton towards the end. Picophytoplankton C:Chl*a* ratios mostly stayed below 150 in the singular and below 100 in the recurring treatments. An impact of upwelling intensity on C:Chla ratios was only recognizable in the singular treatments, where increasing upwelling intensity led to higher values in the total and microphytoplankton fraction.

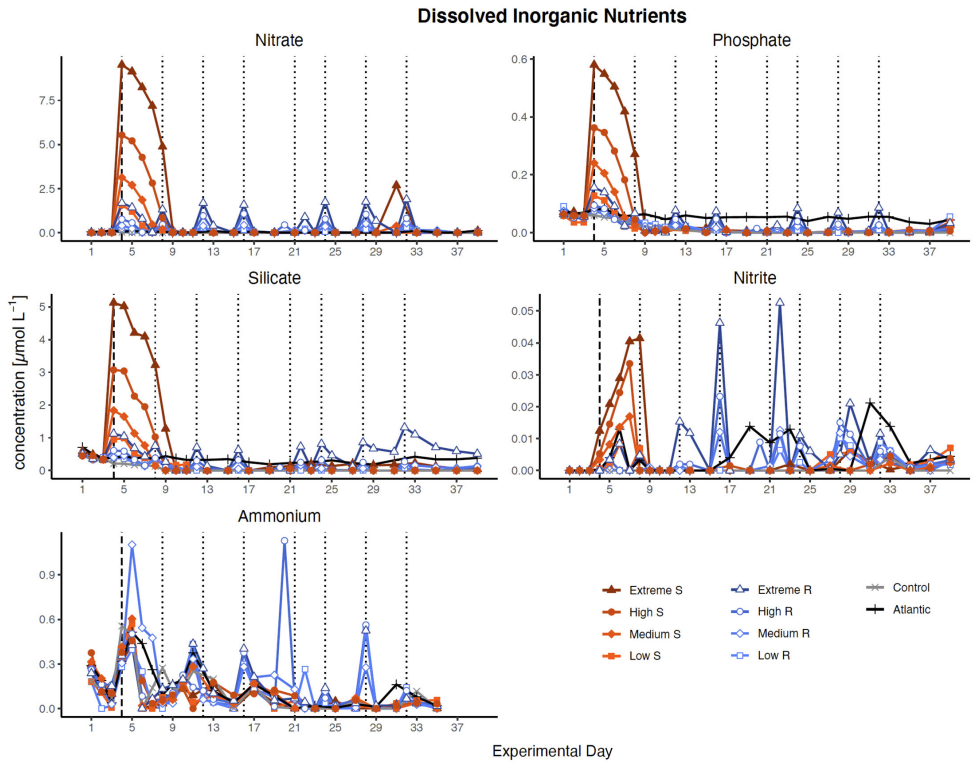

FIGURE 3 | Inorganic nutrient concentration over the course of the study. Dotted lines represent DW additions, dashed line marks the single DW addition to singular treatments. S, singular, R, recurring treatment. Atlantic refers to samples taken from the water surrounding the mesocosm field.

Assimilation numbers (as the rate of carbon produced per unit Chl*a*) were not strongly affected by upwelling intensity nor upwelling mode though variability increased with upwelling intensity among microphytoplankton in the singular treatments. (**Figure 6**; **Supplementary Figure S2**). Mean AN of pico- and nanophytoplankton ranged from 0.59 ± 0.35 - 1.87 ± 1.89 µg C µg Chla^{-1} h^{-1}, while those of microphytoplankton reached values of 1.87 ± 0.82 - 2.98 ± 2.83 µg C µg Chla^{-1} h^{-1}.

4 DISCUSSION

4.1 Developments Within the Primary Producer Community

Poulton et al. (2006) reasonably argued that time is a crucial factor when environmental forcing, in this case artificial upwelling, is applied. On a short time scale the community likely responds through metabolic adaptation, whereas on a long time scale these adaptations lead to actual trophic reorganization. Our results show that, on the primary producer level, both metabolic and trophic adaptation occurred as a consequence of artificial upwelling. This became evident in form of (i) permanent shifts in the dominating size classes towards larger phytoplankton (**Figure 4**), (ii) reduction of PER compared to the control (**Figure 2**) and (iii) increased B build-up and PP_{cum} until the end of our experiment (**Figures 3**, **1C**). While the magnitude of the observed effects mostly increased with increasing upwelling intensity, as expected, some effects such as the increase in PP_{cum} were only very prominent in the high and extreme upwelling intensities. Simultaneously, all observed effects (i)-(iii) were more pronounced under recurring upwelling compared to the respective singular upwelling intensities (or a synthesis of the main results surrounding PP, B and PER see **Figure 7**). This happened most probably because the singular treatments ran into strong nutrient limitation after all nutrients introduced by the DW addition were consumed.

The size class shift was due to a strong increase in diatom abundance, followed by *Prymnesiophyceae* which became more abundant towards the end of the experiment (Ortiz et al., 2022). This is in accordance with large amounts of literature describing succession patterns of small picophytoplankton under oligotrophic to larger microphytoplankton (mainly diatoms) under nutrient replete conditions both in the field and mesocosm experiments (Mann, 1993; Arístegui et al., 2004; Fawcett and Ward, 2011). On the other hand, the *in situ* application of artificial upwelling conducted by Masuda et al. (2010) showed increased growth of pico- and nanophytoplankton rather than diatoms. They suggested this could have been due to low light availability in the artificially

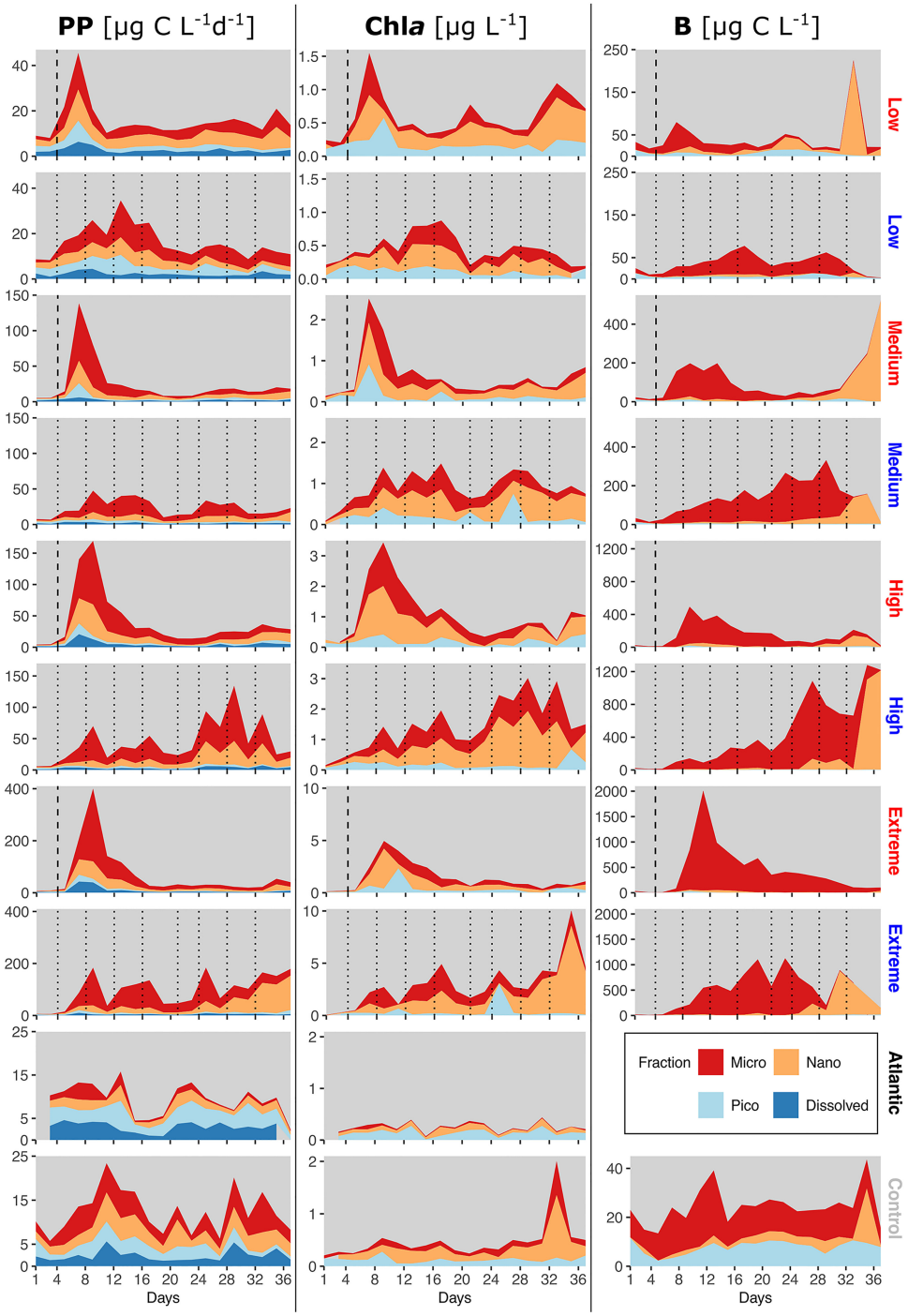

FIGURE 4 | Relative size class contributions of micro-, nano- and picoplankton to total PP rates, Chla concentration and phytoplankton C. PP plots also include PP_{DOC} rates. Mind the different y-axis scales. The blank spot in the Atlantic between d35-37 is due to one missing data point. Dotted lines represent DW additions, dashed line marks the single DW addition to singular treatments. Recurring treatments labelled in blue, singular in red.

fertilized waters combined with insufficient shade adaptation of diatom species, the former of which was not the case in our experiment. Other possibilities such as silicate limitation were not discussed. Compared to an *in situ* application, phytoplankton in the mesocosms can be more strongly affected by differences in the seed communities enclosed at the start. However, we did not find compelling evidence for large differences in the starting communities. Responses to artificial

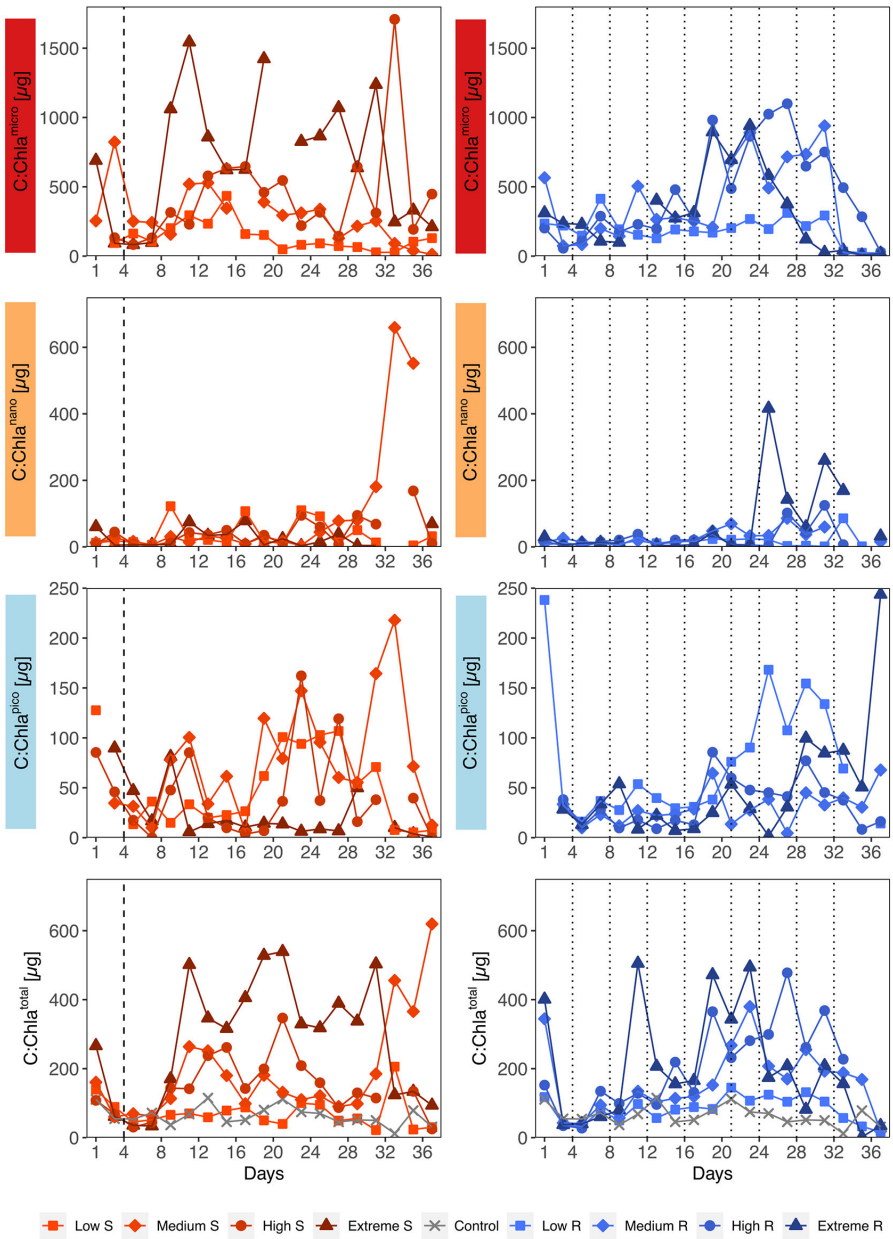

FIGURE 5 | Temporal development of carbon to chlorophyll ratios (C:Chla) separated by size fractions and upwelling mode. S, Singular; R, Recurring. Mind the different y-axis scales. Dotted lines represent DW additions, dashed line marks the single DW addition to singular treatments.

upwelling were spearheaded by Diatoms in all treatments, with *L. danicus*, *L. minimus* and *G. striata* as the main contributors to biomass (Ortiz et al., 2022).

The late *Prymnesiophyceae* increase was, at least in the medium, high and extreme recurring treatment, identified as a strong bloom of coccolithophores from d29 onwards (unpublished data), which explains the almost exclusive contribution of nanophytoplankton to biomass (PP and Chl*a* to a lesser extent) during those last days. What exactly triggered this bloom remains unclear though. In the singular treatments, the extended period of nutrient depletion might have promoted a terminal shift towards more nano- and less microphytoplankton, as smaller cells have been shown to have physiological advantages under oligotrophic conditions (Sommer et al., 2017). Based on experience from previous mesocosm studies we know that *Prochlorococcus*, a globally present and typically dominant species under the oligotrophic conditions in these waters, sometimes doesn't thrive well in the mesocosm

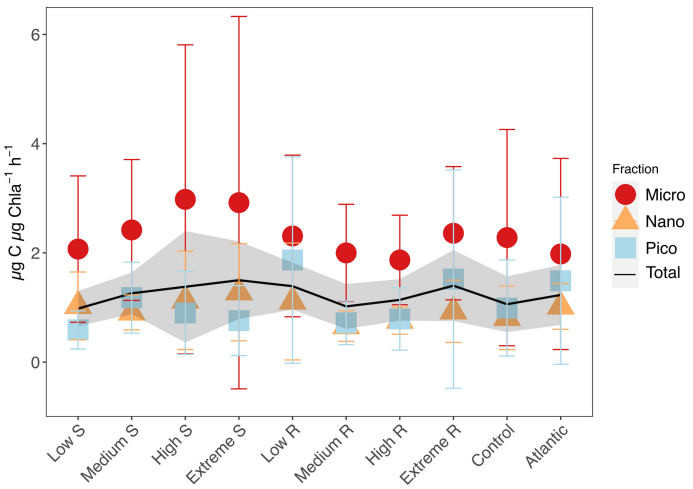

FIGURE 6 | Mean carbon assimilation numbers (AN) and standard deviations for total phytoplankton, microphytoplankton (20-250 μm), nanophytoplankton (2-20 μm) and picophytoplankton (0.2-2 μm). Shaded area shows standard deviation for total phytoplankton AN.

enclosures (Schulz et al., 2017). Apart from the grazing pressure affecting the picophytoplankton overall, this has been attributed to the sudden reduction in the mixed layer depth and consequently higher light exposure inside, to which these genera are more sensitive (Llabrés and Agustí, 2006) and offers an explanation to why they did not pick up more in the singular treatments after these became nutrient-depleted again.

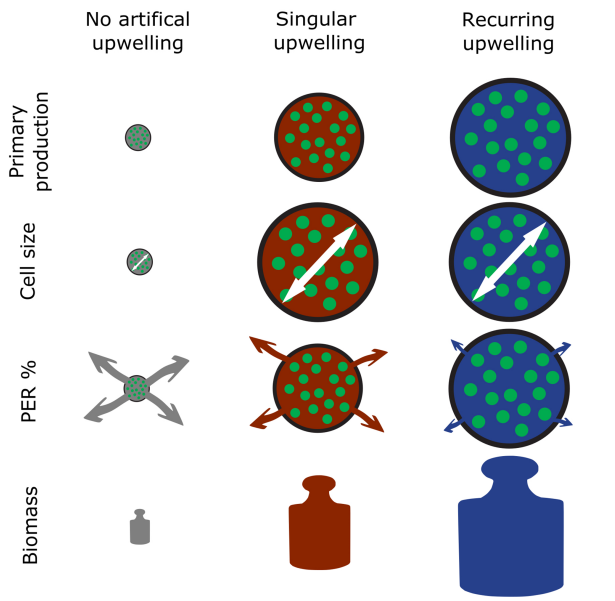

FIGURE 7 | Schematic depiction of the main findings surrounding primary production in this study. PER, Percentage Extracellular Release. The white arrows illustrate cell size and arrows under PER% the magnitude of extracellular release.

Synechococcus, similarly prevalent in these waters, might have failed to increase in abundance due to grazing. In summary, all treatments displayed trophic reorganization, but the extent scaled with upwelling intensity.

Another key message lies in the changes in PER. DOC produced by phytoplankton serves as substrate for heterotrophs. Unless recirculated through the microbial loop, it does not contribute to the pool of particulate organic material consumed by higher trophic levels such as copepods (Fogg, 1983; Cushing, 1989). Compared to the Atlantic, all treatments and the control led to a strong reduction in PER. But PER in the treatments was still consistently lower than in the control, and much more under recurring mode. The negative relationship between PER and the amount of added nutrients in the recurring treatments (**Figures 2A, B**) indicates a better suitability of high intensity recurring upwelling to fuel a food web that ultimately sustains harvestable fish, since less organic carbon would be lost to heterotrophic bacteria. This pattern is also consistent with literature PER values of naturally nutrient-rich (low PER) and oligotrophic (high PER) waters, placing the high and extreme recurring treatments in the spectrum of nutrient-replete upwelling areas (Teira et al., 2001; Teira et al., 2003). It is worth noting that the PER values obtained likely reflect "net" PER at equilibrium with bacterial uptake of PP_{DOC} rather than the gross amount of exudate released given the long incubation times applied (Wolter, 1982), and might therefore be underestimated. Shorter incubation times are commonly used to measure gross amounts of exudate release, as PP_{DOC} rates are influenced by bacterial uptake lag phases in release kinetics (Lancelot, 1979; López-Sandoval et al., 2013). Moreover, nutrient limitation under singular as well as low intensity recurring DW supply likely led to not only increased phytoplankton PER, but also to reduced bacterial uptake of exudates (Obernosterer and Herndl, 1995). In summary with the other main findings (i-iii) this supports the conclusion, that long-term intense recurring upwelling is better suited to achieve a permanent shift from an oligotrophic

community to one resembling that of productive upwelling regions. At least on the primary producer level this change was achieved during our experiment, visible in the higher PP_{cum} and lower PER under elevated upwelling intensity (**Figures 1B**, **2**) as well as the marked shift in PP and B (Chl*a* less so) contributions from pico-/nano- towards nano-/microphytoplankton (**Figure 4**). Though the singular treatments also displayed a similar development, PP rates and B of the high and extreme mostly remained below those of their recurring counterparts, apart from the initial peaks. Ortiz et al. (2022) also reported an analogous development in the metabolic balance (net community production and ratio of gross production versus respiration) of the phytoplankton community: Recurring treatments of medium to extreme upwelling intensity consistently maintained a net autotrophic state whereas singular treatments swiftly reassumed a balanced to net heterotrophic state after nutrient depletion.

Comparison of our data with *in situ* PP measurements from the vicinity of the islands was only possible for total PP rates, since we found no reported measurements on size-fractionated PP for this region except for one dataset from the Atlantic Meridional Transect, several hundred kilometers away, collected by Marañón et al. (2001; 1.2-7.2 μg C L^{-1} d^{-1} with highest rates being PP_{pico}). Peak PP_{POC} rates measured in the Canary Islands area during blooms or higher production periods range from 913 to 2780 mg C m^{-2} d^{-1} (**Supplementary Table 1**). Peak PP rates obtained in the recurring treatments were comparable to this, while the singular extreme treatment reached PP rates almost 1.7 times higher (4689 mg C m^{-2} d^{-1}). The mean PP rates, on the other hand, were within the spectrum found during upwelling periods or other settings supporting elevated production (**Supplementary Table 1**). This confirms that the scenarios simulated in the mesocosms are realistic and that the phytoplankton community adjusted to artificial upwelling the same way it adjusts to natural nutrient input events. The particularly low PP in the control mesocosm and Atlantic samples matches the low productivity season in which the experiment took place (Arístegui, 1990). And although the general trends of increased system productivity under artificial upwelling align, comparative interpretation of the few previous *in situ* applications of artificial upwelling is difficult, due to strongly varying time-scales (hours to years of monitoring) and different parameters used by other authors; such as surface layer Chl*a* values (as opposed to depth integrated), plankton standing stocks or species diversity/richness indexes (Masuda et al., 2010; Jeong et al., 2013).

4.2 Carbon Dynamics and Implications for Primary Production Models

Assimilation numbers (μg C μg Chla^{-1} h^{-1}) were not impacted much by the different treatments except for a slight increase in mean microphytoplankton AN with increasing upwelling intensity (**Figure 6**), which can be attributed to the few very high datapoints that skewed the mean values. Microphytoplankton having generally higher AN than smaller phytoplankton is consistent with literature (Poulton et al., 2006; Cotti-Rausch et al., 2020). The absence of a strong upwelling mode or intensity effect on AN seems counterintuitive, but follows observations made by Harrison and Platt (1980) and Falkowski (1981) that showed no observable relationship between available total inorganic nitrogen and AN. Marra et al. (2007) argued that environmental variability is better described by pigment absorption properties rather than the quantity of Chl*a*. A case also made by Milligan et al. (2015), who further summarized the substantial evidence on AN not reflecting the availability of nutrients. Moreover, AN also decrease due to increased packaging and consequent decreased absorption efficiency when the average cell size increases (Bricaud et al., 1995). All this offers an explanation to the non-existent impact on Chl*a* concentration-based AN in our experiment despite the forcing of substantial stoichiometric changes on the community through the treatment.

We interpret the high variability found across C:Chl*a* ratios in all size fractions and especially among microphytoplankton with some caution, due to constraints related to the biomass estimates discussed later in 4.3. But it nonetheless picks up on an issue that has been raised repeatedly in ecosystem production models: an over-simplified depiction of the primary producer community (Marañón et al., 2000; Marañón et al., 2001; Richardson, 2019). Chl*a*-based models mostly assume constant C:Chl*a* ratios and cell sizes and directly translate changes in Chl*a* to B (Westberry et al., 2008; Silsbe et al., 2016), although it has been shown that the relationship between Chl*a* and B is not necessarily linear (Saba et al., 2010; Pasqueron De Fommervault et al., 2017). Our findings support the critique on this over-simplified approach. Although more recent models like the Carbon-based Productivity Model (CbPM) and the Carbon, Absorption, and Fluorescence Euphotic-resolving model (CAFE) have improved at this, the issue still persists (Westberry and Behrenfeld, 2014). Baklouti et al. (2021) have coherently summarized both the ongoing debate in this topic as well as the importance of considering detailed information and variability on phytoplankton elemental stoichiometry, abundances and cell size shifts, the latter of which is highlighted by our findings. Oddly enough, model validation with *in situ* data also seems to completely ignore the influence of major players in global ocean primary production like eastern boundary upwelling systems.

4.3 Interpretational Limitations

Large mesocosm experiments of this type bring about their own set of caveats and limitations as is thoroughly discussed by, e.g., Bach et al. (2020) (and more generally by Gamble and Davies (1982)). Perhaps the most evident is the small number of replicates imposed by the technical and logistical efforts that go into experiments of this magnitude. In this study we chose two different upwelling modes on top of different intensities in order to enhance the topical scope of the study, although this meant limiting the statistical power since the regression analyses had to be run through a small number of data points only. Moreover, compared to the Atlantic, there was a reduction of both PER (**Figure 2**) and overall picophytoplankton contribution to PP and Chl*a* (**Figure 4**) in the control. Whether this could represent an enclosure effect is unclear, since the Atlantic was obviously subject to constant changes and is therefore not directly comparable to any mesocosm unit. Notwithstanding, all treatments differed strongly from the control in their development and the establishment of

similar starting conditions (see d1-d3 in **Figures 1** and **3**) also worked well. Hence, we are confident that the results discussed are a realistic representation of how oligotrophic communities of the subtropical Atlantic would react to artificial upwelling.

The unusually high C:Chl*a* ratios found among microphytoplankton (**Figure 5**, top row) also demand further discussion, as these exceeded the highest values we found in literature (Sathyendranath et al., 2009). Literature C:Chl*a* values are often based on total particulate organic carbon rather than calculated phytoplankton B and only few authors have gone through the lengths of additional fractionations to differentiate between C:Chl*a* ratios of micro-, nano-, and/or picophytoplankton (e.g., Pérez et al., 2006; Calvo-Díaz et al., 2008). Going into size fractionated C:Chl*a* ratios increases the detail richness of the data, but comes at a cost of added uncertainty. In our case, we assume that we might have slightly overestimated microphytoplankton B, since small errors in size measurements using light microscopy can get enhanced along the conversion from size to biovolume and biovolume to biomass. Which in turn strongly affects the C:Chl*a* ratio, particularly at low Chl*a* concentrations. This is less likely for nano- and picophytoplankton, because the applied method, flow cytometry, is less prone to human error (see section 2.4).

4.4 Conclusions

In summary, artificial upwelling applied to an oligotrophic plankton community led to increases in PP, PP_{cum}, Chl*a* and B that scaled linearly with upwelling intensity (illustrated in **Figure 7**). Larger phytoplankton size classes benefitted disproportionately stronger from the upwelling of inorganic nutrients, leading to a shift in the phytoplankton community composition towards larger cells, predominantly composed of diatoms. The observed stimulation in primary production, build-up in phytoplankton biomass and shift in community structure in response to artificial upwelling are well within the range of the seasonal variation occurring in this region, with enhanced productivity and accumulation of larger-sized phytoplankton typically occurring under intensified vertical mixing in mid to late winter. The observed responses differed with regard to the applied mode of artificial upwelling. Under high upwelling intensity the recurring treatments generated more B than their singular counterparts and yielded significantly higher PP_{cum} per unit of nutrient supply. The loss of primary produced organic matter *via* extracellular release (PER) declined with increasing upwelling intensity and was lower in the recurring compared to the singular upwelling mode. Our results demonstrate that (i) oligotrophic phytoplankton communities are capable to rapidly and effectively adjust to artificial upwelling, (ii) this response is independent of the upwelling intensity, i.e. it scales linearly with the mixing ratio of nutrient-rich deep to nutrient-impoverished surface waters, and (iii) the response differs depending on the upwelling mode, with recurring upwelling yielding higher rates of primary production, stronger biomass build-up per unit of deep-water nutrient supply and lower extracellular release of primary produced organic matter than single pulsed upwelling. These findings indicate that a key objective of artificial upwelling, the efficient use of upwelled nutrients by the larger phytoplankton size fractions, is met even under conditions where the resident community is adapted to highly oligotrophic conditions. This opens up the pathway for either a more efficient transfer of primary produced organic matter to higher trophic levels or enhanced export efficiency *via* organic matter sinking.

DATA AVAILABILITY STATEMENT

The raw data supporting the conclusions of this article will be made available by the authors, without undue reservation.

AUTHOR CONTRIBUTIONS

Experimental concept and design: UR, JA. Execution of the experiment: All authors. Data analysis: JO, NH-H, MF-M. Manuscript writing: JO with input from all co-authors. All authors contributed to the article and approved the submitted version.

FUNDING

This project was conducted in the framework of the project *Ocean Artificial Upwelling* (*Ocean artUp*) funded by an Advanced Grant of the European Research Council. Additional support was provided through Transnational Access funds by the EU project AQUACOSM, EU H2020-INFRAIA-project No. 731065, and by project TRIATLAS (AMD-817578-5) from the European Union's Horizon 2020 to JA. JA was also supported by a Helmholtz International Fellow Award, 2015 (Helmholtz Association, Germany).

ACKNOWLEDGMENTS

The authors are grateful to the Oceanic Platform of the Canary Islands (PLOCAN) and its staff for the use of their facilities, and for their hospitality and help with the logistics and organization of this research campaign. We thank the biological oceanography group of the University of Las Palmas de Gran Canaria (GOB-ULPGC) for providing additional lab facilities. The captain and crew of RV James Cook are thanked for deploying the mesocosms and collecting the deep water. Special thanks go to the KOSMOS team of GEOMAR for taking care of all logistical and technical aspects of this mesocosm campaign and for coordinating the research activities on site as well as the data management and exchange.

SUPPLEMENTARY MATERIAL

The Supplementary Material for this article can be found online at: https://www.frontiersin.org/articles/10.3389/fmars.2022.880550/full#supplementary-material

REFERENCES

Arístegui, J. (1990). La Distribución De La Clorofila a En Aguas De Canarias. *Boletín. Del. Inst. Español. Oceanogr.* 6, 61–71.

Arístegui, J., Barton, E. D., Tett, P., Montero, M. F., García-Muñoz, M., Basterretxea, G., et al. (2004). Variability in Plankton Community Structure, Metabolism, and Vertical Carbon Fluxes Along an Upwelling Filament (Cape Juby, NW Africa). *Prog. Oceanogr.* 62, 95–113. doi: 10.1016/j.pocean.2004.07.004

Aure, J., Strand, Ø., Erga, S. R., and Strohmeier, T. (2007). Primary Production Enhancement by Artificial Upwelling in a Western Norwegian Fjord. *Mar. Ecol. Prog. Ser.* 352, 39–52. doi: 10.3354/meps07139

Bach, L. T., Paul, A. J., Boxhammer, T., von der Esch, E., Graco, M., Schulz, K. G., et al. (2020). Factors Controlling Plankton Community Production, Export Flux, and Particulate Matter Stoichiometry in the Coastal Upwelling System Off Peru. *Biogeosciences* 17, 4831–4852. doi: 10.5194/bg-17-4831-2020

Baklouti, M., Pagès, R., Alekseenko, E., Guyennon, A., and Grégori, G. (2021). On the Benefits of Using Cell Quotas in Addition to Intracellular Elemental Ratios in Flexible-Stoichiometry Plankton Functional Type Models. Application to the Mediterranean Sea. *Prog. Oceanogr.* 197, 102634. doi: 10.1016/j.pocean.2021.102634

Bricaud, A., Babin, M., Morel, A., and Claustre, H. (1995). Variability in the Chlorophyll-Specific Absorption Coefficients of Natural Phytoplankton : Analysis and Parameterization Phytoplankton a • H (A) was Analyzed Using a Data Set Including 815 Spectra Determined Chlorophyll Concentration Range Ph Values Wer. *J. Geophys. Res.* 100, 13321–13332. doi: 10.1029/95JC00463

Calvo-Díaz, A., Morán, X. A. G., and Suárez, L.Á. (2008). Seasonality of Picophytoplankton Chlorophyll a and Biomass in the Central Cantabrian Sea, Southern Bay of Biscay. *J. Mar. Syst.* 72, 271–281. doi: 10.1016/j.jmarsys.2007.03.008

Casareto, B. E., Niraula, M. P., and Suzuki, Y. (2017). Marine Planktonic Ecosystem Dynamics in an Artificial Upwelling Area of Japan: Phytoplankton Production and Biomass Fate. *J. Exp. Mar. Bio. Ecol.* 487, 1–10. doi: 10.1016/j.jembe.2016.11.002

Cermeño, P., Fernández, A., and Marañón, E. (2012). *"Libro Blanco De Métodos Y Técnicas De Trabajo Oceanográfico (MALASPINA 2010): Determinación De La Producción Primaria Fraccionada Por Tamaños"*. Ed. E Moreno-Ostos. (S.A., Spain: Gráficas/85).

Cotti-Rausch, B. E., Lomas, M. W., Lachenmyer, E. M., Baumann, E. G., and Richardson, T. L. (2020). Size-Fractionated Biomass and Primary Productivity of Sargasso Sea Phytoplankton. *Deep. Res. Part I Oceanogr. Res. Pap.* 156, 103141. doi: 10.1016/j.dsr.2019.103141

Cushing, D. H. (1989). A Difference in Structure Between Ecosystems in Strongly Stratified Waters and in Those That are Only Weakly Stratified. *J. Plankton. Res.* 11, 1–13. doi: 10.1093/plankt/11.1.1

Falkowski, P. G. (1981). Light-Shade Adaptation and Assimilation Numbers. *J. Plankton. Res.* 3, 203–216. doi: 10.1093/plankt/3.2.203

Fawcett, S. E., and Ward, B. B. (2011). Phytoplankton Succession and Nitrogen Utilization During the Development of an Upwelling Bloom. *Mar. Ecol. Prog. Ser.* 428, 13–31. doi: 10.3354/meps09070

Fogg, G. E. (1983). The Ecological Significance of Extracellular Products of Phytoplankton Photosynthesis. *Bot. Mar.* 26, 3–14. doi: 10.1515/botm.1983.26.1.3

Frölicher, T. L., Rodgers, K. B., Stock, C. A., and Cheung, W. W. L. (2016). Sources of Uncertainties in 21st Century Projections of Potential Ocean Ecosystem Stressors. *Global Biogeochem. Cycle.* 30, 1224–1243. doi: 10.1111/1462-2920.13280

Gamble, J. C., and Davies, J. M. (1982). ""Application of Enclosures to the Study of Marine Pelagic Systems,"," in *Marine Mesocosms - Biological and Chemical Research in Experimental Ecosystems*. Eds. G. D. Grice and M. R. Reeve (New York: Springer). doi: 10.1007/978-1-4612-5645-8

GESAMP (2019). "High Level Review of a Wide Range of Proposed Marine Geoengineering Techniques," in *GESAMP Reports Stud*, 144. Available at: http://www.gesamp.org/publications/high-level-review-of-a-wide-range-of-proposed-marine-geoengineering-techniques. (London, UK: International Maritime Organisation).

Giraud, M., Boye, M., Garçon, V., Donval, A., and de la Broise, D. (2016). Simulation of an Artificial Upwelling Using Immersed *in Situ* Phytoplankton Microcosms. *J. Exp. Mar. Bio. Ecol.* 475, 80–88. doi: 10.1016/j.jembe.2015.11.006

Handå, A., McClimans, T. A., Reitan, K. I., Knutsen, Ø., Tangen, K., and Olsen, Y. (2014). Artificial Upwelling to Stimulate Growth of non-Toxic Algae in a Habitat for Mussel Farming. *Aquac. Res.* 45, 1798–1809. doi: 10.1111/are.12127

Harrison, W. G., and Platt, T. (1980). Variations in Assimilation Number of Coastal Marine Phyto-Phytoplankton: Effects of Environmental Co-Variates. *J. Plankton. Res.* 2, 249–260. doi: 10.1093/plankt/2.4.249

Hernández-Hernández, N., Bach, L. T., Montero, M. F., Taucher, J., Baños, I., Guan, W., et al. (2018). High CO 2 Under Nutrient Fertilization Increases Primary Production and Biomass in Subtropical Phytoplankton Communities: A Mesocosm Approach. *Front. Mar. Sci.* 5. doi: 10.3389/fmars.2018.00213

Hillebrand, H., Dürselen, C. D., Kirschtel, D., Pollingher, U., and Zohary, T. (1999). Biovolume Calculation for Pelagic and Benthic Microalgae. *J. Phycol.* 35, 403–424. doi: 10.1046/j.1529-8817.1999.3520403.x

Jakobsen, H. H., and Markager, S. (2016). Carbon-To-Chlorophyll Ratio for Phytoplankton in Temperate Coastal Waters: Seasonal Patterns and Relationship to Nutrients. *Limnol. Oceanogr.* 61, 1853–1868. doi: 10.1002/lno.10338

Jeong, Y. K., Lee, H. N., Park, C., Kim, D. S., and Kim, M. C. (2013). Variation of Phytoplankton and Zooplankton Communities in a Sea Area, With the Building of an Artificial Upwelling Structure. *Anim. Cells Syst. (Seoul).* 17, 63–72. doi: 10.1080/19768354.2012.754381

Kirke, B. (2003). Enhancing Fish Stocks With Wave-Powered Artificial Upwelling. *Ocean. Coast. Manage.* 46, 901–915. doi: 10.1016/S0964-5691(03)00067-X

Lancelot, C. (1979). Gross Excretion Rates of Natural Marine Phytoplankton and Heterotrophic Uptake of Excreted Products in the Southern North Sea, as Determined by Short-Term Kinetics. *Mar. Ecol. Prog. Ser.* 1, 179–186. doi: 10.3354/meps001179

Li, G., Cheng, L., Zhu, J., Trenberth, K. E., Mann, M. E., and Abraham, J. P. (2020). Increasing Ocean Stratification Over the Past Half-Century. *Nat. Clim. Change* 10, 1116–1123. doi: 10.1038/s41558-020-00918-2

Llabrés, M., and Agustí, S. (2006). Picophytoplankton Cell Death Induced by UV Radiation: Evidence for Oceanic Atlantic Communities. *Limnol. Oceanogr.* 51, 21–29. doi: 10.4319/lo.2006.51.1.0021

López-Sandoval, D. C., Rodríguez-Ramos, T., Cermeño, P., and Marañón, E. (2013). Exudation of Organic Carbon by Marine Phytoplankton: Dependence on Taxon and Cell Size. *Mar. Ecol. Prog. Ser.* 477, 53–60. doi: 10.3354/meps10174

Lovelock, J. E., and Rapley, C. G. (2007). Ocean Pipes Could Help the Earth to Cure Itself. *Nature* 449, 2007. doi: 10.1038/449403a

Lüdecke, D., Ben-Shachar, M., Patil, I., Waggoner, P., and Makowski, D. (2021). Performance: An R Package for Assessment, Comparison and Testing of Statistical Models. *J.f Open Source Softw* 6 (60), 3139. doi: 10.21105/joss.03139

Mann, K. H. (1993). Physical Oceanography, Food Chains, and Fish Stocks: A Review. *ICES. J. Mar. Sci.* 50, 105–119. doi: 10.1006/jmsc.1993.1013

Marañón, E., Holligan, P. M., Barciela, R., González, N., Mouriño, B., Pazó, M. J., et al. (2001). Patterns of Phytoplankton Size Structure and Productivity in Contrasting Open-Ocean Environments. *Mar. Ecol. Prog. Ser.* 216, 43–56. doi: 10.3354/meps216043

Marañón, E., Holligan, P. M., Varela, M., Mouriño, B., and Bale, A. J. (2000). Basin-Scale Variability of Phytoplankton Biomass, Production and Growth in the Atlantic Ocean. *Deep. Res. Part I Oceanogr. Res. Pap.* 47, 825–857. doi: 10.1016/S0967-0637(99)00087-4

Marra, J., Trees, C. C., and O'Reilly, J. E. (2007). Phytoplankton Pigment Absorption: A Strong Predictor of Primary Productivity in the Surface Ocean. *Deep. Res. Part I Oceanogr. Res. Pap.* 54, 155–163. doi: 10.1016/j.dsr.2006.12.001

Maruyama, S., Tsubaki, K., Taira, K., and Sakai, S. (2004). Artificial Upwelling of Deep Seawater Using the Perpetual Salt Fountain for Cultivation of Ocean Desert. *J. Oceanogr.* 60, 563–568. doi: 10.1023/B:JOCE.0000038349.56399.09

Maruyama, S., Yabuki, T., Sato, T., Tsubaki, K., Komiya, A., Watanabe, M., et al. (2011). Evidences of Increasing Primary Production in the Ocean by Stommel's Perpetual Salt Fountain. *Deep. Res. Part I Oceanogr. Res. Pap.* 58, 567–574. doi: 10.1016/j.dsr.2011.02.012

Masuda, T., Furuya, K., Kohashi, N., Sato, M., Takeda, S., Uchiyama, M., et al. (2010). Lagrangian Observation of Phytoplankton Dynamics at an Artificially Enriched Subsurface Water in Sagami Bay, Japan. *J. Oceanogr.* 66, 801–813. doi: 10.1007/s10872-010-0065-1

McAndrew, P. M., Björkman, K. M., Church, M. J., Morris, P. J., Jachowski, N., Williams, P. J. L. B., et al. (2007). Metabolic Response of Oligotrophic Plankton

Communities to Deep Water Nutrient Enrichment. *Mar. Ecol. Prog. Ser.* 332, 63–75. doi: 10.3354/meps332063

McClimans, T. A., Handå, A., Fredheim, A., Lien, E., and Reitan, K. I. (2010). Controlled Artificial Upwelling in a Fjord to Stimulate non-Toxic Algae. *Aquac. Eng.* 42, 140–147. doi: 10.1016/j.aquaeng.2010.02.002

Menden-Deuer, S., and Lessard, E. J. (2000). Carbon to Volume Relationships for Dinoflagellates, Diatoms, and Other Protist Plankton. *Limnol. Oceanogr.* 45, 569–579. doi: 10.4319/lo.2000.45.3.0569

Milligan, A. J., Halsey, K. H., and Behrenfeld, M. J. (2015). HORIZONS:Advancing Interpretations of 14C-Uptake Measurements in the Context of Phytoplankton Physiology and Ecology. *J. Plankton. Res.* 37, 692–698. doi: 10.1093/plankt/fbv051

Miyabe, H., Kobayashi, H., and Ogiwara, S. (2004). Development of the Floating Structure for the Ocean Nutrient Enhancer "TAKUMI." *Ocean '04 - MTS/IEEE Techno-Ocean '04 Bridg. Across Ocean. - Conf. Proc.* 1, 348–353. doi: 10.1109/oceans.2004.1402940

Obernosterer, I., and Herndl, G. J. (1995). Phytoplankton Extracellular Release and Bacterial Growth: Dependence on the Inorganic N:P Ratio. *Mar. Ecol. Prog. Ser.* 116, 247–258. doi: 10.3354/meps116247

Olenina, I., Hajdu, S., Edler, L., Andersson, A., Wasmund, N., Busch, S., et al. (2006). Biovolumes and Size-Classes of Phytoplankton in the Baltic Sea.

Ortiz, J., Arístegui, J., Taucher, J., and Riebesell, U. (2022). Artificial Upwelling in Singular and Recurring Mode : Consequences for Net Community Production and Metabolic Balance. *Front. Mar. Sci.* 8, 1–10. doi: 10.3389/fmars.2021.743105

Pasqueron De Fommervault, O., Perez-Brunius, P., Damien, P., Camacho-Ibar, V. F., and Sheinbaum, J. (2017). Temporal Variability of Chlorophyll Distribution in the Gulf of Mexico: Bio-Optical Data From Profiling Floats. *Biogeosciences* 14, 5647–5662. doi: 10.5194/bg-14-5647-2017

Perez, F. F., Castro, C. G., Alvarez, M., Kortzinger, A., Santana-casiano, M., Rueda, M. J., et al. (2001). Mixing Analysis of Nutrients, Oxygen and Inorganic Carbon in the Canary Islands Region. *J. Mar. Syst.* 28, 183–201. doi: 10.1016/S0924-7963(01)00003-3

Pérez, V., Fernández, E., Marañón, E., Morán, X. A. G., and Zubkov, M. V. (2006). Vertical Distribution of Phytoplankton Biomass, Production and Growth in the Atlantic Subtropical Gyres. *Deep. Res. Part I Oceanogr. Res. Pap.* 53, 1616–1634. doi: 10.1016/j.dsr.2006.07.008

Poulton, A. J., Holligan, P. M., Hickman, A., Kim, Y. N., Adey, T. R., Stinchcombe, M. C., et al. (2006). Phytoplankton Carbon Fixation, Chlorophyll-Biomass and Diagnostic Pigments in the Atlantic Ocean. *Deep. Res. Part II. Top. Stud. Oceanogr.* 53, 1593–1610. doi: 10.1016/j.dsr2.2006.05.007

Richardson, T. L. (2019). Mechanisms and Pathways of Small-Phytoplankton Export From the Surface Ocean. *Ann. Rev. Mar. Sci.* 11, 57–74. doi: 10.1146/annurev-marine-121916-063627

Riebesell, U., Czerny, J., Von Bröckel, K., Boxhammer, T., Büdenbender, J., Deckelnick, M., et al. (2013a). Technical Note: A Mobile Sea-Going Mesocosm System - New Opportunities for Ocean Change Research. *Biogeosciences* 10, 1835–1847. doi: 10.5194/bg-10-1835-2013

Riebesell, U., Gattuso, J. P., Thingstad, T. F., and Middelburg, J. J. (2013b). Arctic Ocean Acidification: Pelagic Ecosystem and Biogeochemical Responses During a Mesocosm Study. *Biogeosciences* 10, 5619–5626. doi: 10.5194/bg-10-5619-2013

Saba, V. S., Friedrichs, M. A. M., Carr, M. E., Antoine, D., Armstrong, R. A., Asanuma, I., et al. (2010). Challenges of Modeling Depth-Integrated Marine Primary Productivity Over Multiple Decades: A Case Study at BATS and HOT. *Global Biogeochem. Cycle.* 24, 1–21. doi: 10.1029/2009GB003655

Sathyendranath, S., Stuart, V., Nair, A., Oka, K., Nakane, T., Bouman, H., et al. (2009). Carbon-To-Chlorophyll Ratio and Growth Rate of Phytoplankton in the Sea. *Mar. Ecol. Prog. Ser.* 383, 73–84. doi: 10.3354/meps07998

Schlitzer, R., and Mieruch-Schnülle, S. (2021) *webODV Explore*. Available at: https://explore.webodv.awi.de.

Schulz, K. G., Bach, L. T., Bellerby, R. G. J., Bermúdez, R., Büdenbender, J., Boxhammer, T., et al. (2017). Phytoplankton Blooms at Increasing Levels of Atmospheric Carbon Dioxide: Experimental Evidence for Negative Effects on Prymnesiophytes and Positive on Small Picoeukaryotes. *Front. Mar. Sci.* 4. doi: 10.3389/fmars.2017.00064

Silsbe, G. M., Behrenfeld, M. J., Halsey, K. H., Milligan, A. J., and Westberry, T. K. (2016). The CAFE Model: A Net Production Model for Global Ocean Phytoplankton. *Global Biogeochem. Cycle.* 30, 1756–1777. doi: 10.1002/2016GB005521

Sommer, U., Charalampous, E., Genitsaris, S., and Moustaka-Gouni, M. (2017). Benefits, Costs and Taxonomic Distribution of Marine Phytoplankton Body Size. *J. Plankton. Res.* 39, 494–508. doi: 10.1093/plankt/fbw071

Taucher, J., Bach, L. T., Boxhammer, T., Nauendorf, A., Achterberg, E. P., Algueró-Muñiz, M., et al. (2017). Influence of Ocean Acidification and Deep Water Upwelling on Oligotrophic Plankton Communities in the Subtropical North Atlantic: Insights From an *in Situ* Mesocosm Study. *Front. Mar. Sci.* 4. doi: 10.3389/fmars.2017.00085

Teira, E., Abalde, J., Álvarez-Ossorio, M. T., Bode, A., Cariño, C., Cid, Á., et al. (2003). Plankton Carbon Budget in a Coastal Wind-Driven Upwelling Station Off a Coruña (NW Iberian Peninsula). *Mar. Ecol. Prog. Ser.* 265, 31–43. doi: 10.3354/meps265031

Teira, E., Pazó, M. J., Serret, P., and Fernández, E. (2001). Dissolved Organic Carbon Production by Microbial Populations in the Atlantic Ocean. *Limnol. Oceanogr.* 46, 1370–1377. doi: 10.4319/lo.2001.46.6.1370

Utermöhl, H. (1931). Neue Wege in Der Quantitativen Erfassung Des Plankton.(Mit Besonderer Berücksichtigung Des Ultraplanktons.). *SIL. Proceeding. 1922-2010.* 5, 567–596. doi: 10.1080/03680770.1931.11898492

Wang, X. J., Behrenfeld, M., Le Borgne, R., Murtugudde, R., and Boss, E. (2009). Regulation of Phytoplankton Carbon to Chlorophyll Ratio by Light, Nutrients and Temperature in the Equatorial Pacific Ocean: A Basin-Scale Model. *Biogeosciences* 6, 391–404. doi: 10.5194/bg-6-391-2009

Welschmeyer, N. A. (1994). Fluorometric Analysis of Chlorophyll a in the Presence of Chlorophyll B and Pheopigments. *Limnol. Oceanogr.* 39, 1985–1992. doi: 10.4319/lo.1994.39.8.1985

Westberry, T. K., and Behrenfeld, M. J. (2014). "Oceanic Net Primary Production," in *Biophysical Remote of Satellite Applications Sensing*. Ed. J. M. Hanes (Berlin, Germany: Springer), 1–41. doi: 10.1007/978-3-642-25047-7_1

Westberry, T., Behrenfeld, M. J., Siegel, D. A., and Boss, E. (2008). Carbon-Based Primary Productivity Modeling With Vertically Resolved Photoacclimation. *Global Biogeochem. Cycle.* 22, 1–18. doi: 10.1029/2007GB003078

White, A., Björkman, K., Grabowski, E., Letelier, R., Poulos, S., Watkins, B., et al. (2010). An Open Ocean Trial of Controlled Upwelling Using Wave Pump Technology. *J. Atmos. Ocean. Technol.* 27, 385–396. doi: 10.1175/2009JTECHO679.1

Wickham, H. (2016). *Ggplot2* (New York: Springer).

Wolter, K. (1982). Bacterial Incorporation of Organic Substances Released by Natural Phytoplankton Populations. *Mar. Ecol. Prog. Ser.* 7, 287–295. doi: 10.3354/meps007287

Conflict of Interest: The authors declare that the research was conducted in the absence of any commercial or financial relationships that could be construed as a potential conflict of interest.

Publisher's Note: All claims expressed in this article are solely those of the authors and do not necessarily represent those of their affiliated organizations, or those of the publisher, the editors and the reviewers. Any product that may be evaluated in this article, or claim that may be made by its manufacturer, is not guaranteed or endorsed by the publisher.

frontiers | Frontiers in Marine Science

ORIGINAL RESEARCH
published: 29 June 2022
doi: 10.3389/fmars.2022.841894

Expected Limits on the Potential for Carbon Dioxide Removal From Artificial Upwelling

*David A. Koweek**

Ocean Visions, Leesburg, VA, United States

Artificial upwelling, the engineered upward pumping of deep ocean water, has long been proposed as a technique to fertilize the ocean and, more recently, remove atmospheric carbon dioxide. This study investigated the potential of artificial upwelling to contribute to carbon dioxide removal using a simple model with high-resolution (1° × 1°) gridded monthly climatologies of upper ocean and deep ocean physical and chemical properties. The potential for carbon dioxide removal was explored across a range of observationally-informed carbon-to-nitrogen-to-phosphorus ratios for microalgae and macroalgae communities, providing information on the sensitivity of the estimates to any assumed carbon-to-nutrient ratios. Simulated carbon dioxide removal across the tropical-to-subpolar ocean did not exceed 0.66 tons per square kilometer per year for microalgae, and did not exceed 0.85 tons per square kilometer per year for macroalgae. Using current technology, the estimated global aggregate potential for carbon dioxide removal using microalgae was less than 50 megatons (0.05 gigatons) of carbon dioxide annually and the estimated global aggregate potential for carbon dioxide removal using macroalgae was approximately 100 megatons (0.1 gigatons) of carbon dioxide annually. While controlled field trials are needed to validate or invalidate the findings of this study, this study suggests that artificial upwelling is unlikely to support annual carbon dioxide removal at, or close to, the rate of one gigaton of carbon dioxide annually.

Keywords: ocean-based carbon dioxide removal (CDR), ocean-based NETs, Artificial upwelling, Negative Emission Technologies (NETs), Carbon Dioxide Removal (CDR)

OPEN ACCESS

Edited by:
Javier Arístegui, University of Las Palmas de Gran Canaria, Spain

Reviewed by:
Matthew Paul Humphreys, Royal Netherlands Institute for Sea Research (NIOZ), Netherlands
Katja Fennel, Dalhousie University, Canada

***Correspondence:**
David A. Koweek
david.koweek@oceanvisions.org

Specialty section:
This article was submitted to Ocean Solutions, a section of the journal Frontiers in Marine Science

Received: *22 December 2021*
Accepted: *13 May 2022*
Published: *29 June 2022*

Citation:
Koweek DA (2022) Expected Limits on the Potential for Carbon Dioxide Removal From Artificial Upwelling. Front. Mar. Sci. 9:841894. doi: 10.3389/fmars.2022.841894

INTRODUCTION

Between 100 and 1000 gigatons of carbon dioxide removal from the atmosphere are now required to stabilize planetary warming at 1.5°C above pre-industrial temperatures (IPCC, 2018). In the recently released Working Group 1 contribution to the Intergovernmental Panel on Climate Change's (IPCC) Sixth Assessment Report, all shared socioeconomic pathways corresponding to less than 2°C of warming above the pre-industrial also require gigaton-scale deployments of carbon dioxide removal (IPCC, 2021). To meet the urgent and growing demand for carbon dioxide removal, attention has been paid to terrestrial options (e.g., afforestration, soil carbon sequestration) and technological options (e.g., direct air capture, bioenergy with carbon capture and storage) (IPCC, 2018; National Academies, 2019). Although the ocean is the largest reservoir of carbon on the planet

and currently absorbs approximately 31% of all anthropogenic carbon dioxide emissions (Gruber et al., 2019), ocean-based carbon dioxide removal pathways have received far less attention to date. Recent efforts have sought to address this knowledge deficit by accelerating the research and evaluation of ocean-based carbon dioxide removal pathways (Gattuso et al., 2018; GESAMP, 2019; Energy Futures Initiative, 2020; Gattuso et al., 2021; OceanNETs, 2021; Ocean Visions, 2021; National Academies, 2022).

Ocean-based pathways can broadly be categorized into abiotic or biotic pathways. Abiotic pathways use chemical processes to enhance the seawater alkalinity (ocean alkalinity enhancement) or remove carbon dioxide from seawater (direct ocean capture). Biotic pathways use photosynthesis to fix dissolved inorganic carbon into plant biomass (primary production), creating a deficit in the surface ocean aqueous carbon dioxide concentration that can be replenished through invasion of carbon dioxide from the atmosphere (GESAMP, 2019; Energy Futures Initiative, 2020). However, much of the world's surface ocean is nutrient-limited, so additional nutrients are needed to support primary production in the ocean (Sarmiento and Gruber, 2006). Artificial upwelling (the engineered upward pumping of deep ocean water, typically through a pipe) of nutrient-replete deep ocean water could be one means to inject the additional nutrients into the surface ocean where they can support primary production (Stommel et al., 1956; Vershinskiy et al., 1987; Kirke, 2003; Oschlies et al., 2010; Pan et al., 2016).

While artificial upwelling may be an important tool in enhancing surface ocean primary productivity, its potential role in carbon dioxide removal from the atmosphere is far less apparent. In addition to abundant nutrient concentrations, the deep ocean is replete in dissolved inorganic carbon and total alkalinity. Artificial upwelling of deep ocean water to the surface will translocate large quantities of dissolved inorganic carbon and total alkalinity as well as nutrients. Thus the carbon dioxide removal potential of artificial upwelling is a balance between the enhanced primary productivity supported by the upwelled nutrients and the additional deep ocean dissolved carbon dioxide that may be liberated through artificial upwelling to return to the atmosphere. If the newly-produced organic matter has a higher carbon-to-nutrient ratio than the upwelled water *and* can be rapidly exported out of the mixed layer, beyond the depth of upwelling, and into the deep ocean for long-term sequestration, the potential for carbon dioxide removal exists. Otherwise, artificial upwelling may result in a net flux of carbon dioxide from the deep ocean to the atmosphere.

Past studies of artificial upwelling using Earth system models have projected a wide range of carbon dioxide removal potential from less than 0 gigatons of carbon dioxide per year up to 13 gigatons of carbon dioxide per year (Dutreuil et al., 2009; Yool et al., 2009; Oschlies et al., 2010; Keller et al., 2014). This range in projected carbon dioxide removal is enormous: on one end, it would worsen the buildup of atmospheric carbon dioxide, and on the other end, would provide the multi gigaton-scale annual carbon dioxide removal necessary to stabilize planetary warming. The recently released consensus report of the U.S. National Academies of Science, Engineering, and Medicine (2022) suggests a smaller range of carbon dioxide removal potential of between 0.1 and 1 gigaton of carbon dioxide per year, but this range still spans an order of magnitude. More information is needed to narrow this range of possibilities and evaluate the efficacy of artificial upwelling to contribute to removal of atmospheric carbon dioxide.

This study combines a simple model with high-resolution (1° × 1°) gridded monthly climatologies of upper ocean and deep ocean physical and chemical properties to quantify the potential of artificial upwelling to support carbon dioxide removal by lowering the surface ocean aqueous carbon dioxide concentration. In this model, biogeochemical changes in upwelled water are simulated using a range of carbon-to-nitrogen-to-phosphorus ratios determined from observational studies of microalgae and macroalgae communities. This study examines carbon dioxide removal potential of artificial upwelling in two ways: the near-term technological potential based on feasible depth limits of the artificial upwelling pump, and the geophysical potential of artificial upwelling if the depth constraints on pump length did not exist. This study highlights areas of the global tropical-to-subpolar ocean where artificial upwelling may contribute to carbon dioxide removal and quantifies the potential for carbon dioxide removal if upwelling pipes were to be uniformly deployed across the tropical-to-subpolar ocean as a dense network of pipes.

METHODS

Theory

Air-sea exchange of carbon dioxide, J, is often expressed as:

$$J = k\,K_0\left(pCO_{2_{atm}} - pCO_{2_{sw}}\right)$$

Where k is the gas transfer velocity, K_0 is the Henry's law solubility constant, $pCO_{2_{atm}}$ is the partial pressure of carbon dioxide in the atmosphere, and $pCO_{2_{sw}}$ is the partial pressure of carbon dioxide in seawater (Wanninkhof et al., 2009).

Ocean-based carbon dioxide removal technologies lower the partial pressure of carbon dioxide in seawater to allow additional air-to-sea flux of atmospheric carbon dioxide beyond what would have occurred naturally. The additional air-to-sea flux from carbon dioxide removal, CDR, can be expressed as:

$$CDR = J' - J = k\left(K_0\,pCO_{2_{atm}} - K_0'\,pCO'_{2_{sw}}\right) - k\,K_0\left(pCO_{2_{atm}} - pCO_{2_{sw}}\right)$$

where the J' represents the air-sea gas flux due to a perturbed partial pressure of carbon dioxide in seawater, $pCO'_{2_{sw}}$, and K_0' is the corresponding Henry's law solubility constant in the perturbed condition. Note that for ocean-based carbon dioxide removal technologies that do not change the surface water temperature nor the salinity, $K_0' = K_0$. The above equation

simplifies to:

$$CDR = k\left(K_0\, pCO_{2_{sw}} - K_0'\, pCO'_{2_{sw}}\right)$$

Assuming a constant gas transfer velocity k, which is typically represented as an empirical function of wind speed over the open ocean (Wanninkhof et al., 2009), carbon dioxide removal is proportional to the partial pressure gradient between the background partial pressure of carbon dioxide in seawater and the perturbed partial pressure of carbon dioxide in seawater times the Henry's law solubility constant.

$$CDR \propto \left(K_0\, pCO_{2_{sw}} - K_0' pCO'_{2_{sw}}\right)$$

This can also be expressed as a concentration gradient.

$$CDR \propto \left(\left[CO_{2_{sw}}\right] - \left[CO'_{2_{sw}}\right]\right)$$

Introducing the Model

This study models carbon dioxide removal potential from artificial upwelling as the capacity of artificial upwelling to create a surface ocean aqueous carbon dioxide concentration ($[CO_2]$) gradient at longitude x and latitude y pumping from a depth z during month t as:

$$CDR\ Potential\ (x,y,z,t) = \underbrace{f_{light}(y,t)\, n_{pipes}\, \rho(x,y,z)\, \dot{Q}}_{\text{upwelling rate per area in daylight hours}} \times \underbrace{[CO_2]_{ML}(x,y,t) - [CO_2]'(x,y,z,t)}_{\text{maximum aqueous carbon dioxide gradient}}$$

where f_{light} is the fraction of the day in the photoperiod, n_{pipes} is the areal density of upwelling pipes, ρ is the density of upwelled water, $\dot{Q}$ is the volumetric upwelling rate, $[CO_2]_{ML}$ is the background aqueous carbon dioxide concentration in the mixed layer, and $[CO_2]'$ is the predicted aqueous carbon dioxide concentration of upwelled water after biogeochemical modification. All model variables are explained in further detail below.

This model does not directly simulate the additional air-to-sea flux of carbon dioxide necessary for the ocean to uptake additional atmospheric carbon dioxide. Nor does it simulate the fate of newly produced organic matter and its impacts on surface ocean aqueous carbon dioxide concentration via export out of the surface layer, remineralization, ingestion, conversion to dissolved organic matter, or any other pathway. The implications of these simplifications are considered in the Discussion.

Model Variable Descriptions

The Fraction of The Day in the Photoperiod, f_{light}

The fraction of the day in the photoperiod, f_{light}, dictates the potential for photosynthesis to convert high nutrient, high carbon dioxide upwelled deep ocean water to low nutrient, low carbon dioxide at the surface. When f_{light} equals 0, there is no photoperiod to sustain new biological production from artificial upwelling. When f_{light} equals 1, the photoperiod is 24 hours-long. The photoperiod at latitude y during month t was calculated following Forsythe et al. (1995).

Pipe Characteristics: Maximum Depth, Volumetric Flow Rate ($\dot{Q}$), and Areal Density (n_{pipes})

There exists a gap in maximum upwelling pipe depth and volumetric flow rates between experimental field trials and modeling studies with the modeling studies allowing for deeper pipes with higher flow rates (Liu and Jin, 1995; Yool et al., 2009; Oschlies et al., 2010; Keller et al., 2014) than have been produced in experimental field trials (Vershinskiy et al., 1987; Liu, 1999; Kithil, 2007; White et al., 2010; Pan et al., 2019) (**Figure 1**). To more closely understand how near-term engineering constraints may or may not limit carbon dioxide removal potential, I considered two scenarios: one scenario where pipe depth is limited to 500 meters (slightly deeper than the maximum depths tested during field trials) and another scenario where there are no limits to pipe depth. This second scenario simulates a medium-term future scenario where pipe technology is more advanced than the present. Volumetric flow rate, $\dot{Q}$, was held to 0.05 $m^3\ s^{-1}$ in this study to reflect a feasible flow rate based on historical performance of upwelling pipes in field trials. The areal density of upwelling pipes, n_{pipes}, was held fixed at one upwelling pipe per square kilometer. This upwelling pipe areal density was chosen for consistency with past modeling studies (Oschlies et al., 2010) and represents an optimistic scenario for near-term deployment given the lack of field testing of any distributed pipe networks to date.

Density of Upwelled Water, ρ

Deep ocean water density (in units of kg m^{-3}) was calculated from the salinity and potential temperature (θ; referenced to

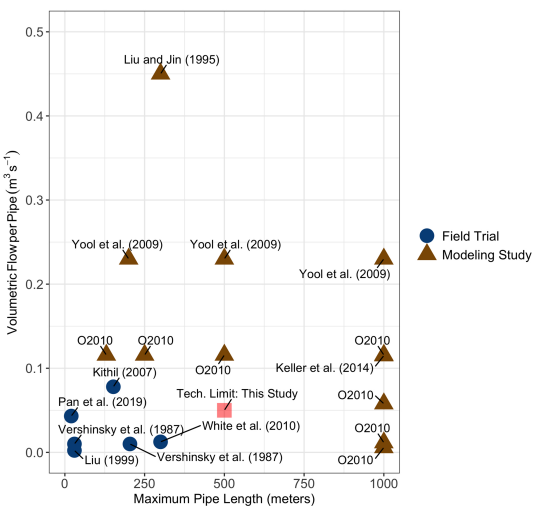

FIGURE 1 | Upwelling pipe volumetric flow rates and maximum depths for field tests (blue circles) and modeling studies (brown triangles). The label 'O2010' refers to Oschlies et al. (2010). Volumetric flow rates for Yool et al. (2009); Keller et al. (2014), and Oschlies et al. (2010) were calculated from the reported upwelling velocities in each study and assuming an areal density of pipes of one pipe per square kilometer as discussed in Oschlies et al. (2010). The maximum depth and flow rate for the scenario where the depth of the upwelling pipe is limited to 500 meters is shown as a red square.

surface pressure) of the depth layer in the GLODAP version 2 data product (Lauvset et al., 2016).

Observed Mixed Layer Carbon Dioxide Concentration: $[CO_2]_{ML}$

The spatially and temporally varying surface layer aqueous carbon dioxide concentration was taken from the OceanSODA-ETHZ gridded monthly pCO_2 climatology data product (Gregor and Gruber, 2021) multiplied by the Henry's law constant (Weiss, 1974). This concentration was applied to mixed layer depths determined from the Holte et al. (2017) monthly climatology of mixed layer depths, with nearest neighbor interpolation used to fill in missing mixed layer depth values each month. By referencing expected changes in aqueous carbon dioxide concentration due to upwelling, $[CO_2]'$, against the dynamic background concentration $[CO_2]_{ML}(x,y,t)$, this model implicitly accounts for the myriad physical and biological factors that control air-sea gas fluxes in the absence of artificial upwelling.

Potential Mixed Layer Carbon Dioxide Concentration Due to Upwelling: $[CO_2]'$

The potential aqueous carbon dioxide concentration of deep ocean water upwelled to the surface from depth z and subject the biogeochemical modification, $[CO_2]'$, was calculated from the potential dissolved inorganic carbon and total alkalinity concentrations after upwelling, $DIC'(z)$ and $TA'(z)$, respectively, along with the salinity, S, at depth z and the potential temperature referenced to surface pressure, θ, using seacarb (Gattuso et al., 2020). $DIC'(z)$ and $TA'(z)$ can be expressed as follows:

$$[CO_2]' = f\left(\theta(z), S(z), \begin{cases} DIC'(z) = DIC(z) + \varepsilon\,\Delta\,DIC(z) \\ TA'(z) = TA(z) + \varepsilon\,\Delta\,TA(z) \end{cases}\right)$$

where $DIC(z)$ and $TA(z)$ are the dissolved inorganic carbon and total alkalinity at depth z, respectively, from GLODAP (Lauvset et al., 2016); ΔDIC and ΔTA are the modeled biogeochemical modifications to DIC and TA, respectively, due to biological production; and ε expresses the effects of light limitation on ΔDIC and ΔTA.

Biogeochemical Modification of DIC and TA: Δ *DIC* and ΔTA

$\Delta DIC(z)$ and $\Delta TA(z)$ are the potential biogeochemical modification to $DIC(z)$ and $TA(z)$, respectively, made possible by the upwelling of nitrate (NO_3^-) and phosphate (PO_4^{3-}) to the surface and the subsequent primary production these nutrients support. ΔDIC was modeled as a co-limitation between nitrate and phosphate as follows:

$$\Delta\,DIC(z) = \begin{cases} -C:P(g) \times \left[PO_4^{3-}\right](z), \text{ if } \frac{\left[NO_3^-\right](z)}{\left[PO_4^{3-}\right](z)} \geq N:P(g) \\ -C:N(g) \times [NO_3^-](z), \ otherwise \end{cases}$$

where g is the microalgae or macroalgae carbon-to-nitrogen-to-phosphorus (C:N:P) stoichiometry (see **Table 1**). $\Delta TA(z)$ was modeled as the uptake of nitrate (Brewer et al., 1975) in this co-limited system as follows:

$$\Delta\,TA(z) = \begin{cases} N:P(g) \times \left[PO_4^{3-}\right](z), \text{ if } \frac{\left[NO_3^-\right](z)}{\left[PO_4^{3-}\right](z)} \geq N:P(g) \\ [NO_3^-](z), \qquad\qquad otherwise \end{cases}$$

The stoichiometries come from published compilations of carbon-to-nitrogen-to-phosphorus ratios for microalgae and macroalgae assemblages. Data sources for microalgae stoichiometries included Galbraith and Martiny (2015) ("Galbraith"), Table 1 in Garcia et al. (2018) ("Garcia Q1" and "Garcia Q3"), and Redfield (1934) ("Redfield" and "Redfield P-limited") for microalgae. The "Redfield P-limited" model is limited only by the availability of phosphorus to represent the possibility that nitrogen fixation could supplement primary production from artifical upwelling as hypothesized by Karl and Letelier (2008). Atkinson and Smith (1983) Table 1 is the data source for the three macroalgae stoichiometries ("Atkinson Q1", "Atkinson Median", and "Atkinson Q3").

Light Limitation: ε

Light limitation was represented as a single coefficient, ε that ranged from 0 to 1 and expressed the relationship between between daily average downwelling irradiance at the ocean's surface during the photoperiod at longitude x, latitude y, and month t and the light saturation parameter, E_k, which also varied spatially, temporally, and as a function of the type of algae (microalgae or macroalgae).

TABLE 1 | Carbon-to-nitrogen-to-phosphorus (C:N:P) ratios for the macroalgae and microalgae considered in this study.

Algae	Model Name	C:N	C:P	N:P	Notes
Microalgae	Galbraith	see below	see below	C:P/C:N	
	Garcia Q1	6.9:1	86.4:1	12.5:1	C:P predicted from 1st quartile N:P
	Garcia Q3	6.5:1	118:1	18.1:1	C:P predicted from 3rd quartile N:P
	Redfield	6.6:1	106:1	16:1	
	Redfield P-limited	6.6:1	106:1	16:1	P-limited only (proxy for N-fixation)
Macroalgae	Atkinson Q1	22:1	440:1	20:1	C:P predicted from 1st quartile N:P
	Atkinson Median	18.4:1	570:1	31:1	C:P predicted from median N:P
	Atkinson Q3	16.1:1	758:1	47:1	C:P predicted from 3rd quartile N:P

The C:N ratio for the Galbraith model is $C:N = (125‰ + 30‰ \times [NO_3^-]/(0.32\mu M + [NO_3^-]))^{-1}$ *and the C:P ratio for the Galbraith model is* $C:P = (7.3 \times [PO_4^{3-}] + 4.8))^{-1}$ *The data used to develop the Atkinson stoichiometries considered Chlorophyta, Phaeophyta, and Rhodophyta only.*

$$\varepsilon = tanh\left(\frac{E(x,y,t)}{E_k(x,y,t,g)}\right)$$

Where $E(x,y,t)$ is the MODIS-Aqua Level 3 monthly climatology of photosynthetically active radiation at 9km resolution spanning the years 2002 to 2019/2020 (NASA, 2020) (data downloaded August 2020), regridded to 1°×1° using the cdo package (Schulzweida, 2019), and divided by the fraction of the day in the photoperiod, f_{light}.

The light saturation parameter, E_k, applied to microalgae stoichiometries (**Table 1**) was determined from the Marine Primary Production: Model Parameters from Space (MAPPS) project (Bouman et al., 2018), where individual reported E_k measurements from the database were grouped by Longhurst biogeochemical province (Longhurst, 2010), hemisphere, and season, from which median values were taken for each of these groupings. Median values ranged from 40 to 370 μmol m^{-2} s^{-1}. This grouping created seasonally-specific polygon groupings of E_k values which were then overlaid onto the 1°×1° grid.

The light saturation parameter, E_k, applied to macroalgae stoichiometries was held fixed at 125 μmol m^{-2} s^{-1} based on the consistency in reported values from red, green, and brown macroalgae (Johansson and Snoeijs, 2002; Gómez et al., 2004).

Global-Scale Estimates of Carbon Dioxide Removal Potential

For each microalgae and macroalgae stoichiometry in **Table 1**, monthly estimates of carbon dioxide removal potential were summed to generate annual scale estimates for each longitude *x*, latitude *y*, and depth *z* combination. At each longitude-latitude pairing, maximum annual carbon dioxide removal potential was selected among depths below the maximum annual mixed layer depth. These maximum carbon dioxide removal potential estimates were integrated across the area of the grid cell. Positive values of this areally-integrated maximum carbon dioxide removal potential estimate from each latitude-longitude pair were summed together to generate global-scale estimates of carbon dioxide removal potential. Negative values were excluded from the summation.

RESULTS

Carbon Dioxide Removal Potential

Microalgae

Median areal flux rates of carbon dioxide removal potential from microalgae stoichiometries were calculated to range from 0.03 to 0.12 tons CO_2 km^{-2} yr^{-1} under the constraint of an upwelling pipe no longer than 500 meters. Maximum areal flux rates ranged from 0.45 to 0.66 tons CO_2 km^{-2} yr^{-1} (**Figures 2**, **3**; **Table 2**). Approximately 90% to 95% of the grid cells were limited to less than 0.5 tons CO_2 km^{-2} yr^{-1}, with the exception of the Galbraith model which did not exceed 0.5 tons CO_2 km^{-2} yr^{-1} under any conditions (**Figure 3**). The models showed some zonal variation with highest estimated rates of carbon dioxide removal poleward of 40° latitude in both hemispheres, especially in the Southern Ocean and in the north Pacific. The eastern equatorial Pacific also shows elevated carbon dioxide removal potential across the range of stoichiometries considered (**Figure 2**). In each of the microalgae models, between 2% and 14% of the model grid cells projected negative carbon dioxide removal (<0 tons CO_2 km^{-2} yr^{-1}), except for the Galbraith model for which 35% of the model grid cells projected negative carbon dioxide removal (**Figure 3**). Negative carbon dioxide removal potential was projected across the microalgae stoichiometries in portions of the eastern tropical north Pacific, the north Atlantic, and the western Indian Ocean (**Figure 2**).

In scenarios where the constraint of a 500 m long upwelling pipe was removed, carbon dioxide removal potential increased slightly across the grid, without substantial change to the spatial pattern (**Figure S1**) or distribution (**Figure 3**) of potential carbon dioxide removal from the depth-limited scenario. The depth of pumping required to generate maximum carbon dioxide removal potential exceeded 1000 meters, and reached 4000 to 5000 meters in much of the north Atlantic and north Pacific (**Figure S2**). That the depth of pumping corresponding to maximum carbon dioxide removal potential exceeded 500 meters indicates that pump length may become a limiting factor on the carbon dioxide removal potential of artificial upwelling. Relaxing the depth constraint eliminated nearly all grid cells projecting negative carbon dioxide removal potential. Model grids cells with projected negative carbon dioxide removal shrunk to between 0.2% and 0.5%, except for the Galbraith model which continued to project 34% of the model grid cells generating negative carbon dioxide removal (**Figure 3**). The persistence of grid cells with negative carbon dioxide removal potential in this scenario suggests that there are locations in the tropical-to-temperate ocean for which no scenario of artificial upwelling would be beneficial for the purposes of carbon dioxide removal.

Macroalgae

Median areal flux rates of carbon dioxide removal potential from macroalgae stoichiometries were calculated to range from 0.3 to 0.35 tons CO_2 km^{-2} yr^{-1} under the constraint of an upwelling pipe no longer than 500 meters. Maximum areal flux rates ranged from 0.8 to 0.85 tons CO_2 km^{-2} yr^{-1} and minimum areal flux rates ranged from -0.33 to -0.23 tons CO_2 km^{-2} yr^{-1} in this scenario (**Figures 2**, **3**; **Table 2**). However, unlike in the microalgae models, the percentage of grid cells in the macroalgae models exhibiting negative carbon dioxide removal potential was negligible (<0.05%). Similar to the microalgae models, greatest carbon dioxide removal potential was projected in the high latitudes of both hemispheres. Eastern boundaries of the south Atlantic and of the Pacific Oceans also showed elevated carbon dioxide removal potential. Elevated carbon dioxide removal potential was projected across much of the eastern equatorial Pacific (**Figure 2**).

In scenarios where the constraint on the depth of the upwelling pipe was removed, projected carbon dioxide removal potential increased across the grid and became more spatially homogeneous across the mid-latitudes (**Figure S1**). In particular, increases in carbon dioxide removal potential were projected for

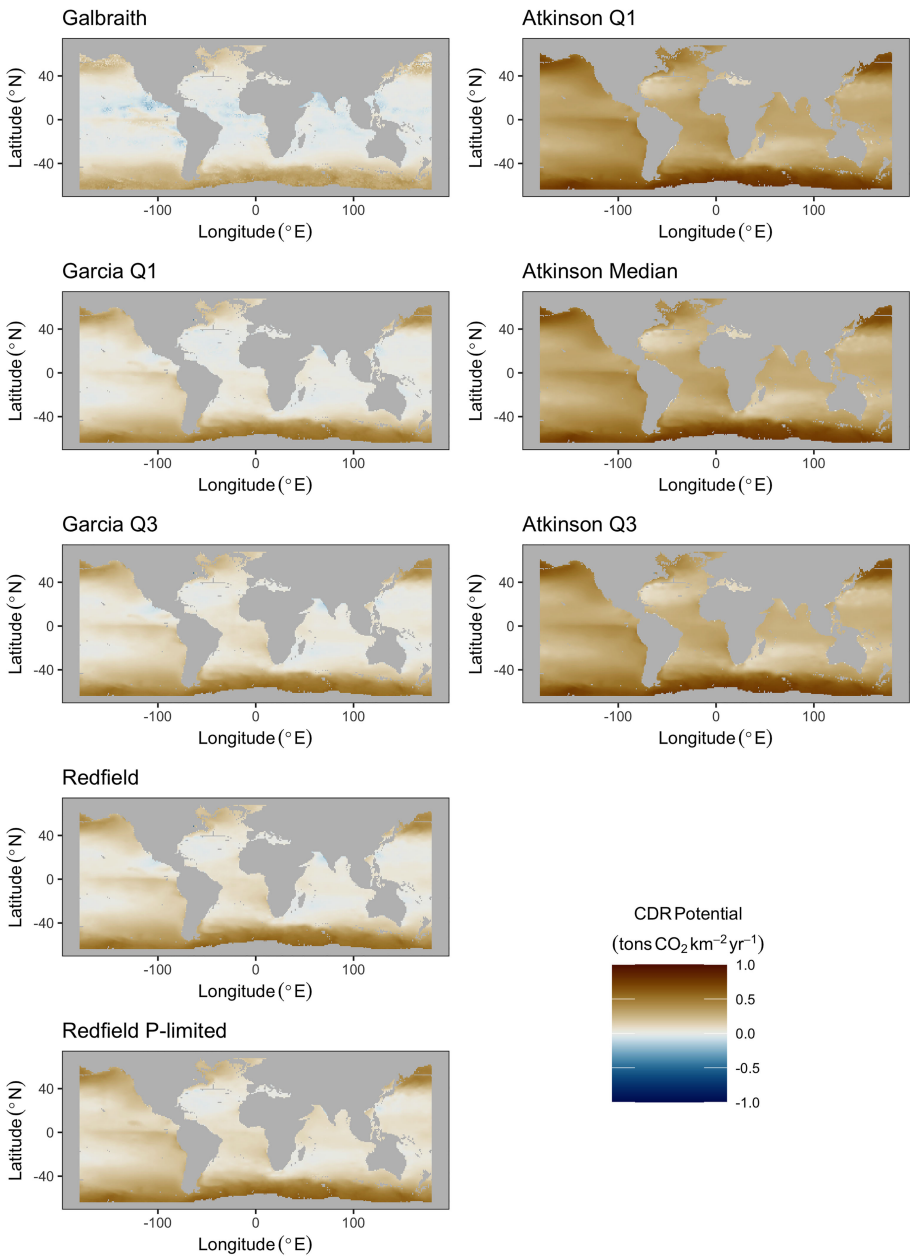

FIGURE 2 | Maps of maximum potential carbon dioxide removal for all microalgae (left column) and macroalgae (right column) stoichiometries under the constraint of an upwelling pipe no longer than 500 meters.

the western margin of the major ocean basins. Maximum carbon dioxide removal was projected when pumping from depths of between 1000 and 2000 meters across most of the major ocean basins (**Figure S2**). The exception to this rule came from the north Atlantic where maximum carbon dioxide removal potential was forecast to come from pumping up from depths of 4000 to 5000 meters. The increased projected carbon dioxide removal serves as evidence that current technological limits on the feasibility of deploying pipes into the deep ocean for artificial upwelling limit carbon dioxide removal potential from macroalgae, although this limitation is typically not more than 0.04 tons CO_2 km^{-2} yr^{-1} (**Table 2**).

Global-Scale Potential

Microalgae

Global aggregated carbon dioxide removal potential from microalgae was calculated to be less than 50 megatons, or 0.05 gigatons, of carbon dioxide per year under the technological

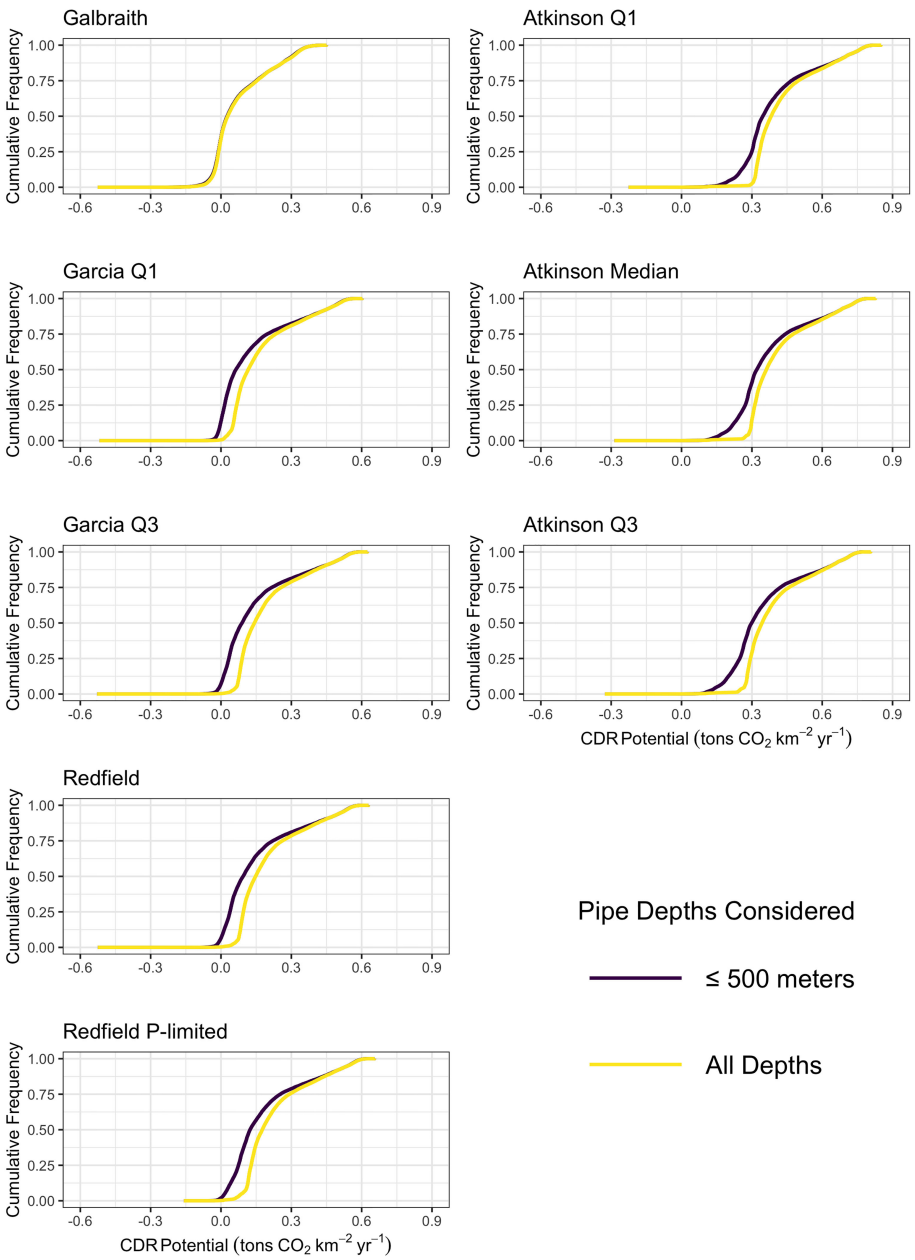

FIGURE 3 | Empirical cumulative distribution functions of the maximum potential carbon dioxide removal for all microalgae (left column) and macroalgae (right column) stoichiometries with the constraint of an upwelling pipe no longer than 500 meters (dark purple) and without limits to the depth of the upwelling pipe (yellow).

constraint of a 500 m length upwelling pipe (**Figure 4**).When this technological constraint was removed, potential carbon dioxide removal increased by between 10 and 15 megatons (0.01-0.015 gigatons) of carbon dioxide per year across all microalgae stoichiometries, except the Galbraith model for which there was a negligible difference (less than one megaton of carbon dixoide per year) (**Figure 4**). In contrast to the other microalgae models, the Galbraith model predicted that the pumping depth for maximum carbon dioxide removal potential would be less than 500 m across much of the tropical-to-subpolar ocean (**Figure S2**). Therefore, removing the technological constraint of a 500 m long upwelling pipe had less impact on the estimates of carbon dioxide removal potential than on other stoichiometries, all of which showed that the depth of pumping for maximal carbon dioxide removal often exceeds 500 meters depth.

Macroalgae

Global aggregated carbon dioxide removal potential for macroalgae stoichiometries was calculated to be between 98 and 113 megatons (0.098 to 0.113 gigatons) of carbon dioxide per year under the technological constraint of a 500 m length upwelling pipe (**Figure 4**). Removing the depth limit on the pipe resulted in an increase of approximately 10 to 15 megatons of carbon dioxide per year across all macroalgae stoichiometries (**Figure 4**).

Controls on Carbon Dioxide Removal Potential

Biogeochemical modification of deep ocean water by microalgae was co-limited by nitrate and phosphate availability. Distributions of nitrate-to-phosphate from locations and depths corresponding to maximum carbon dioxide removal potential without constraints on maximum pump depth (**Figures S1**, **S2**) demonstrated phosphate-limitation for the Garcia Q1 model, nitrate-limitation for the Garcia Q3 and Redfield models, and co-limitation by nitrate and phosphate in the Galbraith model (**Figure 5**). The Redfield P-limited model was phosphate-limited by design (see **Table 1**). In contrast, all three macroalgae models were nitrate-limited (**Figure 5**).

Carbon dioxide removal potential in this study can be explained as linear functions of the ratio of carbon to the limiting nutrient(s) (**Figure 6**). As carbon-to-nutrient ratios in microalgae and macroalgae increase, more carbon is removed per unit nutrients consumed. Microalgae carbon-to-nutrient ratios were represented as the product of carbon-to-nitrogen and carbon-to-phosphorus ratios to reflect the limitation of both

TABLE 2 | Summary statistics of carbon dioxide removal potential from microalgae and macroalgae models across the global grid (tons CO_2 km^{-2} yr^{-1}).

Algae	Model	Min	Q1	Med	Q3	Max
Microalgae	Galbraith	-0.53 (-0.53)	-0.01 (-0.01)	0.03 (0.03)	0.15 (0.15)	0.45 (0.45)
	Garcia Q1	-0.52 (-0.52)	0.02 (0.07)	0.06 (0.12)	0.2 (0.23)	0.6 (0.6)
	Garcia Q3	-0.53 (-0.53)	0.03 (0.09)	0.09 (0.14)	0.22 (0.26)	0.62 (0.62)
	Redfield	-0.53 (-0.53)	0.04 (0.1)	0.09 (0.15)	0.22 (0.26)	0.63 (0.63)
	Redfield P-limited	-0.16 (-0.16)	0.07 (0.13)	0.12 (0.18)	0.25 (0.29)	0.66 (0.66)
Macroalgae	Atkinson Q1	-0.23 (-0.23)	0.3 (0.33)	0.35 (0.38)	0.47 (0.5)	0.85 (0.85)
	Atkinson Median	-0.29 (-0.29)	0.27 (0.31)	0.32 (0.36)	0.44 (0.48)	0.82 (0.83)
	Atkinson Q3	-0.33 (-0.33)	0.25 (0.29)	0.3 (0.34)	0.42 (0.46)	0.8 (0.81)

The table shows minimum (Min), first quartile (Q1), median (Med), third quartile (Q3), and maximum (Max) values for scenarios with a pump depth limit of 500 meters, and those for which pump depth was not limited (values shown in parentheses).

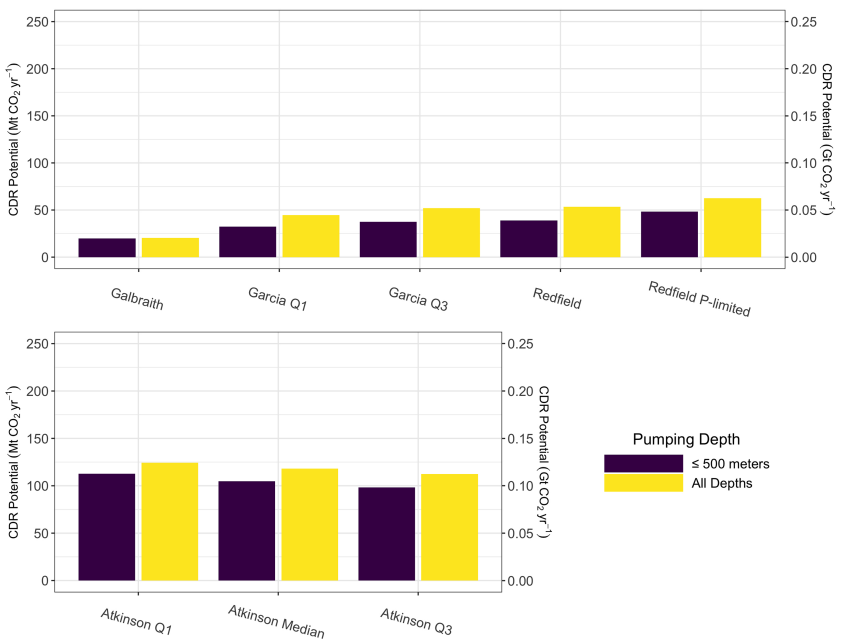

FIGURE 4 | Projected global-scale carbon dioxide removal potential after areally integrating positive potential carbon dioxide removal values from **Figure 2** (purple) and **Figures S1** (yellow) for microalgae stoichiometries (top row) and macroalgae stoichiometries (bottom row).

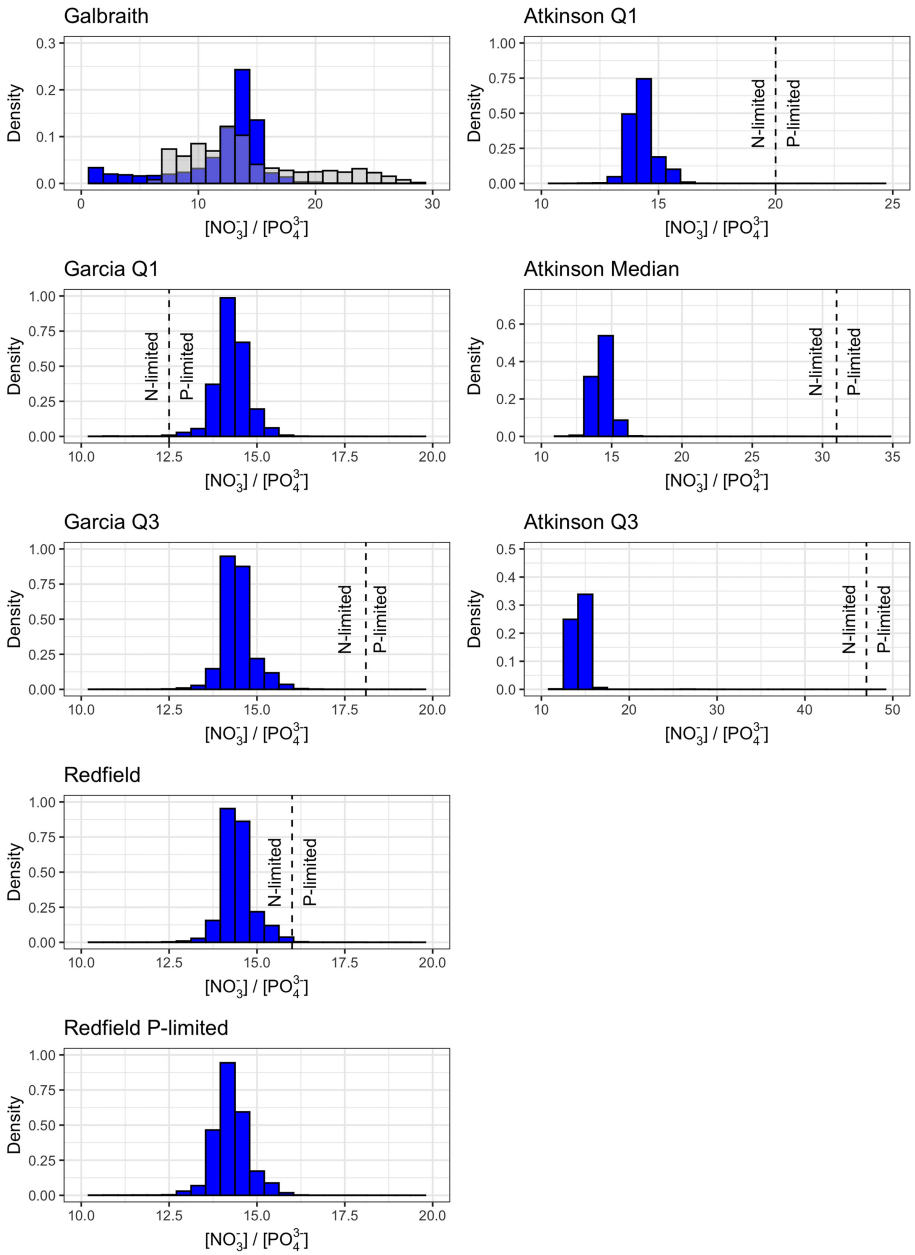

FIGURE 5 | Density histograms of the nitrate-to-phosphate ratio corresponding to maximum carbon dioxide removal potential shown in **Figure S1** for microlage (left column) and macroalgae (right column) stoichiometries. Dashed lines show the nitrogen-to-phosphorus stoichiometry of the microalgae or macroalgae (**Table 1**). Values to the left of the dashed line are nitrogen-limited and values to the right of the dashed line are phosphate-limited. The nitrogen-to-phosphorus stoichiometry of the Galbraith model are shown as the grey overlaying histogram. The nitrogen-to-phosphorus stoichiometry of the Redfield P-limited model is not shown because biogeochemical uptake is limited by phosphate availability only. Axis limits are adjusted between plots to facilitate visualization of the density histograms and their relationship to the nitrogen-to-phosphorus stoichiometry.

nitrate and phosphate on biogeochemical uptake across the suite of microalgae stoichiometries considered. Macroalgae models, being limited by nitrate alone, were explained as a linear function of macroalgae carbon-to-nitrogen ratios across the stoichiometries considered.

DISCUSSION

This study presents estimates of the potential for carbon dioxide removal from artificial upwelling by using a simple model to project the capacity of artificial upwelling to decrease surface

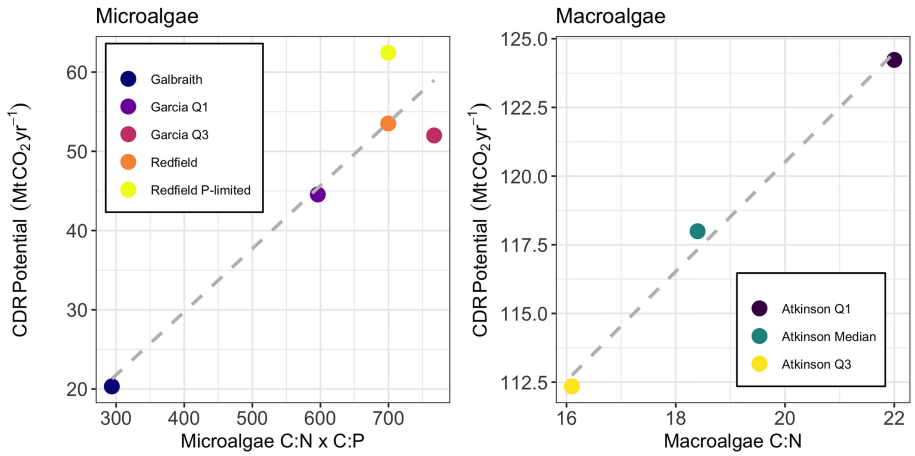

FIGURE 6 | Controls on carbon dioxide removal potential of microalgae (left panel) and macroalgae (right panel). Grey dashed lines show linear models for each type of algae. Carbon-to-nitrogen and carbon-to-phosphorus values for the Galbraith model were chosen by calculating values for all locations and depths displayed in **Figure S2** and selecting the median values of carbon-to-nitrogen and carbon-to-phosphorus from the distributions.

ocean aqueous carbon dioxide concentration. By incorporating a range of observationally-informed carbon-to-nitrogen-to-phosphorus ratios for microalgae communities and for macroalgae (**Table 1**), the simple model can investigate the potential for carbon dioxide removal across a realistic range of possible carbon-to-nutrients ratios. Comparison of the results across the different nutrient stoichiometries serves as a means to analyze the sensitivity of the model results to any assumed carbon-to-nitrogen-to-phosphorus ratio.

This study projects that carbon dioxide removal potential across the tropical-to-subpolar ocean is always less than 1 ton CO_2 km^{-2} yr^{-1} and that global-scale deployment of pipes uniformly deployed at a spacing of one pipe per square kilometer across the tropical-to-subpolar ocean would yield carbon dioxide removal of substantially less than one gigaton of carbon dioxide removal annually. Simulations across a range of assumed microalgae growth stoichiometries without limits on upwelling pipe depth resulted in estimates between 20 and 62 megatons (0.02 to 0.062 gigatons) of potential carbon dioxide removal annually, while simulations across a range of macroalgae growth stoichiometries without limits on upwelling pipe depth resulted in estimates between 98 and 124 megatons (0.098 to 0.124 gigatons) of potential carbon dioxide removal annually. Technological limitations, taken in this study as a maximum pipe depth of 500 meters, are responsible for a reduction of 10 to 15 megatons of potential carbon dioxide removal per year from the theoretical maximum if pipe depth was not a limiting factor (except for the Galbraith model) (**Figure 4**). Under a wide array of microalgae and macroalgae stoichiometries, this study projects that the expected decrease of surface ocean carbon dioxide concentration due to increased primary production from artificial upwelling is largely offset by the effects of upwelling deep ocean water with high concentrations of carbon dioxide.

Study Assumptions

There are a number of assumptions in this study worthy of further consideration. First, this study considers carbon dioxide removal potential from the point of carbon dioxide fixation via photosynthesis. It does not consider losses due to remineralization of organic matter in the surface ocean. If organic matter is not rapidly harvested or exported to the deep ocean, remineralization during export will reduce the efficiency and permanence of carbon dioxide removal from artificial upwelling by returning a large portion of carbon embedded in the biomass back to dissolved carbon dioxide (Baumann et al., 2021; Siegel et al., 2021). By not considering remineralization, this study likely overestimates the quantity and permanence of carbon dioxide removal from artificial upwelling.

There are a number of ideas being considered to reduce surface ocean remineralization of newly produced macroalgae. There is growing interest and exploration in the idea of intentionally sinking macroalgae biomass (GESAMP, 2019; Energy Futures Initiative, 2020; Ocean Visions, 2021) in the deep ocean to sequester the embedded carbon from return to the atmosphere. Recent research suggest that the deep ocean may offer sequestration permanence on timescales of decades-to-millenia depending upon the location where the biomass is sunk and the depth to which it is sunk (Siegel et al., 2021). A second option for macroalgae would involve harvesting the macroalgae for later use as a source of energy coupled with carbon capture and storage (Moreira and Pires, 2016), or for use as a source of energy where the carbon remains in an inert form such as biochar (Roberts et al., 2015).

Microalgae presents unique challenges for ensuring sequestration due to their diffuse concentration and neutral buoyancy in seawater. Coupling artificial upwelling pipes to adjacent artificial downwelling pipes may provide one route for rapid export of additional microalgae biomass into the deep

ocean. Downwelling pipes would need to be a different length than the coupled upwelling pipe to avoid running a closed loop by which the same water parcel is repeatedly upwelled and downwelled without a chance to drawdown atmospheric carbon dioxide in the surface ocean and export newly produced organic matter to the deep ocean.

Second, this study assumes that the change in surface ocean concentration of aqueous carbon dioxide is a reliable indicator of carbon dioxide removal potential because any deficits in surface ocean concentration of aqueous carbon dioxide would be replenished by invasion of atmospheric carbon dioxide. However, changes in aqueous carbon dioxide concentration may only result in uptake of atmospheric carbon dioxide if the carbon dioxide-depleted water remains at the surface long enough for the atmosphere to equilibrate with the surface water. As Bach et al. (2021) showed, carbon dioxide-depleted surface water in the vicinity of the Great Atlantic Sargassum Belt is not exposed to the atmosphere long enough for atmospheric carbon dioxide to invade the surface ocean and re-equilibrate the air-sea equilibrium. In these instances of insufficient equilibration, carbon dioxide removal potential is reduced from the upper bound created by the air-sea concentration gradient. This study does not resolve area(s) of the tropical-to-subpolar ocean over which incomplete equilibration is expected, but one can safely assume that inclusion of this process would reduce the global total estimates of carbon dioxide removal provided here (**Figure 4**).

Third, this study does not consider changes in the vertical structure of the upper water column due to artificial upwelling. The upwelling of deep ocean water from below the winter mixed layer depth into the surface mixed layer will tend to reduce the thermal and haline gradients between the surface ocean and the deep ocean, resulting in reduced stratification between the two layers (Fennel, 2008). This breakdown in stratification accelerates with higher rates of deep water upwelling, but can be inhibited by absorption of solar radiation on the ocean's surface, which heats the surface layer and strengthens stratification (Letelier et al., 2008). Reduced stratification may allow for greater diffusion of high carbon dioxide deep ocean water into the surface mixed layer. These diffusive fluxes of carbon dioxide from within the pycnocline into the mixed layer could offset any drawdown in surface ocean aqueous carbon dioxide caused by upwelling-induced primary production, resulting in diminished estimates of the carbon dioxide removal potential of artificial upwelling.

Fourth, this study relies on monthly climatologies alone to predict annual estimates of carbon dioxide removal potential. It does not resolve sub-monthly variability, nor does it resolve carbon dioxide removal potential on interannual timescales. As such, the carbon dioxide removal potential estimated in this study should serve as an average estimate for a given location, as well as on a global-scale, subject to modification as upper ocean conditions change due to changes in temperature, salinity, surface ocean chemistry, mixed layer depth, and incoming solar radiation.

Fifth, this study focuses on macronutrient fertilization alone. It does not consider the role of micronutrients, such as iron, in supporting enhanced biological productivity. This is a simplification of the model because it is well-established that many regions of the ocean are micronutrient-limited, such as the well-known high-nutrient low-chlorophyll regions (Moore et al., 2013). Excluding micronutrients may bias the carbon dioxide removal potentials presented here to be higher than actually expected. However, this bias may be fully or partially negated because artificial upwelling would translocate micronutrients from depth to the surface alongside macronutrients. For instance, dissolved iron concentration increases with depth consistently across much of the world's major ocean basins (Moore and Braucher, 2008). Regardless, nutrient fertilization is modeled in this study as co-limitation (the least abundant nutrient dictates the extent of new biological production). Incorporating one or more additional co-limiters (e.g., dissolved iron) would result in decreased estimates of the carbon dioxide removal potential of artificial upwelling.

Comparisons With Earth System Modeling Studies

This study estimates carbon dioxide removal potential in each grid cell independent of both past levels of artificial upwelling and other parts of the Earth system. In contrast, past artificial upwelling studies estimated the carbon dioxide removal potential within an Earth system model (Dutreuil et al., 2009; Yool et al., 2009; Oschlies et al., 2010; Keller et al., 2014). While the approach in this study is simpler, and allows for incorporation of recent high resolution (1°×1°) observationally-informed climatologies, it has two main drawbacks relative to Earth system modeling studies. First, Earth system models evolve processes forward in time, such that the past state of a process affects future values. This is a more realistic representation of any intervention as its effects accumulate through space and time (although not all of these models simulate the changes in upper ocean mixing described above due to the required additional complexity of the simulations). By projecting forward in time, Earth system models can address questions that this model is ill-suited to address, such as how using deep ocean nutrients through artificial upwelling may affect nutrient availability to support primary production in downstream ecosystems (the "opportunity cost" of artificial upwelling on biological productivity).

The second drawback of this model relative to Earth system models is that Earth system models allow for exchange of carbon between the ocean, atmosphere, and land, and thus are able to simulate Earth system feedback from artificial upwelling. All carbon dioxide removal pathways are expected to induce Earth system feedbacks that counteract the drawdown of atmospheric carbon dioxide as the various reservoirs of the global carbon cycle re-equilibrate. These feedbacks dictate the ultimate efficacy of any carbon dioxide removal pathway in drawing down atmospheric carbon dioxide concentrations (Cao and Caldeira, 2010; Jones et al., 2016; Keller et al., 2018). For instance, Jones et al. (2016) showed in an Earth system model that the fraction of a given quantity of carbon dioxide removal which remained out of the atmosphere ranged from 55% to 89% (depending upon the RCP scenario) as the global carbon cycle re-equilibrated to a quantity of atmospheric removal.

The spatially-resolved (**Figure 2**) and global summed (**Figure 4**) carbon dioxide removal potential are linearly dependent on the areal mean upwelling rate, which is the product of the areal density of pipes, n_{pipes}, and the volumetric flow rate per pipe, $\dot{Q}$. At n_{pipes} = 1 km^{-2} and $\dot{Q}$ = 0.05 m^3 s^{-1}, the areal mean upwelling rate in this study was approximately 0.4 centimeters per day. For comparison, areal mean upwelling rates in Oschlies et al. (2010) and Keller et al. (2014) were one centimeter per day, and the areal mean upwelling rate in Yool et al. (2009) was two centimeters per day. If the areal mean upwelling rates from the Earth system modeling studies were used in this study, it would increase the carbon dioxide removal potential by a factor of 2.5 (one centimeter per day) or 5 (two centimeters per day). This would increase the estimates of carbon dioxide removal potential for microalgae to between 50 and 310 megatons (0.05 to 0.31 gigatons) annually, and would increase the carbon dioxide removal potential for macroalgae to between ~250 and 625 megatons (0.250 to 0.625 gigatons) annually. These scaled estimates would fall within the range of -0.13 to 0.38 gigatons of microalgae carbon dioxide removal per year projected by Yool et al. (2009). But the scaled estimates would still fall well short of the projected ~3.3 gigatons of carbon dioxide removal per year reported by Oschlies et al. (2010) and of the 6.1 to 13.2 gigatons of carbon dioxide removal per year projected by Keller et al. (2014). However, these discrepancies may not be as large as they may first appear. Oschlies et al. (2010) found that cooling of surface waters due to artificial upwelling depressed land-based respiration, which represented ~80% of the additional carbon storage in their model simulations. This leaves ~0.66 of the 3.3 total gigatons of carbon dioxide removal per year reported by Oschlies et al. (2010) as sequestered in the ocean sink. This study can only estimate uptake potential by the ocean, so a direct comparison between the two studies would find that the estimates of ocean uptake from artificial upwelling in this study are approximately one-sixth that of Oschlies et al. (2010). While this discrepancy clearly leaves room for further investigation, it does not represent a difference of orders of magnitude as it might have initially appeared.

In the short term, two cross-checks between this model and Earth system models could help validate or invalidate the results of this study. First, by incorporating the realistic technical feasibility of pipe performance featured in this study (maximum depth of 500 meters, $\dot{Q}$ = 0.05 m^3 s^{-1}) into Earth system model simulations. Second, by applying this simple diagnostic model to Earth system model output. Regardless of future modeling work, the inconsistencies in reported values between Earth system modeling studies underscore the need for complementary approaches (mesocosms, field tests) to evaluate the efficacy of artificial upwelling for carbon dioxide removal.

Final Thoughts on Study Limitations

Despite its limitations, the simple modeling framework introduced in this study facilitates rapid testing of the upper bound on the potential for carbon dioxide removal from artificial upwelling across a wide range of carbon-to-nitrogen-to-phosphorus ratios for microalgae and macroalgae communities. By considering the near-term technological limits on operational capacities of upwelling pumps, this study helps ground the near-term potential of artificial upwelling to contribute to the removal of atmospheric carbon dioxide. As higher-resolution oceanographic data products and climatologies become available, they can replace the data products used in this study for higher spatial and temporal resolution estimates of the carbon dioxide removal potential from artificial upwelling. Multiple modeling approaches, alongside experimental and observational studies, are likely to provide the most holistic perspective about the range of possible outcomes from artificial upwelling.

Futher Considerations

At the flow rate considered within each pipe here (0.05 m^3 s^{-1}), pipe areal density would need to increase by approximately an order of magnitude to n_{pipes} ~ 10 km^{-2} across the study area to reach gigaton-scale carbon dioxide removal. Substantial technological developments would be needed to reach this areal density because current field trials have been restricted to single pipe studies over short timescales (days-to-weeks) (Pan et al., 2016).

This study may aid in the site selection of experimental programs by identifying sites with large ranges in carbon dioxide removal potential from artificial upwelling, such as in the eastern equatorial Pacific or along the northern boundary of the Southern Ocean among others (**Figure 2**). These sites, which feature large variations in carbon dioxide removal potential over small spatial distances, may prove valuable for experimental programs because they may provide an opportunity to ground truth both upper end and lower end carbon dioxide removal estimates from artificial upwelling.

Environmental impacts from artificial upwelling need to be carefully studied in addition to carbon dioxide removal potential. Possible impacts include whether, and how, artificial upwelling may change phytoplankton community competition via changes in temperature, salinity, nutrients, carbon dioxide, and/or light; and the effects of these changes on marine food webs and carbon export efficiency (Pan et al., 2016; Taucher et al., 2021). Large-scale implementation of artificial upwelling may impact sea surface temperatures with consequences for local circulation, weather, and climate (Kwiatkowski et al., 2015). The Ocean artUp program (https://ocean-artup.eu/) is conducting mesocosm and field experiments, as well as modeling studies to better characterize the environmental impacts (both positive and negative) of artificial upwelling. Observational studies of natural upwelling systems for their carbon sequestration potential may also offer valuable insights into the efficacy of artificial upwelling and its impacts on marine ecosystems (Bach and Boyd, 2021).

CONCLUSION

Gigaton-scale carbon dioxide removal is now required under the shared socioeconomic pathways that limit warming to <2°C above the pre-industrial (IPCC, 2021). Ocean-based pathways may play a valuable role in supplying the needed carbon dioxide removal because of their size, potential for fewer conflicting use needs, and potential advantages with respect to permanence (Siegel et al., 2021). This study suggests artificial upwelling is unlikely to provide gigaton-scale carbon dioxide removal because enhanced biological production supported by deep water

nutrients are largely offset by the correlated release of carbon dioxide from deep ocean water, even before considering inefficiencies from remineralization of newly produced organic matter. Controlled field trials are needed to validate or invalidate the findings of this study and other artificial upwelling modeling studies.

DATA AVAILABILITY STATEMENT

Instructions, code, and data necessary to reproduce the results of this study are freely available at: https://doi.org/10.5281/zenodo.6604122.

AUTHOR CONTRIBUTIONS

The author confirms being the sole contributor of this work and has approved it for publication.

ACKNOWLEDGMENTS

I thank the reviewers for their helpful comments that improved this manuscript. I thank Lydia Kapsenberg for her helpful comments which greatly improved this manuscript before submission. This study was inspired by my participation in the scoping workshops for *Uncharted Waters: Expanding the Options for Carbon Dioxide Removal in Coastal and Ocean Environments*. I thank the workshop co-chairs, Brad Ack and Greg Rau, as well as the Energy Futures Initiative, for the invitation to participate.

SUPPLEMENTARY MATERIAL

The Supplementary Material for this article can be found online at: https://www.frontiersin.org/articles/10.3389/fmars.2022.841894/full#supplementary-material

REFERENCES

Atkinson, M. J., and Smith, S. V. (1983). C:N:P Ratios of Benthic Marine Plants. *Limnol. Oceanog.* 28, 568–574. doi: 10.4319/lo.1983.28.3.0568

Bach, L. T., and Boyd, P. W. (2021). Seeking Natural Analogs to Fast-Forward the Assessment of Marine CO2 Removal. *Proc. Natl. Acad. Sci.* 118, e210614718. doi: 10.1073/pnas.2106147118

Bach, L. T., Tamsitt, V., Gower, J., Hurd, C. L., Raven, J. A., and Boyd, P. W. (2021). Testing the Climate Intervention Potential of Ocean Afforestation Using the Great Atlantic Sargassum Belt. *Nat. Commun.* 12, 1–10. doi: 10.1038/s41467-021-22837-2

Baumann, M., Taucher, J., Allanah, J. P., Heinemann, M., Vanharanta, M., Bach, L. T., et al. (2021). Effect of Intensity and Mode of Artificial Upwelling on Particle Flux and Carbon Export. *Front. Mar. Sci.* 8. doi: 10.3389/fmars.2021.742142

Bouman, H. A., Platt, T., Doblin, M., Figueiras, F. G., Gudmundsson, K., Gudfinnsson, H. G., et al. (2018). Photosynthesis-Irradiance Parameters of Marine Phytoplankton: Synthesis of a Global Data Set. *Earth Sys. Sci. Data* 10, 251–266. doi: 10.5194/essd-10-251-2018

Brewer, P. G., Wong, G. T. F., Bacon, M. P., and Spencer, D. W. (1975). An Oceanic Calcium Problem? *Earth Planet. Sci. Lett.* 26, 81–87. doi: 10.1016/0012-821X(75)90179-X

Cao, L., and Caldeira, K. (2010). Atmospheric Carbon Dioxide Removal: Long-Term Consequences and Commitment. *Environ. Res. Lett.* 5, 0–6. doi: 10.1088/1748-9326/5/2/024011

Dutreuil, S., Bopp, L., and Tagliabue, A. (2009). Impact of Enhanced Vertical Mixing on Marine Biogeochemistry: Lessons for Geo-Engineering and Natural Variability. *Biogeosciences* 6, 901–912. doi: 10.5194/bg-6-901-2009

Energy Futures Initiative (2020). *Uncharted Waters: Expanding the Options for Carbon Dioxide Removal in Coastal and Ocean Environments*. Washington, DC, United States.

Fennel, K. (2008). Widespread Implementation of Controlled Upwelling in the North Pacific Subtropical Gyre Would Counteract Diazotrophic N2 Fixation. *Mar. Ecol. Prog. Ser.* 371, 301–303. doi: 10.3354/meps07772

Forsythe, W. C., Rykiel, E. J., Stahl, R. S., Wu, H.-i., and Schoolfield, R. M. (1995). A Model Comparison for Daylength as a Function of Latitude and Day of Year. *Ecol. Model.* 80, 87–95. doi: 10.1016/0304-3800(94)00034-F

Galbraith, E. D., and Martiny, A. C. (2015). A Simple Nutrient-Dependence Mechanism for Predicting the Stoichiometry of Marine Ecosystems. *Proc. Natl. Acad. Sci. Unite. States America* 112, 8199–8204. doi: 10.1073/pnas.1423917112

Garcia, N. S., Sexton, J., Riggins, T., Brown, J., Lomas, M. W., and Martiny, A. C. (2018). High Variability in Cellular Stoichiometry of Carbon, Nitrogen, and Phosphorus Within Classes of Marine Eukaryotic Phytoplankton Under Sufficient Nutrient Conditions. *Front. Microbiol.* 9. doi: 10.3389/fmicb.2018.00543

Gattuso, J.-P., Epitalon, J.-M., Lavigne, H., and Orr, J. (2020) *Seacarb: Seawater Carbonate Chemistry*. Available at: https://cran.r-project.org/package=seacarb.

Gattuso, J.-P., Magnan, A. K., Bopp, L., Cheung, W. W. L., Duarte, C. M., Hinkel, J., et al. (2018). Ocean Solutions to Address Climate Change and its Effects on Marine Ecosystems. *Front. Mar. Sci.* 5. doi: 10.3389/FMARS.2018.00337

Gattuso, J.-P., Williamson, P., Duarte, C. M., and Magnan, A. K. (2021). The Potential for Ocean-Based Climate Action: Negative Emissions Technologies and Beyond. *Front. Mar. Sci.* 2. doi: 10.3389/fclim.2020.575716

GESAMP (2019). *High Level Review of a Wide Range of Proposed Marine Geoengineering Techniques*. Eds. P. W. Boyd and C. M. G. Vivian (London, England: IMO/FAO/UNESCO-IOC/UNIDO/WMO/IAEA/UN/UN Environment/ UNDP/ISA Joint Group of Experts on the Scientific Aspects of Marine Environmental Protection).

Gómez, I., López-Figueroa, F., Ulloa, N., Morales, V., Lovengreen, C., Huovinen, P., et al. (2004). Patterns of Photosynthesis in 18 Species of Intertidal Macroalgae From Southern Chile. *Mar. Ecol. Prog. Ser.* 270, 103–116. doi: 10.3354/meps270103

Gregor, L., and Gruber, N. (2021). OceanSODA-ETHZ: A Global Gridded Data Set of the Surface Ocean Carbonate System for Seasonal to Decadal Studies of Ocean Acidification. *Earth Sys. Sci. Data* 13, 777–808. doi: 10.5194/essd-13-777-2021

Gruber, N., Clement, D., Carter, B. R., Feely, R. A., van Heuven, S., Hoppema, M., et al. (2019). The Oceanic Sink for Anthropogenic CO_2 From 1994 to 2007. *Science* 363, 1193–1199. doi: 10.1126/science.aau5153

Holte, J., Talley, L. D., Gilson, J., and Roemmich, D. (2017). An Argo Mixed Layer Climatology and Database. *Geophys. Res. Lett.* 44, 5618–5626. doi: 10.1002/2017GL073426

IPCC (2018). "Summary for Policymakers," in *Global Warming of 1.5°C. An Ipcc Special Report on the Impacts of Global Warming of 1.5°C Above Pre-Industrial Levels and Related Global Greenhouse Gas Emission Pathways, in the Context of Strengthening the Global Response to the Threat of Climate Change*. Eds. V. Masson-Delmotte, P. Zhai, H.-O. Pörtner, D. Roberts, J. Skea, P. R. Shukla, et al. Geneva, Switzerland. 32.

IPCC (2021). "The Physical Science Basis. Contribution of Working Group I to the Sixth Assessment Report of the Intergovernmental Panel on Climate Change," in *Climate Change*, vol. 2021 . Eds. V. Masson-Delmotte, P. Zhai, A. Pirani, S. L. Connors, C. Péan, S. Berger, et al (Cambridge University Press). doi: 10.1017/9781009157896

Johansson, G., and Snoeijs, P. (2002). Macroalgal Photosynthetic Responses to Light in Relation to Thallus Morphology and Depth Zonation. *Mar. Ecol. Prog. Ser.* 244, 63–72. doi: 10.3354/meps244063

Jones, C. D., Ciais, P., Davis, S. J., Friedlingstein, P., Gasser, T., Peters, G. P., et al. (2016). Simulating the Earth System Response to Negative Emissions. *Environ. Res. Lett.* 11. doi: 10.1088/1748-9326/11/9/095012

Karl, D. M., and Letelier, R. M. (2008). Nitrogen Fixation-Enhanced Carbon Sequestration in Low Nitrate, Low Chlorophyll Seascapes. *Mar. Ecol. Prog. Ser.* 364, 257–268. doi: 10.3354/meps07547

Keller, D. P., Feng, E. Y., and Oschlies, A. (2014). Potential Climate Engineering Effectiveness and Side Effects During a High Carbon Dioxide-Emission Scenario. *Nat. Commun.* 5, 3304. doi: 10.1038/ncomms4304

Keller, D. P., Lenton, A., Littleton, E. W., Oschlies, A., Scott, V., and Vaughan, N. E. (2018). The Effects of Carbon Dioxide Removal on the Carbon Cycle. *Curr. Climate Change Rep.* 4, 250–265. doi: 10.1007/s40641-018-0104-3

Kirke, B. (2003). Enhancing Fish Stocks With Wave-Powered Artificial Upwelling. *Ocean. Coast. Manage.* 46, 901–915. doi: 10.1016/S0964-5691(03)00067-X

Kithil, P. W. (2007). "Self-Reported Results of Field Trial," in *Ocean-Based Climate Solutions*. Available at: https://ocean-based.com/science.

Kwiatkowski, L., Ricke, K. L., and Caldeira, K. (2015). Atmospheric Consequences of Disruption of the Ocean Thermocline. *Environ. Res. Lett.* 10, 34016. doi: 10.1088/1748-9326/10/3/034016

Lauvset, S. K., Key, R. M., Olsen, A., Van Heuven, S., Velo, A., Lin, X., et al. (2016). A New Global Interior Ocean Mapped Climatology: The 1° × 1° GLODAP Version 2. *Earth Sys. Sci. Data* 8, 325–340. doi: 10.5194/essd-8-325-2016

Letelier, R. M., Strutton, P. G., and Karl, D. M. (2008). Physical and Ecological Uncertainties in the Widespread Implementation of Controlled Upwelling in the North Pacific Subtropical Gyre. *Mar. Ecol. Prog. Ser.* 371, 305–308. doi: 10.3354/meps07773

Liu, C. C. K. (1999). *ROM IOA Newslett.* 10, (4):1–8.

Liu, C. C. K., and Jin, Q. (1995). Artificial Upwelling in Regular Waves. *Ocean. Eng.* 22, 337–350. doi: 10.1016/0029-8018(94)00019-4

Longhurst, A. R. (2010). *Ecological Geography of the Sea* (Elsevier).

Moore, J. K., and Braucher, O. (2008). Sedimentary and Mineral Dust Sources of Dissolved Iron to the World Ocean. *Biogeosciences* 5, 631–656. doi: 10.5194/bg-5-631-2008

Moore, C. M., Mills, M. M., Arrigo, K. R., Berman-Frank, I., Bopp, L., Boyd, P. W., et al. (2013). Processes and Patterns of Oceanic Nutrient Limitation. *Nat. Geosci.* 6, 701–710. doi: 10.1038/ngeo1765

Moreira, D., and Pires, J. C. M. (2016). Atmospheric CO_2 Capture by Algae: Negative Carbon Dioxide Emission Path. *Biores. Technol.* 215, 371–379. doi: 10.1016/j.biortech.2016.03.060

NASA (2020). Moderate-Resolution Imaging Spectroradiometer (MODIS) Aqua Photosynthetically Available Radiation Data; 2018 Reprocessing. *NASA OB.DAAC*. Greenbelt, MD, United States. doi: 10.5067/AQUA/MODIS/L3B/PAR/2018

National Academies of Sciences, Engineering, and Medicine (2019). *Negative Emissions Technologies and Reliable Sequestration: A Research Agenda* (Washington DC: National Academies Press). doi: 10.17226/25259

National Academies of Sciences, Engineering and Medicine (2022). A Research Strategy for Ocean-Based Carbon Dioxide Removal and Sequestration. (Washington, DC: The National Academies Press). doi: 10.17226/26278

OceanNETs (2021) *European Union Horizon 2020 Research; Innovation Programme*. Available at: https://www.oceannets.eu/.

Oschlies, A., Pahlow, M., Yool, A., and Matear, R. J. (2010). Climate Engineering by Artificial Ocean Upwelling: Channelling the Sorcerer's Apprentice. *Geophys. Res. Lett.* 37, 1–5. doi: 10.1029/2009GL041961

Pan, Y., Fan, W., Zhang, D., Chen, J., Huang, H., Liu, S., et al. (2016). Research Progress in Artificial Upwelling and its Potential Environmental Effects. *Sci. China Earth Sci.* 59, 236–248. doi: 10.1007/s11430-015-5195-2

Pan, Y., Li, Y., Fan, W. E. I., Zhang, D., Qiang, Y., Jiang, Z. P., et al. (2019). A Sea Trial of Air-Lift Concept Artificial Upwelling in the East China Sea. *J. Atmosph. Ocean. Technol.* 36, 2191–2204. doi: 10.1175/JTECH-D-18-0238.1

Redfield, A. C. (1934). "On the Proportions of Organic Derivatives in Sea Water and Their Relation to the Composition of Plankton," in *James Johnston Memorial Volume*. Ed. R. J. Daniel (Liverpool, England: University Press Liverpool), 176–192.

Roberts, D. A., Paul, N. A., Dworjanyn, S. A., Bird, M. I., and De Nys, R. (2015). Biochar From Commercially Cultivated Seaweed for Soil Amelioration. *Sci. Rep.* 5, 1–6. doi: 10.1038/srep09665

Sarmiento, J. L., and Gruber, N. (2006). *Ocean Biogeochemical Dynamics* (Princeton, New Jersey: Princeton University Press).

Schulzweida, U. (2019). *CDO User Guide*. doi: 10.5281/zenodo.3539275

Siegel, D. A., DeVries, T., Doney, S. C., and Bell, T. (2021). Assessing the Sequestration Time Scales of Some Ocean-Based Carbon Dioxide Reduction Strategies. *Environ. Res. Lett.* 16, 104003. doi: 10.1088/1748-9326/ac0be0

Stommel, H., Arons, A. B., and Blanchard, D. (1956). An Oceanographical Curiosity: The Perpetual Salt Fountain. *Deep. Sea. Res. (1953).* 3, 152–153. doi: 10.1016/0146-6313(56)90095-8

Taucher, J., Boxhammer, T., Bach, L. T., Paul, A. J., Schartau, M., Stange, P., et al. (2021). Changing Carbon-to-Nitrogen Ratios of Organic-Matter Export Under Ocean Acidification. *Nat. Climate Change* 11, 52–57. doi: 10.1038/s41558-020-00915-5

Vershinskiy, N. V., Pshenichnyy, B. P., and Soloviev, A. V. (1987). Artificial Upwelling Using the Energy of Surface Waves. *Oceanology* 27, 400–402.

Ocean Visions (2021) *Ocean-Based Carbon Dioxide Removal: Road Maps*. Available at: https://oceanvisions.org/roadmaps/.

Wanninkhof, R., Asher, W. E., Ho, D. T., Sweeney, C., and McGillis, W. R. (2009). Advances in Quantifying Air-Sea Gas Exchange and Environmental Forcing. *Annu. Rev. Mar. Sci.* 1, 213–244. doi: 10.1146/annurev.marine.010908.163742

Weiss, R. (1974). Carbon Dioxide in Water and Seawater: The Solubility of a Non-Ideal Gas. *Mar. Chem.* 2, 203–215. doi: 10.1016/0304-4203(74)90015-2

White, A., Björkman, K., Grabowski, E., Letelier, R., Poulos, S., Watkins, B., et al. (2010). An Open Ocean Trial of Controlled Upwelling Using Wave Pump Technology. *J. Atmosph. Ocean. Technol.* 27, 385–396. doi: 10.1175/2009JTECHO679.1

Yool, A., Shepherd, J. G., Bryden, H. L., and Oschlies, A. (2009). Low Efficiency of Nutrient Translocation for Enhancing Oceanic Uptake of Carbon Dioxide. *J. Geophys. Res.: Ocean.* 114, 1–13. doi: 10.1029/2008JC004792

Conflict of Interest: The author declares that the research was conducted in the absence of any commercial or financial relationships that could be construed as a potential conflict of interest.

Publisher's Note: All claims expressed in this article are solely those of the authors and do not necessarily represent those of their affiliated organizations, or those of the publisher, the editors and the reviewers. Any product that may be evaluated in this article, or claim that may be made by its manufacturer, is not guaranteed or endorsed by the publisher.

frontiers | Frontiers in Marine Science

TYPE Original Research
PUBLISHED 14 October 2022
DOI 10.3389/fmars.2022.1006010

OPEN ACCESS

EDITED BY
Jun Sun,
China University of Geosciences
Wuhan, China

REVIEWED BY
Oscar E. Romero,
University of Bremen, Germany
Haocai Huang,
Zhejiang University, China

*CORRESPONDENCE
Isabel Baños
isabel.banos@ieo.csic.es
Javier Arístegui
javier.aristegui@ulpgc.es

SPECIALTY SECTION
This article was submitted to
Marine Biogeochemistry,
a section of the journal
Frontiers in Marine Science

RECEIVED 28 July 2022
ACCEPTED 27 September 2022
PUBLISHED 14 October 2022

CITATION
Baños I, Arístegui J, Benavides M, Gómez-Letona M, Montero MF, Ortiz J, Schulz KG, Ludwig A and Riebesell U (2022) Response of plankton community respiration under variable simulated upwelling events. *Front. Mar. Sci.* 9:1006010. doi: 10.3389/fmars.2022.1006010

Response of plankton community respiration under variable simulated upwelling events

Isabel Baños[1]*, Javier Arístegui[1]*, Mar Benavides[2], Markel Gómez-Letona[1], María F. Montero[1], Joaquín Ortiz[3], Kai G. Schulz[4], Andrea Ludwig[3] and Ulf Riebesell[3]

[1]Oceanografía Biológica, Instituto de Oceanografía y Cambio Global (IOCAG), Universidad de Las Palmas de Gran Canaria, Las Palmas de Gran Canaria, Spain, [2]Aix Marseille Univ., Université de Toulon, CNRS, IRD, MIO, Marseille, France, [3]Marine Biogeochemistry, Biological Oceanography, GEOMAR Helmholtz Center for Ocean Research, Kiel, Germany, [4]Centre for Coastal Biogeochemistry, Southern Cross University, Faculty of Science and Engineering, Lismore, NSW, Australia

Climate change is expected to alter the intensity and frequency of upwelling in high productive coastal regions, thus impacting nutrient fluxes, primary productivity and consequently carbon cycling. However, it is unknown how these changes will impact the planktonic (phytoplankton and bacteria) community structure, which affects community respiration (CR) and hence the carbon available for sequestration or transfer to upper trophic levels. Here we present results from a 37-day mesocosm experiment where we examined the response of CR to nutrient additions by simulating upwelling events at different intensities (low, medium, high and extreme) and modes (singular and recurring additions). We also analysed the potential contribution of different plankton size classes and functional groups to CR. The trend in accumulated CR with respect to nutrient fertilisation (total nitrogen added during the experiment) was linear in the two modes. Microplankton (mostly diatoms) and nanoplankton (small flagellates) dominated under extreme upwelling intensities and high CR in both singular and recurring upwelling modes, explaining >65% of the observed variability in CR. In contrast, prokaryotic picoplankton (heterotrophic bacteria and autotrophic cyanobacteria) explained <43% of the variance in CR under the rest of the upwelling intensities and modes tested. Changes in planktonic community structure, while modulating CR variability, would regulate the metabolic balance of the ecosystem, shifting it towards net-heterotrophy when the community is dominated by small heterotrophs and to net-autotrophy when large autotrophs prevail; although depending on the mode in which nutrients are supplied to the system. This shift in the dominance of planktonic organism will hence affect not only CR but also carbon sequestration in upwelling regions

KEYWORDS

nutrient availability, artificial upwelling, carbon export, EBUS, mesocosm, climate change

1 Introduction

Coastal upwelling regions are among the most productive ecosystems in the ocean (Ryther, 1969). Biological productivity in upwelling systems responds to nutrient inputs from deep layers, which can be highly variable among different regions, depending on wind intensity and frequency, as well as other physical drivers such as wind curl or coastal bathymetry (Kämpf and Chapman, 2016). Overall, nutrient inputs are the main drivers of phytoplankton blooms and organic matter accumulation (Hutchings et al., 1995), which in turn trigger changes in community respiration (CR) rates influencing the amount of carbon available for deep ocean sequestration or transfer to upper trophic levels (Williams and Del Giorgio, 2005; Azam and Malfatti, 2007; Capone and Hutchins, 2013). Climate change is expected to alter coastal wind regimes, impacting upwelling intensity and frequency, and the associated pumping of nutrients to the surface layers (Bakun, 1990; García-Reyes et al., 2015; Basu and Mackey, 2018). These alterations can profoundly impact planktonic community structure and productivity, modifying carbon fluxes at a regional level (Legrende and Michaud, 1998; Tamigneaux et al., 1999; Montero et al., 2007). The balance between the production and the respiratory loss of photosynthetically produced organic matter sets CR as an effective index of the movements of organic matter through ecosystems (Williams and Del Giorgio, 2005). Therefore, CR represents a critical parameter for assessing the metabolic balance of aquatic ecosystems (Basu and Mackey, 2018). However, how perturbations in upwelling intensity and frequency will impact CR in upwelling regions is still unclear.

Mesocosm approaches have been widely used over the last decade to simulate climate change scenarios and assess the effects of multiple stressors such as warming or acidification on marine planktonic communities (e.g., Sommer et al., 2007; Riebesell et al., 2008; Schulz et al., 2017; Taucher et al., 2018). To the best of our knowledge, only one study has previously addressed the effect of different intensities of a simulated upwelling on CR (McAndrew et al., 2007). However, this study lasted only four days, being a very short period to assess stressor responses in planktonic community structure and metabolism (e.g., Filella et al., 2018). Moreover, the study focuses exclusively on the response of the autotrophic component of the community to nutrient fertilisation. Here we use a mesocosm approach to simulate changes in upwelling at different intensities and modes and assess their impact on CR over 37-days. The goal of the study was first to look at the short term variability of CR under nutrient pulses of different intensity and duration, and second to see how the autotrophic vs heterotrophic planktonic community structure contributed to this variability. Our results may therefore help predicting present and future changes in the metabolic balance of upwelling regions due to natural or anthropogenic-induced variability.

2 Materials and methods

2.1 Experimental setup and sampling

Between November and December 2018 (37 days in total) a mesocosms experiment was conducted in Gando Bay (Canary Islands, 27°55.673′ N, 15°21.870′ W) as part of the Ocean artUp project. Nine ~44 m^3 mesocosms (Kiel Off-Shore Mesocosms for future Ocean Simulations or KOSMOS; Riebesell et al., 2013) were moored and filled with *in situ* oligotrophic water. Unfortunately, the planned deep water collection to a depth of ~600m could not be achieved due to technical limitations. Instead, deep water was collected between 28°00′N, 15°18′E and 27°57′N, 15°10′E from 330 m depth (day -10) and from 280 m depth (day 23), respectively, using a custom-built collector with a carrying capacity of 100 m^3 (for technical details see Taucher et al., 2017). Subsequently, deep water was enriched with nitrate (NO_3^-), phosphate (PO_4^{3-}), and silicate [$(Si(OH)_4$] to a final concentration of 25, 1.4, and 12.1 µmol L^{-1}, respectively, necessary to achieve the planned simulated upwelling. Deep water was then added to the mesocosms to simulate different upwelling modes (singular and recurring additions) and intensities (low, medium, high and extreme additions), the latter defined according to the total amount of water volume replaced by deep water (Figure 1). In the recurring mode, four mesocosms (M2, M4, M6, M8) received an addition of deep water every four days starting on day 4, and until the end of the experiment. In the singular mode, another four mesocosms (M1, M3, M7, M9) received a singular deep-water pulse on day 4 and were not further fertilised throughout the experiment. The amount of nutrients added in each of the four intensity levels (low, medium, high and extreme) was similar for both upwelling modes (Figure 1B). No deep water addition was carried out for M5 (Control). 152 samples (19 samplings from each of the 8 mesocosms) were obtained from the entire water column (0-13m) using a depth-integrated water sampler (IWS, Hydro-Bios, Kiel). In the present study, M9 was not sampled due to logistical issues in the supply of the glass bottles. For more details on the experimental setup and sampling procedures see Baumann et al. (2021).

2.2 Community respiration

Mesocosm water samples for community respiration measurements were pre-filtered through a 250 µm mesh and

10.3389/fmars.2022.1006010

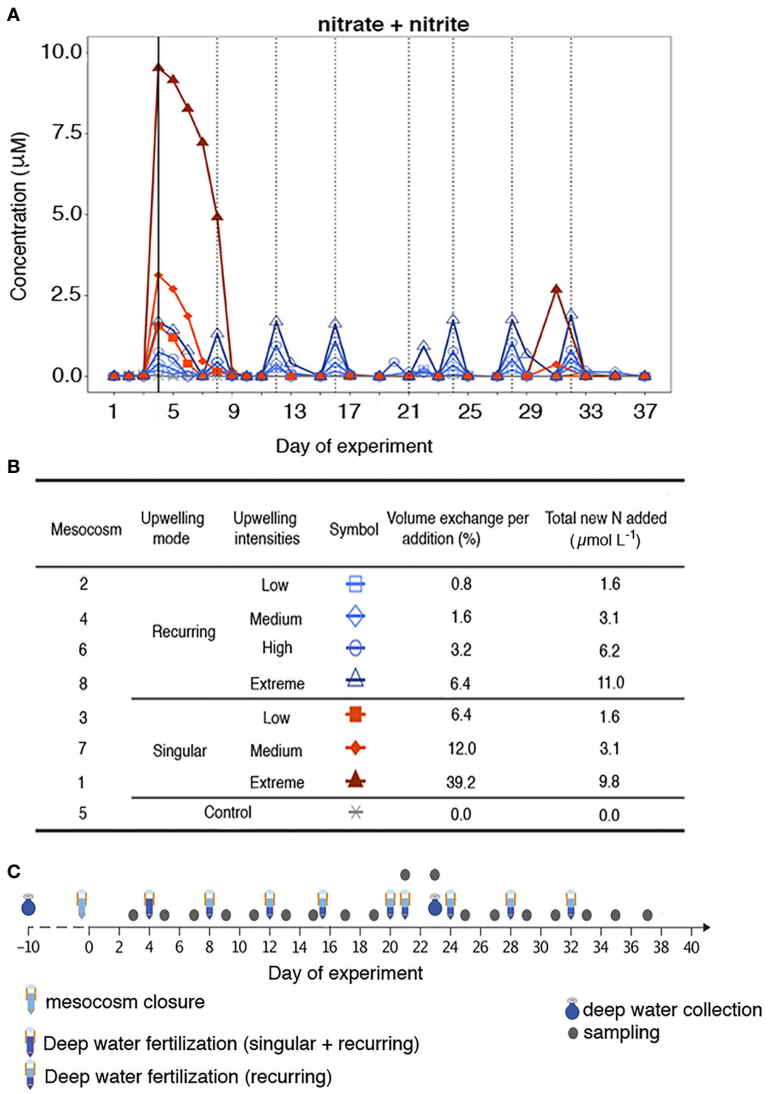

Mesocosm	Upwelling mode	Upwelling intensities	Symbol	Volume exchange per addition (%)	Total new N added (μmol L^{-1})
2	Recurring	Low		0.8	1.6
4		Medium		1.6	3.1
6		High		3.2	6.2
8		Extreme		6.4	11.0
3	Singular	Low		6.4	1.6
7		Medium		12.0	3.1
1		Extreme		39.2	9.8
5	Control			0.0	0.0

FIGURE 1
(A) Nitrate + nitrite evolution during the experiment. The solid black line indicates the first deep-water addition (except in the control). The dotted black lines indicate the addition made only to the recurring treatment. **(B)** Types of treatment, symbol encoded, mesocosms, volume exchange per addition (%) and total new N added (µmol L-1). **(C)** Mesocosms sampling timeline adapted from Baumann et al. (2021).

carefully siphoned using a silicone tube into four replicate "time-zero" and four replicate "dark" 125 mL borosilicate bottles. Dark bottles were incubated in an outdoor pool at seawater temperature (~20.7-21.5°C) for ~24 h. CR was determined by oxygen consumption measured by the Winkler technique, following the recommendations of Carritt and Carpenter (1966); Bryan et al. (1976) and Grasshoff (1983). The entire content of the bottles was titrated during ~3 min by means of an automated, precise titration system with colorimetric end-point detection (Williams and Jenkinson, 1982). The precision achieved in replicates was %CV < 0.07. CR was estimated from the difference in oxygen concentration between the mean of the four time-zero and the mean of the four dark bottles.

2.3 Phytoplankton community composition and biomass

Samples for phytoplankton community composition were filtered onto 0.7 µm pore size glass fiber filters under low pressure (200 mbar, Whatman GF/F, Maidstone, UK). Filters were immediately frozen in liquid nitrogen and subsequently stored at -80°C until analysis. Prior to analysis, samples were mixed with 0.5 mm glass beads and 1.3 mL of 100% high-performance liquid chromatography (HPLC) grade acetone and extracted in a homogenizer. Then, they were centrifuged (10 min, 4°C, 10000 rpm) and the supernatant removed with a syringe and filtered through a PTFE filter (0.2 µm pore size).

Photosynthetic pigments were analyzed through reverse-phase HPLC (Thermo Scientific). The relative contribution to Chla of different phytoplankton classes was calculated using the CHEMTAX algorithm developed by Mackey et al. (1996), applying pigment ratios typically found in the waters off Gran Canaria (Taucher et al., 2018).

The biomass of different phytoplankton groups was estimated by transforming their estimated individual chlorophyll a (Chl-a) concentration to carbon using conversion ratios (g/g) from Sathyendranath et al. (2009): 141 (Prasinophytes and Chlorophytes), 53 (Dinoflagellates), 64 (Diatoms), 88 (Cryptophytes, Chrysophytes and Prymnesiophytes), 140 (Cyanobacteria).

2.4 Heterotrophic bacteria biomass

Seawater samples were fixed with 50 µL of 20% paraformaldehyde (2% final concentration), kept in darkness at 4°C for 30 min and subsequently preserved at -80°C. Heterotrophic bacterial abundance was determined using a FACSCalibur flow cytometer (Becton Dickinson) equipped with an air cooled blue (488nm) argon laser. Briefly, frozen samples were thawed and a 400 µL subsample stained with SYBR Green I (Invitrogen) at room temperature for 15 min. Heterotrophic bacteria were identified in a plot of side scatter (SSC) versus green fluorescence (FL1). Samples were run at low flow rate (22 µL min^{-1}). A suspension of yellow-green 1 µm latex beads (~10^5 - 10^6 beads mL^{-1}) was added as an internal standard (Polysciences, Inc., Warrington, PA, Unites States). Heterotrophic bacterial biomass was estimated by multiplying their abundance by a conversion factor (18 fgC $cell^{-1}$) obtained empirically in coastal waters off Gran Canaria (Montero et al. unpublished).

2.5 Statistics

To assess the effect of upwelling intensity and mode on CR rates a linear mixed-effects (LME) model was applied using "treatment" and "day of experiment" as categorical variables, and "treatment" as a random factor. CR rates were compared by the Dunnet´s test after inspection of normality and homogeneity of the variance. LME models were applied using the *nlme* package in R (v. 3.1-153; Pinheiro et al., 2007). In order to evaluate the variables (biomass of plankton groups) influencing CR during the experiment, multivariate regression models were fitted *via* Stepwise Multiple Linear regressions (SMLR). The contribution of every statistically significant predictor variable to the explained variance was quantified calculating the Relative Importance (%) using the *relaimpo* package in R (v 2.2-6; Grömping, 2006). All statistical analyses were performed in R Statistical Environment (v. 4.1.2; R Core Team, 2021).

3 Results

3.1 Temporal variability in plankton community respiration

CR rates ranged between 19.6 (on average for all mesocosms at the beginning of the experiment) to 292.2 mg O_2 m^{-3} d^{-1} in the singular addition extreme treatment (day 13) and 229.5 mg O_2 m^{-3} d^{-1} in the recurring addition extreme treatment (day 35) (Figure 2). These rates were slightly lower than those previously reported from the Canary Current and NW Africa upwelling (Arístegui and Montero, 1995; Robinson et al., 2002) and Benguela upwelling (Robinson et al., 2002), but higher than those observed in other coastal upwelling systems like the NW Iberian (Moncoiffé et al., 2000) or the Chilean upwelling systems (Daneri et al., 2000).

CR rates differed significantly among upwelling modes and intensities (LME model, $p<0.005$), reaching the highest values in the extreme intensity treatments. In the singular upwelling mode, CR rates increased after day 4 and peaked on day 7, 9 and 13 for low, medium and extreme intensities, respectively. The magnitude of this response increased with upwelling intensity. Following the peak, CR rates decreased and remained relatively constant until the end of the experiment. In contrast, the recurring mode showed a gradual rise in CR rates according to the intensity of the simulated upwelling with some fluctuations until the end of the experiment. In the extreme treatment of the recurring mode, CR rates dropped on day 19 and remained fairly constant until day 31 and increased again from day 33 to day 35, due to the development of a Prymnesiophyceae bloom (see section 3.2). Overall, maximum CR rates were observed on day 35 in all recurring intensities, diminishing at the end of the experiment (day 37), except in the low recurring mode treatment where it remained rather constant.

Cumulative community respiration (CR_{cum}) evolved differently in the various treatments from day 7 onwards (Figure 3A). The CR_{cum} of the singular extreme treatment increased faster than in the rest of the treatments, although it reached similar values to the recurring extreme treatment at the end of the experiment. From day 9 to day 25, CR_{cum} in the low and medium singular mode treatments were higher than those reported in the recurring mode treatments. However, this pattern shifted from day 25 onwards, when CR_{cum} became higher in the low and medium recurring mode treatments than in the singular mode counterparts. CR_{cum} displayed a positive relationship with upwelling intensity (Figure 3B), with a similar effect for both upwelling modes after the last deep water addition to the recurring treatment.

10.3389/fmars.2022.1006010

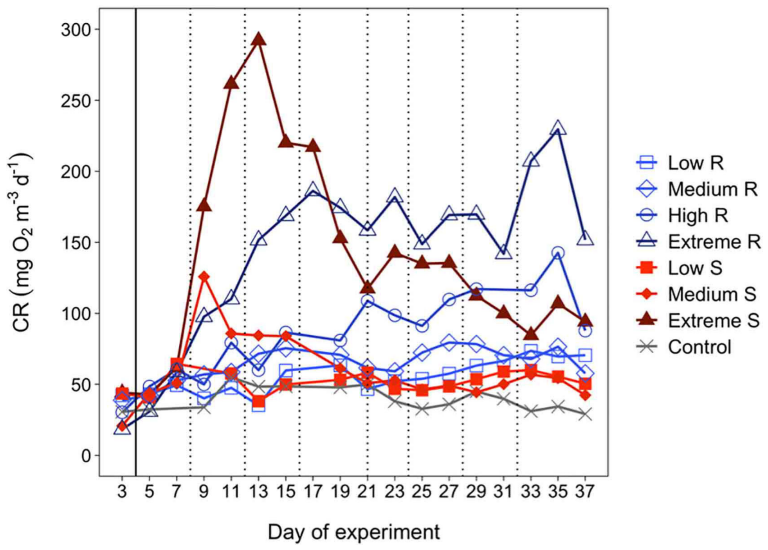

FIGURE 2
Temporal development of plankton community respiration (CR). The solid black line indicates the first deep-water addition (except in the control). The dotted black lines indicate the addition made only to the recurring treatment.

3.2 Contribution of different planktonic groups to total community biomass and respiration

The different upwelling modes and intensities impacted the contribution of different planktonic groups to total community biomass (Figure 4). Microplankton was favoured under extreme upwelling intensities (Figures 4F, G), contributing up to 75% and 50% of the biomass in the singular and recurring modes, respectively. The contribution of nanoplankton to total community biomass was relatively high throughout the experiment in the low treatments of both upwelling modes (Figures 4A, B), as well as in the control (Figure 4H), ranging from 24 to 54%. In the high and extreme recurring mode treatments (Figures 4E–G) the contribution of nanoplankton increased at the end of the experiment (from day 31 onwards), due in large part to the development of a Prymnesiophyceae bloom, representing up to 55% and 60% respectively, but only after the last nutrient addition made on day 32.

The contribution of picoplankton to total community biomass was higher in the control and in the low and medium recurring treatments (Figures 4A, C, H) than in the rest of the treatments. In the low recurring treatment, cyanobacteria represented between 10 and 20% of the biomass, whereas heterotrophic bacteria represented from 25 to 50% of the biomass (Figure 4A). In the low singular treatment, cyanobacteria ranged between 4 and 18%, and heterotrophic bacteria between 25 and 40% (Figure 4B). From day 21 to 31, the contribution of heterotrophic bacteria increased in the extreme singular mode treatment, exceeding the contribution of microplankton to total biomass with values up to 75% (Figure 4F).

Different plankton groups contributed to explaining the variance observed in CR, as revealed by the stepwise multiple regression analysis performed with the biomass of plankton groups and CR during the experiment (Table 1). Particularly, large phytoplankton cells (i.e., microplankton and nanoplankton) were the most important variables explaining the variance in CR during extreme recurring and singular treatments, respectively, but also a notable proportion of the variance in the rest of the treatments, ranging from 57% in the medium recurrent treatment to 87% in the low recurrent treatment. In the case of picoplankton, their contributions to CR turned out to be relevant depending on the upwelling mode intensities. For example, in the recurring mode cyanobacteria explained 22 and 26% of the variance in the high and medium simulated-upwelling treatments, whereas heterotrophic bacteria explained 12 and 16% respectively. However, in the singular mode, heterotrophic bacteria explained 24% and 32% of the CR variance in the medium and low treatments respectively, whereas cyanobacteria did not appear as an explanatory variable.

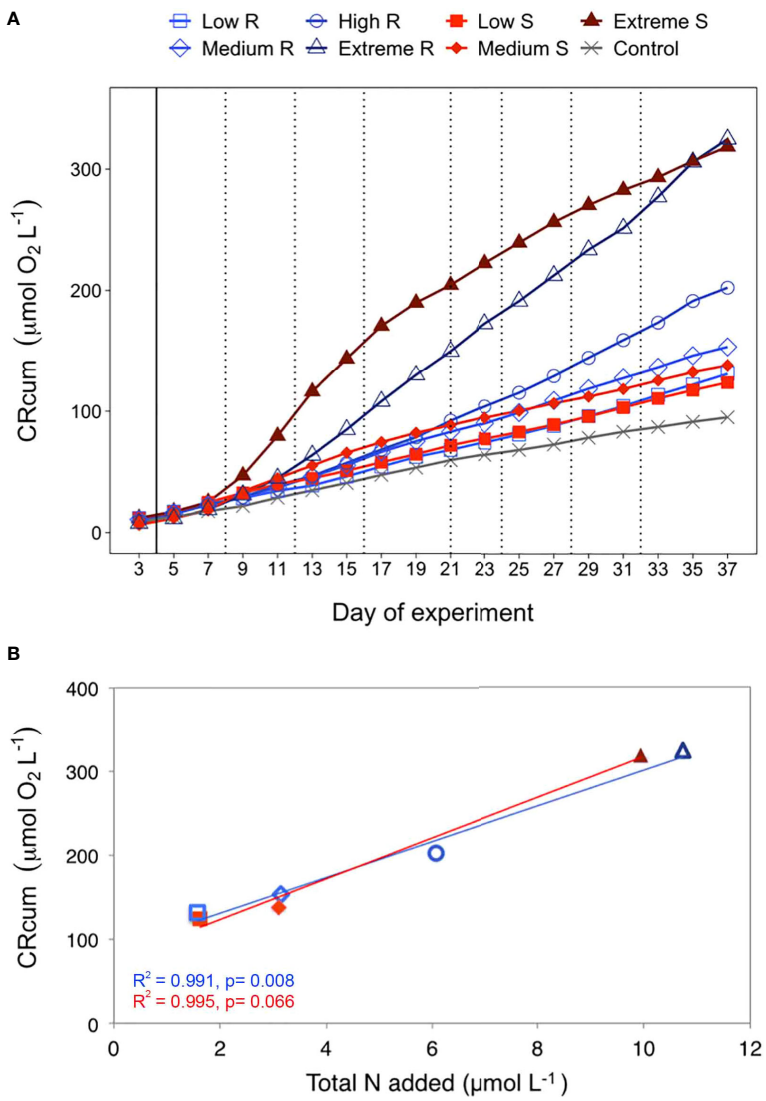

FIGURE 3
(A) Temporal development of plankton community respiration as accumulated rates (CRcum) over the course of the experiment in the control and in the two treatments: singular and recurring. The solid black line indicates the first deepwater addition (except the control). The dotted black lines indicate the additions made only during the recurring treatment. **(B)** Accumulated community respiration (CRcum) at the end of the experiment (day 37) per µmol of nutrients added.

4 Discussion

4.1 Variability in community respiration in the different simulated-upwelling intensity and modes

Here, we tested the effects of different simulated-upwelling modes and intensities in a longer (37-day) experiment and found that CR varied significantly among upwelling modes and intensities (LME model, $p<0.005$, Figure 2), driven by changes in the planktonic community structure.

Following the initial nutrient fertilization on day 4, the temporal variability in CR displayed two distinguishable patterns according to the upwelling modes. Singular treatments induced an abrupt increase in CR rates, reaching their maximum values between days 7 and 13, a few days after the deep-water addition. In contrast, recurring treatments provoked a gradual boost in CR, which reached its maximum rates towards the end of the experiment (day 35). The mode in which upwelling events release nutrients into oligotrophic waters, either through singular or recurring pulses, can consequently modulate CR in the short- or long-term, respectively.

Interestingly, a different timing in the response of CR to nutrient fertilisation was observed under the singular treatments, showing a lag of between 5 and 9 days depending on the simulated-upwelling intensity. These results were also observed in another mesocosm experiment conducted at the same location (Filella et al., 2018). In that study, it took around 5 days for CR to be significantly stimulated after the singular deep-water fertilisation. This could explain the discrepancy between our study and the short-term (4 days) study carried out by McAndrew et al. (2007), as 4 days may not be sufficient to fully detect the CR response. Consequently, we stress that longer experiments (at least > 5 days) are needed to adequately assess the impact of variable upwelling events on CR and thus, to better understand their role within coastal upwelling systems.

The effect of upwelling modes and intensities on CR are also evident from the trend of CRcum along the experiment (Figure 3A). A closer look at the slope of CRcum plotted for each treatment revealed changes throughout the experiment, which could be mainly explained by shifts in the planktonic community structure. For instance, the phytoplankton community under the extreme singular treatment shifted from a microplankton-dominated (between day 7 and day 15) to a pico- (heterotrophic bacteria) and nanoplankton-dominated community (between day 17 and day 29) and finally, was dominated by nano- and microplankton (from day 31 until the end of the experiment). Similarly, the observed changes in CRcum slope under the extreme recurring treatment corresponded to a shift from a microplankton-dominated (from day 13 to day 31) to a nano- and microplankton-dominated community (from day 33 onwards). In contrast, the slope of CRcum in the low and medium singular treatments was only higher than that in the recurring ones coinciding with the incipient microplankton bloom triggered by the nutrient fertilization on day 4 until its vanishing on day 25 (Ortiz et al., 2022), before falling below the slope of the recurring treatments as picoplankton dominated the community. A similar size-related pattern has been described in other coastal upwelling systems (Sherr et al., 2005; Lassiter et al., 2006; Wilkerson et al., 2006; Smayda and Trainer, 2010; Anabalón et al., 2014). Looking into the trend of CRcum relative to nutrient fertilisation (as total nitrogen added until the end of the experiment) (Figure 3B), increases in the intensity of both upwelling modes resulted in a linear rise in CRcum, consequently affecting the amount of carbon cycling.

Our results reveal that changes in CR_{cum} during different simulated upwelling events could therefore be attributed to the ways different plankton community structures responded to changes of upwelling modes and intensities. In the following sections, we describe the plankton functional groups that potentially accounted for the observed variance in CR and how these can affect the metabolic balance and therefore, carbon sequestration of upwelling regions.

4.2 Contribution of plankton functional groups to community respiration and metabolic balance

Diatoms bloomed in the extreme treatments, accounting for up to 75% of the total biomass (Figures 4F ,G). Similar increases in diatom biomass have been previously reported in oceanic regions after inorganic nutrient pulses *via* mixing, eddies, fronts and upwelling events (e.g., Hutchings et al., 1995; Arístegui et al., 2004; Edwards and Richardson, 2004; Arístegui and Montero, 2005; Clayton et al., 2014; Tréguer et al., 2018) as well as in experimental manipulations (Mahaffey et al., 2012; Anil et al., 2021). Temporal variations in CR matched shifts in community structure. Thus, the early rise in diatom biomass (75% on day 13 in the extreme singular treatment and 62% on day 17 in the recurring treatment) coincided with high CR rates (293 and 183 mg O_2 m^{-3} d^{-1}, respectively), meaning that a meaningful fraction of the intracellular carbon pool newly fixed through photosynthesis was potentially lost by autotrophic respiration. Multiple stepwise linear regressions further revealed that diatoms explained between 37% and 47% of the variance in CR, in the extreme singular and recurring treatments, respectively (Table 1). Following nutrient depletion (day 9 and beyond day 32 onwards in the singular and extreme recurring treatment, respectively, Figure 1A), diatoms were outcompeted by nanoplankton (Böttjer et al., 2007). Our results revealed that diatoms and nanoplankton were the main contributors to explaining the variance in CR under extreme upwelling intensities.

Contrary to expectations (e.g., Edwards and Richardson, 2004; Du and Peterson, 2014; Bode et al., 2015), dinoflagellates did not thrive under low upwelling intensities (Figures 4A,B). On the other hand, picoplanktonic organisms (heterotrophic bacteria and cyanobacteria) are usually recognized as extremely efficient in nutrient acquisition at low concentrations due to their small size (i.e., higher surface/volume ratio). Hence, they are deemed to contribute more importantly to carbon fluxes in nutrient deplete rather than in nutrient replete regions (Del Giorgio et al., 1997; Gasol and Duarte, 2000; Zubkov 2014). In our study, heterotrophic bacteria displayed contrasting patterns between upwelling modes, decreasing in relative biomass as the upwelling intensities increased in the recurring mode (from ~40% in the low to 25% in the extreme treatment; Figures 4A-G) and increasing in the singular ones (from ~40% in the low to >80% in the extreme treatment; Figures 4B-F) with a posterior drop (between 25 – 10%) when nutrients were exhausted. Given that large blooms were induced in the extreme treatments (Ortiz et al., 2022) we expected that heterotrophic bacteria would be stimulated by the DOC released and would actively contribute to CR (Blight et al., 1995). Nonetheless, DOC remarkably accumulated in the extreme treatments (Gómez-Letona et al., 2022) suggesting that a major part of this DOC was not utilized by heterotrophic bacteria, which would explain the low contribution to CR in these

10.3389/fmars.2022.1006010

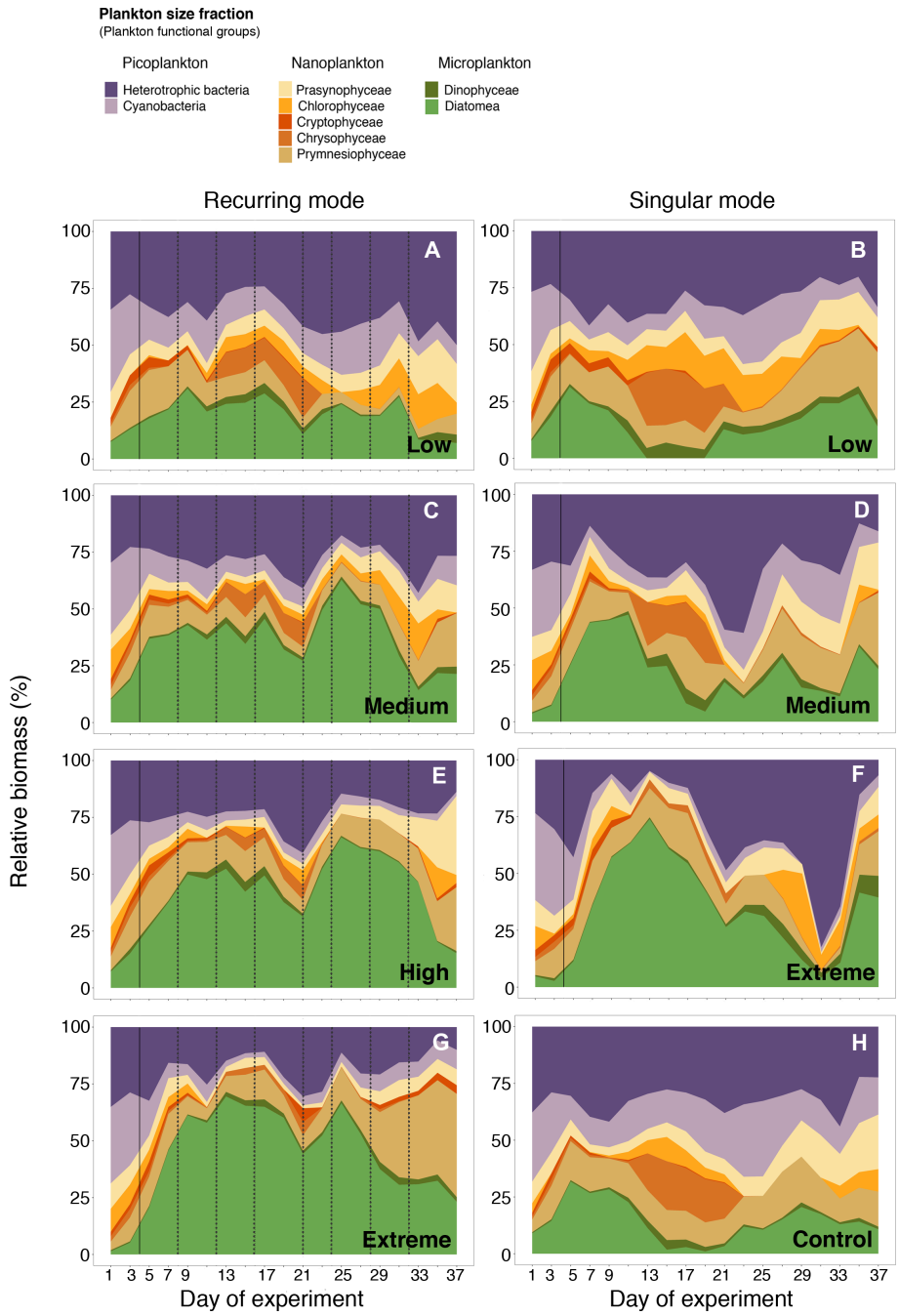

FIGURE 4
Relative contribution of plankton community composition (represented as size fractions: Pico-, Nano- and Microplankton) over the course of the experiment. Picoplankton: heterotrophic bacteria and cyanobacteria; Nanoplankton: prasynophyceae, chlorophyceae, cryptophyceae, chrysophyceae and prymnesiophyceae; Microplankton: dinophyceae and diatomea. The solid black line indicates the first deep-water addition (except in the control). The dotted black lines indicate the addition made only to the recurring treatment. Panels **(A**, **C**, **E**, **G)** refer to recurring mode, and panels **(B**, **D**, **F)** to singular mode from low to extreme upwelling intensities (respectively). Panel **(H)** is the control.

treatments. A variable contribution of heterotrophic bacteria to the variance in CR was found in the other upwelling intensities (16% and 12% under medium and high recurring treatments and 33% and 25% under low and medium singular treatments). The fact that heterotrophic bacteria explained less than 33% of the CR variance in these singular treatments was surprising, given their high relative biomass. This points to a variable metabolic activity of bacteria, that does not depend only on the accumulated biomass.

10.3389/fmars.2022.1006010

TABLE 1 Stepwise multiple linear regression statistics between plankton community respiration (CR) with the biomasses of heterotrophic bacteria (Het. bacteria) and the different phytoplankton groups (Cyanobacteria, Prasynophyceae, Chlorophyceae, Cryptophyceae, Chrysophyceae and Prymnesiophyceae, Diatoms and Dinoflagellates), under the different upwelling modes and intensities, compared to the control (no upwelling).

Upwelling mode	Upwelling intensity	X_i	R^2 adjust	pvalue	F statistic	RI(%)
Recurring	Extreme	DiatomsChlorophyceaeCryptophyceae	0.747	<0.001	17.72	46.6239.9113.47
	High	CryptophyceaeCyanobacteriaDinoflagellatesPrymnesiophyceaeHet.bacteriaChlorophyceae	0.790	<0.001	10.4	25.9622.4914.7112.5712.2612.01
	Medium	DinoflagellatesCyanobacteriaDiatomsHet. bacteria	0.647	<0.01	8.32	36.0526.612116.33
	Low	ChlorophyceaePrymnesiophyceaeCyanobacteriaChrysophyceae	0.578	<0.01	6.48	44.7836.1912.696.34
Control		DinoflagellatesHet.bacteriaChlorophyceaePrymnesiophyceaeDiatoms	0.598	<0.05	4.72	48.3017.1817.138.718.66
Singular	Extreme	DiatomsCryptophyceaePrymnesiophyceae	0.923	<0.0001	69.26	36.8037.8025.41
	Medium	DiatomsHet.bacteriaDinoflagellatesCryptophyceaeChlorophyceae	0.876	<0.0001	23.71	41.6624.5013.9713.526.34
	Low	PrymnesiophyceaeHet.bacteriaDinoflagellatesCryptophyceae	0.484	<0.05	4.51	48.4632.5012.047

X_i, statistically significant predictor variables; R^2 adjust, adjusted correlation coefficient; RI(%), percentage of the variance explained by each group.

A previous study carried out along two latitudinal transects from 50°N to 44°S in the Atlantic Ocean showed that the contribution of bacteria to CR is highly variable (4-77%), suggesting that Chl-a and other factors rather than those assessed in that study (such as nutrient availability and temperature) must be driving such variability (García-Martín et al., 2017). Flagellate grazing is recognized as one of the main factors controlling marine bacterial communities (Böttjer and Morales, 2007; Bunse and Pinhassi, 2017). Accordingly, we observed declines in the relative biomass of heterotrophic bacteria coinciding with the enhancement of nanoplankton biomass, suggesting a strong predation pressure and, therefore, a potential top-down control over heterotrophic bacteria. Such drops in biomass contribution can be observed through the experiment in the different upwelling intensities and modes. Grazing could also affect cyanobacterial populations, which were only identified as predictors of the variance in CR in the singular mode. Nevertheless, we do not discard that other factors external to our observations may be acting. For example, there might be heterogeneity in the respiration rates dynamics of different bacterioplankton groups, derived from the strong metabolic heterogeneity among the different components of bacterial communities (Cottrell and Kirchman, 2000; Alonso-Sáez et al., 2012). Furthermore, viral lysis (not taken into account in this study) may play a significant role in controlling the abundance of different bacterioplankton groups (Breitbart et al., 2008), causing bacterial mortality and thus could affect the patterns observed here.

The planktonic community structure, while modulating CR variability, would display a key role in regulating the metabolic balance of the ecosystem, shifting it towards net-heterotrophy when the planktonic community is dominated by small heterotrophs and to net-autotrophy when large autotrophs prevail (Ortiz et al., 2022). Altogether, our results suggest that upwelling regions subject to low upwelling intensities will tend to display a heterotrophic metabolism dominance during relaxation or low-intensity upwelling episodes, thus decreasing the carbon sequestration capacity. On the contrary, the metabolic balance in upwelling regions subjected to extreme upwelling intensities will depend on the mode in which nutrients are supplied to the system. Thus, in natural systems where upwelling pulses are markedly separated in time or under sudden dust deposition events (similar to our extreme singular treatment), upwelling regions could support a high CR, but decoupled in time from primary production. This would be followed by an increase in net heterotrophy as primary production decreases after the initial bloom. On the other hand, periods of recurring upwelling intensities would lead to a net-autotrophic system, potentially increasing the carbon sequestration of the system.

5 Conclusions

We studied the link between the variability in community respiration rates and shifts in the planktonic community structure

under different modes and intensities of simulated upwelling over a long term (37 days) mesocosm experiment. Our results suggest that CR is particularly sensitive to changes in the upwelling intensities but more significantly to the mode in which nutrients are supplied to the oligotrophic waters. The simulated upwelling events in this study were responsible for profound modifications in planktonic community structure, which in turn acted as a strong driver of CR variability, modulating the carbon respired through the different microbial functional groups. Thus, as upwelling intensity became extreme, planktonic communities were entirely dominated by microplankton (mainly diatoms) and nanoplankton. Particularly in the singular mode, the extreme simulated-upwelling intensity reported the highest CR rates coinciding with a bloom of diatoms, giving evidence of the strong link between the autotrophic component and the observed variance in CR.

On the contrary, less pronounced intensities favoured smaller cells (heterotrophic bacteria and cyanobacteria) identified as better predictors of the variance in CR, potentially channelling a more significant fraction of carbon through the microbial food web. Nonetheless, the contribution to biomass of picoplankton was variable, presumably due to grazing or viral pressure, affecting their contribution to CR.

Our results offer insights into how future alterations in the modes and intensities of upwelling systems can potentially shift the planktonic community structure, affecting CR and therefore, the metabolic balance of the system. Thus, when the type of planktonic community is dominated by small heterotrophs the system shifts toward net-heterotrophy while net-autotrophy is observed when autotrophic-based communities prevailed. This highlights the importance of such changes in the carbon sequestration of upwelling regions. Understanding the link between respiratory losses and planktonic communities is a fundamental requisite to improving our predictive capacity of how these ecosystems will respond to future global change scenarios.

Data availability statement

The raw data supporting the conclusions of this article will be made available by the authors, without undue reservation.

Author contributions

Conceived and designed the study: UR and JA. Execution of the experiment: all authors. Data analysis: IB, JA, MB, JO and KS. Manuscript writing: IB and JA with input from all co-authors. All authors contributed to the article and approved the submitted version.

Funding

This study was carried out within the framework of the Ocean Artificial Upwelling project (Ocean artUp, No. 695094), funded by an Advanced Grant of the European Research Council (ERC). Additional support was provided through projects TRIATLAS (AMD-817578-5) from the European Union's Horizon 2020, FONIAC 2019 (Fundación Caja Canarias and Fundación Bancaria La Caixa), and e-IMPACT (PID2019-109084RB-C2) funded by the Spanish National Science Plan. IB is supported by a FPI fellowship (BES-2016-078407) from the Spanish Ministry of Economy, Industry and Competitiveness (MINECO). MGL is supported by the Ministerio de Ciencia, Innovación y Universidades, Gobierno de España (FPU17-01435) during his PhD. JA was supported by a Helmholtz International Fellow Award, 2015 (Helmholtz Association, Germany). JA also acknowledges support from the United States National Science Foundation grant OCE-1840868 to the Scientific Committee on Oceanic Research (SCOR, United States) WG 155.

Acknowledgments

We would like to thank the Oceanic Platform of the Canary Islands (Plataforma Oceánica de Canarias, PLOCAN) for their support throughout the experiment. We would like to thank the captain and crew of RV James Cook for the deployment of the mesocosms and the deep water collection, and the captain and crew of the vessel J. SOCAS for helping with the second deep water collection and the recovery of the mesocosms. Another special thanks goes to the whole KOSMOS team (GEOMAR) for their invaluable effort, organization and logistical support necessary to conduct the mesocosms experiment. Finally, we would like to thank to Minerva Espino and Acorayda González for their contribution to the CR measurements.

Conflict of interest

The authors declare that the research was conducted in the absence of any commercial or financial relationships that could be construed as a potential conflict of interest.

Publisher's note

References

Alonso-Sáez, L., Sánchez, O., and Gasol, J. M. (2012). Bacterial uptake of low molecular weight organics in the subtropical Atlantic: Are major phylogenetic groups functionally different? *Limnology Oceanography* 57 (3), 798–808. doi: 10.4319/lo.2012.57.3.0798

Anabalón, V., Arístegui, J., Morales, C. E., Andrade, I., Benavides, M., Correa-Ramírez, M. A., et al. (2014). The structure of planktonic communities under variable coastal upwelling conditions off cape ghir (31 n) in the canary current system (NW Africa). *Prog. Oceanography* 120, 320–339. doi: 10.1016/j.pocean.2013.10.015

Anil, A. C., Desai, D. V., Khandeparker, L., Krishnamurthy, V., Mapari, K., Mitbavkar, S., et al. (2021). Short term response of plankton community to nutrient enrichment in central eastern Arabian Sea: Elucidation through mesocosm experiments. *J. Environ. Manage.* 288, 112390. doi: 10.1016/j.jenvman.2021.112390

Arístegui, J., Barton, E. D., Tett, P., Montero, M. F., García-Muñoz, M., Basterretxea, G., et al. (2004). Variability in plankton community structure, metabolism, and vertical carbon fluxes along an upwelling filament (Cape juby, NW Africa). *Prog. Oceanography* 62 (2-4), 95–113. doi: 10.1016/j.pocean.2004.07.004

Arístegui, J., and Montero, M. F. (1995). The relationship between community respiration rate and ETS activity in the ocean. *J. Plankton Res.* 17, 1563–1571. doi: 10.1093/plankt/17.7.1563

Arístegui, J., and Montero, M. F. (2005). Temporal and spatial changes in plankton respiration and biomass in the canary islands region: The effect of mesoscale variability. *J. Mar. System* 54, 65–82. doi: 10.1016/j.jmarsys.2004.07.004

Azam, F., and Malfatti, F. (2007). Microbial structuring of marine ecosystems. *Nat. Rev. Microbiol.* 5 (10), 782–791. doi: 10.1038/nrmicro1747

Bakun, A. (1990). Global climate change and intensification of coastal ocean upwelling. *Science* 247 (4939), 198–201. doi: 10.1126/science.247.4939.198

Basu, S., and Mackey, K. R. (2018). Phytoplankton as key mediators of the biological carbon pump: Their responses to a changing climate. *Sustainability* 10 (3), 869. doi: 10.3390/su10030869

Baumann, M., Taucher, J., Paul, A. J., Heinemann, M., Vanharanta, M., Bach, L. T., et al. (2021). Effect of intensity and mode of artificial upwelling on particle flux and carbon export. *Front. Mar. Sci.* 8, 742142. doi: 10.3389/fmars.2021.742142

Blight, S. P., Bentley, T. L., Lefevre, D., Robinson, C., Rodrigues, R., Rowlands, J., et al. (1995). Phasing of autotrophic and heterotrophic plankton metabolism in a temperate coastal ecosystem. *Mar. Ecol. Prog. Ser.* 128, 61–75. doi: 10.3354/meps128061

Bode, A., Estévez, M. G., Varela, M., and Vilar, J. A. (2015). Annual trend patterns of phytoplankton species abundance belie homogeneous taxonomical group responses to climate in the NE Atlantic upwelling. *Mar. Environ. Res.* 110, 81–91. doi: 10.1016/j.marenvres.2015.07.017

Böttjer, D., and Morales, C. E. (2007). Nanoplanktonic assemblages in the upwelling area off concepción (36S), central Chile: Abundance, biomass, and grazing potential during the annual cycle. *Prog. Oceanography* 75 (3), 415–434. doi: 10.1016/j.pocean.2007.08.024

Breitbart, M., Middelboe, M., and Rohwer, F. (2008). "Marine viruses: community dynamics, diversity and impact on microbial processes," in *Microbial ecology of the oceans*. Ed. D. L. Kirchmam (Hoboken, NJ, USA: John Wiley & Sons Inc), 443–479.

Bryan, J. R., Rlley, J. P., and Williams, P. L. (1976). A winkler procedure for making precise measurements of oxygen concentration for productivity and related studies. *J. Exp. Mar. Biol. Ecol.* 21 (3), 191–197. doi: 10.1016/0022-0981(76)90114-3

Bunse, C., and Pinhassi, J. (2017). Marine bacterioplankton seasonal succession dynamics. *Trends Microbiol.* 25 (6), 494–505. doi: 10.1016/j.tim.2016.12.013

Capone, D. G., and Hutchins, D. A. (2013). Microbial biogeochemistry of coastal upwelling regimes in a changing ocean. *Nat. Geosci.* 6 (9), 711–717. doi: 10.1038/ngeo1916

Carritt, D. E., and Carpenter, J. H. (1966). Comparison and evaluation of currently employed modifications of the winkler method for determining dissolved oxygen in seawater; a NASCO report. *J. Mar. Res.* 24, 286–318.

Clayton, S., Nagai, T., and Follows, M. J. (2014). Fine scale phytoplankton community structure across the kuroshio front. *J. Plankton Res.* 36 (4), 1017–1030. doi: 10.1093/plankt/fbu020

Cottrell, M. T., and Kirchman, D. L. (2000). Natural assemblages of marine proteobacteria and members of the cytophaga-flavobacter cluster consuming low- and high-molecular-weight dissolved organic matter. *Appl. Environ. Microbiol.* 66 (4), 1692–1697. doi: 10.1128/AEM.66.4.1692-1697.2000

Daneri, G., Dellarossa, V., Quiñones, R., Jacob, B., Montero, P., and Ulloa, O. (2000). Primary production and community respiration in the Humboldt current system off Chile and associated oceanic areas. *Mar. Ecol. Prog. Ser.* 197, 41–49. doi: 10.3354/meps197041

Del Giorgio, P. A., Cole, J. J., and Cimbleris, A. (1997). Respiration rates in bacteria exceed phytoplankton production in unproductive aquatic systems. *Nature* 385 (6612), 148–151. doi: 10.1038/385148a0

Du, X., and Peterson, W. T. (2014). Seasonal cycle of phytoplankton community composition in the coastal upwelling system off central Oregon in 2009. *Estuaries Coasts* 37 (2), 299–311. doi: 10.1007/s12237-013-9679-z

Edwards, M., and Richardson, A. J. (2004). Impact of climate change on marine pelagic phenology and trophic mismatch. *Nature* 430, 881–884. doi: 10.1038/nature02808

Filella, A., Baños, I., Montero, M. F., Hernández-Hernández, N., Rodríguez-Santos, A., Ludwig, A., et al. (2018). Plankton community respiration and ETS activity under variable CO2 and nutrient fertilization during a mesocosm study in the subtropical north Atlantic. *Front. Mar. Sci.* 5. doi: 10.3389/fmars.2018.00310

García-Martín, E. E., Aranguren-Gassis, M., Hartmann, M., Zubkov, M. V., and Serret, P. (2017). Contribution of bacterial respiration to plankton respiration from 50 n to 44 s in the Atlantic ocean. *Prog. oceanography* 158, 99–108. doi: 10.1016/j.pocean.2016.11.006

García-Reyes, M., Sydeman, W. J., Schoeman, D. S., Rykaczewski, R. R., Black, B. A., Smit, A. J., et al. (2015). Under pressure: Climate change, upwelling, and eastern boundary upwelling ecosystems. *Front. Mar. Sci.* 2. doi: 10.3389/fmars.2015.00109

Gasol, J. M., and Duarte, C. M. (2000). Comparative analyses in aquatic microbial ecology: how far do they go? *FEMS Microbiol. Ecol.* 31 (2), 99–106. doi: 10.1111/j.1574-6941.2000.tb00675.x

Gómez-Letona, M., Sebastian, M., Baños, I., Montero, M. F., Barrancos, C. P., Baumann, M., et al. (2022). Artificial upwelling leads to a large increase in surface dissolved organic matter concentrations. *bioRxiv*. doi: 10.1101/2022.06.27.496799

Grasshoff, K. (1983). Determination of oxygen. *Methods seawater Anal.*, 61–72.

Grömping, U. (2006). Relative importance for linear regression in r: The package relaimpo. *J. Stat. Software* 17 (1), 1–27. doi: 10.18637/jss.v017.i01

Hutchings, L., Pitcher, G. C., Probyn, T. A., and Bailey, G. W. (1995). The chemical and biological consequences of coastal upwelling. *Environ. Sci. Res. Rep. Es* 18, 65–82.

Kämpf, J., and Chapman, P. (2016). *Upwelling systems of the world* (Switzerland: Springer International Publishing), 31–42.

Lassiter, A. M., Wilkerson, F. P., Dugdale, R. C., and Hogue, V. E. (2006). Phytoplankton assemblages in the CoOP-WEST coastal upwelling area. *Deep Sea Res. Part II: Topical Stud. Oceanography* 53 (25-26), 3063–3077. doi: 10.1016/j.dsr2.2006.07.013

Legendre, L., and Michaud, J. (1998). Flux of biogenic carbon in oceans: Size-dependent regulation by pelagic food webs. *Mar. Ecol. Prog. Ser.* 164, 1–11. doi: 10.3354/meps164001

Mackey, M. D., Mackey, D. J., Higgins, H. W., and Wright, S. W. (1996). CHEMTAX-a program for estimating class abundances from chemical markers: application to HPLC measurements of phytoplankton. *Mar. Ecol. Prog. Ser.* 144, 265–283. doi: 10.3354/meps144265

Mahaffey, C., Björkman, K. M., and Karl, D. M. (2012). Phytoplankton response to deep seawater nutrient addition in the north pacific subtropical gyre. *Mar. Ecol. Prog. Ser.* 460, 13–34. doi: 10.3354/meps09699

McAndrew, P. M., Björkman, K. M., Church, M. J., Morris, P. J., Jachowski, N., Williams, P. J. L. B., et al. (2007). Metabolic response of oligotrophic plankton communities to deep water nutrient enrichment. *Mar. Ecol. Prog. Ser.* 332, 63–75. doi: 10.3354/meps332063

Moncoiffé, G., Alvarez-Salgado, X. A., Figueiras, F. G., and Savidge, G. (2000). Seasonal and short-time-scale dynamics of microplankton community production and respiration in an inshore upwelling system. *Mar. Ecol. Prog. Ser* 196, 111–126. doi: 10.3354/meps196111

Montero, P., Daneri, G., Cuevas, L. A., González, H. E., Jacob, B., Lizárraga, L., et al. (2007). Productivity cycles in the coastal upwelling area off concepción: The importance of diatoms and bacterioplankton in the organic carbon flux. *Prog. Oceanography* 75 (3), 518–530. doi: 10.1016/j.pocean.2007.08.013

Ortiz, J., Arístegui, J., Taucher, J., and Riebesell, U. (2022). Artificial upwelling in singular and recurring mode: Consequences for net community production and metabolic balance. *Front. Mar. Sci* 8, 743105. doi: 10.3389/fmars.2021.743105

Pinheiro, J., Bates, D., DebRoy, S., Sarkar, D., and Team, R. C. (2007). Linear and nonlinear mixed effects models. *R Package versions* 3 (57), 1–89.

Riebesell, U., Bellerby, R. G. J., Grossart, H. P., and Thingstad, F. (2008). Mesocosm CO 2 perturbation studies: from organism to community level. *Biogeosciences* 5 (4), 1157–1164. doi: 10.5194/bg-5-1157-2008

Riebesell, U., Czerny, J., von Bröckel, K., Boxhammer, T., Büdenbender, J., Deckelnick, M., et al. (2013). A mobile sea-going mesocosm system–new opportunities for ocean change research. *Biogeosciences* 10 (3), 1835–1847. doi: 10.5194/bg-10-1835-2013

Robinson, C., Serret, P., Tilstone, G., Teira, E., Zubkov, M. V., Rees, A. P., et al. (2002). Plankton respiration in the eastern Atlantic ocean. *Deep Sea Res. Part I: Oceanographic Res. Papers* 49 (5), 787–813. doi: 10.1016/S0967-0637(01)00083-8

Ryther, J. H. (1969). Photosynthesis and fish production in the sea. *Science* 166 (3901), 72–76. doi: 10.1126/science.166.3901.72

Sathyendranath, S., Stuart, V., Nair, A., Oka, K., Nakane, T., Bouman, H., et al. (2009). Carbon-to-chlorophyll ratio and growth rate of phytoplankton in the sea. *Mar. Ecol. Prog. Ser.* 383, 73–84. doi: 10.3354/meps07998

Schulz, K. G., Bach, L. T., Bellerby, R. G. J., Bermúdez, R., Büdenbender, J., Boxhammer, T., et al. (2017). Phytoplankton blooms at increasing levels of atmospheric carbon dioxide: Experimental evidence for negative effects on prymnesiophytes and positive on small picoeukaryotes. *Front. Mar. Sci.* 4. doi: 10.3389/fmars.2017.00064

Sherr, E. B., Sherr, B. F., and Wheeler, P. A. (2005). Distribution of coccoid cyanobacteria and small eukaryotic phytoplankton in the upwelling ecosystem off the Oregon coast during 2001 and 2002. *Deep Sea Res. Part II: Topical Stud. Oceanography* 52 (1-2), 317–330. doi: 10.1016/j.dsr2.2004.09.020

Smayda, T. J., and Trainer, V. L. (2010). Dinoflagellate blooms in upwelling systems: Seeding, variability, and contrasts with diatom bloom behaviour. *Prog. Oceanography* 85, 92–107. doi: 10.1016/j.pocean.2010.02.006

Sommer, U., Aberle, N., Engel, A., Hansen, T., Lengfellner, K., Sandow, M., et al. (2007). An indoor mesocosm system to study the effect of climate change on the late winter and spring succession of Baltic Sea phyto- and zooplankton. *Oecologia* 150 (4), 655–667. doi: 10.1007/s00442-006-0539-4

Tamigneaux, E., Legendre, L., Klein, B., and Mingelbier, M. (1999). Seasonal dynamics and potential fate of size-fractionated phytoplankton in a temperate nearshore environment (Western gulf of St Lawrence, Canada). *Estuarine Coast. Shelf Sci.* 48 (2), 253–269. doi: 10.1006/ecss.1999.0416

Taucher, J., Arístegui, J., Bach, L. T., Guan, W., Montero, M. F., Nauendorf, A., et al. (2018). Response of subtropical phytoplankton communities to ocean acidification under oligotrophic conditions and during nutrient fertilization. *Front. Mar. Sci.* 5. doi: 10.3389/fmars.2018.00330

Taucher, J., Bach, L. T., Boxhammer, T., Nauendorf, A., Achterberg, E. P., Algueró-Muñiz, M., et al. (2017). Influence of ocean acidification and deep water upwelling on oligotrophic plankton communities in the subtropical north Atlantic: insights from an *in situ* mesocosm study. *Front. Mar. Sci.* 4. doi: 10.3389/fmars.2017.00085

Tréguer, P., Bowler, C., Moriceau, B., Dutkiewicz, S., Gehlen, M., Aumont, O., et al. (2018). Influence of diatom diversity on the ocean biological carbon pump. *Nat. Geosci.* 11, 27–37. doi: 10.1038/s41561-017-0028-x

Wilkerson, F. P., Lassiter, A. M., Dugdale, R. C., Marchi, A., and Hogue, V. E. (2006). The phytoplankton bloom response to wind events and upwelled nutrients during the CoOP WEST study. *Deep Sea Res. Part II: Topical Stud. Oceanography* 53 (25-26), 3023–3048. doi: 10.1016/j.dsr2.2006.07.007

Williams, P. L. B., and Del Giorgio, P. A. (2005). Respiration in aquatic ecosystems: history and background. *Respiration Aquat. Ecosyst.*, 1–17. doi: 10.1093/acprof:oso/9780198527084.003.0001

Williams, P. L., and Jenkinson, N. W. (1982). A transportable microprocessor controlled precise winkler titration suitable for field station and shipboard use 1. *Limnology Oceanography* 27 (3), 576–584. doi: 10.4319/lo.1982.27.3.0576

Zubkov, M. V. (2014). Faster growth of the major prokaryotic versus eukaryotic CO2 fixers in the oligotrophic ocean. *Nat.Commun.* 5 (1), 1–6. doi: org/10.1038/ncomms4776

frontiers | Frontiers in Marine Science

TYPE Original Research
PUBLISHED 08 November 2022
DOI 10.3389/fmars.2022.969714

OPEN ACCESS

EDITED BY
Jun Sun,
China University of Geosciences
Wuhan, China

REVIEWED BY
Michael William Lomas,
Bigelow Laboratory For Ocean
Sciences, United States
Norman B. Nelson,
University of California, Santa Barbara,
United States

*CORRESPONDENCE
Markel Gómez-Letona
markel.gomezletona@ulpgc.es
Javier Arístegui
javier.aristegui@ulpgc.es

SPECIALTY SECTION
This article was submitted to
Marine Biogeochemistry,
a section of the journal
Frontiers in Marine Science

RECEIVED 15 June 2022
ACCEPTED 24 October 2022
PUBLISHED 08 November 2022

CITATION
Gómez-Letona M, Sebastián M,
Baños I, Montero MF, Barrancos CP,
Baumann M, Riebesell U and
Arístegui J (2022) The importance of
the dissolved organic matter pool for
the carbon sequestration potential of
artificial upwelling.
Front. Mar. Sci. 9:969714.
doi: 10.3389/fmars.2022.969714

The importance of the dissolved organic matter pool for the carbon sequestration potential of artificial upwelling

Markel Gómez-Letona[1]*, Marta Sebastián[2], Isabel Baños[1], María Fernanda Montero[1], Clàudia Pérez Barrancos[1,3], Moritz Baumann[4], Ulf Riebesell[4] and Javier Arístegui[1]*

[1]Instituto de Oceanografía y Cambio Global, Universidad de Las Palmas de Gran Canaria, Las Palmas, Spain, [2]Department of Marine Biology and Oceanography, Institut de Ciències del Mar (ICM), Consejo Superior de Investigaciones Científicas, Barcelona, Spain, [3]Instituto Español de Oceanografía, Consejo Superior de Investigaciones Científicas (CSIC), Centro Oceanográfico de Canarias, Santa Cruz de Tenerife, Spain, [4]Marine Biogeochemistry, Biological Oceanography, GEOMAR Helmholtz Centre for Ocean Research Kiel, Kiel, Germany

In the face of climate change there is a need to reduce atmospheric CO_2 concentrations. Artificial upwelling of nutrient-rich deep waters has been proposed as a method to enhance the biological carbon pump in oligotrophic oceanic regions in order to increase carbon sequestration. Here we examine the effect of different artificial upwelling intensities and modes (single pulse versus recurring pulses) on the dynamics of the dissolved organic matter pool (DOM). We introduced nutrient-rich deep water to large scale mesocosms (~44 m^3) in the oligotrophic subtropical North Atlantic and found that artificial upwelling strongly increased DOM concentrations and changed its characteristics. The magnitude of the observed changes was related to the upwelling intensity: more intense treatments led to higher accumulation of dissolved organic carbon (>70 μM of excess DOC over ambient waters for the most intense) and to comparatively stronger changes in DOM characteristics (increased proportions of chromophoric DOM (CDOM) and humic-like fluorescent DOM), suggesting a transformation of the DOM pool at the molecular level. Moreover, the single upwelling pulse resulted in higher CDOM quantities with higher molecular weight than the recurring upwelling mode. Together, our results indicate that under artificial upwelling, large DOM pools may accumulate in the surface ocean without being remineralized in the short-term. Possible reasons for this persistence could be a combination of the molecular diversification of DOM due to microbial reworking, nutrient limitation and reduced metabolic capabilities of the prokaryotic communities within the mesocosms. Our study demonstrates the importance of the DOC pool when assessing the carbon sequestration potential of artificial upwelling.

KEYWORDS

dissolved organic carbon, chromophoric dissolved organic matter, fluorescent dissolved organic matter, carbon sequestration, artificial upwelling, fertilization, mesocosm

Introduction

Primary producers and bacterioplankton require the uptake of inorganic nutrients from their surrounding waters to grow and keep their metabolism functioning (Azam and Malfatti, 2007). Inorganic nutrients are found in high concentrations below the photic layer (Levitus et al., 1993; Johnson et al., 1997), due to the absence of nutrient-consuming, light-driven primary production and the predominance of nutrient-releasing remineralization of organic matter. These nutrient-rich waters can reach the surface by a range of physical processes, such as winter convection (Severin et al., 2017), wind-driven coastal upwelling (Jacox et al., 2018), mesoscale eddies (McGillicuddy et al., 2007) or diapycnal diffusion (Arcos-Pulido et al., 2014), and play a key role in driving primary production and, consequently, CO_2 fixation in the surface ocean (Field et al., 1998). A fraction of this newly produced organic matter is in turn exported, *via* multiple pathways, out of the photic layer into the deep ocean, where it is ultimately remineralised, releasing inorganic nutrients and carbon back to seawater. This process is known as the biological carbon pump (Le Moigne, 2019).

The biological carbon pump plays a major role in the atmosphere-ocean CO_2 dynamics and acts as a key mechanism in the sequestration of CO_2 in the deep ocean (Le Moigne, 2019). Nonetheless, there are great extents of the global oceans –such as the subtropical gyres that make up ~40% of Earth's surface (Polovina et al., 2008)– where the vertical input of nutrients is limited and, thus, phytoplankton rely on nutrients recycled within the photic layer, resulting in low primary production and CO_2 fixation (Field et al., 1998). In the context of climate change and increasing CO_2 emissions, the possibility of fertilizing these nutrient-poor waters to fuel primary production has been put forward as a climate intervention approach to enhance CO_2 sequestration in the ocean and help reduce its atmospheric concentration (Williamson et al., 2012; Fawzy et al., 2020). One of the proposed fertilization methods consists in bringing nutrient-rich deep waters into the surface, an approach known as artificial upwelling (Pan et al., 2016). Artificial upwelling is envisioned to enhance the biological carbon pump by increasing primary production in nutrient-limited oceanic regions, amplifying carbon export and ideally yielding a net increase in carbon sequestration (if the C: N and C: P ratios of the exported organic matter are higher than the Redfield ratio). However, the efficiency of artificial upwelling to sequester atmospheric CO_2 has been questioned (Shepherd et al., 2007; Yool et al., 2009), evidencing the need of further research.

Dissolved organic carbon (DOC) represents the largest pool of reduced carbon in the ocean and its downward flux is an important contributor to the biological carbon pump (Hansell et al., 2009; Le Moigne, 2019). The efficiency of the DOC pathway of carbon export will depend on the extent of its remineralization by prokaryotes and the depth at which it occurs in the water column. Some DOM is readily consumed by prokaryotes, and this process influences the absorption spectrum and fluorescence characteristics of DOM (Catalá et al., 2015b; Catalá et al., 2018). A fraction of it however seems to escape remineralization and is accumulated. Two main hypotheses seek to explain this persistence (Dittmar et al., 2021): on the one hand, the intrinsic inability (or very reduced ability) of prokaryotes to consume some classes of organic molecules would lead to their accumulation and the long-term persistence of a fraction of DOM. On the contrary, the accumulated DOM might not be inherently resistant to degradation, its persistence being instead a consequence of complex ecological interactions between the vast molecular diversity of DOM (Zark et al., 2017b) and the wide metabolic capabilities of prokaryotes (Sunagawa et al., 2015; Acinas et al., 2021). In this scenario, all compounds would be continuously produced and degraded, stabilization occurring as a consequence of parallel decreases in the concentration of specific compounds and the abundance of prokaryotes able to degrade them (Dittmar et al., 2021). For instance, in the subtropical North Atlantic, seasonally accumulated DOC has been shown to resist remineralization by surface prokaryotic communities, but it is remineralized when exported into the mesopelagic layer (Carlson et al., 2004). In summary, the balance between the transport of DOM to the ocean's interior and how rapidly remineralization occurs above the permanent pycnocline (which depends on both physical dynamics and the ability of prokaryotes to consume DOM) will determine the net contribution of DOC to carbon sequestration. This balance will consequently influence the efficiency of artificial upwelling, making DOM a major factor to consider when addressing carbon sequestration by this approach.

In the present work we studied the effect of the intensity and mode of artificial upwelling on the DOM pool in an oligotrophic marine environment. Using mesocosms that simulate ecological systems in close-to-natural conditions, we introduced nutrient-rich deep water into nutrient-depleted surface waters, aiming to investigate how the quantity, stoichiometry and composition of DOM is affected by upwelling and the subsequent enhancement of primary production. Deep-water addition was done simulating two modes of artificial upwelling: a singular addition, representing a moored system that upwells water into passing water patches, fertilizing them once (e.g., Zhang et al., 2016), and recurring deep water additions, simulating a system that drifts within a water parcel, repeatedly upwelling water into it (e.g., Maruyama et al., 2011). We aimed to study DOM dynamics under the different artificial upwelling scenarios to gain insights into the short-term fate of DOM and the potential long-term implications for the efficiency of carbon sequestration.

Materials and methods

Experimental setup and sampling

Our experiment was conducted in Gando Bay (27° 55′ 41′′ N, 15° 21′ 55′′ W, Gran Canaria, Canary Islands) during the autumn of 2018 as a part of the Ocean artUp project. Nine KOSMOS (Kiel Off-Shore Mesocosms for Ocean Simulations; Riebesell et al., 2013) were deployed (M1-M9) and filled with *in situ* oligotrophic water (mean volume 43.775 ± 1.352 m^3). To simulate artificial upwelling, nutrient-rich deep water was collected off Gran Canaria from 330 m (on day -10) and 280 m depth (on day 23), and added to the mesocosms in two different treatment modes (Table 1): a *singular* mode (M3, M7, M9, M1), in which a single deep-water (DW) addition was performed (on day 4), and a *recurring* mode (M2, M4, M6, M8), in which consecutive deep-water additions were performed (on days 4, 8, 12, 16, 21, 24, 28 and 32). For each artificial upwelling mode, four levels of intensity were simulated, with increasing quantities of DW added to them: *low* (M2, M3), *medium* (M7, M4), *high* (M6, M9) and *extreme* (M8, M1). For the same intensity level, the singular and recurring modes had overall similar amounts of nutrients added during the entire course of the experiment, yielding comparable treatments (Table 1). A characterization of the DOM found in the deep water can be found in Table S1. No deep water was added to M5 (*Control*) and ambient waters outside of the mesocosms were monitored during regular sampling (*Atlantic*). A detailed description of the experimental set up and sampling procedures can be found in Baumann et al. (2021b).

Integrated samples of the water column within the mesocosms were collected using depth-integrated water samplers (IWS, HYDRO-BIOS, Kiel) and stored in acid-cleaned shaded glass bottles. To minimize photobleaching and degradation, samples were kept in dark, cool conditions until freezing/analysis (see below) on the same day. Prior to analysis/freezing, samples for dissolved organic matter quantification and characterization were filtered through precombusted (450°C, 6h) glass fiber filters (GF/F, 0.7 µm nominal pore size) using acid-cleaned syringes and filter holders.

Dissolved organic carbon, nitrogen and phosphorus

For DOC measurements, 10 mL of filtered samples were stored in high density polyethylene bottles and frozen (-20°C) until analysis. Samples were analyzed with a Shimadzu TOC-5000 analyzer (Sharp et al., 1993). Prior to the analysis, samples were thawed, acidified with 50 µL of H_3PO_4 (50%) and sparged with CO_2-free air for several minutes to remove inorganic carbon. DOC concentrations were estimated based on standard curves (30–200 µM) of potassium hydrogen phthalate produced every day (Thomas et al., 1995). Reference material of deep-sea water (DSW, 42–45 µM C) provided by D. A. Hansell laboratory (University of Miami) was analyzed daily.

DON and DOP samples were collected in acid-rinsed, high-density polyethylene (HDPE) bottles and analyzed according to Hansen and Koroleff (1999). Upon arrival in the laboratory, 40 mL of the samples were filtered (0.45 µm cellulose acetate filters, Whatman) under sterile conditions. Total dissolved nitrogen and phosphorus were decomposed to phosphate and nitrate by adding one spoon of the oxidizing reagent Oxisolv (Merck) and cooking the solution for approximately one hour (90-100°C). The samples were left to cool overnight, and the next day total dissolved nitrogen and phosphorus concentrations were measured spectrophotometrically on a continuous flow analyzer (QuAAtro AutoAnalyzer, SEAL Analytical). Triplicates of artificial seawater were treated and measured similarly on each measurement day. They acted as blanks and were averaged and subtracted from the samples. DON and DOP concentrations were calculated from the total dissolved nitrogen and phosphorus by subtracting the dissolved inorganic nitrogen and phosphate concentrations.

TABLE 1 Information of the treatments applied to each mesocosm.

Mesocosm	Upwelling mode	Upwelling intensity	Added deep water volume [m^3]	Added deep water volume [%]*	Added N [µmol·L^{-1}]	Added P [µmol·L^{-1}]	Added Si [µmol·L^{-1}]
M5	Control		0.0	0.0	0.00	0.000	0.00
M2	Recurring	Low	2.8	6.3	1.61	0.094	0.69
M4	Recurring	Medium	5.6	12.7	3.15	0.187	1.35
M6	Recurring	High	11.2	25.6	6.16	0.363	2.64
M8	Recurring	Extreme	22.4	51.1	10.97	0.682	4.96
M3	Singular	Low	2.8	6.4	1.62	0.094	0.74
M7	Singular	Medium	5.3	12.0	3.07	0.177	1.41
M9	Singular	High	9.8	22.4	5.56	0.325	2.63
M1	Singular	Extreme	17.2	39.2	9.80	0.567	4.58

*Considering average mesocosm volume of 43.775 m^3.
Total additions of deep water (as absolute values and % relative to the volume of the mesocosms), nitrogen (N), phosphorus (P) and silica (Si). N, P and Si values include both inorganic and organic forms.

Chromophoric dissolved organic matter characterization

Absorbance spectra were determined using an Ocean Optics USB2000+UV-VIS-ES Spectrometer alongside a World Precision Instruments liquid waveguide capillary cell (LWCC) with a path length of 0.9982 m. For each sample, absorbance was measured across a wavelength spectrum between 178 nm and 878 nm, performing a blank measurement prior to each sample using ultrapure Milli-Q water. Data processing was done in R (v. 4.1.2; R Core Team, 2021): raw spectra (samples and blanks) were cropped between 250 and 700 nm, blank spectra were subtracted from sample spectra and a baseline correction was performed by subtracting the average absorbance of each sample between 600 and 700 nm to the whole spectrum. The effect of refractive index changes due to salinity on the absorbance measurements of our equipment was negligible (as reported in Catalá et al., 2018) and, thus, no corrections were applied.

After processing, absorbance was transformed into absorption following the definition of the Napierian absorption coefficient:

$$a_\lambda = 2.303 \cdot \frac{Abs_\lambda}{L}$$

Where, for each wavelength λ, the absorption coefficient a_λ is given by the absorbance at wavelength λ (Abs_λ), the path length of the cuvette (L, in meters; here 0.9982) and 2.303 (the factor that converts from decadic to natural logarithms).

From a_λ spectra values at 254 and 325 nm were considered. Both are proxies of CDOM concentration, although for different fractions of it: while a_{254} represents conjugated double bonds a_{325} is related to the aromatic fraction (Lønborg and Álvarez-Salgado, 2014; Catalá et al., 2016; Catalá et al., 2018). Furthermore, spectral slopes between 275-295 nm and 350-400 nm were estimated from the natural log transformed absorption spectra following Helms et al. (2008). These regions of the spectra (as well as their ratio, S_R) have been shown to be especially sensitive to changes in the molecular weight of CDOM, with higher slopes denoting lower average molecular weight (Helms et al., 2008; Helms et al., 2013). Moreover, these spectral slope parameters have been related to the microbial reworking of organic matter in the ocean, decreasing values being associated to increased transformation of DOM by prokaryotes (Catalá et al., 2015a; Catalá et al., 2018).

Fluorescent dissolved organic matter characterization

Fluorescence measurements were performed with a Jobin Yvon Horiba Fluoromax-4 spectrofluorometer, exciting the water samples in a wavelength range of 240-450 nm (10 nm increments), and measuring the fluorescence emission in a range of 300-560 nm (2 nm increments), with excitation and emission slit widths of 5 nm, and an integration time of 0.25 s. Fluorescence measurements were collected into excitation-emission matrices. To correct for lamp spectral properties and be able to compare results with other studies, excitation-emission matrices were measured in signal-to-reference mode with instrument-specific excitation and emission corrections applied during collection (Sc : Rc).

Excitation-emission matrices were processed using the DOMFluor toolbox (v. 1.7; Stedmon and Bro, 2008) for Matlab (R2017a). Alongside seawater samples, each sampling day three blank samples were measured using ultrapure Milli-Q water (at the beginning, middle and end of the measurement process). A weighted mean of the blanks was subtracted from each sample. Furthermore, excitation-emission matrices were normalized to the Raman area using the emission scan at 350 nm of ultrapure water blanks, calculating the area following the trapezoidal integration method (Lawaetz and Stedmon, 2009). Inner-filter correction was not performed as the average absorption coefficient of CDOM at 250 nm in all samples was 2.120 ± 0.544 m^{-1} (mean ± sd, n = 208; max. = 3.4 m^{-1}), which was lower than the threshold of 10 m^{-1} above which this correction is considered to be necessary (Stedmon and Bro, 2008). Rayleigh scatter bands of 1st ($Em = Ex \pm bandwidth$) and 2nd ($Em = 2{\cdot}Ex \pm 2{\cdot}bandwith$) orders were cut at each wavelength pair.

Parallel factor analysis of fluorescence data

The processed excitation-emission matrices (n = 175, samples with measurement errors were removed) were analyzed applying a (PARAFAC) analysis (Stedmon et al., 2003; Stedmon and Bro, 2008) using the DOMFluor toolbox. A model consisting of five components (Table S2 and Figure S1) was validated by split-half validation and random initialization. For each sample, the fluorescence maximum (F_{max}) of the components was recorded.

The optical characteristics of the five fluorescent DOM (FDOM) components are summarized in Table S2, along with similar fluorophores found in the literature. The identification of previously described fluorophores was performed using the OpenFluor database (openfluor.lablicate.com, Murphy et al., 2014), based on the combined Tucker Congruence Coefficient of the excitation and emission spectra ($TCC_{ex\text{-}em}$). C1, C2, C4 and C5 had 17, 28, 11 and 6 matches with high congruence ($TCC_{ex\text{-}em}$ >0.95), respectively. C1 presented characteristics similar to fluorophores identified as amino acid-/tryptophan-like, with primary and secondary excitation maxima at 300 and 240 nm, respectively, and an emission maximum at 354 nm (Table S2). Such amino acid-like compounds have been previously described as partially bioavailable for prokaryotic

consumption (Lønborg et al., 2010). C2 (excitation maxima at 250 and 330 nm, emission maximum at 410 nm) displayed high similarities with humic-like fluorophores (peak M, Table S2) that have been observed to be positively correlated to apparent oxygen utilization in the ocean (Catalá et al., 2015b). C4 was also similar to previously identified humic-like components but, unlike C2, its signal presented peaks at higher wavelengths (excitation maxima at 260 and 370 nm, emission maximum at 466 nm). It resembled a mixture of peaks A and C, formed by compounds with high aromaticity (Table S2). Similarly to C1, C5 also presented excitation and emission spectra highly congruent with amino acid-/tryptophan-like fluorophores, but had lower maxima than C1 (excitation and emission maxima at 270 and 342 nm, respectively; Table S2). Notably, the spectrum of this component was highly similar to that of indole (Wünsch et al., 2015). As opposed to the other components, C3 presented matches with congruence lower than 0.95. With excitation maximum below 240 nm and a broad emission spectrum (maximum at 330 – 472 nm), it was identified as similar to fluorophores potentially related to fluorometer artifacts (Table S2). Thus, the C3 component was not further considered in the analyses.

Prokaryotic heterotrophic production and cell abundance

Prokaryotic heterotrophic production (PHP) was estimated *via* the incorporation of ^{3}H-leucine using the centrifugation method (Smith and Azam, 1992). ^{3}H-leucine (Perkin-Elmer, specific activity 160 Ci mmolL^{-1}) was added at final concentration (20 nmol L^{-1}) to quadruplicate 1 mL subsamples. Blanks were established by adding 100 µL of 50% trichloroacetic acid (TCA) to duplicate blanks screw-cap microcentrifuge tubes 15 min prior to radioisotope addition. The microcentrifuge tubes were incubated at *in situ* temperature (± 1°C) in the dark for 2 h. Incorporation of leucine in the quadruplicate tubes was stopped by adding 100 µL ice-cold 50% TCA and tubes were kept together with the blanks at -20°C until further processing as in Smith and Azam (1992). The mean disintegrations per minute (DPM) of the TCA-killed blanks were removed from the mean DPM of the respective samples and succeeding DPM value converted into leucine incorporation rates. PHP was calculated using a conservative theoretical conversion factor of 1.55 kg C molL^{-1} Leu assuming no internal isotope dilution (Kirchman, 1993). The PHP data are available at the PANGAEA repository (Baumann et al., 2021a).

Samples for prokaryotic cell abundance were collected into 2 mL cryovials, fixed with a 2% final concentration of paraformaldehyde and stored at -80°C. After thawing, 400 µL subsamples were stained with 4 µL of the fluorochrome SYBR Green I (Molecular Probes) diluted in dimethyl sulfoxide (1:10) and analyzed in a FACSCalibur (Becton-Dickinson) flow cytometer. Fluorescent beads (1 µm, Polysciences) were added for internal calibration (10^{5} mL^{-1}). Prokaryotic cells were identified in green fluorescence *vs.* side scatter cytograms.

Inorganic nutrients, chlorophyll-a and particulate organic carbon

Nitrate (NO_3^-), nitrite (NO_2^-), ammonium (NH_4^+), phosphate (PO_4^{3-}) and silicic acid ($Si(OH)_4$) were quantified spectrophotometrically on a five channel continuous flow analyzer (QuAAtro AutoAnalyzer, SEAL Analytical Inc., Mequon, United States). Chlorophyll-a (Chl-a) was measured with an HPLC Ultimate 3000 (Thermo Scientific GmbH, Schwerte, Germany). Particulate organic carbon (POC) in the water column was measured using a CN analyzer (Euro EA-CN, HEKAtech). See Baumann et al. (2021b) for details. Chl-a and POC data are available at the PANGAEA repository (Baumann et al., 2021a).

Statistical analyses

All statistical analyses and data representations were performed in R (v. 4.1.2; R Core Team, 2021). Linear regressions were performed to assess the relationships between upwelling intensity (as N addition, in µM) and the dissolved organic matter variables. Normality and homoscedasticity of residuals were tested with Shapiro-Wilk (*stats* package, v. 4.1.2) and Breusch-Pagan (*lmtest* package, v. 0.9.39; Zeileis and Hothorn, 2002) tests, respectively. Data representations were done with *ggplot2* (v. 3.3.5; Wickham, 2016).

Results

Response of primary producers

Artificial upwelling led to large phytoplankton blooms after the first deep water addition, increasing primary production and shifting the community composition towards a diatom dominated assemblage (Ortiz et al., 2022b). Changes were in accordance with the intensity level of upwelling: the largest Chl-a build-ups were registered in the singular extreme treatment, where Chl-a reached 11.2 µg·L^{-1} on day 9 (Figure 1A). Upwelling modes however differed in their outcomes after the first deep water addition. In the singular treatments the blooms rapidly collapsed and Chl-a remained low until the end of the experiment, while in the recurring treatments subsequent deep water additions allowed to sustain the blooms (with oscillating Chl-a concentrations, Figure 1A) throughout the experiment. Particulate organic carbon (POC) concentrations in the water column (Figure 1B) showed accumulations following the

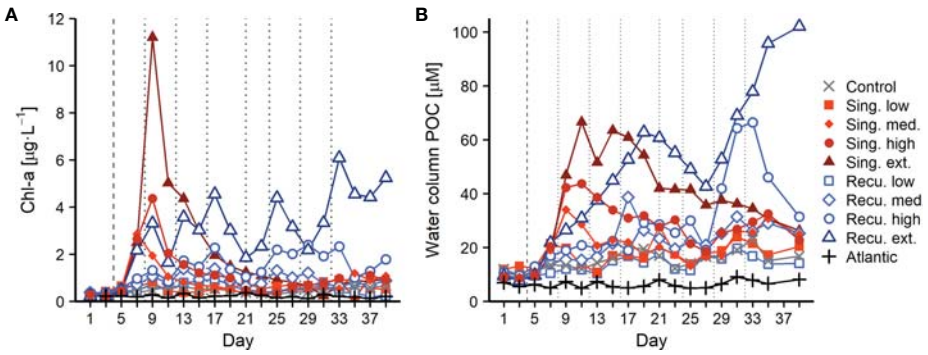

FIGURE 1
Chl-a **(A)** and particulate organic carbon (POC) **(B)** concentrations during the experiment. Vertical lines indicate deep water additions of singular (dashed) and recurring (dashed and dotted) treatments.

phytoplankton bloom dynamics. Singular treatments accumulated the highest POC values after the initial bloom, reaching 66 µM in the extreme intensity level, followed by a steady decrease. The response in the recurring treatments was slower but POC accumulated until day ~20 (63 µM in the extreme treatment). While the least intense levels ended with similar concentrations to those of the singular mode, in the high and extreme recurring treatments POC values were markedly higher after day 27 (maximum of 102 µM).

Dissolved organic matter concentration and elemental composition

Artificial upwelling yielded large increases in the DOM pool, in direct positive relationship with upwelling intensity (Figures 2, 3). Extreme treatments presented DOC concentrations that were +70 µM compared to starting conditions (Figure 2A). Average DOC concentrations prior to the first deep water addition on day 4 ranged between 70.6-78.1 µM. After the deep water addition DOC remained relatively stable without exceeding initial values until day 9, when concentrations started to raise in all treatments coinciding with the peak of the diatom bloom (Figure 1). After day 9, while the bloom in the singular treatments started to collapse, DOC concentrations continued to increase, especially in the singular treatments: on day 13, the extreme, high and medium singular treatments showed the highest DOC values with 155, 109 and 106 µM respectively (Figure 2A). After day 13, DOC in these mesocosms did not continue to increase and tended to stabilize until the end of the experiment.

In the recurring treatments, where phytoplankton abundances experienced smaller initial increases but did not collapse (Figure 1), DOC increases were not as abrupt. Only between days 16-20, when the bloom in the extreme recurring treatment presented a major decrease, DOC displayed pronounced increases, reaching its peak on day 19 (154 µM) and subsequently sustained similar values, while the high treatment experienced a steady increase throughout the experiment (Figure 2A). During days 33-39, average DOC values were of 143-145, 115-125, 103-106 and 95-97 µM for extreme, high, medium and low treatments, respectively. After the final deep water addition to the recurring treatments (days ≥33), average DOC concentrations showed a significant positive relationship with upwelling intensity (Figure 3A), with a similar effect for both upwelling modes (Table S3). During the entire experiment, DOC concentrations in the control mesocosm trailed those in the low treatments, while the Atlantic remained relatively stable with far smaller values (mean ± sd = 68.5 ± 5.1 µM).

Increases in DON and DOP concentrations were more subtle than in DOC (Figures 2B, C). Initial values ranged between 4.65-5.70 µM and 0.102-0.109 µM, respectively. On days 11-13 DON values started to raise in the extreme singular treatment, followed by the extreme recurring treatment on day 19. These mesocosms reached maximum values of 7-8 µM during days 27-31. In contrast to DOC concentrations, DON values departed less from initial conditions and presented higher variability. Nonetheless, increasing DON concentrations were associated with increasing upwelling intensity, with similar effects for both modes (Figures 2B, 3B and Table S3). Similarly, differences in DOP between treatments were minor until day 11, when the extreme singular treatment started to increase, reaching values above 0.15 µM and fluctuating until the end of the experiment. The extreme recurring treatment began to separate from less intense treatments on day 19, peaking during days 23-27 at ~0.17 µM and slowly decreasing towards the end (Figure 2C). Despite variability, overall treatments subject to more intense upwelling presented higher DOP concentrations: average DOP values on days ≥33 showed

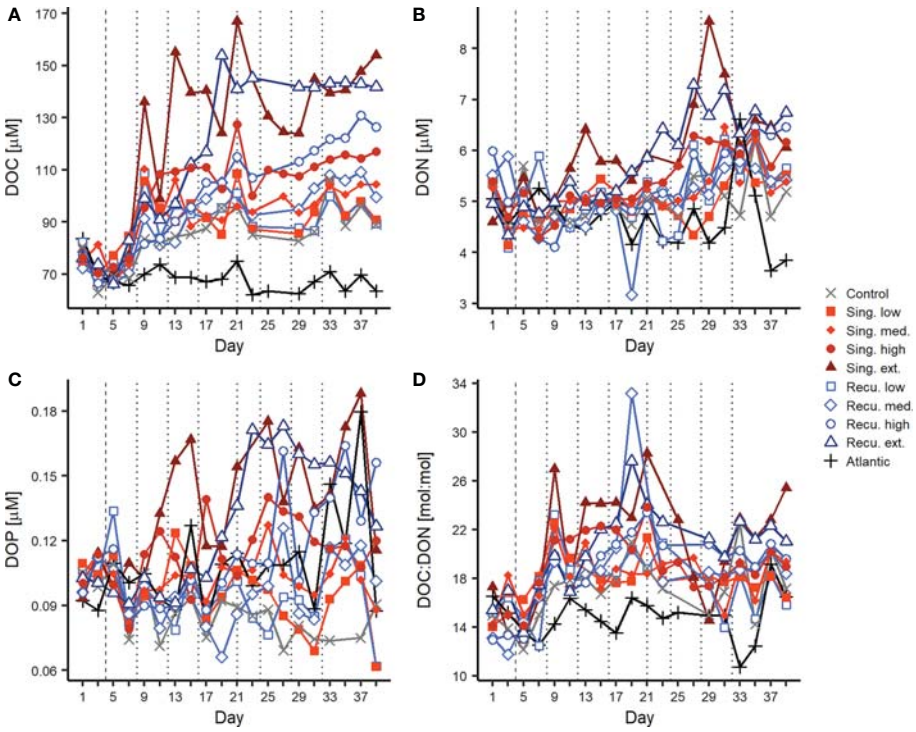

FIGURE 2
Changes in dissolved organic matter concentrations and elemental ratios ratios during the experiment. Temporal evolution of **(A)** DOC, **(B)** DON, **(C)** DOP, **(D)** DOC : DON. Vertical lines indicate deep water additions of singular (dashed, day 4) and recurring (dashed and dotted) treatments. Results for DOC : DOP and DON : DOP ratios can be found in Figure S2.

significant positive relationships with upwelling intensity both for singular and recurring upwelling modes (Figure 3C, Table S3).

The differential changes in DOC, DON and DOP were reflected in the elemental ratios (Figures 2D, S2), with notable increases in the values of the DOC : DON and DOC : DOP ratios, leading to DOM with higher relative C content. The average DOC : DON : DOP ratio across mesocosms prior to the first deep water addition was 704:48:1 (DOC : DON ~15 : 1). After the addition and following the DOC build up, carbon ratios started to increase, although consistent differences between treatments were only observed for DOC : DON (Figure 2D), but not DOC : DOP (Figure S2). During days 13-21, DOC : DON ratios were highest, particularly in mesocosms with more intense upwelling: extreme singular and recurring treatments showed average values of 25:1 and 23:1, respectively, while low treatments only reached 19:1. Average DOC : DOP ratios ranged between 927:1-1178:1 for this same period. During days 33-39, DOC : DON values experienced a slight decrease, but still were higher than initial ratios and showed consistent differences between treatments (17:1-23:1 across intensity levels). In fact, DOC : DON showed a positive relationship with upwelling intensity (Figure 3D). While DON : DOP values showed considerable variability and no consistent temporal trend throughout the experiment (Figure S2), the more intense treatments tended to show lower values. After the last deep water addition, DON : DOP ratios showed negative relationships with upwelling intensity, although only significant for the singular treatments (Figure S3).

Optical characteristics of dissolved organic matter

The chromophoric and fluorescent fractions of the dissolved organic matter presented pronounced increases in response to artificial upwelling. CDOM concentrations, as depicted by a_{254} (Figure 4A), increased in all mesocosms once the first water addition was done (including the control despite no nutrients were added). Initial values ranged between 1.22-1.39 m^{-1} and steadily increased for most of the experiment, reaching 2.90 m^{-1} (extreme recurring) and 3.17 m^{-1} (extreme singular). The extreme and high singular treatments displayed a pronounced increase on days 9-17 (during and post phytoplankton bloom, Figure 1), and the extreme recurring treatment on days 13-17, but subsequently continued to raise at a gentler rate until the end

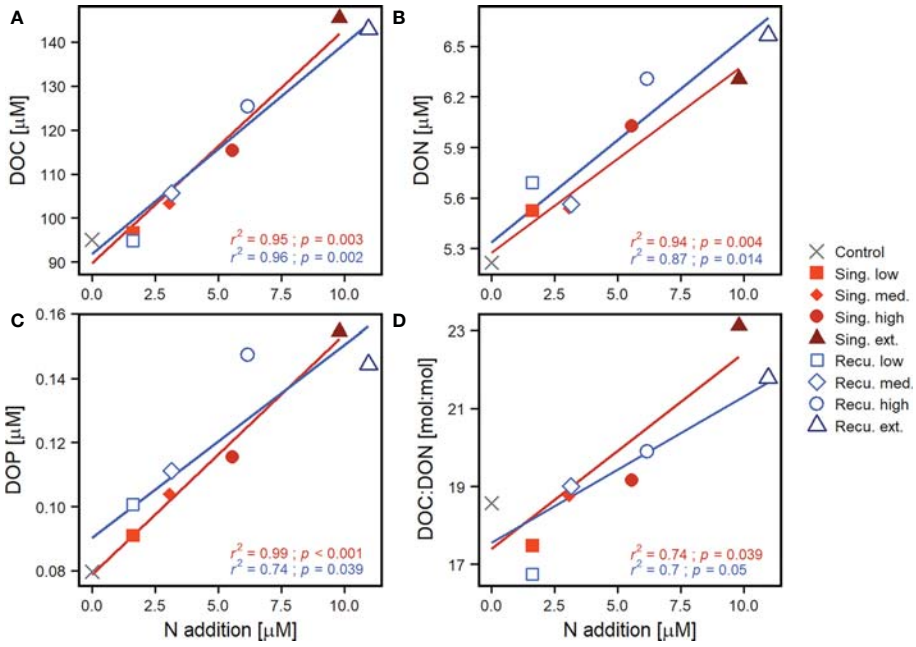

FIGURE 3
Effect of upwelling intensity on dissolved organic matter. Shown are linear regressions of **(A)** DOC, **(B)** DON, **(C)** DOP and **(D)** DOC : DON values against upwelling intensity (N addition) per upwelling mode. DOM values were averaged after the last deep water addition (≥ day 33). The coefficient of determination (r^2) and p-value (p) of the regressions are included. Only the lines for significant regressions ($p < 0.05$) are displayed (see Table S3 for detailed test statistics). Results for DOC : DOP and DON : DOP ratios can be found in Figure S3.

of experiment. Resulting CDOM quantities were higher in mesocosms with more intense simulated upwelling and were overall greater in the singular treatments: recurring treatments displayed values that were comparable to the previous intensity level in singular treatments (Figure 4A). While both upwelling modes showed significant positive relationships between a_{254} and upwelling intensity (Figure 5A), the slope of the singular mode was steeper than the recurring one even when considering the 95% confidence interval (Table S3). The aromatic fraction of CDOM, represented by a_{325} (Figure S4), followed patterns very similar to a_{254}, starting at 0.17-0.19 m^{-1} and ending at 0.53-0.99 m^{-1}. a_{325} showed a positive relationship with upwelling intensity (Figure S5 and Table S3).

Spectral slopes ($S_{275\text{-}295}$ and $S_{350\text{-}400}$), which provide insights into the average molecular weight of the CDOM pool, also experienced marked changes. $S_{275\text{-}295}$ (Figure 4B) began at 36.0-37.9 μm^{-1} and decreased throughout the experiment, signaling an increase in average molecular weight, as compounds of higher molecular weight tend to absorb light at higher wavelengths, thus decreasing the slopes. Coupled with changes in a_{254}, $S_{275\text{-}295}$ in the high and extreme singular treatments showed a very pronounced decline between days 9-13, while a sharp decrease was registered on days 13-17 in the extreme recurring treatment. After day 17 values tended to stabilize in the more intense simulated upwelling treatments while less intense treatments continued to steadily decrease (Figure 4B). The extreme singular treatment displayed the lowest $S_{275\text{-}295}$, reaching average values of 19.4 ± 0.3 μm^{-1} during days ≥33. Average $S_{275\text{-}295}$ values for this period showed significant negative relationship with upwelling intensity for both modes (Figure 5B) but, as for a_{254}, $S_{275\text{-}295}$ values in singular treatments were comparable to the previous intensity level in recurring treatments. $S_{350\text{-}400}$ (initial values of 13.5-14.9 μm^{-1}, Figure 4C) on the other hand presented opposite trends for each upwelling mode: while singular treatments presented increases (the extreme reaching 16-17 μm^{-1} on days 17-29), the recurring treatments tended to decrease. This resulted in different outcomes after day 33: despite the increase, singular treatments did not show a significant relationship with upwelling intensity, while recurring treatments showed a significant negative one (Figure 5C). Resulting S_R values overall were dominated by the marked changes in $S_{275\text{-}295}$ and followed its patterns (Figure 4D): initially at 2.48-2.74, decreases were observed specially in high and extreme singular patterns (the latter reaching minimum values close to 1.25) until day 17 and subsequently tended to stabilize. However, the different fates of $S_{350\text{-}400}$ for the two upwelling modes were reflected in S_R: at the end of the experiment, singular treatments displayed a significant

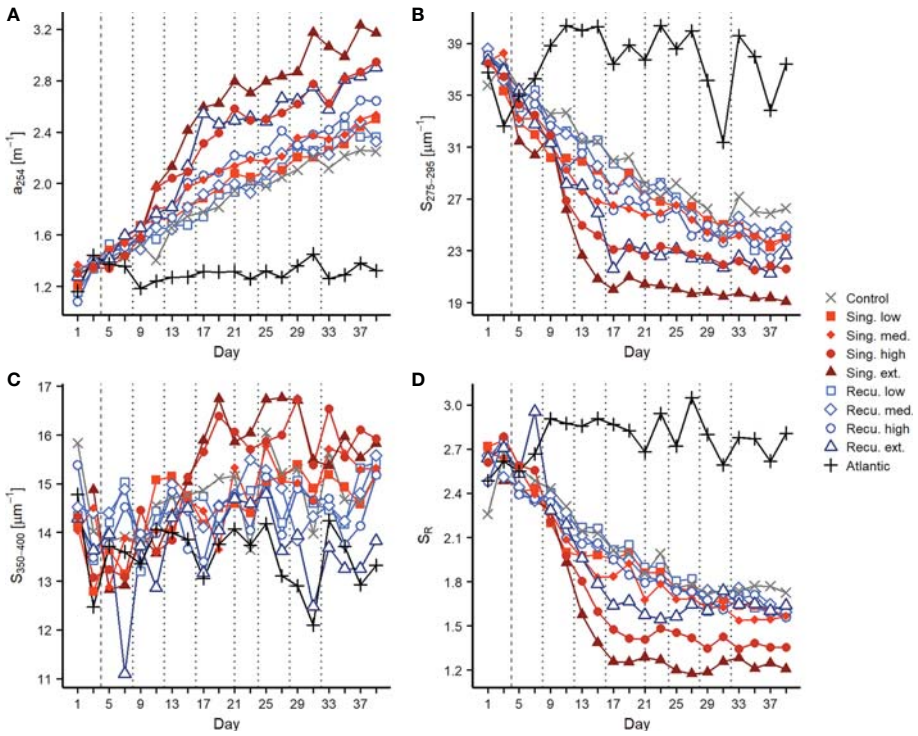

FIGURE 4
Changes in chromophoric dissolved organic matter during the experiment. Temporal development of **(A)** CDOM quantity as a_{254}, **(B)** $S_{275-295}$, **(C)** $S_{350-400}$, and **(D)** S_R. Vertical lines indicate deep water additions of singular (dashed) and recurring (dashed and dotted) treatments. See explanation of parameters in the Methods section.

relationship with upwelling intensity (Figure 5D), but recurring ones did not and tended to converge around S_R values of 1.65 (Figure 4D).

Fluorescence measurements provided further details into the composition of the DOM pool. Components C1 and C5 of the PARAFAC model were similar to fluorophores described as amino acid-like/tryptophan-like compounds that are at least partially bioavailable to prokaryotic consumption (Table S2). Both C1 and C5 (Figures 6A, D) presented increases in the intensity of their signal across mesocosms after the first deep water addition. For C1 the extreme singular treatment experienced a fluorescence intensification that was clearly superior to any other treatment, increasing from 0.009 RU to 0.070 RU on day 15, and continued to increase until reaching 0.087 RU at the end of the experiment. Other treatments also displayed increases until day 15 (although smaller) and tended to stabilize afterwards, despite variability, ending within a range of 0.032 (high singular) and 0.044 RU (low recurring). Despite the extreme singular treatment showed markedly high values, no consistent relationship was found between C1 and upwelling intensity at the end of the experiment (Figure 7A). For C5 (Figure 6D) all treatments exhibited relatively similar patterns. Initial values ranged between 0.001-0.007 RU, fluorescence signals increasing until day 21 and subsequently maintaining relatively similar values, ending at 0.011-0.021 RU. C5 did display significant positive relationships with upwelling intensity for both upwelling modes (Figure 7D).

Components representing humic-like compounds (C2 and C4), which have been associated to the microbial transformation of DOM, displayed nearly continuous increases in fluorescence signals (Figures 6B, C). C2 started at values of 0.003-0.008 RU and increased throughout the experiment in all mesocosms, treatments with greater upwelling intensity exhibiting more intense fluorescence signals. Positive significant relationships were found with upwelling intensity after the final deep water addition (Figure 7B). Singular treatments presented slightly higher values than recurring ones: e.g., during days ≥33, average C2 values for the extreme singular and recurring treatments were 0.0206 ± 0.0005 and 0.0190 ± 0.0005 RU, respectively. C4 also displayed fluorescence signals that consistently increased throughout the experiment (Figure 6C) and, as C2, presented significant positive relationships with upwelling intensity for both modes at the end of the experiment (Figure 7C).

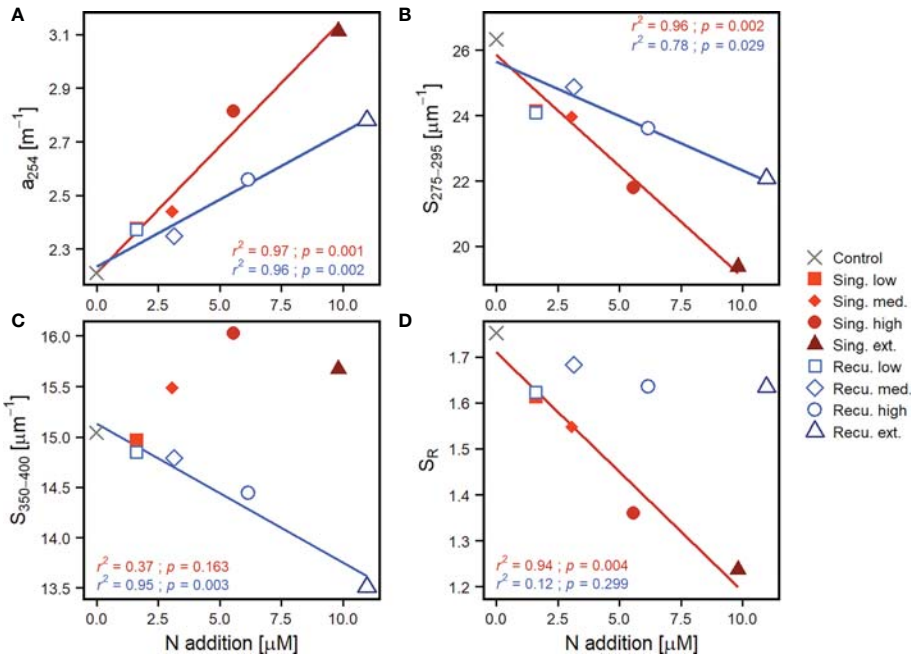

FIGURE 5
Linear regressions of average values after the last deep water addition to recurring treatments (≥ day 33) of **(A)** CDOM quantity as a_{254}, **(B)** $S_{275-295}$, **(C)** $S_{350-400}$ and **(D)** S_R against upwelling intensity (as N addition), per upwelling mode. The coefficient of determination (r^2) and p-value (p) of the regressions are included. Only lines for significant regressions ($p < 0.05$) are displayed. Regression parameters are detailed in Table S3.

Discussion

DOC accumulation in the water column

Initial concentrations of DOC were similar to those typically found in surface waters of the Canary Islands oceanic region (Arístegui et al., 2003; Arístegui et al., 2004; Arístegui et al., 2020; Burgoa et al., 2020) and other locations in the North Atlantic subtropical gyre (Goldberg et al., 2010; Lomas et al., 2013). Concentrations quickly increased following nutrient depletion and the collapse of the diatom-dominated phytoplankton bloom (Ortiz et al., 2022b). In the case of extreme treatments (~140 µM), values reached levels far exceeding DOC concentrations observed in the Canary Current upwelling system (100-110 µM, Arístegui et al., 2003; Burgoa et al., 2020). Similar DOC levels have previously been reported in deep water addition mesocosm experiments in oligotrophic waters (Zark et al., 2017a).

Diatoms are known to release DOC upon nutrient limitation (Norrman et al., 1995; Zark et al., 2017a), but the source of the observed DOC (~70 µM increase in extreme treatments by day 21) was not limited to dissolved primary production (that is, recently photosynthesized DOC). Accumulated dissolved primary production by day 21 was 20.53 µmol $C{\cdot}L^{-1}$ (11.91% of total primary production) and 6.58 µmol $C{\cdot}L^{-1}$ (5.07% of total primary production) for the extreme singular and recurring treatments, respectively (Figure S6; Ortiz et al., 2022a). Given these values, most of the DOC increase must have originated from a source other than dissolved primary production. This DOC increase in extreme singular and recurring treatments represented 43% and 58% of cumulative total primary production by day 21, respectively (35% and 55% of cumulative particulate primary production after removing the dissolved primary production contribution to the DOC increase), higher than the 23% of total new production accumulated as DOC reported by Norrman et al. (1995) during a coastal diatom bloom.

The arising question is how such vast amounts of organic carbon were channeled into the dissolved matter pool in such a short period of time (~10 days). Processes such as exudation by diatoms (Mühlenbruch et al., 2018), extracellular enzymatic activity on particles and gel structures (Arnosti, 2011), grazing and sloppy feeding (Steinberg and Landry, 2017), viral lysis (Breitbart et al., 2018) and programmed cell death (Spungin et al., 2018) result in release of DOM. The large amounts of particles (including transparent exopolymer particles) that were formed following the diatom bloom (Baumann et al., 2021b) provided the substrate for prokaryotes to consume POC, and this could have contributed to the production of DOC. The stabilization of DOC after day 21 despite continued primary production, in conjunction with sustained community respiration (Baños et al., 2022) and prokaryotic heterotrophic production (PHP) rates (Figure S7), indicates that prokaryotes

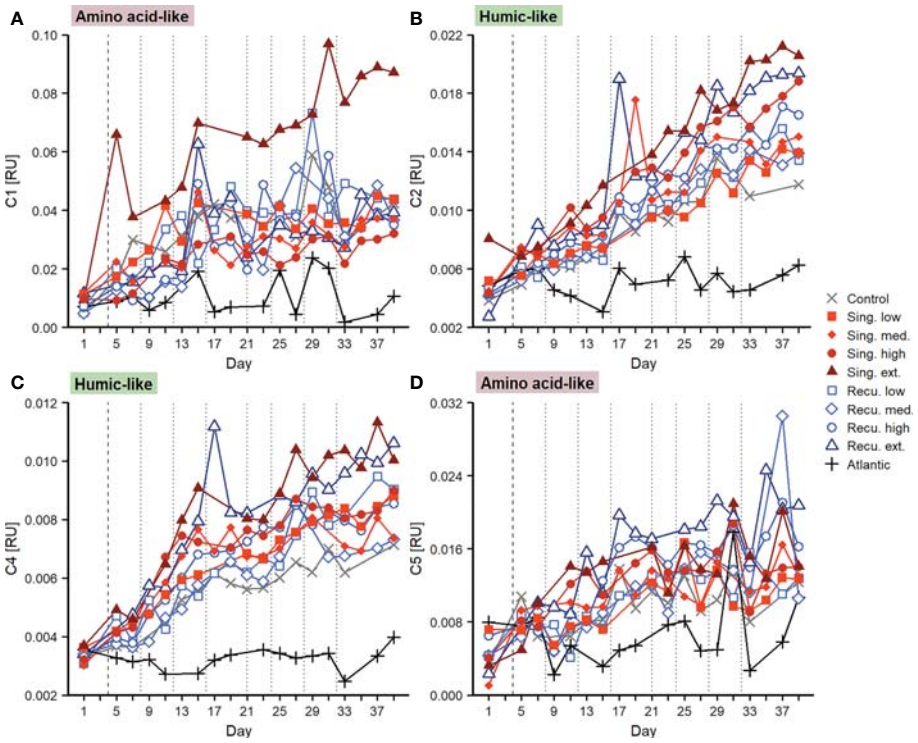

FIGURE 6
Changes in fluorescent dissolved organic matter during the experiment. Temporal evolution of PARAFAC components **(A)** C1, **(B)** C2, **(C)** C4 and **(D)** C5. Vertical lines indicate deep water additions of singular (dashed) and recurring (dashed and dotted) treatments.

were consuming at least a fraction of the DOM pool and, consequently, at least part of the DOC accumulated in the water column could eventually be remineralised.

Increase in the relative C content of DOM

Artificial upwelling enhanced the C:N ratio in the DOM pool from ~15 to 19-27. Initial DOC : DON values (Figure 2D) were within the range of values reported for the subtropical North Atlantic (Hansell and Carlson, 2001; Valiente et al., 2022). Subsequent increases in DOC : DON ratios as a result of artificial upwelling were similar to those observed in other experimentally-induced diatom blooms (Norrman et al., 1995). This increase was probably a combination of the release of C-rich polysaccharides by diatoms (Engel, 2001; Mühlenbruch et al., 2018) and the preferential degradation of DON by prokaryotes (Hach et al., 2020). The blooming diatom community itself was probably a major source of DON in the form of free amino acids, proteins and aminosugars, as suggested by the initial increase in amino acid-like fluorescence (Figure 6; Granum et al., 2002). Over the course of the experiment the amino acid-like fluorescence was not clearly related to upwelling intensity (Figures 6, 7), which may indicate ongoing consumption by prokaryotes. While the organic molecules generating the humic-like fluorescence signal probably also contained N, they tend not to be degraded by prokaryotes (Lønborg et al., 2010). Amino acid-like fluorescence did not return to initial levels, meaning that a fraction of this signal corresponded to molecules that were not readily consumed by prokaryotes (Lønborg et al., 2010). Amino acid release through viral lysis (Middelboe and Jørgensen, 2006) and, for recurring treatments, more constant releases of amino acid-containing molecules by the prolonged diatom blooms throughout the experiment (Ortiz et al., 2022b) could have also contributed to the sustained amino acid-like fluorescence signal.

DOC : DOP ratios were also similar to previous estimates for the subtropical North Atlantic (Ammerman et al., 2003) but, as opposed to DOC : DON, no clear relationship with upwelling intensity was observed for DOC : DOP (Figures S2, S3). Overall, DOC : DOP values slightly increased from initial conditions and, thus, preferential DOP consumption might have existed to a certain degree (Hach et al., 2020). Prokaryotes are known to utilize DOP as a source of P through the use of alkaline phosphatases when inorganic P is limiting, as measured previously in the study area (Sebastián et al., 2004). Particulate organic matter stoichiometry also tended to shift to higher

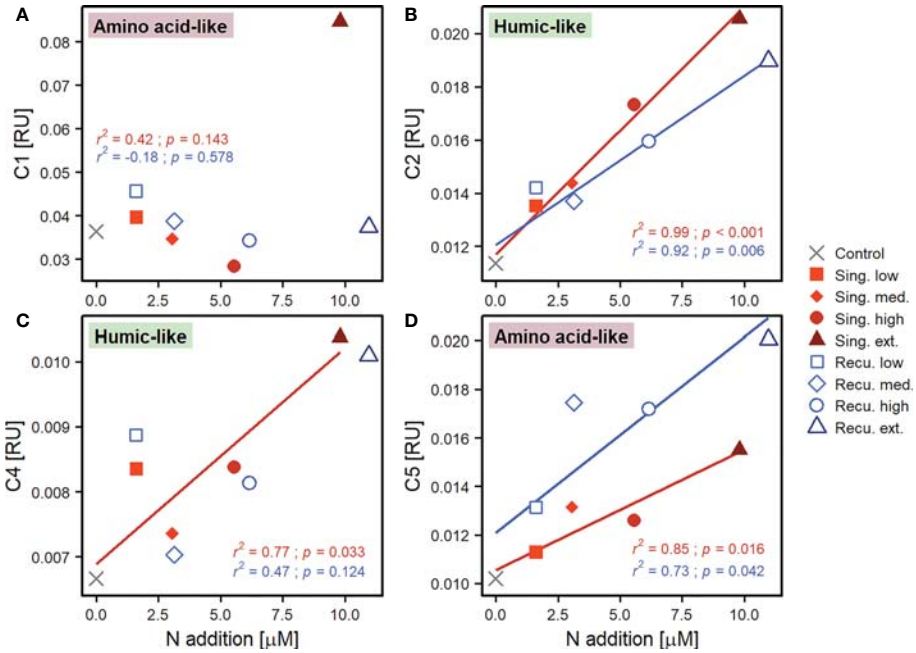

FIGURE 7
Linear regressions of average values after the last deep water addition to recurring treatments (≥ day 33) of FDOM components **(A)** C1, **(B)** C2, **(C)** C4 and **(D)** C5 against upwelling intensity (as N addition), per upwelling mode. The coefficient of determination (r^2) and p-value (p) of the regressions are included. Only lines for significant regressions ($p < 0.05$) are displayed. Regression parameters are detailed in Table S3.

relative content of C (Baumann et al., 2021b), supporting the idea that not only the consumption of DON and DOP, but also the production of C-rich organic matter, yielded higher C content of DOM. While DOP concentrations fluctuated considerably (Figure 2C), DON : DOP values tended to decrease with increasing upwelling intensity at the end of the experiment (Figure S2), suggesting that DON might have been consumed over DOP to compensate for the lower N availability, as NO_3^- : PO_4^- ratios decreased after deep water additions (Figure S8).

Shift towards high molecular weight, humic-like DOM

CDOM increases have been previously observed associated with phytoplankton production (Romera-Castillo et al., 2010), including communities in nutrient-depleted conditions after a blooming phase (Loginova et al., 2015). Hence, as with DOC, the initial post-bloom increase in a_{254} (Figure 4A) and a_{325} (Figure S4) was probably partly associated with DOM released by diatoms. While DOC tended to stabilize, CDOM continued to accumulate (to a greater degree in singular treatments), including an intensification of the humic-like fluorescence signal (Figure 6). The sustained accumulation throughout the experiment seems to be the result of the generation of CDOM and humic-like FDOM as by-products of the prokaryotic reworking of organic matter (Nelson and Siegel, 2013; Catalá et al., 2015b). The fact that cumulative PHP was strongly correlated with CDOM absorption, spectral slopes and humic-like FDOM intensity (Figure 8) would support that interpretation, as cumulative PHP has been previously observed to be correlated to DOM transformation (Zark et al., 2017a).

CDOM average molecular weight also changed markedly: initial values of spectral slopes were similar to those found in other oligotrophic regions (e.g. Catalá et al., 2018) but markedly decreased after the initial bloom (Figures 4B, C), suggesting an increase in average molecular weight (Helms et al., 2008). Artificial upwelling modes, however, had different outcomes, with higher CDOM molecular weight in the singular treatments and differences in composition (Figures 4B-D). According to the size-reactivity continuum theory (Benner and Amon, 2015), larger size classes of DOM (e.g., macromolecules of combined forms of carbohydrates and amino acids) tend to be preferentially degraded by prokaryotes. The degradation of this high molecular weight DOM, which here probably included polysaccharides and molecules containing amino acids, would result in the generation of CDOM (and FDOM) of higher molecular weight than what was initially present in the mesocosms, hence yielding the observed changes in spectral slopes. Similar results have been reported for the open ocean, as

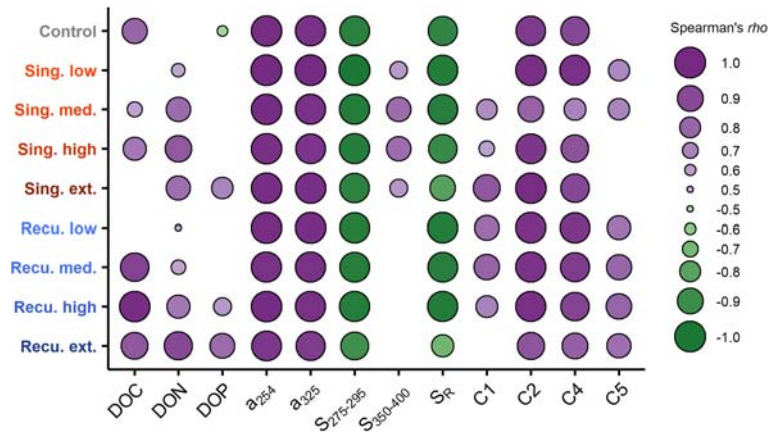

FIGURE 8
Relationship between cumulative prokaryotic heterotrophic production (PHP) and dissolved organic matter (DOM) parameters. Shown are Spearman's *rho* (ρ) correlation coefficients per mesocosm. Only significant correlations ($p < 0.05$) are displayed.

apparent oxygen utilization has been linked to the decreases in $S_{275\text{-}295}$ and increases in humic-like fluorescence (Catalá et al., 2015b; Martínez-Pérez et al., 2017; Catalá et al., 2018).

Implications for carbon sequestration

Long-term nutrient addition experiments (weeks to >1 year) have shown that following large DOM accumulations, a significant fraction of it can be remineralised in the weeks following the diatom bloom, but as much as ~30% remain for at least several months (Fry et al., 1996; Meon and Kirchman, 2001). Here, the fertilization with nutrient-rich deep water caused an accumulation of DOC with no visible decrease during the duration of the experiment (~5.5 weeks). The magnitude of the excess DOC was comparable to the carbon that sunk out of the mesocosms in the form of POC (Baumann et al., 2021b), highlighting that DOC represents a pool of major importance for carbon sequestration. DOC is known to accumulate in the oligotrophic waters of the North Atlantic subtropical gyre (Goldberg et al., 2010; Lomas et al., 2013) as surface prokaryotic communities are not able to remineralize it (Carlson et al., 2004). Mesopelagic and bathypelagic prokaryotes, however, have been shown to consume surface DOC when they come into contact with it, suggesting that deep ocean prokaryotic communities possess a wider range of metabolic capabilities (Carlson et al., 2004; Sebastián et al., 2021). As artificial upwelling is not merely limited to nutrient addition but involves the translocation of deep prokaryotic communities into surface waters, their inoculation into the surface DOM pool could enhance DOC remineralization. However, this will depend on whether deep ocean prokaryotes are able to thrive when introduced among the surface prokaryotic assemblages in the course of the successions that happen during and following phytoplankton blooms (Pontiller et al., 2022).

During our experiment, while no decreases in DOC concentrations were found following the post-bloom accumulation, DOM transformation seemed to be taking place. The production of CDOM and humic-like FDOM (Figures 4, 6) and their correlation with cumulative PHP (Figure 8) are indicative of ongoing microbial transformation of DOM (Nelson and Siegel, 2013; Catalá et al., 2015b). This has been previously observed in mesocosm fertilization experiments also at the molecular level (Zark et al., 2017a). Oceanic DOM is known to undergo rapid molecular diversification following the consumption and transformation of newly produced organic matter by prokaryotes, resulting in an extremely diverse mixture of organic molecules (Lechtenfeld et al., 2015; Hach et al., 2020). The complex web of ecological interactions between the resulting diverse DOM and the prokaryotic community likely contributed to the stabilization of the organic matter pool (Dittmar et al., 2021). Nutrients were quickly depleted after deep water additions (Ortiz et al., 2022a), and their limitation could partially explain the lack of DOM consumption (Letscher et al., 2015). Additionally, predation (Jürgens and Massana, 2008) and viral infection (Breitbart et al., 2018) of prokaryotes, whose abundance markedly decreased during the diatom bloom collapse (Figure S9), could also have reduced bulk DOM degradation rates. In conjunction, these factors could contribute to the persistence of DOC, hindering remineralization and potentially leading to its long-term storage.

The accumulated persistent DOC could be ultimately subducted below the permanent pycnocline (Boyd et al., 2019; Le Moigne, 2019), leading to potential carbon sequestration. A long monitoring period (multiple weeks, months) and tracing of DOC dynamics would be required to reliably assess the fate of DOC. Additionally, while mesocosms are a useful tool to study pelagic communities in close-to-natural conditions, they cannot reproduce the multi-dimensional physical dynamics of the real ocean. Downwelling or convective mixing would need to be considered, as they transport DOC to the deep ocean (Boyd et al., 2019; Baetge et al., 2020), which is a requirement for long-term sequestration. Moreover, horizontal advection would potentially limit the accumulation of DOC, thereby reducing its concentrations and making potential downwelling less effective. All these factors would need to be considered in conjunction with POC dynamics to assess the viability of artificial upwelling as a climate mitigation measure in natural open-sea conditions.

Conclusions

The artificial upwelling of deep, nutrient-rich waters into the oligotrophic subtropical North Atlantic yielded marked increases in the DOM concentration and its carbon content, and shifts in DOM characteristics. The magnitude of the observed changes was mostly related to the upwelling intensity, as mesocosms subject to more intense upwelling presented higher concentrations of DOC. Increases over 70 µM for extreme treatments show the potential of artificial upwelling to transfer inorganic carbon to the dissolved organic fraction. The resulting DOC pool was as large as the POC that sunk in the mesocosms, highlighting the importance that DOC has for carbon sequestration estimations. Upwelling intensity led to increases in the C content of DOM relative to N and P, increases in concentration and average molecular weight of CDOM, and the intensification of humic-like FDOM signals. The generation of CDOM, and specifically humic-like FDOM, has been associated with the reworking of organic matter, suggesting ongoing transformation and molecular diversification of DOM during the experiment. The artificial upwelling mode yielded partially different outcomes: while it did not result in differences in DOC concentrations during the time period of the experiment, the treatments reproducing a singular upwelling event presented higher CDOM quantities and average molecular weight than recurring treatments, as well as differences in the spectral slope ratios. These differences in the CDOM pool likely indicate that the singular upwelling event yielded conditions where the by-products of the microbial transformation of DOM accumulated to a greater extent than in recurring upwelling, where periodic additions of deep water resulted in sustained diatoms blooms and new inputs of DOM. Nonetheless, in both upwelling modes no decreases in DOM quantity were observed. This persistence could be associated with a combination of the molecular diversification of DOM due to microbial reworking, unfavorable environmental conditions (nutrient limitation) and inadequate metabolic capabilities of the prokaryotic communities in the mesocosms. While the temporal scale of the experiment leaves an open question regarding the mid- and long-term fate of the accumulated DOM (long-term persistence *vs.* gradual remineralization), our results highlight the importance of considering DOC along POC when assessing the carbon sequestration potential of artificial upwelling. A monitoring period of multiple weeks/months would be required to reliably estimate the extent of DOM remineralization and studies in open-sea conditions would be necessary to include the effects of the physical processes involved in carbon export.

Data availability statement

The data presented in the study are deposited in the PANGAEA repository, DOI https://doi.pangaea.de/10.1594/PANGAEA.946776 (Gómez-Letona et al., 2022).

Author contributions

Experimental concept and design: UR and JA. Execution of experiment and sample analyses: all authors. Data analysis: MG-L with contributions from all authors. MG-L wrote the original draft with input from all authors. All authors contributed to the article and approved the submitted version.

Funding

This study is a contribution to the Ocean Artificial Upwelling project (Ocean artUp), funded by an Advanced Grant of the European Research Council (No. 695094). Additional support was provided through projects TRIATLAS (AMD-817578-5) from the European Union's Horizon 2020 and e-IMPACT (PID2019-109084RB-C21) funded by the Spanish National Science Plan. MG-L is supported by the Ministerio de Ciencia, Innovación y Universidades, Gobierno de España (FPU17-01435) during his PhD. MS is supported by the Project MIAU (RTI2018-101025-B-I00) and the 'Severo Ochoa Centre of Excellence' accreditation (CEX2019-000928-S). JA is supported by a Helmholtz International Fellow Award, 2015 (Helmholtz Association, Germany). JA is supported by the United States National Science Foundation grant OCE-

1840868 to the Scientific Committee on Oceanic Research (SCOR, United States) WG 155.

Acknowledgments

The authors thank the Plataforma Oceánica de Canarias (PLOCAN) for their extensive support throughout the experiment, including the use of their facilities and their assistance during the sampling of the mesocosms. The authors thank the captain and crew of RV James Cook for the deployment of the mesocosms and the deep water collection, and the captain and crew of the vessel J. SOCAS for helping with the second deep water collection and the recovery of the mesocosms at the end of the experiment. The authors especially thank the whole KOSMOS team (GEOMAR) for their relentless effort organizing and carrying out all the logistic and technical work necessary for the experiment, and to the biological oceanography group of the University of Las Palmas de Gran Canaria (GOB-ULPGC) for providing lab facilities and technical support. Particular thanks go to Acorayda González for her contribution to the measurement of dissolved organic carbon.

Conflict of interest

The authors declare that the research was conducted in the absence of any commercial or financial relationships that could be construed as a potential conflict of interest.

Publisher's note

All claims expressed in this article are solely those of the authors and do not necessarily represent those of their affiliated organizations, or those of the publisher, the editors and the reviewers. Any product that may be evaluated in this article, or claim that may be made by its manufacturer, is not guaranteed or endorsed by the publisher.

Supplementary material

The Supplementary Material for this article can be found online at: https://www.frontiersin.org/articles/10.3389/fmars.2022.969714/full#supplementary-material

References

Acinas, S. G., Sánchez, P., Salazar, G., Cornejo-Castillo, F. M., Sebastián, M., Logares, R., et al. (2021). Deep ocean metagenomes provide insight into the metabolic architecture of bathypelagic microbial communities. *Commun. Biol.* 4, 604. doi: 10.1038/s42003-021-02112-2

Ammerman, J. W., Hood, R. R., Case, D. A., and Cotner, J. B. (2003). Phosphorus deficiency in the Atlantic: An emerging paradigm in oceanography. *Eos Trans. Am. Geophys. Union* 84, 165–170. doi: 10.1029/2003EO180001

Arcos-Pulido, M., Rodríguez-Santana, A., Emelianov, M., Paka, V., Arístegui, J., Benavides, M., et al. (2014). Diapycnal nutrient fluxes on the northern boundary of cape ghir upwelling region. *Deep-Sea Res. Part I Oceanogr. Res. Pap.*, 100–109, 84. doi: 10.1016/j.dsr.2013.10.010

Arístegui, J., Barton, E. D., Montero, M. F., García-Muñoz, M., and Escánez, J. (2003). Organic carbon distribution and water column respiration in the NW Africa-canaries coastal transition zone. *Aquat. Microb. Ecol.* 33, 289–301. doi: 10.3354/ame033289

Arístegui, J., Barton, E. D., Tett, P., Montero, M. F., García-Muñoz, M., Basterretxea, G., et al. (2004). Variability in plankton community structure, metabolism, and vertical carbon fluxes along an upwelling filament (Cape juby, NW Africa). *Prog. Oceanogr.* 62, 95–113. doi: 10.1016/j.pocean.2004.07.004

Arístegui, J., Montero, M. F., Hernández-Hernández, N., Alonso-González, I. J., Baltar, F., Calleja, M. L., et al. (2020). Variability in water-column respiration and its dependence on organic carbon sources in the canary current upwelling region. *Front. Earth Sci.* 8. doi: 10.3389/feart.2020.00349

Arnosti, C. (2011). Microbial extracellular enzymes and the marine carbon cycle. *Ann. Rev. Mar. Sci.* 3, 401–425. doi: 10.1146/annurev-marine-120709-142731

Azam, F., and Malfatti, F. (2007). Microbial structuring of marine ecosystems. *Nat. Rev. Microbiol.* 5, 782–791. doi: 10.1038/nrmicro1747

Baetge, N., Graff, J. R., Behrenfeld, M. J., and Carlson, C. A. (2020). Net community production, dissolved organic carbon accumulation, and vertical export in the Western north Atlantic. *Front. Mar. Sci.* 7. doi: 10.3389/fmars.2020.00227

Baños, I., Arístegui, J., Benavides, M., Gómez-Letona, M., Montero, M. F., Ortiz, J., et al. (2022). Response of plankton community respiration under variable simulated upwelling events. *Front. Mar. Sci.* 9, 1006010. doi: 10.3389/fmars.2022.1006010

Baumann, M., Sswat, M., Ortiz Cortes, J., Hernández-Hernández, N., Baños Cerón, I., Vanharanta, M., et al. (2021a). KOSMOS 2018 gran canaria mesocosm study: water column biogeochemistry. *PANGAEA*. doi: 10.1594/PANGAEA.933090

Baumann, M., Taucher, J., Paul, A. J., Heinemann, M., Vanharanta, M., Bach, L. T., et al. (2021b). Effect of intensity and mode of artificial upwelling on particle flux and carbon export. *Front. Mar. Sci.* 8. doi: 10.3389/fmars.2021.742142

Benner, R., and Amon, R. M. W. (2015). The size-reactivity continuum of major bioelements in the ocean. *Ann. Rev. Mar. Sci.* 7, 185–205. doi: 10.1146/annurev-marine-010213-135126

Boyd, P. W., Claustre, H., Levy, M., Siegel, D. A., and Weber, T. (2019). Multi-faceted particle pumps drive carbon sequestration in the ocean. *Nature* 568, 327–335. doi: 10.1038/s41586-019-1098-2

Breitbart, M., Bonnain, C., Malki, K., and Sawaya, N. A. (2018). Phage puppet masters of the marine microbial realm. *Nat. Microbiol.* 3, 754–766. doi: 10.1038/s41564-018-0166-y

Burgoa, N., Machín, F., Marrero-Díaz, Á., Rodríguez-Santana, Á., Martínez-Marrero, A., Arístegui, J., et al. (2020). Mass, nutrients and dissolved organic carbon (DOC) lateral transports off northwest Africa during fall 2002 and spring 2003. *Ocean Sci.* 16, 483–511. doi: 10.5194/os-16-483-2020

Carlson, C. A., Giovannoni, S. J., Hansell, D. A., Goldberg, S. J., Parsons, R., and Vergin, K. (2004). Interactions among dissolved organic carbon, microbial processes, and community structure in the mesopelagic zone of the northwestern Sargasso Sea. *Limnol. Oceanogr.* 49, 1073–1083. doi: 10.4319/lo.2004.49.4.1073

Catalá, T. S., Álvarez-Salgado, X. A., Otero, J., Iuculano, F., Companys, B., Horstkotte, B., et al. (2016). Drivers of fluorescent dissolved organic matter in the global epipelagic ocean. *Limnol. Oceanogr.* 61, 1101–1119. doi: 10.1002/lno.10281

Catalá, T. S., Martínez-Pérez, A. M., Nieto-Cid, M., Álvarez, M., Otero, J., Emelianov, M., et al. (2018). Dissolved organic matter (DOM) in the open Mediterranean sea. i. basin–wide distribution and drivers of chromophoric DOM. *Prog. Oceanogr.* 165, 35–51. doi: 10.1016/j.pocean.2018.05.002

Catalá, T. S., Reche, I., Álvarez, M., Khatiwala, S., Guallart, E. F., Benítez-Barrios, V. M., et al. (2015a). Water mass age and aging driving chromophoric dissolved organic matter in the dark global ocean. *Global Biogeochem. Cycles* 29, 917–934. doi: 10.1002/2014GB005048

Catalá, T. S., Reche, I., Fuentes-Lema, A., Romera-Castillo, C., Nieto-Cid, M., Ortega-Retuerta, E., et al. (2015b). Turnover time of fluorescent dissolved organic matter in the dark global ocean. *Nat. Commun.* 6, 5986. doi: 10.1038/ncomms6986

Dittmar, T., Lennartz, S. T., Buck-Wiese, H., Hansell, D. A., Santinelli, C., Vanni, C., et al. (2021). Enigmatic persistence of dissolved organic matter in the ocean. *Nat. Rev. Earth Environ.* 2, 570–583. doi: 10.1038/s43017-021-00183-7

Engel, A. (2001). Carbon and nitrogen content of transparent exopolymer particles (TEP) in relation to their alcian blue adsorption. *Mar. Ecol. Prog. Ser.* 219, 1–10. doi: 10.3354/meps219001

Fawzy, S., Osman, A. I., Doran, J., and Rooney, D. W. (2020). Strategies for mitigation of climate change: a review. *Environ. Chem. Lett.* 18, 2069–2094. doi: 10.1007/s10311-020-01059-w

Field, C. B., Behrenfeld, M. J., Randerson, J. T., and Falkowski, P. (1998). Primary production of the biosphere: Integrating terrestrial and oceanic components. *Science* 281, 237–240. doi: 10.1126/science.281.5374.237

Fry, B., Hopkinson, C. S.Jr., Nolin, A., Norrman, B., and Zweifel, U. L. (1996). Long-term decomposition of DOC from experimental diatom blooms. *Limnol. Oceanogr.* 41, 1344–1347. doi: 10.4319/lo.1996.41.6.1344

Goldberg, S. J., Carlson, C. A., Bock, B., Nelson, N. B., and Siegel, D. A. (2010). Meridional variability in dissolved organic matter stocks and diagenetic state within the euphotic and mesopelagic zone of the north Atlantic subtropical gyre. *Mar. Chem.* 119, 9–21. doi: 10.1016/j.marchem.2009.12.002

Gómez-Letona, M., Baumann, M., González, A., Pérez Barrancos, C., Sebastian, M., Baños Cerón, I., et al. (2022). KOSMOS 2018 Gran Canaria mesocosm study: dissolved organic matter. *PANGAEA* doi: 10.1594/PANGAEA.946776

Granum, E., Kirkvold, S., and Myklestad, S. M. (2002). Cellular and extracellular production of carbohydrates and amino acids by the marine diatom skeletonema costatum: diel variations and effects of n depletion. *Mar. Ecol. Prog. Ser.* 242, 83–94. doi: 10.3354/meps242083

Hach, P. F., Marchant, H. K., Krupke, A., Riedel, T., Meier, D. V., Lavik, G., et al. (2020). Rapid microbial diversification of dissolved organic matter in oceanic surface waters leads to carbon sequestration. *Sci. Rep.* 10, 13025. doi: 10.1038/s41598-020-69930-y

Hansell, D. A., and Carlson, C. A. (2001). Biogeochemistry of total organic carbon and nitrogen in the Sargasso Sea: control by convective overturn. *Deep Sea Res. Part II Top. Stud. Oceanogr.* 48, 1649–1667. doi: 10.1016/S0967-0645(00)00153-3

Hansell, D. A., Carlson, C. A., Repeta, D. J., and Schlitzer, R. (2009). Dissolved organic matter in the ocean: A controversy stimulates new insights. *Oceanography* 22, 202–211. doi: 10.5670/oceanog.2009.109

Hansen, H. P., and Koroleff, F. (1999). "Determination of nutrients," in *Methods of seawater analysis*. Eds. K. Grasshoff, K. Kremling and M. Ehrhardt (Weinheim, Germany: Wiley Verlag Chemie GmbH), 159–228. doi: 10.1002/9783527613984.ch10

Helms, J. R., Stubbins, A., Perdue, E. M., Green, N. W., Chen, H., and Mopper, K. (2013). Photochemical bleaching of oceanic dissolved organic matter and its effect on absorption spectral slope and fluorescence. *Mar. Chem.* 155, 81–91. doi: 10.1016/j.marchem.2013.05.015

Helms, J. R., Stubbins, A., Ritchie, J. D., Minor, E. C., Kieber, D. J., and Mopper, K. (2008). Absorption spectral slopes and slope ratios as indicators of molecular weight, source, and photobleaching of chromophoric dissolved organic matter. *Limnol. Oceanogr.* 53, 955–969. doi: 10.4319/lo.2008.53.3.0955

Jacox, M. G., Edwards, C. A., Hazen, E. L., and Bograd, S. J. (2018). Coastal upwelling revisited: Ekman, bakun, and improved upwelling indices for the U.S. West coast. *J. Geophys. Res. Ocean.* 123, 7332–7350. doi: 10.1029/2018JC014187

Johnson, K. S., Michael Gordon, R., and Coale, K. H. (1997). What controls dissolved iron concentrations in the world ocean? *Mar. Chem.* 57, 137–161. doi: 10.1016/S0304-4203(97)00043-1

Jürgens, K., and Massana, R. (2008). Protistan grazing on marine bacterioplankton. *Microb. Ecol. Ocean.*, Kirchman, D. L. (Ed.) 383–441. doi: 10.1002/9780470281840.ch11

Kirchman, D. L. (1993). "Leucine incorporation as a measure of biomass production by heterotrophic bacteria," in *Handbook of methods in aquatic microbial ecology*. Eds. P. F. Kemp, B. F. Sherr, E. B. Sherr and J. J. Cole (Boca Raton, FL: CRC Press), 509–512. doi: 10.1201/9780203752746

Lønborg, C., and Álvarez-Salgado, X. A. (2014). Tracing dissolved organic matter cycling in the eastern boundary of the temperate north Atlantic using absorption and fluorescence spectroscopy. *Deep Sea Res. Part I Oceanogr. Res. Pap.* 85, 35–46. doi: 10.1016/j.dsr.2013.11.002

Lønborg, C., Álvarez-Salgado, X. A., Davidson, K., Martínez-García, S., and Teira, E. (2010). Assessing the microbial bioavailability and degradation rate constants of dissolved organic matter by fluorescence spectroscopy in the coastal upwelling system of the ría de vigo. *Mar. Chem.* 119, 121–129. doi: 10.1016/j.marchem.2010.02.001

Lawaetz, A. J., and Stedmon, C. A. (2009). Fluorescence intensity calibration using the raman scatter peak of water. *Appl. Spectrosc.* 63, 936–940. doi: 10.1366/000370209788964548

Lechtenfeld, O. J., Hertkorn, N., Shen, Y., Witt, M., and Benner, R. (2015). Marine sequestration of carbon in bacterial metabolites. *Nat. Commun.* 6, 6711. doi: 10.1038/ncomms7711

Le Moigne, F. A. C. (2019). Pathways of organic carbon downward transport by the oceanic biological carbon pump. *Front. Mar. Sci.* 6. doi: 10.3389/fmars.2019.00634

Letscher, R. T., Knapp, A. N., James, A. K., Carlson, C. A., Santoro, A. E., and Hansell, D. A. (2015). Microbial community composition and nitrogen availability influence DOC remineralization in the south pacific gyre. *Mar. Chem.* 177, 325–334. doi: 10.1016/j.marchem.2015.06.024

Levitus, S., Conkright, M. E., Reid, J. L., Najjar, R. G., and Mantyla, A. (1993). Distribution of nitrate, phosphate and silicate in the world oceans. *Prog. Oceanogr.* 31, 245–273. doi: 10.1016/0079-6611(93)90003-V

Loginova, A. N., Borchard, C., Meyer, J., Hauss, H., Kiko, R., and Engel, A. (2015). Effects of nitrate and phosphate supply on chromophoric and fluorescent dissolved organic matter in the Eastern tropical north Atlantic: a mesocosm study. *Biogeosciences* 12, 6897–6914. doi: 10.5194/bg-12-6897-2015

Lomas, M. W., Bates, N. R., Johnson, R. J., Knap, A. H., Steinberg, D. K., and Carlson, C. A. (2013). Two decades and counting: 24-years of sustained open ocean biogeochemical measurements in the Sargasso Sea. *Deep Sea Res. Part II Top. Stud. Oceanogr.* 93, 16–32. doi: 10.1016/j.dsr2.2013.01.008

Martínez-Pérez, A. M., Álvarez-Salgado, X. A., Arístegui, J., and Nieto-Cid, M. (2017). Deep-ocean dissolved organic matter reactivity along the Mediterranean Sea: does size matter? *Sci. Rep.* 7, 5687. doi: 10.1038/s41598-017-05941-6

Maruyama, S., Yabuki, T., Sato, T., Tsubaki, K., Komiya, A., Watanabe, M., et al. (2011). Evidences of increasing primary production in the ocean by stommel's perpetual salt fountain. *Deep-Sea Res. Part I Oceanogr. Res. Pap.* 58, 567–574. doi: 10.1016/j.dsr.2011.02.012

McGillicuddy, D. J., Anderson, L. A., Bates, N. R., Bibby, T., Buesseler, K. O., Carlson, C. A., et al. (2007). Eddy/Wind interactions stimulate extraordinary mid-ocean plankton blooms. *Science* 316, 1021–1026. doi: 10.1126/science.1136256

Meon, B., and Kirchman, D. L. (2001). Dynamics and molecular composition of dissolved organic material during experimental phytoplankton blooms. *Mar. Chem.* 75, 185–199. doi: 10.1016/S0304-4203(01)00036-6

Middelboe, M., and Jørgensen, N. O. G. (2006). Viral lysis of bacteria: an important source of dissolved amino acids and cell wall compounds. *J. Mar. Biol. Assoc. United Kingdom* 86, 605–612. doi: 10.1017/S0025315406013518

Mühlenbruch, M., Grossart, H.-P., Eigemann, F., and Voss, M. (2018). Mini-review: Phytoplankton-derived polysaccharides in the marine environment and their interactions with heterotrophic bacteria. *Environ. Microbiol.* 20, 2671–2685. doi: 10.1111/1462-2920.14302

Murphy, K. R., Stedmon, C. A., Wenig, P., and Bro, R. (2014). OpenFluor- an online spectral library of auto-fluorescence by organic compounds in the environment. *Anal. Methods* 6, 658–661. doi: 10.1039/c3ay41935e

Nelson, N. B., and Siegel, D. A. (2013). The global distribution and dynamics of chromophoric dissolved organic matter. *Ann. Rev. Mar. Sci.* 5, 447–476. doi: 10.1146/annurev-marine-120710-100751

Norrman, B., Zwelfel, U. L., Hopkinson, C. S.Jr., and Brian, F. (1995). Production and utilization of dissolved organic carbon during an experimental diatom bloom. *Limnol. Oceanogr.* 40, 898–907. doi: 10.4319/lo.1995.40.5.0898

Ortiz, J., Arístegui, J., Hernández-Hernández, N., Fernández-Méndez, M., and Riebesell, U. (2022a). Oligotrophic phytoplankton community effectively adjusts to artificial upwelling regardless of intensity, but differently among upwelling modes. *Front. Mar. Sci.* 9. doi: 10.3389/fmars.2022.880550

Ortiz, J., Arístegui, J., Taucher, J., and Riebesell, U. (2022b). Artificial upwelling in singular and recurring mode: Consequences for net community production and metabolic balance. *Front. Mar. Sci.* 8. doi: 10.3389/fmars.2021.743105

Pan, Y. W., Fan, W., Zhang, D. H., Chen, J. W., Huang, H. C., Liu, S. X., et al. (2016). Research progress in artificial upwelling and its potential environmental effects. *Sci. China Earth Sci.* 59, 236–248. doi: 10.1007/s11430-015-5195-2

Polovina, J. J., Howell, E. A., and Abecassis, M. (2008). Ocean's least productive waters are expanding. *Geophys. Res. Lett.* 35, L03618. doi: 10.1029/2007GL031745

Pontiller, B., Martínez-García, S., Joglar, V., Amnebrink, D., Pérez-Martínez, C., González, J. M., et al. (2022). Rapid bacterioplankton transcription cascades regulate organic matter utilization during phytoplankton bloom progression in a coastal upwelling system. *ISME J* 16, 2360–2372. doi: 10.1038/s41396-022-01273-0

R Core Team (2021). *R: A language and environment for statistical computing* (Vienna, Austria: R Foundation for Statistical Computing). Available at: https://www.R-project.org/.

Riebesell, U., Czerny, J., Von Bröckel, K., Boxhammer, T., Büdenbender, J., Deckelnick, M., et al. (2013). Technical note: A mobile sea-going mesocosm system

- new opportunities for ocean change research. *Biogeosciences* 10, 1835–1847. doi: 10.5194/bg-10-1835-2013

Romera-Castillo, C., Sarmento, H., Álvarez-Salgado, X. A., Gasol, J. M., and Marraséa, C. (2010). Production of chromophoric dissolved organic matter by marine phytoplankton. *Limnol. Oceanogr.* 55, 446–454. doi: 10.4319/lo.2010.55.1.0446

Sebastián, M., Arístegui, J., Montero, M. F., Escanez, J., and Xavier Niell, F. (2004). Alkaline phosphatase activity and its relationship to inorganic phosphorus in the transition zone of the north-western African upwelling system. *Prog. Oceanogr.* 62, 131–150. doi: 10.1016/j.pocean.2004.07.007

Sebastián, M., Forn, I., Auladell, A., Gómez-Letona, M., Sala, M. M., Gasol, J. M., et al. (2021). Differential recruitment of opportunistic taxa leads to contrasting abilities in carbon processing by bathypelagic and surface microbial communities. *Environ. Microbiol.* 23, 190–206. doi: 10.1111/1462-2920.15292

Severin, T., Kessouri, F., Rembauville, M., Sánchez-Pérez, E. D., Oriol, L., Caparros, J., et al. (2017). Open-ocean convection process: A driver of the winter nutrient supply and the spring phytoplankton distribution in the northwestern Mediterranean Sea. *J. Geophys. Res. Ocean.* 122, 4587–4601. doi: 10.1002/2016JC012664

Sharp, J. H., Peltzer, E. T., Alperin, M. J., Cauwet, G., Farrington, J. W., Fry, B., et al. (1993). Procedures subgroup report. *Mar. Chem.* 41, 37–49. doi: 10.1016/0304-4203(93)90104-V

Shepherd, J., Iglesias-Rodriguez, D., and Yool, A. (2007). Geo-engineering might cause, not cure, problems. *Nature* 449, 781. doi: 10.1038/449781a

Smith, D., and Azam, F. (1992). A simple, economical method for measuring bacterial protein synthesis rates in seawater using. *Mar. Microb. Food webs* 6, 107–114.

Spungin, D., Belkin, N., Foster, R. A., Stenegren, M., Caputo, A., Pujo-Pay, M., et al. (2018). Programmed cell death in diazotrophs and the fate of organic matter in the western tropical south pacific ocean during the OUTPACE cruise. *Biogeosciences* 15, 3893–3908. doi: 10.5194/bg-15-3893-2018

Stedmon, C. A., and Bro, R. (2008). Characterizing dissolved organic matter fluorescence with parallel factor analysis: A tutorial. *Limnol. Oceanogr. Methods* 6, 572–579. doi: 10.4319/lom.2008.6.572

Stedmon, C. A., Markager, S., and Bro, R. (2003). Tracing dissolved organic matter in aquatic environments using a new approach to fluorescence spectroscopy. *Mar. Chem.* 82, 239–254. doi: 10.1016/S0304-4203(03)00072-0

Steinberg, D. K., and Landry, M. R. (2017). Zooplankton and the ocean carbon cycle. *Ann. Rev. Mar. Sci.* 9, 413–444. doi: 10.1146/annurev-marine-010814-015924

Sunagawa, S., Coelho, L. P., Chaffron, S., Kultima, J. R., Labadie, K., Salazar, G., et al. (2015). Structure and function of the global ocean microbiome. *Science* 348, 1261359. doi: 10.1126/science.1261359

Thomas, C., Cauwet, G., and Minster, J.-F. (1995). Dissolved organic carbon in the equatorial Atlantic ocean. *Mar. Chem.* 49, 155–169. doi: 10.1016/0304-4203(94)00061-H

Valiente, S., Fernández-Castro, B., Campanero, R., Marrero-Díaz, A., Rodríguez-Santana, A., Gelado-Cabellero, M. D., et al. (2022). Dissolved and suspended organic matter dynamics in the cape Verde frontal zone (NW Africa). *Prog. Oceanogr.* 201, 102727. doi: 10.1016/j.pocean.2021.102727

Wickham, H. (2016). *ggplot2: Elegant graphics for data analysis* (New York: Springer-Verlag).

Williamson, P., Wallace, D. W. R., Law, C. S., Boyd, P. W., Collos, Y., Croot, P., et al. (2012). Ocean fertilization for geoengineering: A review of effectiveness, environmental impacts and emerging governance. *Process Saf. Environ. Prot.* 90, 475–488. doi: 10.1016/j.psep.2012.10.007

Wünsch, U. J., Murphy, K. R., and Stedmon, C. A. (2015). Fluorescence quantum yields of natural organic matter and organic compounds: Implications for the fluorescence-based interpretation of organic matter composition. *Front. Mar. Sci.* 2. doi: 10.3389/fmars.2015.00098

Yool, A., Shepherd, J. G., Bryden, H. L., and Oschlies, A. (2009). Low efficiency of nutrient translocation for enhancing oceanic uptake of carbon dioxide. *J. Geophys. Res. Ocean.* 114, C08009. doi: 10.1029/2008JC004792

Zark, M., Broda, N. K., Hornick, T., Grossart, H.-P., Riebesell, U., and Dittmar, T. (2017a). Ocean acidification experiments in Large-scale mesocosms reveal similar dynamics of dissolved organic matter production and biotransformation. *Front. Mar. Sci.* 4. doi: 10.3389/fmars.2017.00271

Zark, M., Christoffers, J., and Dittmar, T. (2017b). Molecular properties of deep-sea dissolved organic matter are predictable by the central limit theorem: Evidence from tandem FT-ICR-MS. *Mar. Chem.* 191, 9–15. doi: 10.1016/j.marchem.2017.02.005

Zeileis, A., and Hothorn, T. (2002). Diagnostic checking in regression relationships. *R News* 2, 7–10. Availble at: https://journal.r-project.org/articles/RN-2002-018/.

Zhang, D., Fan, W., Yang, J., Pan, Y., Chen, Y., Huang, H., et al. (2016). Reviews of power supply and environmental energy conversions for artificial upwelling. *Renew. Sustain. Energy Rev.* 56, 659–668. doi: 10.1016/j.rser.2015.11.041

frontiers | Frontiers in Marine Science

TYPE Original Research
PUBLISHED 25 November 2022
DOI 10.3389/fmars.2022.1015188

OPEN ACCESS

EDITED BY
Alessandro Bergamasco,
National Research Council (CNR), Italy

REVIEWED BY
Heather McNair,
University of Rhode Island,
United States
Oscar E. Romero,
University of Bremen, Germany

*CORRESPONDENCE
Silvan Urs Goldenberg
sgoldenberg@geomar.de

SPECIALTY SECTION
This article was submitted to Marine Biogeochemistry, a section of the journal Frontiers in Marine Science

RECEIVED 09 August 2022
ACCEPTED 19 October 2022
PUBLISHED 25 November 2022

CITATION
Goldenberg SU, Taucher J, Fernández-Méndez M, Ludwig A, Arístegui J, Baumann M, Ortiz J, Stuhr A and Riebesell U (2022) Nutrient composition (Si:N) as driver of plankton communities during artificial upwelling.
Front. Mar. Sci. 9:1015188.
doi: 10.3389/fmars.2022.1015188

Nutrient composition (Si:N) as driver of plankton communities during artificial upwelling

Silvan Urs Goldenberg[1]*, Jan Taucher[1], Mar Fernández-Méndez[1,2], Andrea Ludwig[1], Javier Arístegui[3], Moritz Baumann[1], Joaquin Ortiz[1], Annegret Stuhr[1] and Ulf Riebesell[1]

[1]Marine Biogeochemistry, Biological Oceanography, Geomar Helmholtz Centre for Ocean Research Kiel, Kiel, Germany, [2]Polar Biological Oceanography Section, Alfred Wegener Institute Helmholtz Centre for Polar and Marine Research, Bremerhaven, Germany, [3]Instituto de Oceanografía y Cambio Global, IOCAG, Universidad de Las Palmas de Gran Canaria, Las Palmas de Gran Canaria, Spain

Artificial upwelling brings nutrient-rich deep water to the sun-lit surface to boost fisheries or carbon sequestration. Deep water sources under consideration range widely in inorganic silicon (Si) relative to nitrogen (N). Yet, little is known about how such differences in nutrient composition may influence the effectiveness of the fertilization. Si is essential primarily for diatoms that may increase food web and export efficiency *via* their large size and ballasting mineral shells, respectively. With a month-long mesocosm study in the subtropical North Atlantic, we tested the biological response to artificial upwelling with varying Si:N ratios (0.07-1.33). Community biomass increased 10-fold across all mesocosms, indicating that basic bloom dynamics were upheld despite the wide range in nutrient composition. Key properties of these blooms, however, were influenced by Si. Photosynthetic capacity and nutrient-use efficiency doubled from Si-poor to Si-rich upwelling, leading to C:N ratios as high as 17, well beyond Redfield. Si-rich upwelling also resulted in 6-fold higher diatom abundance and mineralized Si and a corresponding shift from smaller towards larger phytoplankton. The pronounced change in both plankton quantity (biomass) and quality (C:N ratio, size and mineral ballast) for trophic transfer and export underlines the pivotal role of Si in shaping the response of oligotrophic regions to upwelled nutrients. Our findings indicate a benefit of active Si management during artificial upwelling with the potential to optimize fisheries production and CO_2 removal.

KEYWORDS

ocean fertilization, diatoms, stoichiometry, silicic acid, ecosystem-based aquaculture, negative emission technology, carbon dioxide removal

Introduction

Food security and climate change are recognized as two great challenges of the 21st century and beyond (Godfray et al., 2010; IPCC 2014). But how do we best develop food production and the capacity to neutralize green-house gas emissions to meet the global growth in human prosperity and population? Terrestrial and coastal resources are already utilized intensively by competing societal sectors, limiting the expansion of farmland and negative emission technologies (Minx et al., 2018; Fuhrman et al., 2020; Macreadie et al., 2021). Open-ocean ecosystems, in contrast, which cover over half of our planet, still hold vast amounts of untapped resources (Moore et al., 2013; Gattuso et al., 2021). They cannot be sourced, however, by the traditional 'hunter-gatherer' approach to ocean management. Here, seafood yield is limited by the existing productivity (Pauly and Christensen, 1995; Costello et al., 2020), while the ocean's natural ability to take up CO_2 is allowed to degrade unchecked (Matear and Hirst, 1999; Steinacher et al., 2010). Ground-breaking innovations in ocean food production and CO_2 removal are thus needed to achieve global environmental and social sustainability.

Ocean artificial upwelling is a nature-based solution with the potential to boost ecosystem services in regions of low biological activity. The warm, nutrient-poor surface waters in tropical and subtropical seas are characterized by low productivity (Steinacher et al., 2010; Armengol et al., 2019). Here, the nutrients are locked away in cold (i.e. heavier) deep water below the surface mixed layer (Moore et al., 2013; Dulaquais et al., 2014). Artificial upwelling, however, could break the density gradient and force nutrient-rich deep water to the sun-lit surface stimulating primary productivity (Pan et al., 2016). As in natural upwelling systems, the enhanced biomass production may be transfered to exploitable fish (Chavez and Messie, 2009; Messie et al., 2009) or exported to the ocean's interior where it may be stored longer-term (Boyd et al., 2019). The vertical mixing, in turn, could counter enhanced stratification under climate change and the expansion of 'ocean deserts' (Polovina et al., 2008; Boyce et al., 2010; Steinacher et al., 2010; Fu et al., 2016). Artificial upwelling may thus be evaluated as (1) ecosystem-based aquaculture that is, contrary to conventional fish farming, not limited by animal feed (Tacon and Metian, 2015), (2) a biological CO_2 sink more scalable than blue carbon in coastal areas (Macreadie et al., 2021), and (3) a nature conservation tool to restore pelagic habitats degraded by human-induced warming and stratification.

The 'classical' view of pelagic ecosystems identifies two food web models of contrasting potential for fisheries and carbon export (Ryther, 1969; Eppley and Peterson, 1979; Cushing, 1989). In oligotrophic, low productivity systems, small phytoplankton dominate and organic matter is recycled rather than exported. Here, multiple trophic steps, each entailing a loss of energy, are required to reach larger crustacean grazers. Eutrophic, high productivity systems are instead based on upwelled nutrients that favour large phytoplankton. These allow direct grazing by crustaceans that in-turn support small pelagic fish (Cury et al., 2000; Espinoza and Bertrand, 2008). Such short food webs are considerably more efficient in transferring energy (Eddy et al., 2020) leading to exceptional fisheries yields (Chavez and Messie, 2009). The biological pump is also highly active here. It removes CO_2 from the atmosphere where the exported organic carbon exceeds the upwelled inorganic carbon (Eppley and Peterson, 1979; Karl and Letelier, 2008); a balance that partly hinges on the carbon to nutrient ratio of biological processes (Hessen et al., 2004). Diatoms are given a key role in driving these ecosystem services. They dominate new production in natural upwelling systems and spring blooms in coastal seas and their large size makes them ideal food for crustacean plankton (Sommer et al., 2002).

Diatoms build silica (SiO_2) cell walls that characterize their role in elemental cycles and their nutrient requirements. To the organisms, the shells may serve multiple functions including grazer protection and nutrient and light harvesting (Mitchell et al., 2013; Romann et al., 2015; Pancic et al., 2019). Following cell growth, the mineral shells provide ballast to aggregates and fecal pellets, accelerating the sequestration of carbon through increased sinking velocities (Ragueneau et al., 2000; Armstrong et al., 2001; Jin et al., 2006). For the biomineralization of their shells, however, diatoms require dissolved silicate ($Si(OH)_4$), whilst other primary producers are often limited only by nitrate (NO_3) and phosphate (PO_4) (Moore et al., 2013). The relative availibility of silicate over other macro-nutrients therefore shapes the environmental and ecological niche of diatoms (Dugdale and Wilkerson, 1998; Sommer et al., 2002; Allen et al., 2005; Bibby and Moore, 2011). A nutrient ratio of silicate to nitrate of 1:1 has been considered optimal, yet with considerable variability between and within diatom species (Sarthou et al., 2005). In principle, lower silicate limits diatom growth and shifts the competitive balance towards other primary producers, while higher silicate reduces the energetic cost for biomineralization favouring diatom dominance.

Silicate shows a distinct distribution pattern across the world's oceans. At the sun-lit surface, silicate is often limiting (Griffiths et al., 2013; Dulaquais et al., 2014) and any newly introduced silicate is thus quickly depleted by diatoms (Dugdale and Wilkerson, 1998; Sarmiento et al., 2004; Allen et al., 2005). The vertical profile of silicate differs from that of the other macro-nutrients due to the slower remineralization of silica shells compared to organic nitrogen or phosphorus during the downward flux of particles (Ragueneau et al., 2000). Whilst silicate increases slower with depth than nitrate and phosphate at first ($Si:N < 1$), it catches up on the other macro-nutrients at greater depth and finally exceeds them ($Si:N > 1$) (Griffiths et al., 2013; Dulaquais et al., 2014). The latitudinal and longitudinal distribution of silicate is, instead, determined by the longer-term

biogeochemical history of the water bodies that are moved globally *via* ocean currents (Sarmiento et al., 2004; Bibby and Moore, 2011).

By sourcing deep water with specific Si concentrations during artificial upwelling, would it be possible to boost beneficial primary producers (i.e. diatoms) and thereby maximize the effectiveness of the fertilization? Natural systems often deviate from biogeochemical paradigms at smaller spatiotemporal scales. The grazing of diatoms by crustaceans for trophic transfer (Ban et al., 1997; Decima and Landry, 2020) and the carbon to nutrient ratio of organic matter for export (Geider and La Roche, 2002; Martiny et al., 2013) are particularly variable. Generalization of such central processes and properties severely limits our predictive understanding of how nature-based solutions may enhance fisheries production and carbon sequestration (Dutreuil et al., 2009; Yool et al., 2009; Chassot et al., 2010; Baumann et al., 2021). Artificial upwelling would force sudden eutrophication onto a plankton community which is adapted, in its species composition and physiology, to an oligotrophic environment. Such an artificial system may produce extremes, including harmful side-effects but also unexpected benefits, and thus requires a rigorous testing and re-evaluation of established principles.

Here, we investigate the effect of nutrient composition (Si relative to N) on oligotrophic plankton communities during artificial upwelling. In the subtropical North Atlantic (Canary Islands), we simulated recurring fertilization with nutrient-rich deep water of constant nitrate but varying silicate levels. Over the course of 33 days, we employed a pelagic mesocosm system that captures much of the natural biogeochemical and ecological complexity (Figure 1B). The developing plankton blooms were closely monitored for organic matter assimilation (quantity) and composition (quality), with a special focus on diatoms. Shifts in fundamental community properties indicated a benefit of active Si management during artificial upwelling with the potential to optimize trophic transfer to fisheries and export for CO_2 removal.

Methods

Study system

The experiment took place on the island of Gran Canaria located at the eastern side of the North Atlantic gyre, where it is continuously swept with oceanic water by the Canary Current (Barton et al., 1998) (Figure 1A). Phytoplankton biomass and fisheries production is low and stratification prominent in these warm, subtropical waters (Aristegui et al., 2001; Neuer et al., 2007; Popescu and Ortega Gras, 2015). Vertical profiles indicate only a slow increase of inorganic nutrients with depth, which would translate into higher costs for artificial upwelling compared to other regions (Llinás et al., 1999; Neuer et al., 2007). Our aim, however, is not to evaluate the feasibility of

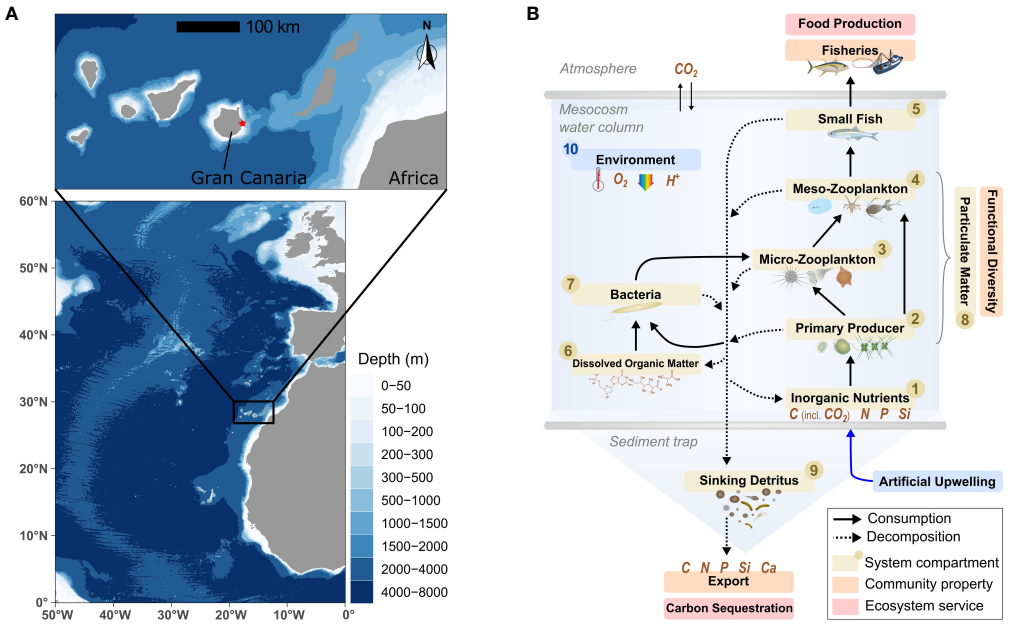

FIGURE 1
(A) Study site in the subtropical North Atlantic (red dot) (created with ggOceanMaps, Vihtakari, 2021). **(B)** Conceptualization of our pelagic mesocosms system. An overview of the parameters assessed for compartments #1-10 is provided by Table S1. Symbols from the Integration and Application Network (ian.umces.edu/media-library).

artificial upwelling locally but to conduct a general test of how an oligotrophic surface community responds to upwelling of nutrient-rich deep water.

Mesocosm facility

Eight floating mesocosms were installed in October 2019 inside Taliarte harbour (27°59'24" N, 15°22'8" W; Figures S1A, B), ~250 m from the laboratory facilities of the Plataforma Oceánica de Canarias (PLOCAN, https://www.plocan.eu) and the University of Las Palmas de Gran Canaria (ULPGC). Each mesocosm consisted of a transparent 1 mm polyurethane bag with cylindrical trunk and conical sediment trap, holding on average (± SD) 8292 ± 70 L of seawater. The bags were cleaned regularly to minimize growth of fouling organisms (Figure 2B). A large ring with rubber lips was scrubbed tightly along the inside walls (Riebesell et al., 2013) and the sediment traps and outside walls were brushed. This mesocosm system was previously deployed (Bach et al., 2019) and is the "in-shore" equivalent of the "Kiel Off-Shore Mesocosms for Oceanographic Studies" (KOSMOS) (Riebesell et al., 2013; Boxhammer et al., 2016; Taucher et al., 2017).

All mesocosm bags were filled in parallel with water from outside the harbour at 2-8 m depth (10-15 m bottom depth), using hoses (Ø 37 mm), a peristaltic pump (14 m^3 h^{-1}, KUNZ SPF60, Flexodamp FD-50) and mechanical flow meters. The natural plankton community was included, while larger organisms such as fish were excluded *via* a 3 mm mesh. The well-filled and firmly shaped mesocosm bags were measured by divers for a geometrical volume determination. Mesocosm volumes were then aligned by adjusting water removal during the first deep water addition on day 6.

Upwelling simulation

Small amounts of deep water were added to all mesocosms in short, regular intervals according to a continuous upwelling regime. Every second day, 320 L of mesocosm water was replaced by deep water, corresponding to a mixing ratio of deep water to mesocosm of 4%. Starting on day 6, this scheme totalled in 14 additions and a 56% replacement (Figure 2B). To assure a representative removal of mesocosm water and an even injection of the deep water, a special distribution device was moved up and down in the water column during pumping (Figure S1C).

To test the effect of nutrient composition, a gradient in silicon relative to nitrogen (Si:N) was established during the upwelling based on the eight mesocosms (Figure 2A). This Si:N treatment was achieved by adjusting the silicate ($Si(OH)_4$) concentration in the deep water specifically for each mesocosm while nitrate (NO_3), as well as phosphate (PO_4) and dissolved inorganic carbon (DIC), were kept constant.

Our Si:N range encompasses relevant natural and artificial upwelling scenarios (Sarmiento et al., 2004; Griffiths et al., 2013; Dulaquais et al., 2014). The lower boundary of 0.07 represented

A

Si:N treatment	0.07	0.33	0.50	0.67	0.83	1.00	1.17	1.33			
Nutrient	$Si(OH)_4$								NO_3	PO_4	DIC_{excess}
Deep water [µmol L^{-1}]	2	10	15	20	25	30	35	40	30	1.9	199
Mesocosm after addition [µmol L^{-1}]	0.08	0.38	0.58	0.77	0.96	1.15	1.35	1.54	1.15	0.07	7.65
Mesocosm accumulative [µmol L^{-1}]	1.1	5.4	8.1	10.8	13.5	16.2	18.8	21.5	16.2	1.01	91.8*
Si* = [Si] - [N] [µmol L^{-1}]	-28	-20	-15	-10	-5	0	5	10			
Mesocosm #	3	5	7	1	6	2	8	4			
Symbol											

DIC_{excess} ≙ dissolved inorganic carbon in excess of the hypothetical deep water baseline; *no extra DIC added in first two additions

B

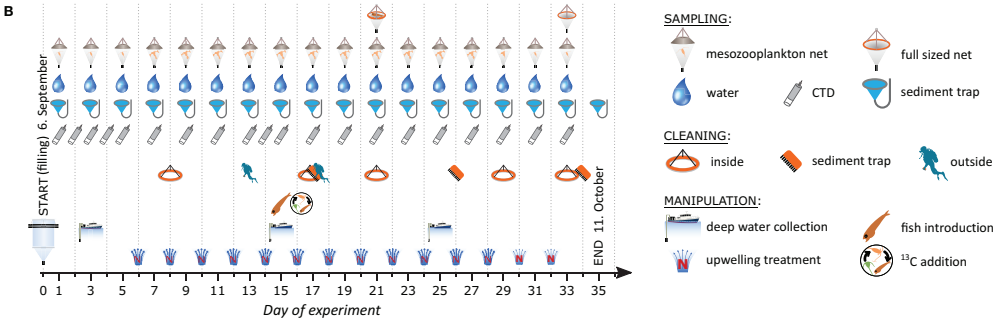

FIGURE 2
Experimental design to simulate artificial upwelling. **(A)** Nutrient regime with a gradient in silicate and constant levels of the other macro-nutrients (at Redfield). Each of the 14 additions exchanged 4% of the mesocosm (320 L). **(B)** Experimental schedule.

the lowest achievable Si:N given the silicate already present in the collected deep water. Increasing silicate is then hypothesized to benefit diatoms until a Si:N of 1 from which point onwards silicate may be less limiting (Sarthou et al., 2005). Specifically in the oligotrophic study system, Si:N in potential source water for artificial upwelling ranges from around 0.5 at 500 m depth to above 1.2 at depth greater than 2000 m (Llinás et al., 1999). Our upper Si:N boundary of 1.33 assures the inclusion of extreme scenarios.

Deviations from the planned addition scheme occurred. Due to initial uncertainty over the mesocosm volume, mesocosm 7 experienced a minimally higher mixing ratio of 4.2% during the 1st and 2nd addition. Further exceptions were the 10th addition, where 100 L less water was removed from each mesocosm to compensate for evaporation, and the 12th addition, where no water was removed before addition due to technical issues. Lastly, the 5th addition was based on surface water that had been treated with UV light and filtered at 5 µm, as the prior deep water collection failed. Despite these irregularities, the nutrient manipulation was overall fairly consistent, with standard deviations for mixing ratios between additions (n = 112) and mesocosms (n = 8) of 0.026% and of 0.010%, respectively.

Deep water

Deep water was collected on three occasions east of Gran Canaria at a minimum bottom-depth of 170 m (27°52'16" N, 15° 18'48" W or 28°00'01"N, 15°20'11"W). During each collection, a hose (Ø 37 mm) with a submersible pump (Grundfos SP-17-5R, flow rate 20 m^3 h^{-1}) was lowered to a depth of ~120-160 m and water was pumped into 12 opaque 1-m^3 food grade plastic containers. These were stored at 7°C degrees for use in the following days.

Our deep water source needed to meet the specific requirements of the study. On the one hand, a sufficient depth below the photic zone (~100 m) assured low chlorophyll *a* and low abundance of surface organisms (Neuer et al., 2007). On the other hand, we could not go too deep to keep nitrate levels well below our treatment target levels. The latter was necessary, given the silicate present besides nitrate in the collected water, to establish the wide Si:N treatment gradient *via* artificial supplementation of nutrients. The collected water contained (mean ± SD, n = 14 additions) 5.8 ± 1.6 µmol L^{-1} nitrate (NO_2 and NH_4 negligibly low concentrations), 0.38 ± 0.07 µmol L^{-1} phosphate, 2.12 ± 0.44 µmol L^{-1} silicate and 2358 ± 20 µmol L^{-1} DIC. Particulate organic nitrogen and carbon were at 0.24 ± 0.02 and 1.09 ± 0.12 µmol L^{-1} (mean ± SD, n = 3 collection containers), respectively, which is <1% of the final inorganic nutrient levels (Figure 2A) and ~10% of the particulate matter of the oligotrophic surface water in the mesocosms before the first upwelling treatment.

The collected deep water was amended to the desired nutrient levels immediately before each deep water addition (Figure 2A). Nitrate is the limiting nutrient in the study region (Figures 3F, G; Moore et al., 2013) and is also considered key in driving primary production in natural (Chavez and Messie, 2009) and artificial upwelling systems (Ortiz et al., 2022). Nitrate thus served as reference nutrient for our manipulation, representative of upwelling intensity. Deep water nitrate levels were topped up to 30 µmol L^{-1}, and phosphate and DIC were provided in Redfield ratio (C:N:P = 106:16:1) (Redfield, 1958). This nitrate concentration lies in the upper range of water supplied during natural upwelling (Messie et al., 2009) and could readily be sourced during artificial upwelling below a depth of a few hundred meters in some oligotrophic regions (Griffiths et al., 2013; Dulaquais et al., 2014). Nutrient salts were used to obtain the target nitrate ($NaNO_3$), phosphate (Na_2HPO_4) and DIC ($NaHCO_3$) concentrations. All salts were first dissolved in MilliQ water and equilibrated with HCl for proton-balance. Lastly, the Si:N treatment gradient was established by adding specific amounts of silicate salt (Na_2SiO_3) to the deep water designated for the respective mesocosms.

Trophic structure

A coastal pelagic zooplanktivore, the silverside *Atherina presbyter*, was caught locally and introduced to each mesocosm as early juvenile (n = 45, length = 17 mm) and young larva (n = 36, length = 9 mm) on day 15 after the sampling. Six days later, they were removed using a large net (1 mm mesh size) to assess growth and survival. Meso-zooplankton populations could not recover from the strong top-down control that had been exerted by the fish and remained at very low levels for the remainder of the experiment (day 21-33). Whilst the exact consequences for the smaller plankton, the focus of the current article, are unknown, we are certain about two aspects of this trophic restructuring. Firstly, it was identical for all mesocosms and thus not biasing the Si:N treatment. Secondly, it did not trigger the prominent temporal shift in the Si:N effect from the 'initial' to the 'longer-term' phase (Figures 4C–E). This effect originated from the carbon overconsumption during primary production that only afterwards accumulated in the particulate organic matter. As evident from chlorophyll *a* (Figure 4E) and O_2 production (Ortiz, unpublished data), the Si:N effect on carbon overconsumption peaks already on day 11 and has entirely vanished by the time the fish were introduced on day 15.

Sample collection

Sampling took place in the morning in two-day intervals (Figure 2B), always with the same order of parameters. Sampling

devices were gently lowered through the centre of the mesocosm to target depth using a smooth, abrasion resistant plastic line guided over an overhanging pulley (Figure S1B). Samples were transported to the nearby laboratory facilities in cooling boxes at ambient seawater temperature and immediately processed or preserved.

At dawn (~7-8:30 am), the sedimented material that had been collected over the past 48 h was transferred into 5 L glass bottles by means of a vacuum pump (Figure S1A, Boxhammer et al., 2016). Depth-integrated water samples were taken with a 2.5-m plastic tube (Ø 53 mm, 5.13 L) submersed vertically into the mesocosm (~8-10:30 am). Then, set-valves at both ends of the tube were shut – the lower valve *via* a string-system – and the extracted water column transferred to various parameter-specific storage containers. An average (± SD) of 8.7 ± 0.2 tubes corresponding to 44.4 ± 0.9 L were sampled per day and mesocosm. Meso-zooplankton was sampled *via* tubes and nets (Apstein Ø 17 cm, 56.7 L, 55 µm mesh size). To conclude the sampling day (~10-10:30 am), environmental conditions were recorded with three replicate CTD casts (CTD167M, Sea and Sun Technologies) to 3.5 m depth. The probe included sensors for depth, temperature, salinity, oxygen, pH, density, photosynthetically active radiation and chlorophyll *a* (see Schulz and Riebesell, 2013 for details).

Parameters

The major compartments of the pelagic system were assessed including mass and fluxes of both organic and inorganic matter (Figure 1B). This article focuses on suspended particulate matter and the community of larger phytoplankton. All other parameters measured in the context of this experiment are listed in Table S1.

To measure inorganic water chemistry, the water was directly subsampled into small bottles without air headspace. Particulate matter was removed *via* filtration (before day 17: 0.2 µm; on and after day 17: 0.45 µm, Sarstedt) and samples were stored at 4 °C until analysis on the same or the following day. The inorganic nutrients NO_3, NO_2, PO_4 and $Si(OH)_4$ were measured photometrically following Hansen and Koroleff (1999) and NH_4 fluorometrically following Holmes et al. (1999), each in triplicates. Total alkalinity (TA) was measured in duplicates *via* open cell titration (Metrohm 862 Compact Titrosampler with 907 Titrando unit) (Dickson et al., 2003). Dissolved inorganic carbon (DIC) was measured in triplicates *via* an Autonomous Infra-Red Inorganic Carbon Analyser (AIRICA; Marianda). TA and DIC measures were accurate within 1% of certified reference material (A. Dickson, Scripps Institution of Oceanography) (Dickson et al., 2007).

For the analysis of suspended particulate matter, the water was transferred into 10 L polyethylene containers and stored in a climate chamber at 15°C. Over the course of the day, these containers were subsampled for the different parameters. Sample volumes were continuously adjusted according to the development of the plankton bloom to avoid clogging, from 1 L at the start of the experiment to 0.2 L at the end. Samples were filtered with a negative pressure of 200 mbar onto glass fibre filters (>0.7 µm, GF/F Whatman, pre-combusted except for pigments) for total particulate carbon (TPC), particulate organic carbon and nitrogen (POC/N), particulate organic phosphorus (POP), and photosynthetically active pigments. Biogenic silica (BSi) was filtered in the same manner using cellulose acetate filters (>0.65 µm, Whatman). To remove particulate inorganic carbon (PIC), POC/N filters were acidified with 1 ml of 1 M HCl. Subsequently, POC/N and TPC filters were dried in an oven at 60 °C for 24 h. They were then packed in tin capsules and stored in desiccators until elemental analysis (Euro EA-CN HEKAtech) following Sharp (1974). Filters for POP and BSi were stored at -20 °C and analysed in the following days according to Hansen and Koroleff (1999). Filters for photosynthetic pigment analysis were stored at -80 °C until extraction and reverse-phase high-performance liquid chromatography (HPLC) (Ultimate 3000, Thermo Scientific) (Barlow et al., 1997). More details on the analytical procedures for these parameters are provided in Paul et al. (2015).

We found no consistent evidence for the presence of PIC. The difference between TPC and POC varied randomly around 0 and was unrelated to the Si:N treatment (Figure S2). We therefore considered PIC to be negligible and treated the TPC as second POC dataset. The precision of our POC (and also PON) estimate benefited considerably from the averaging across two separate filters and elemental analyses.

Larger phytoplankton was visually assessed using Utermöhl microscopy (Edler and Elbrächter, 2010; Bach et al., 2019). Water samples were filled in 250 ml brown glass bottles and fixed with acidic Lugol's iodine. A subsample of 20-50 ml was settled in a settling chamber for 24 h. Phytoplankton cells larger than ~5 µm were counted and identified to the lowest taxonomic level possible. The taxonomic composition of diatoms, the dominant group, was investigated, including indexes for species richness, evenness and diversity (Pielou, 1966). The dimensions of abundant taxa were measured regularly and those of rare taxa extracted from the literature for a geometrical estimation of cell biovolume following Olenina (2006). Finally, total biovolume of the diatom assemblage was calculated to serve as a proxy for biomass.

A potential shift in phytoplankton size distribution was assessed *via* flow cytometry. For this, 0.5-2 ml were analysed within 3 h of sampling using a Cytosense imaging flow cytometer (CytoBuoy, Woerden, Netherlands), with instrument settings optimal for the nano and micro scale. This technique structures natural plankton communities into clusters of similar cells based on fluorescence and light scatter properties (Dubelaar and Jonker, 2000; Veldhuis and Kraay, 2000). The three clusters representing the largest phytoplankton increased

most strongly following the nutrient addition and may thus be considered as the eutrophic specialists: 10-40 µm with high fluorescence, 10-40 µm with low fluorescence, and >40 µm chain-forming. For our analysis, the two 10-40 µm clusters were pooled to obtain two distinct groups of larger autotrophs, one ranging from large nano- to small microphytoplankton (10-40 µm) and one comprising larger microphytoplankton (>40 µm). These clusters represented the natural size structure in our system, which is not congruent with the commonly applied plankton size structure. Finally, cell abundances were standardized against the chlorophyll *a* of the entire autotroph community as measured by HPLC. These variables hence express the relative contribution of larger phytoplankton to the overall photosynthetic capacity.

Data analysis

All parameters followed the same basic data structure: a gradient of Si:N with 8 independent mesocosms that was repeatedly sampled over the course of the experiment. We used linear mixed models with random intercept to establish the general effect of Si:N and its change over time (restricted maximum likelihood fit, type III test, Kenward-Roger approximation, Bates et al., 2015; Kuznetsova et al., 2017; Singmann and Kellen, 2019). Si:N was employed as continuous explanatory variable, Mesocosm as random effect, and experimental Day and its interaction with Si:N as factors of the repeated design (Quinn and Keough, 2002). Potential deviations from normality of residuals and random effects were checked with normal Q-Q plots and homogeneity of variance with residual versus fitted plots. Data was transformed if necessary. Finally, we investigated the day-to-day development of the Si:N effect size. For this, individual linear regressions were conducted for each sampling day and their slopes plotted with 95% confidence intervals. All data analyses were performed at a significance level of $\alpha = 0.05$ with R version 4.0.5 (R Core Team, 2021; RStudio Team, 2021).

Results

A pronounced plankton bloom developed in all mesocosms following the addition of nutrient-rich deep water. The universally essential nutrients N and P dominated the overall build-up of biomass (particulate organic N, P and C) and the potential for primary production (chlorophyll *a*). In contrast, Si that is required specifically by diatoms determined the composition of the plankton community (C:N ratio, biogenic silica, diatoms, size). Consequently, Si in deep water may be seen as primary driver of plankton bloom quality that acts on top

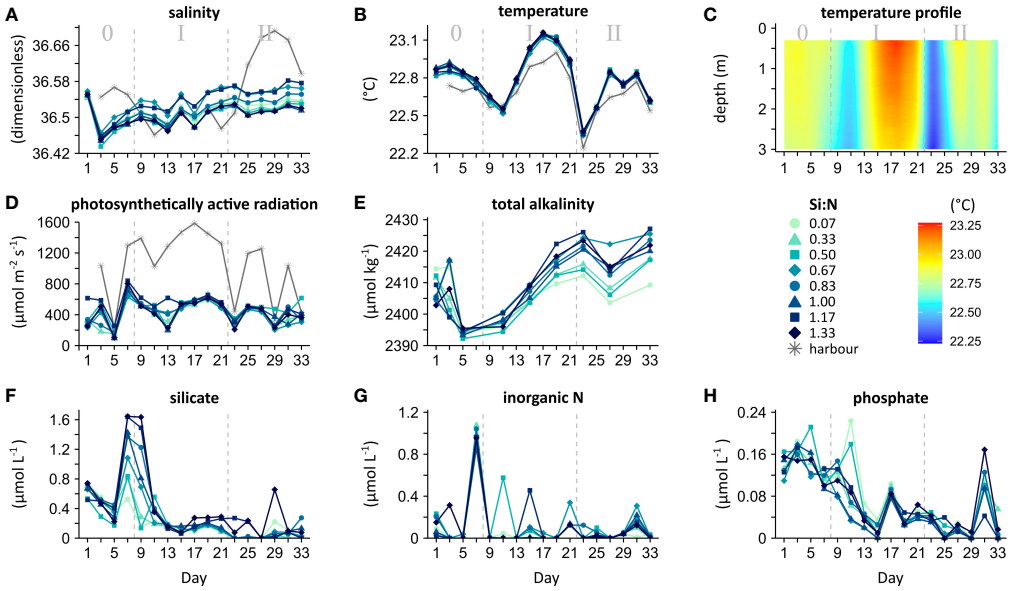

FIGURE 3
Environmental conditions and nutrient concentrations in the mesocosms. *In situ* measurements with averages from 0.3 to 2.5 m depth for each mesocosm **(A, B, D)** and a vertical profile averaged across all mesocosms **(C)**. Laboratory measurements of integrated water samples from 0 to 2.3 m depth **(E-H)**. Experimental phases: 0 = oligotrophic baseline, I = initial response, II = longer-term response.

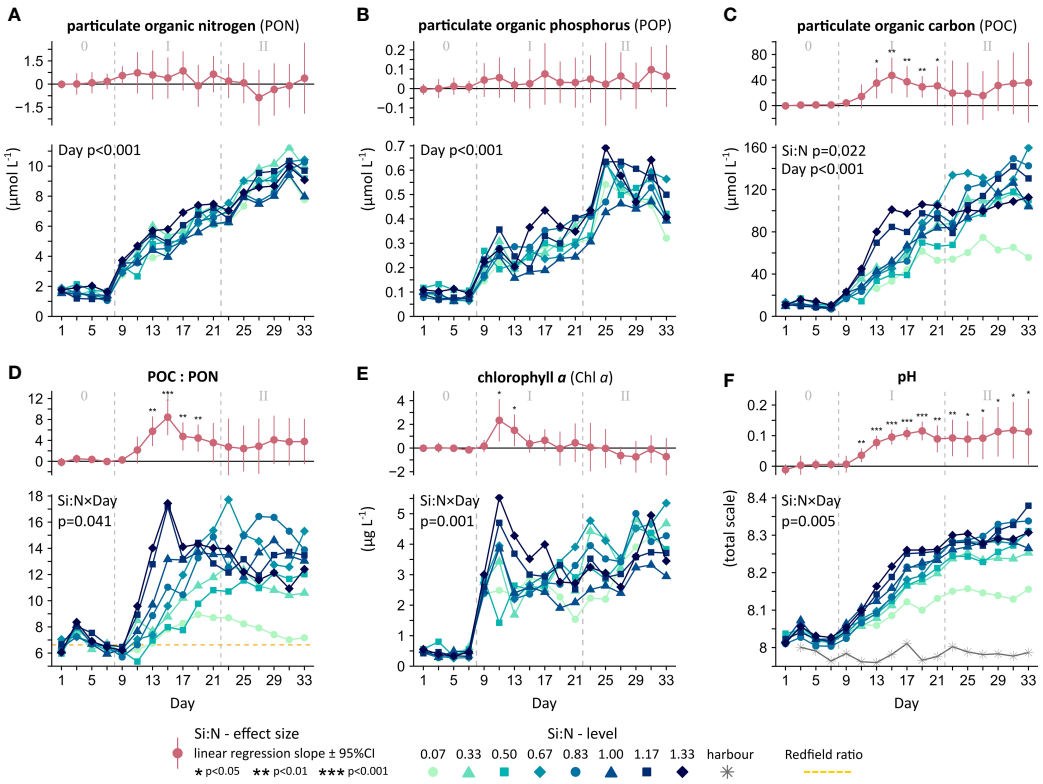

FIGURE 4
Biomass development under upwelling with varying deep water Si:N, including **(A-D)** particulate organic matter, **(E)** photosynthetic capacity, and **(F)** metabolic balance. Provided are the overall significances across time (Si:N, Day or Si:N×Day) and the daily Si:N effect (in red). Experimental phases: 0 = oligotrophic baseline, I = initial response, II = longer-term response.

of N and P upwelling determining quantity. To facilitate interpretation of the Si:N-effect, we distinguish between the three phases 'oligotrophic baseline' (0), 'initial response' (I) and 'longer-term response' (II), based on the distinct temporal pattern.

Environmental conditions

Environmental conditions were similar for all mesocosms and stayed relatively constant over the entire experimental period (Figures 3A–E and Tables S2A-D). Yet, there were slight variations from day to day, as characteristic of mesocosm systems. Salinity increased slowly over time due to evaporation (Figure 3A). Fluctuations in temperature closely followed the surrounding harbour water (Figure 3B). The absence of thermal stratification was indicative of a homogenous water column (Figure 3C). Photosynthetically active radiation varied with cloud cover as suggested by the matching harbour light pattern (Figure 3D). The phytoplankton bloom, in contrast, did not markedly reduce light availability. Whilst total alkalinity diverged following the Si:N gradient (Table S2D), absolute differences were small and likely biologically insignificant (Figure 3E).

Inorganic nutrients

The macro-nutrients added through the upwelling simulation were fully consumed by the plankton community (Figures 3F–H). Upon the first deep water addition (day 6), N (nitrate, nitrite and ammonia) and Si (silicate) peaked steeply. Whilst this increase was equal across mesocosms for N, Si varied matching the Si:N gradient (Figure 2A), which confirms a correct treatment application. During the following upwelling events every other day, the added nutrients were taken up quickly. In this eutrophic state (phase I and II), Si and P (phosphate) dropped to well below their oligotrophic levels (phase 0). It appears that our communities became first N, then N-Si and finally N-P-Si limited. We found no evidence for an effect of deep water Si:N on the consumption of N and P (Tables S2F, G). Si depletion was slightly slower in the high Si:N mesocosms (Table S2E), which however did not lead to Si accumulation (Figure 3F). Overall, our results suggest that,

after a brief period of adjustment, nutrient provisioning through recurring upwelling and primary productivity were in-phase, with efficient uptake of all macro-nutrients independent of their stoichiometry.

Biomass

Particulate organic matter – that is, the bulk measure across all suspended organisms and their remains including bacteria, phytoplankton, micro-zooplankton and smaller meso-zooplankton – grew steadily over the 27-days of upwelling (Figures 4A–C). Particulate organic nitrogen (PON) and phosphorus (POP) concluded with a ~5-fold higher mass compared to the oligotrophic baseline (Figures 4A, B - bottom). This accumulation of PON and POP was driven by the upwelling of N and P that was applied uniformly to all mesocosms and is incorporated in the factor 'Day' (Tables S3A, B). The Si:N treatment instead had no influence on PON and POP, neither overall (Table S3A, B) nor on a day by day basis as demonstrated by the insignificant daily regression slopes (Figures 4A, B - top). Consequently, their elemental ratio (PON : POP) also remained unchanged (Figure S3 and Table S3C). In agreement with the inorganic nutrients, these clear-cut results suggest that N and P cycling occurred independently of the Si levels in the deep water.

The production of carbon biomass, in contrast, was considerably accelerated under Si-rich upwelling. Over the first 2 weeks, the community with the largest excess in Si (Si:N = 1.33) grew 3-fold more particulate organic carbon (POC) than the one with the most severe Si deficiency (Si:N = 0.07) (Figure 4C - phase I, Table S3D). In parallel, carbon to nitrogen ratios of communities under high Si upwelling rose to more than twice that of the ocean-wide average Redfield stoichiometry (C:N ratio from ~6.6 to 17) (Figure 4D - phase I). This exceptionally rapid growth in POC has thus been achieved through a more efficient use of the upwelled N and P. The clear linear effect of Si:N on POC and organic matter stoichiometry was lost, however, over the longer term (Figures 4C, D - phase II). Instead, a curvilinear relationship characterized the second phase of our simulation with highest C:N ratios at intermediate levels of Si:N (Figure S4). Communities across the Si:N gradient finalised with about 10-fold higher POC and a doubling in C:N ratios compared to the oligotrophic baseline. Only the extreme low Si:N community followed an altogether different path in agreement with Redfield, possibly indicating a lower threshold in Si availability below which community functioning shifts drastically.

The development of chlorophyll *a*, as proxy for phytoplankton biomass and potential of photosynthesis, was influenced by the Si:N treatment in a pattern similar to POC (Figure 4E and Table S3F). We observed a sharp rise in chlorophyll *a* over the first 4 days of upwelling, peaking at double the concentration under excess Si compared to extreme Si deficiency (phase I). While there was still ample Si remaining from the oligotrophic state (day 7-9) (Figure 3F), the rate of chlorophyll *a* build-up was equally rapid in all mesocosms. Si only became truly limiting for a further rapid growth of chlorophyll *a* once this left-over had been depleted in the low Si:N mesocosms (day 9-11). This strong positive effect of Si:N on chlorophyll *a* was only characteristic of the immediate response to the regime shift. In the longer term (phase II), mesocosms evened out at around 4 μg L^{-1} chlorophyll *a* irrespective of the Si:N treatment.

Throughout the month-long upwelling simulation, communities across the wide range of Si:N maintained net-autotrophy. This positive metabolic balance, where primary production exceeds respiration, is indicated by the steady increase in pH (Figure 4F). Silicate-rich upwelling further accelerated the rise in pH over the first two weeks (phase I), indicating particularly high photosynthetic activity and associated consumption of CO_2 (Table S3G). Net-autotrophy and the accumulation of PON, POP and POC indicate a surplus in energy and organic matter that could be transferred from the plankton to fish (trophic transfer) and the deep ocean (carbon sequestration).

Larger phytoplankton

Diatoms responded strongly to the added nutrients. Throughout the entire manipulation, the biomineralization of dissolved Si (silicate) into particulate Si (biogenic silica) increased linearly with the Si:N treatment (Figure 5A and Table S4A). Being the major producers of biogenic silica, the microscopically assessed diatoms matched this pattern. Whilst diatoms were practically absent in the oligotrophic state, they quickly grew large populations in the mesocosms under high but not low Si-upwelling (Figure 5B and S3B; Table S4 B, C). Here, effect sizes were particularly large with a 6- and 7-fold increase in biogenic silica and diatoms, respectively, along our Si:N gradient. Other larger autotrophic taxa, in contrast, showed no consistent response to Si:N and were generally outnumbered by diatoms, even under Si-deficiency (Figure S3C and Table S4D).

Diatom composition was also shaped by the upwelling simulation. Assemblages under high Si upwelling were slightly richer in species (Figure S3D and Table S4E, 38 diatom taxa recorded) and more evenly composed (Figure S3E and Table S4F), resulting in higher diatom diversity (Figure S3F and Table S4G). However, only two genera dominated the upwelling-induced blooms across Si:N (Figure 5C). *Pseudo-nitzschia* was most prominent initially and *Leptocylindrus* over the longer-

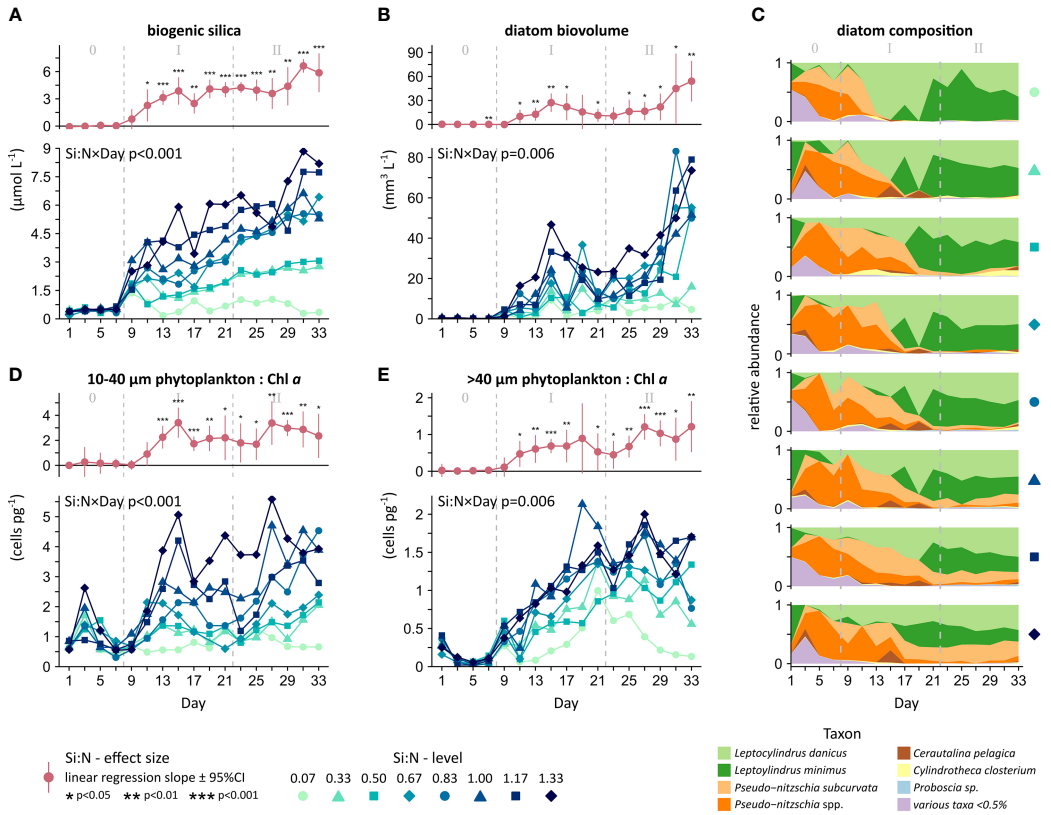

FIGURE 5
Larger phytoplankton under upwelling with varying deep water Si:N, including **(A)** biomineralized Si, **(B, C)** diatoms only (via microscopy), and **(D, E)** the abundance of all larger phytoplankton (via flow cytometry) relative to the chlorophyll *a* of the entire autotrophic community. Provided are the overall significances across time (Si:N, Day or Si:N×Day) and the daily Si:N effect (in red). Experimental phases: 0 = oligotrophic baseline, I = initial response, II = longer-term response.

term. Still, *Pseudo-nitzschia* was able to maintain significant populations under Si:N ratios of ≥1. Concluding, the observed increase in diatoms due to Si was primarily driven by an increase in the same species.

Phytoplankton size was strongly and positively affected by the Si in the deep water. As expected, phytoplankton at the nano and micro scale were only a minor component of the phytoplankton community during the oligotrophic state (Figures 5D, E). Upon the start of upwelling, populations of these larger phytoplankton grew most rapidly when provided with an excess of Si. Their contribution to overall photosynthetic capacity increased on average 6-fold (cluster 10-40 µm) and 3-fold (cluster >40 µm) from low to high Si:N (Figures 5D, E and Tables S4H, I). The general agreement with biogenic silica and diatom microscopy suggests that diatoms were responsible for differences in phytoplankton size. This Si-driven dominance of diatoms and their key traits (large size and mineral shells) persisted over time, in contrast to the response in carbon biomass (compare Figures S4, S5). Accordingly, Si availability was identified as a stronger driver than N and P for responses related to community composition (variation explained by 'Si:N', Tables S3E, S4).

Discussion

Our study demonstrates how the nutrient composition in deep water can drive plankton bloom dynamics during artificial upwelling. We now evaluate these responses to varying Si:N and explore possible implications for fisheries production and carbon sequestration (Figure 6).

Organic matter production

Basic plankton bloom functionality was upheld across our wide range in Si-availability. The cycling of N and P within the community was not measurably altered under extreme Si deficiency, which is surprising given the key role of diatoms in eutrophic systems (Dugdale and Wilkerson, 1998; Sarthou et al.,

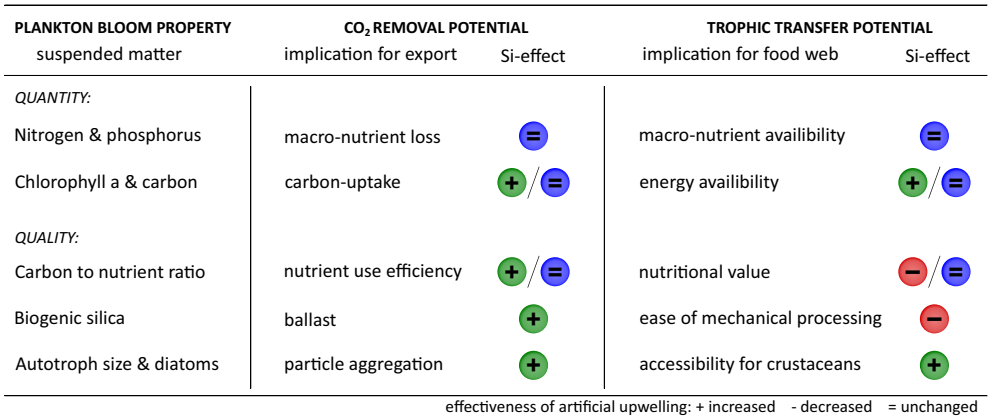

FIGURE 6
Possible consequences of varying Si:N in deep water for the effectiveness of artificial upwelling. Our findings for suspended matter are conceptually related to trophic transfer towards fisheries and carbon removal *via* the biological pump. Signs indicate increased (+), decreased (–) or unchanged (=) effectiveness. Two signs are given in case of a temporal pattern in the Si-effect: left for initial (first 2 weeks) and right for longer-term (following 2 weeks). This overview is limited to the simplified, 'classical' model of pelagic systems.

2005; Bibby and Moore, 2011). Even the influence of Si on photosynthetic capacity and carbon biomass dissipated with time. N and P availability, instead, was the primary driver of biomass synthesis, as presumed in previous studies on natural (Pitcher et al., 1991; Messie et al., 2009) and artificial upwelling (Karl and Letelier, 2008; Yool et al., 2009; Ortiz et al., 2022). Consequently, all our Si:N levels could maintain a photosynthetic capacity (2.5-5 μg L^{-1} chlorophyll *a*) similar to that of shelf seas and natural upwelling regions that support high zooplankton and fish production (Chavez and Messie, 2009; Gohin, 2011). Solely based on the energy and matter available for trophic transfer and export, the relative amount of Si in source water may not be critical for artificial upwelling facilities that maintain the bloom state long-term.

CO_2 removal potential

Our communities developed high carbon to nutrient ratios under upwelling in general, indicating a potential for carbon drawdown from the atmosphere. Nutrient-use efficiencies of our artificial systems were about twice that of the ocean wide average Redfield stoichiometry (Redfield, 1958) that would have to be exceeded for net carbon removal (Hessen et al., 2004; Karl and Letelier, 2008). Natural upwelling areas, in contrast, stay close to Redfield and may even act as a net source of CO_2 (Takahashi et al., 1997; Martiny et al., 2013). Accordingly, theoretical models on artificial upwelling employ Redfield stoichiometries and grant this technology only very limited potential for CO_2 sequestration (Dutreuil et al., 2009; Yool et al., 2009). Phytoplankton is exceptionally plastic, however, and can produce an excess in carbon-rich molecules under nutrient limitation (Geider and La Roche, 2002; Talmy et al., 2014; Mari et al., 2017). Such carbon overconsumption was possibly encouraged in our simulation, where the regularly added nutrients were rapidly exhausted by the elevated phytoplankton biomass causing intermittent N-limitation.

Si in deep water was an additional driver of carbon to nutrient ratios in our plankton blooms. During the first days of upwelling, the hypothetical carbon capture potential increased ~6-fold from communities with low (C:N = ~8) to high Si (C:N = ~16), when accounting for the inorganic carbon brought to the surface (C:N = 6.6, Redfield). Large phytoplankton such as diatoms are particularly well suited for the build-up of carbon-rich energy stores (Granum et al., 2002; Talmy et al., 2014) or the release of carbohydrates that aggregate to transparent exopolymer particles (TEP) (Mari et al., 2017). This possibly explains the strong Si-effect in the early phase of our bloom and the observed increase in C:N ratios in temperate mesocosms studies under nutrient limitation (Gilpin et al., 2004; Makareviciute-Fichtner et al., 2021). Clearly, fertilization strategies and seed communities that enable the biological pump to operate beyond the canonical Redfield ratio need better characterization. Only then, theoretical models may re-evaluate the potential of artificial upwelling as a negative emission technology.

The temporal shift in the influence of Si may reflect the progress in ecological adjustment. The environmental stability of the oligotrophic open ocean allows for a relatively precise adaptation of communities to low levels of regenerated nutrients (Landry, 2002;

Mojica et al., 2015). A strong upwelling of new nutrients stresses this balance and demands a drastic re-organisation towards traits beneficial under the alternate trophic state (Smetacek, 1999; Smith et al., 2009). Our results suggest that boosting diatoms *via* Si accelerates this transition so that high photosynthetic capacity, biomass and carbon to nutrient ratios are reached faster. Approaching the new steady-state, in contrast, our communities compensated for the varying nutrient stoichiometry, likely through functional redundancy (Rosenfeld, 2002). Low Si availability may have been offset either within diatoms, *via* lighter per capita silica shells (Sarthou et al., 2005) or higher per capita assimilation activity (Sathyendranath et al., 2009), or by non-silicifying primary producers (Dutkiewicz et al., 2021). The larger 'seed' communities involved in a real-world application would further increase the probability of including organisms that are essential to maintain ecological functioning across fertilizations scenarios.

Favourable properties for the formation and ballasting of sinking particles under high Si upwelling were maintained throughout the entire experiment. Suspended biogenic silica, and thus its availability for export, scaled proportionally with the Si treatment. Such mineral ballast in cells or zooplankton fecal pellets can considerably increase particle sinking velocity and therefore shorten the time-window for respiration of organic carbon before sequestration depths are reached (Armstrong et al., 2001; Jin et al., 2006). Diatoms are also thought to be efficient exporters due to their larger size, appendices and transparent exopolymer particles that facilitate aggregation and can further enhance sinking velocities (Thornton, 2002, but see also Mari et al., 2017 and Baumann et al., 2021). In conclusion, high Si upwelling altered the quality of suspended matter with a potential benefit for carbon removal, including carbon to nutrient ratios, the availability of mineral ballast and phytoplankton size. Our findings are, however, limited to the production of matter in the surface water, the first step towards carbon sequestration. Whether the subsequent export is efficient is uncertain and depends on complex ecological and biogeochemical processes involved in the formation and sinking of particles.

Trophic transfer potential

A pronounced shift towards larger phytoplankton occurred under high-Si upwelling, as hypothesized by benefiting diatoms. Cell size continued to increase even under Si:N ratios in excess of average diatom requirements (Si:N = 1:1, Sarthou et al., 2005). The shift in food size from the pico towards the nano and micro scale should make the primary production directly accessible for calanoid copepods (Kleppel, 1993; Harris et al., 2000; Sommer et al., 2002) and krill (Stuart, 1989; Riquelme-Bugueno et al., 2020). These crustacean taxa dominate grazing, including on diatoms, in productive shelf and upwelling systems, and provide a trophic shortcut to small pelagic fish (Cury et al., 2000; Espinoza and Bertrand, 2008). Under this traditional view of pelagic food webs (Cushing, 1989; Sommer et al., 2002), artificial upwelling with high Si may thus favour a short and efficient food web with increased fisheries potential.

The benefit of diatoms for crustaceans, however, is not universal. A range of diatom defences can function in naturally eutrophic systems with regular diatom blooms, despite the selective pressure in grazers to overcome them (Ianora and Miralto, 2010; Pancic et al., 2019). These mechanisms that hamper trophic transfer may prove more severe under artificial upwelling, where oligotrophic zooplankton conditioned to low diatom abundances dominate, at least initially (Hernandez-Leon, 1998; Mojica et al., 2015). We observed two changes under high Si upwelling that may impede grazing by crustaceans: the prominence of mineral shells that complicate mechanical handling and add ballast during digestion (Pancic et al., 2019) and the unusually high carbon to nutrient ratio that lead to nutritional imbalance (Anderson et al., 2005; Steinberg et al., 2017). Eventually, the benefit of Si upwelling for fisheries production may hinge on the presence of crustacean grazers that are highly adapted to silicified food of low nutritional value.

Conclusion

We identify Si:N nutrient stoichiometry as a strong driver of plankton bloom quality, and to a lesser extent quantity, during artificial upwelling (Figure 6). This Si-effect is likely to interact with major design aspects of an upwelling facility, such as the mode and duration of nutrient provisioning. Being constrained to a short time window, the effect on carbon assimilation may be taken advantage of by a stationary facility where a water mass receives only a single pulse of nutrients ('plume' type fertilization). The increase of phytoplankton size and mineral ballast by high Si proved instead more stable over time. These community properties may thus benefit a free-floating facility that maintains the eutrophic state long-term ('patch' type fertilisation). In any case, the chosen Si-strategy may not be capable to improve trophic transfer and carbon sequestration simultaneously. Maximizing CO_2 removal *via* mineral ballast and high carbon to nutrient ratios of organic matter implies a low food palatability that may, in turn, impair trophic transfer in the absence of highly adapted crustacean grazers.

The insights provided herein are limited to the growth-phase of the bloom. An entirely different response to Si could emerge under post-bloom dynamics, when upwelling is discontinued and plankton falls out en mass. We are clearly only beginning to understand the potential and risks of artificial upwelling as negative emission technology and ecosystem-based aquaculture.

Time is running out to evaluate such nature-based solutions for society's path out of the climate crisis and towards global food security.

Data availability statement

The raw data supporting the conclusions of this article will be made available by the authors, without undue reservation, *via* PANGAEA (https://www.pangaea.de/?q=campaign:%22KOSMOS_2019%22).

Author contributions

All authors designed the study and conducted the experiment. SG analyzed the data. SG wrote the manuscript with input from all authors. All authors contributed to the article and approved the submitted version.

Funding

This study was conducted within the projects Ocean Artificial Upwelling (Ocean artUp) funded by an Advanced Grant of the European Research Council and Road Testing Ocean Artificial Upwelling (Test-ArtUp) funded by the German Marine Research Alliance (DAM). Further support was provided through Transnational Access funds by the EU project AQUACOSM and by project TRIATLAS (AMD-817578-5) from the European Union's Horizon 2020. JA was also supported by a Helmholtz International Fellow Award, 2015 (Helmholtz Association, Germany).

Acknowledgments

We thank the Plataforma Oceánica de Canarias (PLOCAN) for providing facilities and logistical and technical support throughout the experiment. Further, we thank all the staff and students from the KOSMOS team of GEOMAR and the biological oceanography group of ULPGC who organised and carried out the experiment and Greta Wunderlich for her microscopical assessment of the phytoplankton community.

Conflict of interest

The authors declare that the research was conducted in the absence of any commercial or financial relationships that could be construed as a potential conflict of interest.

Publisher's note

Supplementary material

The Supplementary Material for this article can be found online at: https://www.frontiersin.org/articles/10.3389/fmars.2022.1015188/full#supplementary-material

References

Allen, J. T., Brown, L., Sanders, R., Moore, C. M., Mustard, A., Fielding, S., et al. (2005). Diatom carbon export enhanced by silicate upwelling in the northeast Atlantic. *Nature* 437, 728–732. doi: 10.1038/nature03948

Anderson, T. R., Hessen, D. O., Elser, J. J., and Urabe, J. (2005). Metabolic stoichiometry and the fate of excess carbon and nutrients in consumers. *Am. Nat.* 165, 1–15. doi: 10.1086/426598

Aristegui, J., Hernandez-Leon, S., Montero, M. F., and Gomez, M. (2001). The seasonal planktonic cycle in coastal waters of the canary islands. *Scientia Marina* 65, 51–58. doi: 10.3989/scimar.2001.65s151

Armengol, L., Calbet, A., Franchy, G., Rodriguez-Santos, A., and Hernandez-Leon, S. (2019). Planktonic food web structure and trophic transfer efficiency along a productivity gradient in the tropical and subtropical Atlantic ocean. *Sci. Rep.* 9, 19. doi: 10.1038/s41598-019-38507-9

Armstrong, R. A., Lee, C., Hedges, J. I., Honjo, S., and Wakeham, S. G. (2001). A new, mechanistic model for organic carbon fluxes in the ocean based on the quantitative association of POC with ballast minerals. *Deep-Sea Res. Part Ii-Topical Stud. Oceanogr.* 49, 219–236. doi: 10.1016/S0967-0645(01)00101-1

Bach, L. T., Hernandez-Hernandez, N., Taucher, J., Spisla, C., Sforna, C., Riebesell, U., et al. (2019). Effects of elevated CO2 on a natural diatom community in the subtropical NE Atlantic. *Front. Mar. Sci.* 6, 16. doi: 10.3389/fmars.2019.00075

Ban, S. H., Burns, C., Castel, J., Chaudron, Y., Christou, E., Escribano, R., et al. (1997). The paradox of diatom-copepod interactions. *Mar. Ecol. Prog. Ser.* 157, 287–293. doi: 10.3354/meps157287

Barlow, R. G., Cummings, D. G., and Gibb, S. W. (1997). Improved resolution of mono- and divinyl chlorophylls a and b and zeaxanthin and lutein in phytoplankton extracts using reverse phase c-8 HPLC. *Mar. Ecol. Prog. Ser.* 161, 303–307. doi: 10.3354/meps161303

Barton, E., Arıstegui, J., Tett, P., Cantón, M., Garcıa-Braun, J., Hernández-León, S., et al. (1998). The transition zone of the canary current upwelling region. *Prog. Oceanogr.* 41, 455–504. doi: 10.1016/S0079-6611(98)00023-8

Bates, D., Machler, M., Bolker, B. M., and Walker, S. C. (2015). Fitting linear mixed-effects models using lme4. *J. Stat. Software* 67, 1–48. doi: 10.18637/jss.v067.i01

Baumann, M., Taucher, J., Paul, A. J., Heinemann, M., Vanharanta, M., Bach, L. T., et al. (2021). Effect of intensity and mode of artificial upwelling on particle flux and carbon export. *Front. Mar. Sci.* 1579. doi: 10.3389/fmars.2021.742142

Bibby, T. S., and Moore, C. M. (2011). Silicate: nitrate ratios of upwelled waters control the phytoplankton community sustained by mesoscale eddies in sub-tropical north Atlantic and pacific. *Biogeosciences* 8, 657–666. doi: 10.5194/bg-8-657-2011

Boxhammer, T., Bach, L. T., Czerny, J., and Riebesell, U. (2016). Technical note: Sampling and processing of mesocosm sediment trap material for quantitative biogeochemical analysis. *Biogeosciences* 13, 2849–2858. doi: 10.5194/bg-13-2849-2016

Boyce, D. G., Lewis, M. R., and Worm, B. (2010). Global phytoplankton decline over the past century. *Nature* 466, 591–596. doi: 10.1038/nature09268

Boyd, P. W., Claustre, H., Levy, M., Siegel, D. A., and Weber, T. (2019). Multi-faceted particle pumps drive carbon sequestration in the ocean. *Nature* 568, 327–335. doi: 10.1038/s41586-019-1098-2

Chassot, E., Bonhommeau, S., Dulvy, N. K., Melin, F., Watson, R., Gascuel, D., et al. (2010). Global marine primary production constrains fisheries catches. *Ecol. Lett.* 13, 495–505. doi: 10.1111/j.1461-0248.2010.01443.x

Chavez, F. P., and Messie, M. (2009). A comparison of Eastern boundary upwelling ecosystems. *Prog. Oceanogr.* 83, 80–96. doi: 10.1016/j.pocean.2009.07.032

Core Team, R. (2021). *R: A language and environment for statistical computing* (Vienna, Austria: R Foundation for Statistical Computing).

Costello, C., Cao, L., Gelcich, S., Cisneros-Mata, M. A., Free, C. M., Froehlich, H. E., et al. (2020). The future of food from the sea. *Nature* 588, 95–100. doi: 10.1038/s41586-020-2616-y

Cury, P., Bakun, A., Crawford, R. J. M., Jarre, A., Quinones, R. A., Shannon, L. J., et al. (2000). Small pelagics in upwelling systems: patterns of interaction and structural changes in "wasp-waist" ecosystems. *Ices J. Mar. Sci.* 57, 603–618. doi: 10.1006/jmsc.2000.0712

Cushing, D. H. (1989). A difference in structure between ecosystems in strongly stratified waters and in those that are only weakly stratified. *J. Plankton Res.* 11, 1–13. doi: 10.1093/plankt/11.1.1

Decima, M., and Landry, M. R. (2020). Resilience of plankton trophic structure to an eddy-stimulated diatom bloom in the north pacific subtropical gyre. *Mar. Ecol. Prog. Ser.* 643, 33–48. doi: 10.3354/meps13333

Dickson, A. G., Afghan, J. D., and Anderson, G. C. (2003). Reference materials for oceanic CO2 analysis: a method for the certification of total alkalinity. *Mar. Chem.* 80, 185–197. doi: 10.1016/S0304-4203(02)00133-0

Dickson, A. G., Sabine, C. L., and Christian, J. R. (2007). *Guide to best practices for ocean CO2 measurements* (Sidney, BC, Canada: North Pacific Marine Science Organization).

Dubelaar, G. B. J., and Jonker, R. R. (2000). Flow cytometry as a tool for the study of phytoplankton. *Scientia Marina* 64, 135–156. doi: 10.3989/scimar.2000.64n2135

Dugdale, R. C., and Wilkerson, F. P. (1998). Silicate regulation of new production in the equatorial pacific upwelling. *Nature* 391, 270–273. doi: 10.1038/34630

Dulaquais, G., Boye, M., Rijkenberg, M. J. A., and Carton, X. (2014). Physical and remineralization processes govern the cobalt distribution in the deep western Atlantic ocean. *Biogeosciences* 11, 1561–1580. doi: 10.5194/bg-11-1561-2014

Dutkiewicz, S., Boyd, P. W., and Riebesell, U. (2021). Exploring biogeochemical and ecological redundancy in phytoplankton communities in the global ocean. *Global Change Biol.* 27, 1196–1213. doi: 10.1111/gcb.15493

Dutreuil, S., Bopp, L., and Tagliabue, A. (2009). Impact of enhanced vertical mixing on marine biogeochemistry: lessons for geo-engineering and natural variability. *Biogeosciences* 6, 901–912. doi: 10.5194/bg-6-901-2009

Eddy, T. D., Bernhardt, J. R., Blanchard, J. L., Cheung, W. W., Colléter, M., Du Pontavice, H., et al. (2020). Energy flow through marine ecosystems: Confronting transfer efficiency. *Trends Ecol. Evol* 36:76–86. doi: 10.1016/j.tree.2020.09.006

Edler, L., and Elbrächter, M. (2010). The utermöhl method for quantitative phytoplankton analysis. *Microscopic Mol. Methods quantitative phytoplankton Anal.* 110, 13–20.

Eppley, R. W., and Peterson, B. J. (1979). Particulate organic-matter flux and planktonic new production in the deep ocean. *Nature* 282, 677–680. doi: 10.1038/282677a0

Espinoza, P., and Bertrand, A. (2008). Revisiting Peruvian anchovy (Engraulis ringens) trophodynamics provides a new vision of the Humboldt current system. *Prog. Oceanogr.* 79, 215–227. doi: 10.1016/j.pocean.2008.10.022

Fuhrman, J., McJeon, H., Patel, P., Doney, S. C., Shobe, W. M., and Clarens, A. F. (2020). Food-energy-water implications of negative emissions technologies in a+1.5 degrees c future. *Nat. Clim. Change* 10, 920. doi: 10.1038/s41558-020-0876-z

Fu, W. W., Randerson, J. T., and Moore, J. K. (2016). Climate change impacts on net primary production (NPP) and export production (EP) regulated by increasing stratification and phytoplankton community structure in the CMIP5 models. *Biogeosciences* 13, 5151–5170. doi: 10.5194/bg-13-5151-2016

Gattuso, J.-P., Williamson, P., Duarte, C. M., and Magnan, A. K. (2021). The potential for ocean-based climate action: negative emissions technologies and beyond. *Front. Climate* 2, 37. doi: 10.3389/fclim.2020.575716

Geider, R. J., and La Roche, J. (2002). Redfield revisited: variability of c : N : P in marine microalgae and its biochemical basis. *Eur. J. Phycology* 37, 1–17. doi: 10.1017/S0967026201003456

Gilpin, L. C., Davidson, K., and Roberts, E. C. (2004). The influence of changes in nitrogen: silicon ratios on diatom growth dynamics. *J. Sea Res.* 51, 21–35. doi: 10.1016/j.seares.2003.05.005

Godfray, H. C. J., Beddington, J. R., Crute, I. R., Haddad, L., Lawrence, D., Muir, J. F., et al. (2010). Food security: The challenge of feeding 9 billion people. *Science* 327, 812–818. doi: 10.1126/science.1185383

Gohin, F. (2011). Annual cycles of chlorophyll-a, non-algal suspended particulate matter, and turbidity observed from space and *in-situ* in coastal waters. *Ocean Sci.* 7, 705–732. doi: 10.5194/os-7-705-2011

Granum, E., Kirkvold, S., and Myklestad, S. M. (2002). Cellular and extracellular production of carbohydrates and amino acids by the marine diatom skeletonema costatum: diel variations and effects of n depletion. *Mar. Ecol. Prog. Ser.* 242, 83–94. doi: 10.3354/meps242083

Griffiths, J. D., Barker, S., Hendry, K. R., Thornalley, D. J. R., van de Flierdt, T., Hall, I. R., et al. (2013). Evidence of silicic acid leakage to the tropical Atlantic *via* Antarctic intermediate water during marine isotope stage 4. *Paleoceanography* 28, 307–318. doi: 10.1002/palo.20030

Hansen, H. P., and Koroleff, F. (1999). *Determination of nutrients* (Weinheim, Germany: Wiley-VCH).

Harris, R. P., Irigoien, X., Head, R. N., Rey, C., Hygum, B. H., Hansen, B. W., et al. (2000). Feeding, growth, and reproduction in the genus calanus. *Ices J. Mar. Sci.* 57, 1708–1726. doi: 10.1006/jmsc.2000.0959

Hernandez-Leon, S. (1998). Annual cycle of epiplanktonic copepods in canary island waters. *Fisheries Oceanogr.* 7, 252–257. doi: 10.1046/j.1365-2419.1998.00071.x

Hessen, D. O., Agren, G. I., Anderson, T. R., Elser, J. J., and De Ruiter, P. C. (2004). Carbon, sequestration in ecosystems: The role of stoichiometry. *Ecology* 85, 1179–1192. doi: 10.1890/02-0251

Holmes, R. M., Aminot, A., Kerouel, R., Hooker, B. A., and Peterson, B. J. (1999). A simple and precise method for measuring ammonium in marine and freshwater ecosystems. *Can. J. Fisheries Aquat. Sci.* 56, 1801–1808. doi: 10.1139/f99-128

Ianora, A., and Miralto, A. (2010). Toxigenic effects of diatoms on grazers, phytoplankton and other microbes: a review. *Ecotoxicology* 19, 493–511. doi: 10.1007/s10646-009-0434-y

IPCC and Core Writing Team (2014). "Climate change 2014: Synthesis report," in *Contribution of working groups I, II and III to the fifth assessment report of the intergovernmental panel on climate change*. Eds. R. K. Pachauri and L. A. Meyer (Geneva, Switzerland: IPCC).

Jin, X., Gruber, N., Dunne, J. P., Sarmiento, J. L., and Armstrong, R. A. (2006). Diagnosing the contribution of phytoplankton functional groups to the production and export of particulate organic carbon, CaCO3, and opal from global nutrient and alkalinity distributions. *Global Biogeochem. Cycles* 20. doi: 10.1029/2005GB002532

Karl, D. M., and Letelier, R. M. (2008). Nitrogen fixation-enhanced carbon sequestration in low nitrate, low chlorophyll seascapes. *Mar. Ecol. Prog. Ser.* 364, 257–268. doi: 10.3354/meps07547

Kleppel, G. S. (1993). On the diets of calanoid copepods. *Mar. Ecol. Prog. Ser.* 99, 183–195. doi: 10.3354/meps099183

Kuznetsova, A., Brockhoff, P. B., and Christensen, R. H. B. (2017). lmerTest package: Tests in linear mixed effects models. *J. Stat. Software* 82, 1–26. doi: 10.18637/jss.v082.i13

Landry, M. R. (2002). Integrating classical and microbial food web concepts: evolving views from the open-ocean tropical pacific. *Hydrobiologia* 480, 29–39. doi: 10.1023/A:1021272731737

Llinás, O., Leon, A., Siedler, G., and Wefer, G. (1999). ESTOC data report 95/96. *Instituto Canario Cienc. Marinas Telde*.

Macreadie, P. I., Costa, M. D. P., Atwood, T. B., Friess, D. A., Kelleway, J. J., Kennedy, H., et al. (2021). Blue carbon as a natural climate solution. *Nat. Rev. Earth Environ* 2:826–839. doi: 10.1038/s43017-021-00224-1

Makareviciute-Fichtner, K., Matthiessen, B., Lotze, H. K., and Sommer, U. (2021). Phytoplankton nutritional quality is altered by shifting Si:N ratios and selective grazing. *J. Plankton Res.* 43, 325–337. doi: 10.1093/plankt/fbab034

Mari, X., Passow, U., Migon, C., Burd, A. B., and Legendre, L. (2017). Transparent exopolymer particles: Effects on carbon cycling in the ocean. *Prog. Oceanogr.* 151, 13–37. doi: 10.1016/j.pocean.2016.11.002

Martiny, A. C., Vrugt, J. A., Primeau, F. W., and Lomas, M. W. (2013). Regional variation in the particulate organic carbon to nitrogen ratio in the surface ocean. *Global Biogeochemical Cycles* 27, 723–731. doi: 10.1002/gbc.20061

Matear, R. J., and Hirst, A. C. (1999). Climate change feedback on the future oceanic CO2 uptake. *Tellus Ser. B-Chem. Phys. Meteorol.* 51, 722–733. doi: 10.3402/tellusb.v51i3.16472

Messie, M., Ledesma, J., Kolber, D. D., Michisaki, R. P., Foley, D. G., and Chavez, F. P. (2009). Potential new production estimates in four eastern boundary upwelling ecosystems. *Prog. Oceanogr.* 83, 151–158. doi: 10.1016/j.pocean.2009.07.018

Minx, J. C., Lamb, W. F., Callaghan, M. W., Fuss, S., Hilaire, J., Creutzig, F., et al. (2018). Negative emissions-part 1: Research landscape and synthesis. *Environ. Res. Lett.* 13:063001. doi: 10.1088/1748-9326/aabf9b

Mitchell, J. G., Seuront, L., Doubell, M. J., Losic, D., Voelcker, N. H., Seymour, J., et al. (2013). The role of diatom nanostructures in biasing diffusion to improve uptake in a patchy nutrient environment. *PloS One* 8, e59548. doi: 10.1371/journal.pone.0059548

Mojica, K. D. A., van de Poll, W. H., Kehoe, M., Huisman, J., Timmermans, K. R., Buma, A. G. J., et al. (2015). Phytoplankton community structure in relation to vertical stratification along a north-south gradient in the northeast Atlantic ocean. *Limnol. Oceanogr.* 60, 1498–1521. doi: 10.1002/lno.10113

Moore, C. M., Mills, M. M., Arrigo, K. R., Berman-Frank, I., Bopp, L., Boyd, P. W., et al. (2013). Processes and patterns of oceanic nutrient limitation. *Nat. Geosci.* 6, 701–710. doi: 10.1038/ngeo1765

Neuer, S., Cianca, A., Helmke, P., Freudenthal, T., Davenport, R., Meggers, H., et al. (2007). Biogeochemistry and hydrography in the eastern subtropical north Atlantic gyre. results from the European time-series station ESTOC. *Prog. Oceanogr.* 72, 1–29. doi: 10.1016/j.pocean.2006.08.001

Olenina, I. (2006). Biovolumes and size-classes of phytoplankton in the Baltic Sea. *HELCOM Baltic Sea Environ. Proc. No.106*. 144.

Ortiz, J., Arístegui, J., Taucher, J., and Riebesell, U. (2022). Artificial upwelling in singular and recurring mode: Consequences for net community production and metabolic balance. *Front. Mar. Sci.* 8. doi: 10.3389/fmars.2021.743105

Pancic, M., Torres, R. R., Almeda, R., and Kiorboe, T. (2019). Silicified cell walls as a defensive trait in diatoms. *Proc. R. Soc. B-Biol. Sci.* 286, 9. doi: 10.1098/rspb.2019.0184

Pan, Y. W., Wei, F., Zhang, D. H., Chen, J. W., Huang, H. C., Liu, S. X., et al. (2016). Research progress in artificial upwelling and its potential environmental effects. *Sci. China-Earth Sci.* 59, 236–248. doi: 10.1007/s11430-015-5195-2

Paul, A. J., Bach, L. T., Schulz, K. G., Boxhammer, T., Czerny, J., Achterberg, E. P., et al. (2015). Effect of elevated CO2 on organic matter pools and fluxes in a summer Baltic Sea plankton community. *Biogeosciences* 12, 6181–6203. doi: 10.5194/bg-12-6181-2015

Pauly, D., and Christensen, V. (1995). Primary production required to sustain global fisheries. *Nature* 374, 255–257. doi: 10.1038/374255a0

Pielou, E. C. (1966). The measurement of diversity in different types of biological collections. *J. Theor. Biol.* 13, 131–144. doi: 10.1016/0022-5193(66)90013-0

Pitcher, G. C., Walker, D. R., Mitchellinnes, B. A., and Moloney, C. L. (1991). Short-term variability during an anchor station study in the southern benguela upwelling system – phytoplankton dynamics. *Prog. Oceanogr.* 28, 39–64. doi: 10.1016/0079-6611(91)90020-M

Polovina, J. J., Howell, E. A., and Abecassis, M. (2008). Ocean's least productive waters are expanding. *Geophysical Res. Lett.* 35, 5. doi: 10.1029/2007GL031745

Popescu, I., and Ortega Gras, J. J. (2015). Fisheries in the canary islands. *European Parliament, Directorate-General for Internal Policies of the Union*. doi: 10.2861/18051

Quinn, G. P., and Keough, M. J. (2002). *Experimental design and data analysis for biologists* (New York, USA: Cambridge University Press).

Ragueneau, O., Treguer, P., Leynaert, A., Anderson, R. F., Brzezinski, M. A., DeMaster, D. J., et al. (2000). A review of the Si cycle in the modem ocean: recent progress and missing gaps in the application of biogenic opal as a paleoproductivity proxy. *Global Planetary Change* 26, 317–365. doi: 10.1016/S0921-8181(00)00052-7

Redfield, A. C. (1958). The biological control of chemical factors in the environment. *Am. Sci.* 46, 205–221.

Riebesell, U., Czerny, J., von Brockel, K., Boxhammer, T., Budenbender, J., Deckelnick, M., et al. (2013). Technical note: A mobile sea-going mesocosm system - new opportunities for ocean change research. *Biogeosciences* 10, 1835–1847. doi: 10.5194/bg-10-1835-2013

Riquelme-Bugueno, R., Pantoja-Gutierrez, S., Jorquera, E., Anabalon, V., Srain, B., and Schneider, W. (2020). Fatty acid composition in the endemic Humboldt current krill, euphausia mucronata (Crustacea, euphausiacea) in relation to the phytoplankton community and oceanographic variability off dichato coast in central Chile. *Prog. Oceanogr.* 188, 11. doi: 10.1016/j.pocean.2020.102425

Romann, J., Valmalette, J. C., Chauton, M. S., Tranell, G., Einarsrud, M. A., and Vadstein, O. (2015). Wavelength and orientation dependent capture of light by diatom frustule nanostructures. *Sci. Rep.* 5, 6. doi: 10.1038/srep17403

Rosenfeld, J. S. (2002). Functional redundancy in ecology and conservation. *Oikos* 98, 156–162. doi: 10.1034/j.1600-0706.2002.980116.x

RStudio Team (2021). *RStudio: Integrated development environment for r* (Boston, MA: RStudio, PBC).

Ryther, J. H. (1969). Photosynthesis and fish production in the sea. *Science* 166, 72–76. doi: 10.1126/science.166.3901.72

Sarmiento, J. L., Gruber, N., Brzezinski, M. A., and Dunne, J. P. (2004). High-latitude controls of thermocline nutrients and low latitude biological productivity. *Nature* 427, 56–60. doi: 10.1038/nature02127

Sarthou, G., Timmermans, K. R., Blain, S., and Treguer, P. (2005). Growth physiology and fate of diatoms in the ocean: A review. *J. Sea Res.* 53, 25–42. doi: 10.1016/j.seares.2004.01.007

Sathyendranath, S., Stuart, V., Nair, A., Oka, K., Nakane, T., Bouman, H., et al. (2009). Carbon-to-chlorophyll ratio and growth rate of phytoplankton in the sea. *Mar. Ecol. Prog. Ser.* 383, 73–84. doi: 10.3354/meps07998

Schulz, K. G., and Riebesell, U. (2013). Diurnal changes in seawater carbonate chemistry speciation at increasing atmospheric carbon dioxide. *Mar. Biol.* 160, 1889–1899. doi: 10.1007/s00227-012-1965-y

Sharp, J. H. (1974). Improved analysis for "particulate" organic carbon and nitrogen from seawater. *Limnol. Oceanogr.* 19, 984–989. doi: 10.4319/lo.1974.19.6.0984

Singmann, H., and Kellen, D. (2019). An introduction to mixed models for experimental psychology. *New Methods Cogn. Psychol.* 28, 4–31. doi: 10.4324/9780429318405-2

Smetacek, V. (1999). Diatoms and the ocean carbon cycle. *Protist* 150, 25–32. doi: 10.1016/S1434-4610(99)70006-4

Smith, M. D., Knapp, A. K., and Collins, S. L. (2009). A framework for assessing ecosystem dynamics in response to chronic resource alterations induced by global change. *Ecology* 90, 3279–3289. doi: 10.1890/08-1815.1

Sommer, U., Stibor, H., Katechakis, A., Sommer, F., and Hansen, T. (2002). Pelagic food web configurations at different levels of nutrient richness and their implications for the ratio fish production: primary production. *Hydrobiologia* 484, 11–20. doi: 10.1023/A:1021340601986

Steinacher, M., Joos, F., Frolicher, T. L., Bopp, L., Cadule, P., Cocco, V., et al. (2010). Projected 21st century decrease in marine productivity: a multi-model analysis. *Biogeosciences* 7, 979–1005. doi: 10.5194/bg-7-979-2010

Steinberg, D. K., Landry, M. R., and Annual, R. (2017). Zooplankton and the ocean carbon cycle. *Annu. Rev. Mar. Sci.* 9, 413–444. doi: 10.1146/annurev-marine-010814-015924

Stuart, V. (1989). Observations on the feeding of euphausia lucens on natural phytoplankton suspensions in the southern benguela upwelling region. *Continent. Shelf Res.* 9, 1017–1028. doi: 10.1016/0278-4343(89)90005-8

Tacon, A. G. J., and Metian, M. (2015). Feed matters: Satisfying the feed demand of aquaculture. *Rev. Fisheries Sci. Aquaculture* 23, 1–10. doi: 10.1080/23308249.2014.987209

Takahashi, T., Feely, R. A., Weiss, R. F., Wanninkhof, R. H., Chipman, D. W., Sutherland, S. C., et al. (1997). Global air-sea flux of CO2: An estimate based on measurements of sea-air pCO2 difference. *Proc. Natl. Acad. Sci. U. S. A.* 94, 8292–8299. doi: 10.1073/pnas.94.16.8292

Talmy, D., Blackford, J., Hardman-Mountford, N. J., Polimene, L., Follows, M. J., and Geider, R. J. (2014). Flexible c : N ratio enhances metabolism of large phytoplankton when resource supply is intermittent. *Biogeosciences* 11, 4881–4895. doi: 10.5194/bg-11-4881-2014

Taucher, J., Bach, L. T., Boxhammer, T., Nauendorf, A., Achterberg, E. P. , Algueró-Muñiz, M., et al. (2017). Influence of ocean acidification and deep water upwelling on oligotrophic plankton communities in the subtropical north Atlantic: insights from an *in situ* mesocosm study. *Front. Mar. Sci.* 4, 85. doi: 10.3389/fmars.2017.00085

Thornton, D. C. O. (2002). Diatom aggregation in the sea: Mechanisms and ecological implications. *Eur. J. Phycology* 37, 149–161. doi: 10.1017/S0967026202003657

Veldhuis, M. J. W., and Kraay, G. W. (2000). Application of flow cytometry in marine phytoplankton research: current applications and future perspectives. *Scientia Marina* 64, 121–134. doi: 10.3989/scimar.2000.64n2121

Vihtakari, M. (2021). *ggOceanMaps: Plot data on oceanographic maps using 'ggplot2'* (R package). Available at: https://CRAN.R-project.org/package=ggOceanMaps.

Yool, A., Shepherd, J. G., Bryden, H. L., and Oschlies, A. (2009). Low efficiency of nutrient translocation for enhancing oceanic uptake of carbon dioxide. *J. Geophysical Research-Oceans* 114, C08009. doi: 10.1029/2008JC004792

frontiers | Frontiers in Marine Science

TYPE Original Research
PUBLISHED 05 July 2023
DOI 10.3389/fmars.2023.1181351

OPEN ACCESS

EDITED BY
Rob Middag,
Royal Netherlands Institute for Sea Research (NIOZ), Netherlands

REVIEWED BY
Yang Xiang,
University of Washington, United States
Daniel Ohnemus,
University of Georgia, United States

*CORRESPONDENCE
Moritz Baumann
mbaumann@geomar.de

RECEIVED 07 March 2023
ACCEPTED 31 May 2023
PUBLISHED 05 July 2023

CITATION
Baumann M, Goldenberg SU, Taucher J, Fernández-Méndez M, Ortiz J, Haussmann J and Riebesell U (2023) Counteracting effects of nutrient composition (Si:N) on export flux under artificial upwelling.
Front. Mar. Sci. 10:1181351.
doi: 10.3389/fmars.2023.1181351

Counteracting effects of nutrient composition (Si:N) on export flux under artificial upwelling

Moritz Baumann[1]*, Silvan Urs Goldenberg[1], Jan Taucher[1], Mar Fernández-Méndez[2], Joaquin Ortiz[1], Jacqueline Haussmann[1] and Ulf Riebesell[1]

[1]Biological Oceanography, GEOMAR Helmholtz Centre for Ocean Research, Kiel, Germany, [2]Biosciences, Polar Biological Oceanography, Alfred-Wegener-Institut Helmholtz-Zentrum für Polar- und Meeresforschung, Bremerhaven, Germany

To keep global warming below 1.5°C, technologies that remove carbon from the atmosphere will be needed. Ocean artificial upwelling of nutrient-rich water stimulates primary productivity and could enhance the biological carbon pump for natural CO_2 removal. Its potential may depend on the Si availability in the upwelled water, which regulates the abundance of diatoms that are key carbon exporters. In a mesocosm experiment, we tested the effect of nutrient composition (Si relative to N) in artificially upwelled waters on export quantity and quality in a subtropical oligotrophic environment. Upwelling led to a doubling of exported particulate matter and increased C:N ratios to well beyond Redfield (9.5 to 11.1). High Si availability stimulated this carbon over-consumption further, resulting in a temporary ~5-fold increase in POC export and ~30% increase in C:N ratios compared to Si-scarce upwelling. Whilst the biogenic Si ballast of the export flux increased more than 3.5-fold over the Si:N gradient, these heavier particles did not sink faster. On the contrary, sinking velocity decreased considerably under high Si:N, most likely due to reduced particle size. Respiration rates remained similar across all treatments indicating that biogenic Si did not protect particles against microbial degradation. Si availability thus influenced key processes of the biological carbon pump in counteracting ways by increasing the export magnitude and associated C:N ratios but decreasing the efficiency of carbon transfer to depth. These opposing effects need to be considered when evaluating the potential of artificial upwelling as negative emission technology.

KEYWORDS

artificial upwelling, biological carbon pump, particulate matter export, sinking velocity, remineralization rate, carbon sequestration, diatoms, mesocosms

1 Introduction

Carbon dioxide removal (CDR) on a grand scale is likely to be a critical component of any feasible plan to keep global warming below 1.5°C (IPCC, 2018). The oceanic realm constitutes the biggest non-geological carbon reservoir of our planet, and it offers vast space for carbon dioxide removal techniques to be deployed. Artificial upwelling is one such technology, which aims to enhance biological productivity in the surface ocean by transporting nutrient-rich water from deeper layers to the oligotrophic surface (Pan et al., 2016). Much like in natural upwelling systems, the increase in primary productivity should theoretically cause an enhanced vertical export flux of sinking particulate organic matter, which transports organically bound carbon to depth. Once the carbon reaches the deep ocean (generally below 1,000 m), it is regarded as sequestered on the time scale of up to centuries (Siegel et al., 2021). This natural process is called the "biological carbon pump" (e.g. Volk and Hoffert, 1985), whose strength might be enhanced using artificial upwelling.

The carbon sequestration potential of artificial upwelling via the biological carbon pump is mainly determined by (a) how much material sinks out of the surface ocean, (b) the efficiency with which it is transferred to depth, i.e. the vertical carbon flux attenuation (Henson et al., 2012a), and (c) the carbon to nutrient ratio of sequestered particulate matter. The first is affected by the pelagic community composition and productivity. The export efficiency is controlled by the velocity with which exported material sinks and the rate at which it is remineralized back to the dissolved inorganic carbon (DIC) pool (McDonnell et al., 2015). The exported matter carbon to nutrient ratio is affected by the community composition in the surface (Coale et al., 2004) and remineralization processes in the sub-surface (Boyd and Trull, 2007). It is critical because the upwelled water contains not only excess nutrients but also excess DIC, which needs to be compensated for (e.g. Oschlies et al., 2010). When all upwelled nutrients are eventually exported, the carbon to nutrient ratio of sequestered matter needs to be higher than that of the upwelled nutrients (e.g. excess DIC : NO_3^-) to achieve net carbon sequestration (Baumann et al., 2021).

Nutrient composition shapes phytoplankton community structure, with implications for food webs and ultimately ecosystem services, such as carbon export. The relative availability of dissolved silicate (orthosilicic acid, $Si(OH)_4$) is perhaps the most important characteristic when it comes to defining the phytoplankton community structure under meso- or eutrophic conditions. Under abundant silicate, diatoms (*Bacillariophyceae*) thrive, whereas under Si scarcity usually phyto-flagellates dominate (Sommer, 1994).

Diatoms are important players in the ocean carbon cycle (Field et al., 1998), contributing 40% to the global particulate organic carbon (POC) export (Jin et al., 2006). Many species are chain-forming, especially those constituting the yearly spring blooms at high latitudes and seasonal blooms in coastal upwelling regions (Smetacek, 1985; Smetacek, 1999). When the limiting nutrient is exhausted (usually nitrate or silicic acid), they form aggregates and export large amounts of biogenic carbon from the euphotic zone to the deep sea (Honjo and Manganini, 1993). Diatom blooms are short-lived, but can be sustained by recurring silicic acid fertilization and the associated carbon sequestration upheld on time scales of weeks to months (Dugdale and Wilkerson, 1998; Allen et al., 2005). Diatoms incorporate the silicic acid into their cell walls as biogenic silica (BSi, opal), a biomineral twice as heavy as particulate organic carbon (Klaas and Archer, 2002). As biogenic ballast material, it is considered to increase particle sinking velocities (Armstrong et al., 2009) and it might as well act as a protective barrier against microbial remineralization (Armstrong et al., 2002; Klaas and Archer, 2002). Furthermore, aggregation processes can be facilitated by the exudation of transparent exopolymer particles (TEP), which are often exuded at the termination of a bloom (Obernosterer and Herndl, 1995) and promote the formation of larger marine snow particles. This suggests that increased Si availability and consequently higher diatom abundances would increase the transfer efficiency of biogenic matter to depth.

However, diatoms do not necessarily promote efficient carbon export. In fact, their blooms can result in relatively inefficient transfer of particulate organic matter from the surface ocean to depth (Guidi et al., 2009; Henson et al., 2012b; Maiti et al., 2013). Exuded TEP itself is positively buoyant and can thus decrease the density of particulate matter in aggregates, thereby leading to its retention in the surface (Mari et al., 2017). Furthermore, diatom-originated aggregates are usually relatively porous, which can reduce sinking velocities and facilitate bacterial remineralization rates (Lam et al., 2011; Puigcorbé et al., 2015; Bach et al., 2019). How these positive and negative effects on carbon export will balance out during artificial upwelling is uncertain.

We here investigate the carbon sequestration potential of artificial upwelling under varying levels of Si availability and diatom dominance. In a mesocosm experiment in the subtropical North Atlantic, we fertilized a natural oligotrophic plankton community with nutrient-rich deep water composed of different Si:N ratios (gradient from 0.07–1.33 mol:mol). During the month-long experiment, Si availability altered plankton community properties in potentially beneficial ways regarding carbon sequestration (Goldenberg et al., 2022). Our study tests how these changes in the surface water were carried over to key export properties including the flux, composition, velocity and remineralization of sinking biogenic matter. By linking plankton communities to the functioning of the biological carbon pump, we characterize the role of diatoms during carbon export and evaluate artificial upwelling as a negative emission technology.

2 Materials and methods

2.1 Experimental setup

The 35 day-long mesocosm experiment was carried out in autumn 2019 in the subtropical North Atlantic. Inside the harbor of Taliarte, Spain (27°59'24" N, 15°22'8" W), we deployed eight

floating *in situ* mesocosms, which are the shorter equivalents of the KOSMOS mesocosm design (Riebesell et al., 2013). They are 2 m in diameter, 4 m long and possess a 1 mm thick bag made of transparent polyurethane. Their cylindrical main body tapers off into a conical sediment trap at the bottom, from which sinking material can regularly be sampled. On the 6th of September (experimental day 0) they were filled simultaneously with ~8 m^3 of oligotrophic water from outside the harbor. During the filling, a 3 mm mesh at the water inlet kept larger organisms from entering the mesocosms.

During the 35 day-long experiment, the enclosed plankton communities were subjected to recurring additions of nutrient-rich deep water. The water was collected west of Gran Canaria at ~120-160 m depth at two different locations (27°52'16" N, 15° 18'48" W and 28°00'01"N, 15°20'11"W). Before the deep water addition to the mesocosms, inorganic nutrients were added to reach our desired nutrient levels. Thereby, C, N and P were supplied at Redfield ratios (C:N:P = 106:16:1), reaching nitrate concentrations of 30 µmol L^{-1} with corresponding 1.9 µmol L^{-1} of phosphate and 199 µmol L^{-1} of additional dissolved inorganic carbon. Nitrate thereby served as the reference for the Si:N treatment. Silicic acid ($Si(OH)_4$) was added in different amounts (between 2 and 40 µmol L^{-1}, Figure 1A) to achieve the specific treatment levels. These were chosen to mimic the different stoichiometries of potential source waters from different locations (Sarmiento et al., 2004; Griffiths et al., 2013) and depths (Llinás et al., 1994; Sarmiento et al., 2007). The first upwelling treatment was carried out on day 6, and was repeated every other day until day 32 (Figure 1B).

Iron influences Si:N ratios in pelagic systems. Upwelled deep waters stripped of iron, for example, can limit productivity and elevate the uptake of Si relative to other nutrients by diatoms (Hutchins and Bruland, 1998; Hutchins et al., 1998; Jickells et al., 2005). Yet, given the geographic location and experimental facility, we did not control for iron in our study. Firstly, iron inputs are plentiful around Gran Canaria through atmospheric dust deposition (López-García et al., 2021) and resuspension from shelf sediments. Secondly, contamination via measurement devices generally causes relatively high dissolved iron (dFe) concentrations inside mesocosms. In another one of our studies at the same location and in the same season that deployed the same set of mesocosms, dFe ranged from 0.54 to 4.15 nM (pers. comm. Magdalena Santana). The same mesocosm system off the coast of Peru ranged from 3.1 to 17.8 nM dFe (Bach et al., 2020). These dFe concentrations are substantially higher than in Atlantic Ocean surface waters (0 to ~1.0 nM, Sarthou et al., 2003; Bergquist and Boyle, 2006; Rijkenberg et al., 2014; Hatta et al., 2015; Tonnard et al., 2020). Iron was likely also abundant in our experiment and not limiting diatoms.

To maintain the pelagic quality of the enclosed ecosystems, the mesocosm bags were cleaned regularly using a ring-shaped wiper or by divers equipped with brushes to prevent the attachment of fouling organisms (Figure 1B). For more information on the experimental setup, the mesocosm maintenance and the deep water collection see Goldenberg et al. (2022).

The small pelagic silverside *Atherina presbyter* was introduced to each mesocosm as early juvenile (n = 45, length = 17 mm) and young larvae (n = 36, length = 9 mm) on day 15. They were removed from the mesocosms on day 21 to assess survival and growth. The mesozooplankton community was depleted by the fish and could not recover. Given that all mesocosms were affected equally, this restructuring of the food web unlikely biased our Si:N treatment. Before fish introduction, there had already been a pronounced mismatch between phyto- and mesozooplankton in all mesocosms, as primary producers with short generation times rapidly outgrew their grazers (Goldenberg, unpublished data). During the experimental period organic matter export was hence

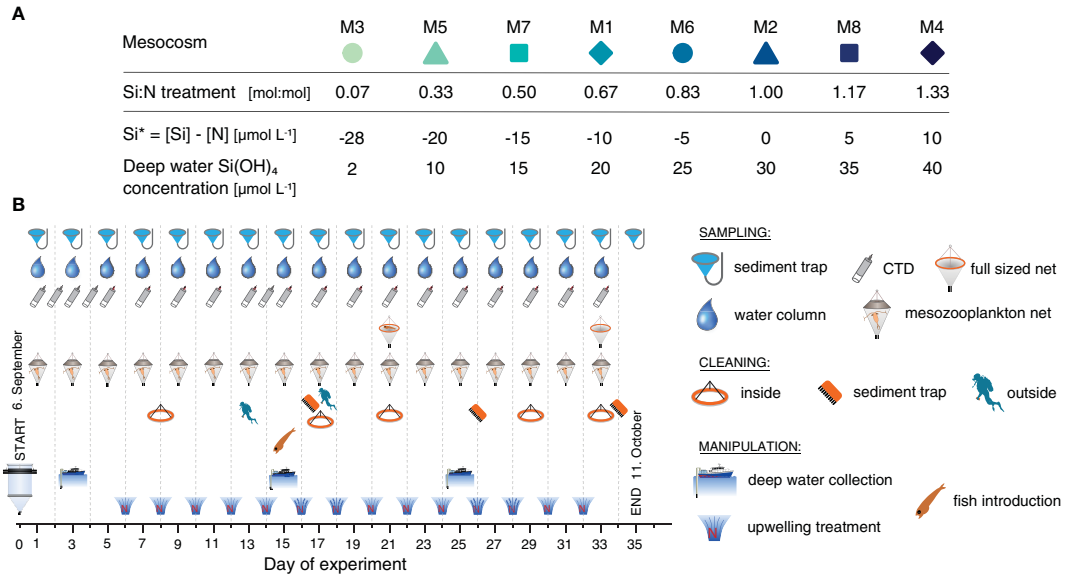

FIGURE 1
Si:N treatment per mesocosm **(A)** and experimental timeline with sampling, cleaning and manipulation schedule **(B)**.

based on a truncated food web, in which phytoplankton could grow unchecked by mesozooplankton grazers.

2.2 Sampling procedure

Water column and sediment trap samples were taken every to every second experimental day for the analysis of various biogeochemical and ecological parameters. The samples were analyzed in the nearby laboratory facilities of the Plataforma Oceánica de Canarias (PLOCAN) and the University of Las Palmas de Gran Canaria (ULPGC). Integrated water column samples were taken using submersible, 2.5 m long plastic tubes (Ø 53 mm, 5.13 L). They were transferred to 10 L carboys and stored dark and cold until arrival in the laboratory. There, they were subsampled for the analysis of phytoplankton abundances, composition and biomass and concentrations of particulate biogenic matter. Mesozooplankton samples were taken with tubes and nets (Apstein Ø 17 cm, 56.7 L, 55 µm mesh size). Sedimented material was sampled every second day through the hose attached to the sediment traps by means of a manual vacuum pump (<0.3 bar). It was collected in 5 L glass bottles (Schott Scandinavia, Denmark) and stored dark until further processing. In the lab, the sediment bottles were gently rotated to homogenize the material, and subsequently subsampled for measurements of sinking velocity and remineralization rates. The remainder of the material was prepared for the analysis of particulate biogenic matter, including particulate organic carbon, nitrogen and phosphorus (POC, PON, POP), total particulate carbon (TPC) and biogenic silica (BSi).

2.3 Sample processing and measurement

2.3.1 Sediment trap material

After subsampling, the settled biogenic matter had to be separated from sea water (see Boxhammer et al., 2016). 3 mol L^{-1} of ferric chloride ($FeCl_3$) were added to the sediment bottles to make the material flocculate, followed by 3 mol L^{-1} of NaOH as a pH buffer, after which the bottles were left alone for 1 h to let the material settle. Subsequently, the supernatant sea water was carefully decanted. The sediment suspension was then centrifuged at ~5,200 *g* for 10 min in a 6–16KS centrifuge (Sigma Laborzentrifugen, Germany), and then again at ~5,000 *g* for 10 min in a 3K12 centrifuge (Sigma). This yielded sediment pellets, which were frozen at –20°C and transported to Kiel, where their elemental composition was analyzed. In Kiel, the pellets were freed of any leftover moisture by freeze-drying and ground in a cell mill (Edmund Bühler, Germany), to obtain fine and homogeneous sediment powder. This powder was then weighed and subsequently subsampled for TPC, POC, PON, BSi and POP measurements.

Subsamples for TPC and PON were transferred into tin cups (8 × 8 × 15 mm, LabNeed, Germany) and measured after Sharp (1974) in duplicates on a Euro EA-CN analyzer (HEKAtech, Germany). POC subsamples were fumed with 1 mol L^{-1} HCl to remove the particulate inorganic carbon (PIC) fraction and dried at 50°C overnight before they were measured similarly. The PIC content was estimated as the difference between TPC and POC. As there were no treatment effects on PIC export, this parameter is not shown in this study. Biogenic silica and particulate organic phosphorus concentrations were measured spectrophotometrically following Hansen and Koroleff (1999). The mass fluxes to the sediment trap were calculated by upscaling the measured C, N, Si and P concentrations in the subsamples to the total sample weight. The mass fluxes were then normalized to the time between sample collection (48 h) and to the mesocosm volume to obtain daily mass fluxes in µmol L^{-1} d^{-1}. The relative contribution of BSi (BSi fraction) to the total export flux as a proxy for BSi ballasting was calculated according to Bach et al. (2016).

$$BSi\ \ fraction = \frac{2.1\ \frac{g}{cm^3} * BSi}{1.06\ \frac{g}{cm^3} * POC + 2.1\ \frac{g}{cm^3} * BSi + 2.7\ \frac{g}{cm^3} * PIC} \quad (1)$$

where the daily export fluxes of BSi, POC and PIC are multiplied with their respective densities (Klaas and Archer, 2002).

2.3.2 Water column samples

The integrated water samples were analyzed for their POC, PON and total particulate carbon (TPC) concentrations. Therefore, subsamples were taken in our on-shore labs and the suspended particles were collected on pre-combusted glass fiber filters (0.7 µm, Whatman). Filters for POC and PON analyses were acidified for ~2 h with 1 mol L^{-1} HCl to remove the inorganic carbon fraction. Filters for POC/N and TPC were then dried for 24 h at 60°C in pre-combusted glass petri dishes. They were packed into tin cups and transported back to Kiel, where their carbon and nitrogen contents were measured on a CN analyzer, as described for sedimented matter above. The particulate inorganic carbon content was estimated as the difference between TPC and POC. Since we did not find consistent evidence for the presence of particulate inorganic carbon (Goldenberg et al., 2022), we pooled the TPC and POC/N filters to obtain POC and PON duplicates.

Diatom biovolume was estimated using the Utermöhl method (Edler and Elbrächter, 2010). Water samples were fixed with Lugol's iodine (final concentration of 1%) and stored inside 250 mL brown glass bottles. Subsamples were transferred to settling chambers (20–50 mL), from which cells were counted after 24 h using inverse light microscopy. A minimum of 500 phytoplankton cells per taxa were counted and identified to the lowest possible taxonomic level. Due to the high phytoplankton abundances, not all cells per subsample were counted, but a minimum of 500 cells across all taxa. The dimensions of the dominant taxa were regularly measured, and, based on average sizes, their specific biovolumes were calculated (Olenina et al., 2006). Total diatom biovolume was calculated from cell abundances and per capita biovolume.

2.3.3 Sinking velocity of sediment trap particles

In order to assess the potential transfer efficiency of sinking particles, we measured sinking velocities (SV) of particles in the 40–1000 µm size spectrum. We therefore used a video microscopy method, which was developed by Bach et al. (2012) and further reworked by Bach et al. (2019) and Baumann et al. (2021). Diluted

sediment subsamples were transferred to a sinking chamber (1 x 1 cm edge length), which was vertically mounted on a FlowCam device (Fluid Imaging Technologies, United States). Settling particles were therein recorded for 20 min at ~7 fps. Particle sinking velocities were calculated by fitting a linear model to the y-positions of multiple captures of the same particle and their respective time stamps. The calculations were carried out using the MATLAB software (version R2018b). Particles out of focus were excluded from the analysis based on the blurriness of their contour lines. Wall effects of the sinking chamber were corrected for using the equation in Ristow (1997). Because of the temperature-dependence of sinking velocity measurements (Bach et al., 2012), our laboratory was temperature-controlled and set to 22–23°C, depending on the daily *in situ* mesocosm temperatures.

Alongside sinking velocity, particle size as equivalent spherical diameter (ESD) and porosity (i.e. compactness) as a size-normalized measure for particle intensity (P_{int}) were measured. The underlying assumption of our porosity-proxy was that porous particles appear brighter (translucent) whereas more compact ones appear darker (opaque). High intensity values (i.e. brighter images) thus resulted in high porosities and vice versa. As large particles are generally more porous than small ones (Laurenceau-Cornec et al., 2020), our porosity-proxy is size-dependent, and was calculated following Bach et al. (2019):

$$P_{int} = (intensity/255)^2 * ESD \quad (2)$$

We analyzed sinking velocity and particle properties in four different particle classes: small (40–100 µm), medium (100–250 µm) and large particles (250–1000 µm), as well as the fastest 10% of sinking particles across the three size fractions. For every measurement (i.e., mesocosm X on day Y) we calculated mean sinking velocities and particle properties in each of these classes across all measured particles. As fast sinking particles are particularly important for carbon sequestration processes (see Section 4.1) and since we detected the strongest treatment effects in this particle class, we mainly focus on the fast sinking particle class in our analysis. Note that size fractions that included fewer than five particles were removed from the analysis, which encompassed the 250–1000 µm size fraction of M4 on days 5 and 21. This threshold shall prevent outliers based on a handful of data points to drastically affect statistical data analysis.

2.3.4 Remineralization rates of sinking particles

The other factor that determines the transfer efficiency of particulate matter exported via the biological carbon pump is its remineralization rate. The higher it is, the lower the efficiency of carbon transfer to depth. Here, we measured the carbon-specific remineralization rate of sedimented material every 4 days via the oxygen depletion rate in dark-incubated sediment. Therefore, seven 330 mL glass bottles (Schott) were sampled headspace-free from the water column of each mesocosm. Four of these were used as replicates and three as controls ((4 + 3) bottles × 8 mesocosms = 56 bottles in total). They were transported dark and cool to the temperature-controlled lab (daily *in situ* temperature), where they acclimatized for 2 h in a water bath. There, between 0.5–3 mL of sediment suspension from sediment subsamples of the respective mesocosm was carefully added to the replicate bottles, while the controls were left untreated. A plastic pipette with a widened tip was used for the sediment addition to keep aggregates intact. All bottles were then incubated in darkness on a rotating plankton wheel (~1 rpm), and oxygen depletion over time was measured. O_2 measurements were carried out non-invasively on PSt3 optodes (PreSens Precision Sensing, Germany) mounted inside the bottles using a handheld optical measurement device (Fibox4 Trace, PreSens). They were automatically corrected for temperature, which was measured in a dummy bottle, and for atmospheric pressure measured by the Fibox4. Salinity was corrected for using the respective mesocosm salinity, measured by CTD casts on the respective day. The eight incubations lasted on average ~27 h, during which 5–8 O_2 measurement were carried out in intervals of 2–6 h. After the incubations the particulate matter inside the bottles was collected on pre-combusted glass fiber filters (0.7 µm, Whatman) and their POC contents analyzed similarly as for the suspended particle filters.

Carbon-specific remineralization rates (C_{remin}, d^{-1}) were calculated by dividing the O_2 depletion rate (r in µmol O_2 L^{-1} d^{-1}) of the sediment material by its measured POC content (µmol C L^{-1}) at the end of the incubation:

$$C_{remin} = \frac{(r * RQ)}{(POC + r * RQ * \Delta t)} \quad (3)$$

Thereby, RQ is the respiratory quotient (µmol C µmol O_2^{-1}), commonly regarded as 1, i.e. 1 mol CO_2 produced: 1 mol O_2 consumed (Ploug and Grossart, 2000; Iversen and Ploug, 2013; Bach et al., 2019), and the time interval between the start of the incubation and the filtration start is factored in as Δt (d). C-specific remineralization rates were calculated for both sediment-containing bottles and blank bottles with only mesocosm water. The remineralization rates of the sedimented particulate matter were calculated by correcting the rates of the sediment-containing bottles for the rates in the blank bottles.

Finally, we calculated the remineralization length scale (RLS, m) as the quotient of sinking velocity (SV, m d^{-1}) and carbon-specific remineralization rates (C_{remin}, d^{-1}). It resembles the vertical distance over which 63% of the sinking POC flux are being remineralized back to inorganic carbon (Cavan et al., 2017).

$$RLS = \frac{SV}{C_{remin}} \quad (4)$$

2.4 Data analysis

The eight mesocosms were replicates along the established Si:N artificial upwelling gradient, sampled repetitively throughout the experiment. Linear mixed effects models with random intercept were used to detect effects of the upwelled Si:N ratio and its change over time on export parameters (vertical fluxes and stoichiometries, particle sinking velocities and degradation rates). Si:N and experimental Day were employed as continuous and categorical fixed effect, respectively, and Mesocosm as random effect. The

interaction term of Si:N × Day was employed as additional fixed effect to test how the Si:N effect changed over time. This is particularly relevant for pelagic food webs, in which temporal dynamics can strongly affect ecosystem responses to environmental changes such as upwelling. To assess the effect of silicon-associated export mechanisms (e.g. BSi ballasting) on particle sinking velocity more directly, the exported Si:N ratio (i.e. exported BSi to exported PON, Figure S1) was established as continuous explanatory variable in addition to upwelled Si:N (see Tables S2F–I).

The models were fit using restricted maximum likelihood and a type III test with Satterthwaite's approximation. All data analyses were carried out with R (version 4.1.2, R Core Team, 2021; RStudio Team, 2022). For data exploration and visualization the "tidyverse" package was used (Wickham et al., 2019). Statistical testing was performed using "lme4" (Bates et al., 2015) and "lmerTest" (Kuznetsova et al., 2017) at a significance level of $\alpha = 0.05$. Normality of residuals and random effects were checked with Q-Q plots, homogeneity of variance with residuals versus fitted plots (package "performance" (Lüdecke et al., 2021). Data was transformed where necessary. In addition, the temporal development of the Si:N effect was examined. Therefore, linear regressions for each sampling day were computed and their slopes ± 95% confidence intervals plotted over time.

Based on the daily export fluxes and stoichiometric ratios (see Figures 2B–E; Figure S1), we segmented the experiment into three phases to be able to discuss our results more comprehensively: oligotrophic baseline (days 3–9), initial response (days 11–21) and long-term response (days 23–35).

3 Results

3.1 Diatom community and particulate matter export

Artificial upwelling fueled diatom growth in all mesocosms. High Si fertilization additionally accelerated bloom development during the initial growth phase (Goldenberg et al., 2022). The diatom blooms were formed mainly by the chain-forming *Leptocylindrus* and the pennate *Pseudo-nitzschia* genera. Both are ubiquitous (Trainer et al., 2012; Ajani et al., 2021) and *Leptocylindrus* has often been abundant in mesocosm experiments (Roberts, 2003; Taucher et al., 2018b; Ortiz et al., 2022). *Pseudo-nitzschia* is known to produce the toxin domoic acid, of which we found no relevant concentrations in our experiment. Throughout the treatment application, diatom abundances and total biovolume were higher under Si-rich upwelling than under Si scarcity (Figure 2A), indicating that abundant Si promoted plenty of building material for frustules.

The diatom blooms caused increased export of freshly produced particulate matter to the sediment traps (Figure 2B). This material was characterized by elevated C:N ratios compared to pre-upwelling conditions (Figure 2C). Higher upwelled Si:N ratios further enhanced both particulate organic carbon export and exported C:N ratios during the initial treatment response phase (days 11–21). Actively managing silicon to nutrient ratios thus affected the export of organically bound carbon during the system's adjustment to artificial upwelling.

Increased export fluxes as a response to upwelling and to high Si:N ratios were primarily observed for carbon, nitrogen and silicon pools (see Figures 2B, D; Figure S1). Particulate organic carbon and nitrogen export increased on average 3- and 2.5-fold from the pre-treatment (days 3–9) to the initial response phase (days 11–21), respectively, while biogenic silica export increased 1.7-fold. In contrast, the export of total particulate phosphorus did not increase (Figure S1). The Si:N treatment was reflected most clearly by the biogenic silica flux, the BSi fraction of the total flux (Figures 2D–E) and the exported Si:N ratio during the initial and long-term response phases (Figure S1). Si-rich upwelling did thus not only cause a higher BSi flux, but also increased the BSi ballasting of sinking particles (Table S1). Both effects persisted throughout the initial and long-term response phases. In contrast, the positive Si:N effect on POC export and exported C:N ratios disappeared during the long-term response phase. The peak in the export flux parameters on day 19 (Figures 2B, D; Figure S1) was likely a consequence of the cleaning of the inside mesocosm walls and the sediment traps on day 17 (compare Figure 1; Figures 2B, D). This removed the biofilm and fouling organisms from the vertical mesocosm walls and brushed particles off the walls of the funnel-shaped sediment trap into the collection container.

3.2 Sinking particle characteristics

The nutrient composition in the upwelled water affected the properties of sinking particles. Surprisingly, high Si:N in upwelled waters temporarily decreased sinking velocity and size of the fastest sinking particles (Figures 3B–F). The effect was similar, although slightly weaker, for sinking velocities classified by particle size (Figure S2; Table S2). These effects occurred mainly between days 17 to 25. During this time, the relationship between the exported Si:N ratio and sinking velocity (or particle size) yielded similar results (Figures 3D, H; Table S2F-I). This shows that a high proportion of biogenic silica ballast correlated with smaller sizes and lower sinking speeds of the fast sinking particle fraction. Moreover, the reduced sinking speeds in the high Si:N treatments were not only associated with smaller sizes, but possibly also with lower particle porosities (Figure 3G).

The remineralization rates of sinking particulate matter increased when freshly produced material sank to the sediment traps at the onset of the upwelling treatment and subsequently decreased again towards the end of the experiment (Figure 3A). In contrast to sinking velocities, remineralization rates were however not affected by the upwelled Si:N ratio (Table S2), except for day 15, on which there was a small positive effect.

We found that high sinking velocities of fast sinking particles were associated with low to moderate diatom presence, whereas high diatom abundances did seemingly not allow for fast sinking (Figure 4A). Likewise, fast sinking particles and high C:N ratios did not co-occur while the Si:N treatment effect was strongest (Figure 3E; Figure 4B). Hence, the exported particles in between days 17 and 25 were either fast sinking or carbon-rich, but not both. Finally, only a part of the over-consumed carbon under high Si:N upwelling was exported. Under high Si:N, the C:N ratios of

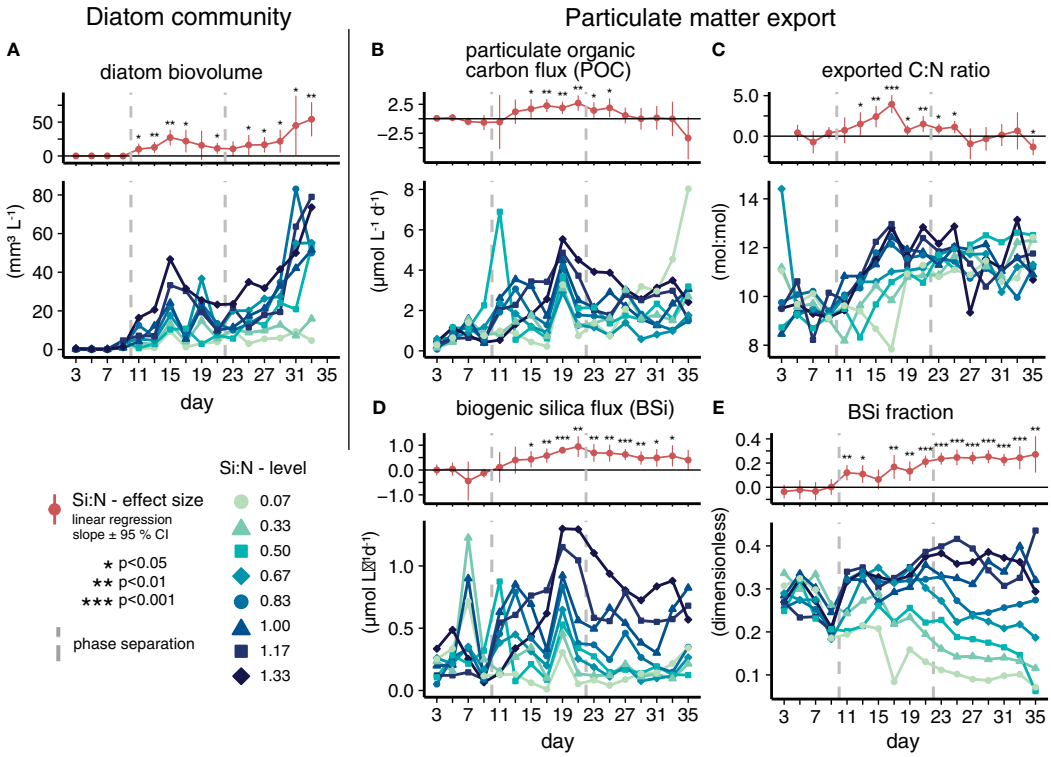

FIGURE 2
Suspended diatoms **(A)** and particulate matter export **(B–E)** under varying Si:N of upwelled water. The detailed development of individual mesocosms (lower subpanels) and the effect of the Si:N treatment across all 8 mesocosms on each day (upper subpanels) are provided. Units are valid for both panels.

suspended particles were very high (~10–17.5 mol:mol), however, the exported matter was carbon-depleted relative to the suspended material (Figure 4C). This indicates a retention of C in the water column. In contrast, under low Si:N, suspended particle C:N ratios were relatively low (~5–12 mol:mol), and exported matter was carbon-enriched compared to the suspended material (retention of N in the water column, Figure 4C). This indicates that the additionally taken-up carbon under high Si:N was partly retained as suspended POC (i.e. non-sinking particles) in the water column instead of being channeled into export production. The amount of silicon relative to nitrogen in artificially upwelled water thus affected export-related parameters in counteracting ways.

4 Discussion

4.1 Counteracting effects of Si:N upwelling

POC export and associated C:N ratios increased after the onset of artificial upwelling. This finding is similar to an earlier artificial upwelling mesocosm study (Baumann et al., 2021). The Si:N composition in the artificially upwelled water had positive effects on the magnitude of the export flux as well as its C:N stoichiometry, both of which is beneficial for potential carbon sequestration. This was caused by higher diatom abundances and elevated C:N ratios of suspended particles during the initial response phase of Si-rich upwelling (Goldenberg et al., 2022). Upwelled Si:N further had a lasting positive effect on biogenic silica export and the relative contribution of BSi ballast to sedimented matter. High upwelled Si:N ratios thus promoted several key factors which should in theory favor the carbon sequestration potential.

Curiously though, the more than 3-fold increase in BSi ballast under Si-rich upwelling did not result in higher particle sinking velocities. On the contrary, particles under enhanced BSi ballasting in the highest Si:N treatment temporarily sank only about half as fast as particles in the lowest Si:N treatment. The reason for this was most likely that particles under Si-replete conditions were ~100 µm smaller than the ones experiencing Si-scarce upwelling. As sinking velocity is usually positively affected by particle size for similar particle types (Cael et al., 2021), the decreased particle size apparently outweighed the positive effect of enhanced BSi ballast. Although we found this negative Si:N effect on sinking velocities for almost all considered particle size classes, it was most prominent for those particles that sank fastest (Table S2). These fast sinking particles can be considered the most important contributor to the biological pump as they reach the sequestration depth most rapidly and spend the least amount of time in the mesopelagic zone, where the majority of remineralization occurs (Mayor et al., 2014; García-Martín et al., 2021). Additionally, they are often large and hence incorporate high amounts of organic carbon. The speed with which the fastest particles sink is thus an important predictor for carbon sequestration processes (Riley et al., 2012).

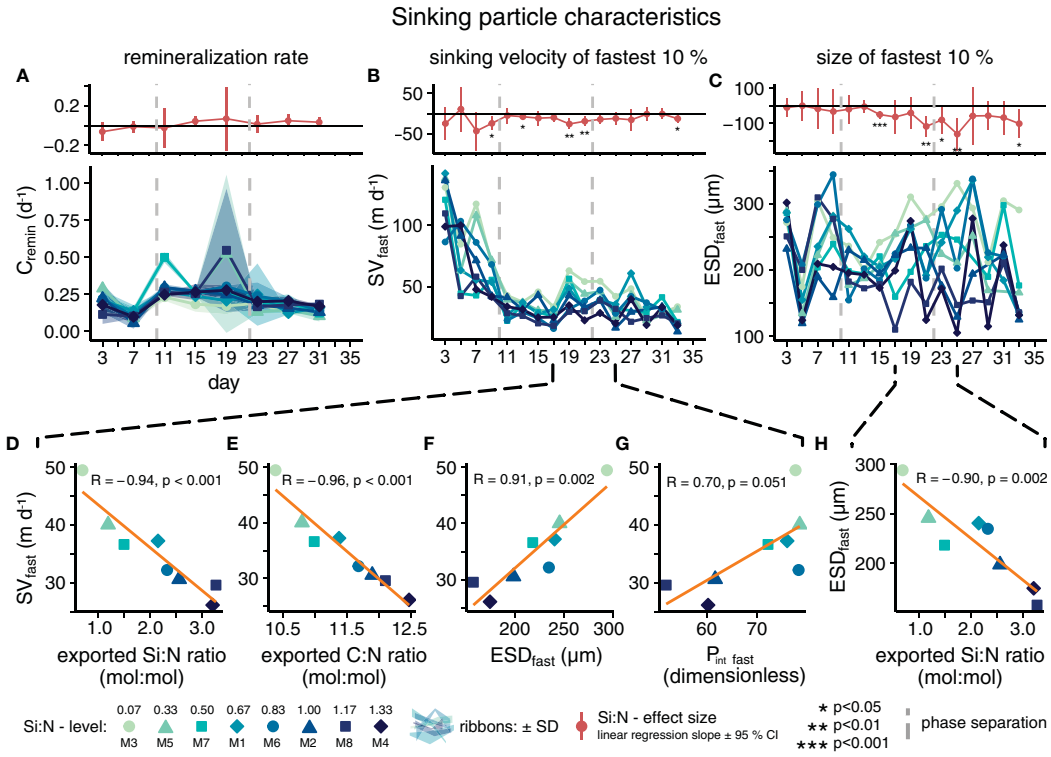

FIGURE 3
Development of sinking particle characteristics over time with daily Si:N effect sizes **(A–C)** and relationship between key export parameters **(D–H)**. Particle sinking velocities, sizes and porosities in **(B–H)** are means of the fastest 10% of sinking particles **(B–F)**. **(D–H)** incorporate mean data from days 17 to 25, the period of strongest, negative Si:N effects.

Our *ex situ* sinking velocity measurements may have been affected by our sediment sampling and processing: Both aggregation and disaggregation processes might thereby have altered the particle size distribution and sinking velocities to some (unknown) extent. As all samples were handled equally, they might have all been affected similarly by such systematical methodological artefacts. However, since the quality of sinking particles varied across Si:N treatments, it is possible that the handling influenced samples in different ways. For instance, more fragile aggregates might have been affected more strongly than sturdier ones. Thus, we cannot exclude the possibility that the negative Si:N effect on particle size was influenced by sample handling, i.e. that samples

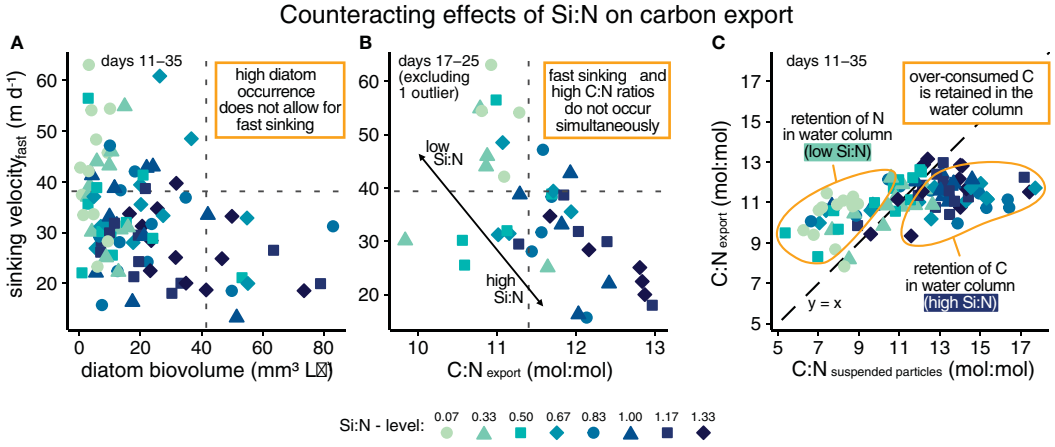

FIGURE 4
Summary figure displaying the counteracting effects of upwelled Si:N on export related parameters **(A-C)**. The dashed line in **(C)** indicates no change in C:N ratios from suspended to exported particles. Note that the data point M3 on day 17 was excluded as an outlier (exported C:N ratio: 7.8 mol: mol, sinking velocity of fastest 10%: 33.4 m d^{-1}).

under high Si:N were more fragile and experienced more disaggregation than under Si scarcity.

Another counterintuitive finding was the positive – albeit borderline insignificant – correlation between sinking velocity and particle porosity at the end of the initial response phase (Figure 3G). Theoretically, porosity should negatively affect a particle's sinking velocity by lowering its density (Laurenceau-Cornec et al., 2020). We assume that the reason for our contradictory result is the size-dependency of porosity (see Equation (2)). Very porous particles were also large and therefore likely sank more quickly (Alldredge and Gotschalk, 1988; Xiang et al., 2022). Increasing size might have accelerated particles despite decreasing BSi ballast and increasing porosity.

The question remains why increased Si availability drove smaller sizes and lower sinking velocities during the end of the adjustment phase. The slower sinking could possibly be explained by elevated exudation of transparent exopolymer particles (TEP) under Si-rich upwelling. TEP can act as "biological glue" and promote aggregation, but it can also retain suspended matter in the surface layer due to its positive buoyancy (Mari et al., 2017). During an earlier mesocosm campaign in the Canary island region, TEP increased sharply following a simulated artificial upwelling event (Taucher et al., 2018a), and was provided as the reason for the decrease of particle sinking velocities (Bach et al., 2019). Whilst we did not measure TEP in the current study, the association of high C:N ratios with slow sinking velocities hint at its presence . The conditions for its exudation were favorable under high Si:N upwelling. Firstly, nutrients were quickly depleted following each deep water addition (Goldenberg et al., 2022), resulting in regular nutrient limitation that encourages TEP exudation (Obernosterer and Herndl, 1995; Mari et al., 2017). Secondly, diatoms that are typical TEP producers under post-bloom conditions (Taucher et al., 2015; Taucher et al., 2018a) were more abundant under Si-rich upwelling.

TEP exudation could explain why carbon-rich particulate matter sank slowly under high upwelled Si:N. However, one would concurrently expect increased aggregation and hence larger particles. Yet, we observed the opposite. Figure 5 shows representative images of a subsample of sedimented material aligned along the Si:N upwelling gradient. Under Si scarcity particles were large and contrasted strongly with the background, whereas under abundant Si, single particles were smaller and hardly distinguishable. Potentially, TEP exuded under high Si:N was more numerous but less sticky, leading to smaller, more slowly sinking aggregates. Another possibility is that sampling procedures broke apart aggregates under high upwelled Si more easily. In the end, these explanation attempts remain speculative and the mechanism for the negative Si:N effect on sinking velocities and particle sizes cannot be fully disclosed.

Summing up, enhancing the proportion of Si in artificially upwelled water increased BSi ballasting of sinking particles but also resulted in a rather counter-intuitive decrease in particle sizes and ultimately lower sinking velocities. Furthermore, remineralization of sinking particles did not change with upwelled Si:N ratio, indicating that BSi apparently did not shield organic matter from respiration (Boyd and Trull, 2007). High BSi ballasting did thus not go hand in hand with beneficial particle properties for transfer efficiency. When considering the correlations between BSi and POC fluxes in the deep ocean (Klaas and Archer, 2002), our findings suggest that in the surface ocean the positive effects of BSi ballasting on POC fluxes are superimposed by other drivers. For example, the enhanced formation of positively buoyant TEP could exert a negative control on sinking velocities (Azetsu-Scott and Passow, 2004) and retain carbon-rich material in the surface (Mari et al., 2017). As particles sink through the epi- and mesopelagic zones, the preferential remineralization of organic material, including TEP, might leave a higher fraction of BSi behind and could thus be the reason for the observed correlations between POC and BSi at depth (Sanders et al., 2010). It is important

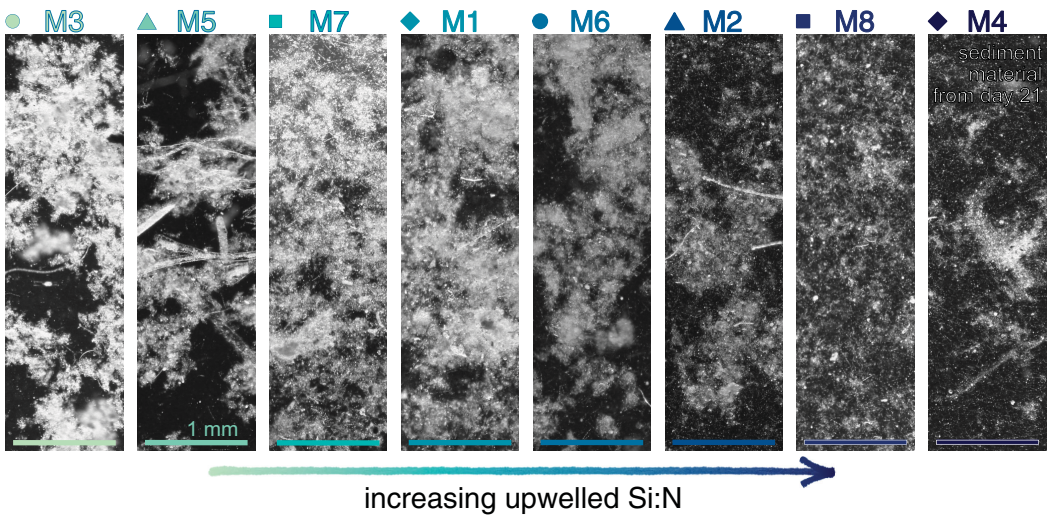

FIGURE 5
Material sampled from the sediment trap of each mesocosm on day 21. Pictures were taken on a stereo microscope (Stemi 305, ZEISS) and are displayed on a greyscale to emphasize structural differences.

to note that due to the strong mismatch between phytoplankton and mesozooplankton grazers during this experiment, the latter did not play a major role for export production via e.g. repackaging and fecal pellet production. Therefore, our findings on how the upwelled Si:N ratio affected export parameters may not apply to systems in which mesozooplankton exerts a strong top-down control. Under such conditions, reworking of suspended and sinking particles might lead to different particle types sinking, possibly promoting a BSi ballast effect.

4.2 Implications for artificial upwelling as negative emission technology

The various Si:N effects on export parameters in our study were of counteracting nature. Some imply an increased potential for carbon sequestration and thus carbon removal from the atmosphere, others are unfavorable in that aspect (Figure 6). In the following, we will discuss the relative importance of our findings in respect to the carbon removal potential of artificial upwelling.

The key Si:N effects concerning the carbon sequestration potential are the positive effects on POC flux, exported matter C:N ratios and BSi ballasting on the one side, and the negative effects on sinking velocities and the relative difference between suspended and exported C:N ratios on the other (Figure 6). Si-replete conditions temporarily caused more material to be exported from the surface and positively affected the C:N ratio of exported matter, both of which strengthens the biological carbon pump. However, the C:N effect was potentially buffered by the retention of parts of the over-consumed carbon as suspended POC in the water column, and additionally, sinking velocities decreased, which hampered the potential for efficient carbon transfer to depth.

The question is whether the increased POC flux and elevated C:N ratios, or the decreased sinking velocities would have had a larger impact on the realized carbon deep export. The remineralization length scale (RLS), a proxy for the POC transfer efficiency, helps to get an understanding of the relative importance of flux quantity versus quality. Figure 7 shows surface POC fluxes, the RLS and theoretical attenuated POC fluxes at the respective RLS depth for the lowest and highest Si:N treatment on day 21. On this day, there were pronounced and rather linear Si:N effects, making this comparison representative of the range of upwelled Si:N ratios tested here. Due to the 2.5-fold higher particle sinking velocities under low Si:N, the transfer of organic carbon to depth would have likely been more efficient in the lowest compared to the highest treatment (RLS depth more than 2-fold deeper). Nonetheless, the 6-fold higher POC flux under the highest Si availability would have probably led to more POC sinking out of the euphotic zone (50–100 m depth) in this treatment. We can, however, not say whether the enhanced flux attenuation under high Si:N would ultimately lead to less POC reaching the deep ocean than under Si-scarcity. The flux and sinking velocity measurements herein stem from the very surface layer (4 m depth), and it is complicated to predict the fate of sinking matter fluxes to greater depths. Even for approximations, a sophisticated flux attenuation model would be needed, which is beyond the scope of this study. We hence emphasize the importance of incorporating our experimental findings into biogeochemical models. This would help to resolve the relative importance of counteracting effects of artificial upwelling as a carbon removal technique.

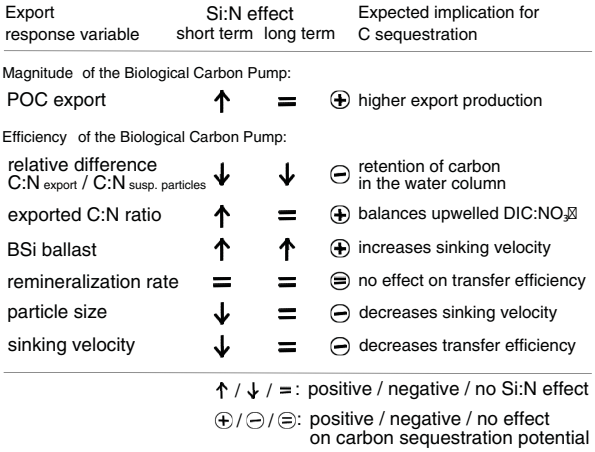

FIGURE 6
Summary of Si:N effects under artificial upwelling on export-related parameters and their implications for the carbon sequestration potential. Short-term (initial response phase, days 11–21) and long-term (long-term response phase, days 23–35) effects are displayed.

When discussing the implications of our results, it is important to differentiate between short and long term effects. The observed short term Si:N effects carry more weight for stationary artificial upwelling applications, which result in one-time fertilization of water patches, e.g. a moored wave pump (Liu et al., 1999; Fan, 2016). Also the remineralization rates, which increased after the onset of artificial upwelling, subsequently decreased again towards the end of the experiment, and thus only temporarily hampered the efficiency of particle transfer. The long-term effects are more important regarding the application of drifting artificial upwelling devices, which fertilize the same patch of water over longer time periods. Concerning recurring upwelling, most of the Si:N effects are thus not crucial, and instead the benefit of increased POC fluxes and enhanced sinking matter C:N ratios would come into play. Those elevated carbon to nutrient ratios would, however, be buffered under Si-rich upwelling by the retention of over-consumed carbon as suspended POC in the water column.

In summary, artificial upwelling enhanced surface ocean POC fluxes and associated C:N ratios, and did so on the time scale of multiple weeks. Additionally, the upwelled Si:N ratio temporarily enhanced carbon assimilation and consequently the POC flux and exported matter C:N ratios. However, the over-consumed carbon was partly retained in the water column, possibly due to the enhanced formation of positively buoyant TEP under high diatom abundances. Furthermore, although Si-rich upwelling enhanced BSi ballasting manifold, changes in particle properties led to temporarily decreased sinking velocities and hence less efficient particle export. Actively managing Si availability under artificial upwelling thus caused conflicting changes to export-relevant system properties of the surface ocean. This indicates that in a real world application it could be challenging to find the

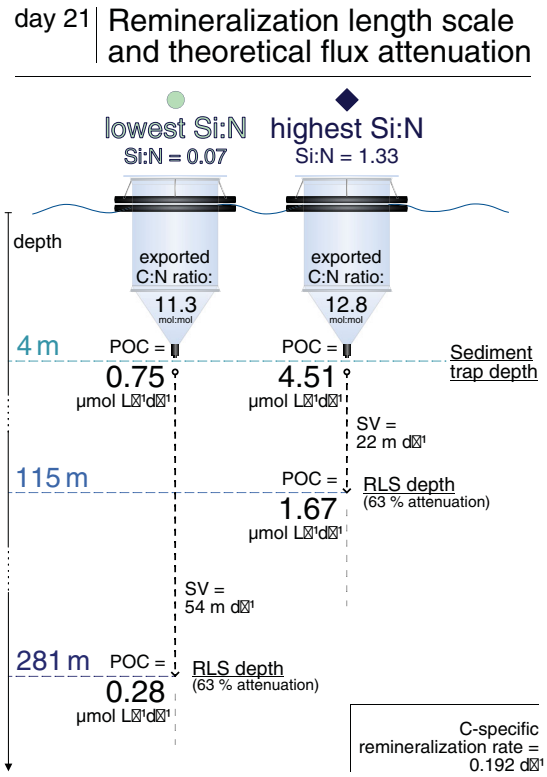

FIGURE 7
Remineralization length scale (RLS) and resulting flux attenuation for the highest and lowest Si:N treatments on day 21. RLSs were calculated from sinking velocities (SV) of the fastest sinking particles on day 21 and remineralization rates from day 23 averaged across mesocosms. See Figure S2 for further RLS data.

right balance between favorable and unfavorable effects on carbon sequestration. In a next step, modelling approaches could help to resolve the relative importance of these findings by incorporating them into POC flux attenuation simulations. Ultimately, artificial upwelling research will need open ocean trials with sophisticated deep flux monitoring in order to verify previous results and accurately assess its carbon sequestration potential.

Data availability statement

The datasets presented in this study can be found in online repositories. The names of the repository/repositories and accession number(s) can be found below: PANGAEA data repository (https://doi.org/10.1594/PANGAEA.956371).

Author contributions

Experimental concept and design: UR, JT, SG, MF-M. Execution of the experiment: MB, SG, JT, MF-M, JO and UR. Data analysis: MB, SG, JH. Manuscript writing: MB with input from all co-authors. All authors contributed to the article and approved the submitted version.

Funding

This study was conducted in the framework of the Ocean Artificial Upwelling (Ocean artUp) and the Road Testing Ocean Artificial Upwelling (Test-ArtUp) projects. The former was funded by an Advanced Grant of the European Research Council, the latter by the German Marine Research Alliance (DAM). The EU project AQUACOSM and the project TRIATLAS (AMD-817578-5) from the European Union's Horizon 2020 provided additional Transnational Access funds.

Acknowledgments

We thank the Oceanic Platform of the Canary Islands (Plataforma Oceánica de Canarias, PLOCAN) and the Marine Science and Technology Park (Parque Cientiífico Tecnoloìgico Marino, PCTM) from the University of Las Palmas (Universidad de Las Palmas de Gran Canaria, ULPGC) for providing research facilities as well as logistical and technical support before, during and after this experiment. We are grateful to the staff and students from the KOSMOS team (GEOMAR) and the ULPGC biological oceanographers for organizing and carrying out the experiment. Finally, we thank Greta Wunderlich, Jana Meyer and Levka Hansen for their contribution to data analysis and data exchange.

Conflict of interest

The authors declare that the research was conducted in the absence of any commercial or financial relationships that could be construed as a potential conflict of interest.

Publisher's note

Supplementary material

The Supplementary Material for this article can be found online at: https://www.frontiersin.org/articles/10.3389/fmars.2023.1181351/full#supplementary-material

SUPPLEMENTARY FIGURE 1
Particulate matter export flux (daily flux, cumulative flux and elemental ratios) and daily Si:N effect sizes. Effect sizes of exported C:N and exported Si:N ratios on day 3 were removed in order to improve readability (-1.64 ± 4.15 and -4.55 ± 9.14 mol mol^{-1}, respectively).

SUPPLEMENTARY FIGURE 2
Sinking velocities for different size fractions of the 40–1000 µm size spectrum and remineralization length scale (RLS) including daily Si:N effect sizes. RLS was calculated by dividing velocities of the fastest 10% of sinking

particles (SV_{fast}) by particle remineralization rates (C_{remin}) and is limited to the days for which there are remineralization rate measurements.

SUPPLEMENTARY TABLE 1
Linear mixed models showing the effects of artificial upwelling on particulate matter flux and stoichiometries. Si:N, Day (day 11–33) and Si:N × Day were deployed as fixed effects and Mesocosm as random effect. Significant fixed effects to be interpreted are displayed in bold. MS: mean squares; df_{Num} and df_{Den}: numerator and denominator degrees of freedom; $R^2_{marginal}$: proportion of variation explained by all fixed effects

SUPPLEMENTARY TABLE 2
(A–E): Linear mixed models showing the effects of artificial upwelling on sinking velocities and carbon-specific remineralization rate. **(F-I)**: Linear mixed models showing the relationship between sinking velocities and the Si:N ratio of the particulate export flux (BSi : PON). Si:N (or exported Si:N ratio for **(F-I)**), Day (day 11–33) and Si:N × Day were deployed as fixed effects and Mesocosm as random effect. Significant fixed effects to be interpreted are displayed in bold. MS: mean squares; df_{Num} and df_{Den}: numerator and denominator degrees of freedom; $R^2_{marginal}$: proportion of variation explained by all fixed effects

References

Ajani, P. A., Petrou, K., Larsson, M. E., Nielsen, D. A., Burke, J., and Murray, S. A. (2021). Phenotypic trait variability as an indication of adaptive capacity in a cosmopolitan marine diatom. *Environ. Microbiol.* 23, 207–223. doi: 10.1111/1462-2920.15294

Alldredge, A. L., and Gotschalk, C. (1988). In situ settling behavior of marine snow. *Limnol. Oceanogr.* 33, 339–351. doi: 10.4319/lo.1988.33.3.0339

Allen, J. T., Brown, L., Sanders, R., Mark Moore, C., Mustard, A., Fielding, S., et al. (2005). Diatom carbon export enhanced by silicate upwelling in the northeast Atlantic. *Nature* 437, 728–732. doi: 10.1038/nature03948

Armstrong, R. A., Lee, C., Hedges, J. I., Honjo, S., and Wakeham, S. G. (2002). A new, mechanistic model for organic carbon fluxes in the ocean based on the quantitative association of POC with ballast minerals. *Deep. Sea. Res. Part II.: Topical. Stud. Oceanogr.* 49, 219–236 doi: 10.1016/s0967-0645(01)00101-1

Armstrong, R. A., Peterson, M. L., Lee, C., and Wakeham, S. G. (2009). Settling velocity spectra and the ballast ratio hypothesis. *Deep. Sea. Res. Part II.: Topical. Stud. Oceanogr.* 56, 1470–1478. doi: 10.1016/j.dsr2.2008.11.032

Azetsu-Scott, K., and Passow, U. (2004). Ascending marine particles: significance of transparent exopolymer particles (TEP) in the upper ocean. *Limnol. Oceanogr.* 49, 741–748. doi: 10.4319/lo.2004.49.3.0741

Bach, L. T., Boxhammer, T., Larsen, A., Hildebrandt, N., Schulz, K. G., and Riebesell, U. (2016). Influence of plankton community structure on the sinking velocity of marine aggregates: sinking velocity of marine aggregates. *Global Biogeochem. Cycles.* 30, 1145–1165. doi: 10.1002/2016GB005372

Bach, L. T., Paul, A. J., Boxhammer, T., von der Esch, E., Graco, M., Schulz, K. G., et al. (2020). Factors controlling plankton community production, export flux, and particulate matter stoichiometry in the coastal upwelling system off Peru. *Biogeosciences* 17, 4831–4852. doi: 10.5194/bg-17-4831-2020

Bach, L. T., Riebesell, U., Sett, S., Febiri, S., Rzepka, P., and Schulz, K. G. (2012). An approach for particle sinking velocity measurements in the 3–400 µm size range and considerations on the effect of temperature on sinking rates. *Mar. Biol.* 159, 1853–1864. doi: 10.1007/s00227-012-1945-2

Bach, L. T., Stange, P., Taucher, J., Achterberg, E. P., Algueró-Muñiz, M., Horn, H., et al. (2019). The influence of plankton community structure on sinking velocity and remineralization rate of marine aggregates. *Global Biogeochem. Cycles.* 33, 971–994. doi: 10.1029/2019GB006256

Bates, D., Mächler, M., Bolker, B., and Walker, S. (2015). Fitting linear mixed-effects models using lme4. *J. Stat. Software.* 67, 1–48. doi: 10.18637/jss.v067.i01

Baumann, M., Taucher, J., Paul, A. J., Heinemann, M., Vanharanta, M., Bach, L. T., et al. (2021). Effect of intensity and mode of artificial upwelling on particle flux and carbon export. *Front. Mar. Sci.* 8. doi: 10.3389/fmars.2021.742142

Bergquist, B. A., and Boyle, E. A. (2006). Dissolved iron in the tropical and subtropical Atlantic ocean. *Global Biogeochem. Cycles.* 20, n/a–n/a. doi: 10.1029/2005GB002505

Boxhammer, T., Bach, L. T., Czerny, J., and Riebesell, U. (2016). Technical note: sampling and processing of mesocosm sediment trap material for quantitative biogeochemical analysis. *Biogeosciences* 13, 2849–2858. doi: 10.5194/bg-13-2849-2016

Boyd, P. W., and Trull, T. W. (2007). Understanding the export of biogenic particles in oceanic waters: is there consensus? *Prog. Oceanogr.* 72, 276–312. doi: 10.1016/j.pocean.2006.10.007

Cael, B. B., Cavan, E. L., and Britten, G. L. (2021). Reconciling the size-dependence of marine particle sinking speed. *Geophys. Res. Lett.* 48. doi: 10.1029/2020GL091771

Cavan, E. L., Trimmer, M., Shelley, F., and Sanders, R. (2017). Remineralization of particulate organic carbon in an ocean oxygen minimum zone. *Nat. Commun.* 8, 14847. doi: 10.1038/ncomms14847

Coale, K. H., Johnson, K. S., Chavez, F. P., Buesseler, K. O., Barber, R. T., Brzezinski, M. A., et al. (2004). Southern ocean iron enrichment experiment: carbon cycling in high- and low-Si waters. *Science* 304, 408–414. doi: 10.1126/science.1089778

Dugdale, R. C., and Wilkerson, F. P. (1998). Silicate regulation of new production in the equatorial pacific upwelling. *Nature* 391, 270–273. doi: 10.1038/34630

Edler, L., and Elbrächter, M. (2010). *The utermöhl method for quantitative phytoplankton analysis, in: microscopic and molecular methods for quantitative phytoplankton analysis* Vol. 55, 13–20 (Paris: UNESCO).

Fan, W. (2016). Experimental study on the performance of a wave pump for artificial upwelling. *Ocean. Eng.* 10. doi: 10.1016/j.oceaneng.2015.12.056

Field, C. B., Behrenfeld, M. J., Randerson, J. T., and Falkowski, P. (1998). Primary production of the biosphere: integrating terrestrial and oceanic components. *Science* 281, 237–240. doi: 10.1126/science.281.5374.237

García-Martín, E. E., Davidson, K., Davis, C. E., Mahaffey, C., McNeill, S., Purdie, D. A., et al. (2021). Low contribution of the fast-sinking particle fraction to total plankton metabolism in a temperate shelf Sea. *Global Biogeochem. Cycles.* 35. doi: 10.1029/2021GB007015

Goldenberg, S. U., Taucher, J., Fernández-Méndez, M., Ludwig, A., Arístegui, J., Baumann, M., et al. (2022). Nutrient composition (Si:N) as driver of plankton communities during artificial upwelling. *Front. Mar. Sci.* 9. doi: 10.3389/fmars.2022.1015188

Griffiths, J. D., Barker, S., Hendry, K. R., Thornalley, D. J. R., van de Flierdt, T., Hall, I. R., et al. (2013). Evidence of silicic acid leakage to the tropical Atlantic via Antarctic intermediate water during marine isotope stage 4. *Paleoceanography* 28, 307–318. doi: 10.1002/palo.20030

Guidi, L., Stemmann, L., Jackson, G. A., Ibanez, F., Claustre, H., Legendre, L., et al. (2009). Effects of phytoplankton community on production, size, and export of large aggregates: a world-ocean analysis. *Limnol. Oceanogr.* 54, 1951–1963. doi: 10.4319/lo.2009.54.6.1951

Hansen, H. P., and Koroleff, F. (1999). *Determination of nutrients, in: methods of seawater analysis, third, completely revised and extended edition* (WILEY-VCH), 159–228.

Hatta, M., Measures, C. I., Wu, J., Roshan, S., Fitzsimmons, J. N., Sedwick, P., et al. (2015). An overview of dissolved fe and Mn distributions during the 2010–2011 U.S. GEOTRACES north Atlantic cruises: GEOTRACES GA03. *Deep. Sea. Res. Part II.: Topical. Stud. Oceanogr.* 116, 117–129. doi: 10.1016/j.dsr2.2014.07.005

Henson, S. A., Lampitt, R. S., and Johns, D. (2012b). Variability in phytoplankton community structure in response to the north Atlantic oscillation and implications for organic carbon flux. *Limnol. Oceanogr.* 57, 1591–1601. doi: 10.4319/lo.2012.57.6.1591

Henson, S. A., Sanders, R., and Madsen, E. (2012a). Global patterns in efficiency of particulate organic carbon export and transfer to the deep ocean: export and transfer efficiency. *Global Biogeochem. Cycles.* 26, 34–1. doi: 10.1029/2011GB004099

Honjo, S., and Manganini, S. J. (1993). Annual biogenic particle fluxes to the interior of the north Atlantic ocean; studied at 34°N 21°W and 48°N 21°W. *Deep. Sea. Res. Part II.: Topical. Stud. Oceanogr.* 40, 587–607. doi: 10.1016/0967-0645(93)90034-K

Hutchins, D. A., and Bruland, K. W. (1998). Iron-limited diatom growth and Si:N uptake ratios in a coastal upwelling regime. *Nature* 393, 561–564. doi: 10.1038/31203

Hutchins, D. A., DiTullio, G. R., Zhang, Y., and Bruland, K. W. (1998). An iron limitation mosaic in the California upwelling regime. *Limnol. Oceanogr.* 43, 1037–1054. doi: 10.4319/lo.1998.43.6.1037

IPCC. (2018). Summary for Policymakers, in: Global warming of 1.5°C. An IPCC Special Report on the impacts of global warming of 1.5°C above pre-industrial levels and related global greenhouse gas emission pathways, in the context of strengthening the global response to the threat of climate change, sustainable development, and efforts to eradicate poverty, edited by: Masson-Delmotte,, V., Zhai,, P., Pörtner,, H.-O., Roberts,, D., Skea,, J., Shukla,, P. R., Pirani,, A., Moufouma-Okia,, W., Péan,, C., Pidcock,, R., Connors,, S., Matthews,, J. B. R., Chen,, Y., Zhou,, X., Gomis,, M. I., Lonnoy,, E., Maycock,, T., Tignor,, M., and Waterfield,, T. (Cambridge, UK: Cambridge University Press), 2018.

Iversen, M. H., and Ploug, H. (2013). Temperature effects on carbon-specific respiration rate and sinking velocity of diatom aggregates – potential implications for deep ocean export processes. *Biogeosciences* 10, 4073–4085. doi: 10.5194/bg-10-4073-2013

Jickells, T. D., An, Z. S., Andersen, K. K., Baker, A. R., Bergametti, G., Brooks, N., et al. (2005). Global iron connections between desert dust, ocean biogeochemistry, and climate. *Science* 308, 67–71. doi: 10.1126/science.1105959

Jin, X., Gruber, N., Dunne, J. P., Sarmiento, J. L., and Armstrong, R. (2006). Diagnosing the contribution of phytoplankton functional groups to the production and export of particulate organic carbon, CaCO3, and opal from global nutrient and alkalinity distributions. *Global Biogeochem. Cycles.* 2. doi: 10.1029/2005gb002532

Klaas, C., and Archer, D. (2002). Association of sinking organic matter with various types of mineral ballast in the deep sea: implications for the rain ratio. *Global Biogeochem. Cycles*. 16, 63. doi: 10.1029/2001gb001765

Kuznetsova, A., Brockhoff, P. B., and Christensen, R. H. B. (2017). lmerTest package: tests in linear mixed effects models. *J. Stat. Soft.*, 82. doi: 10.18637/jss.v082.i13

Lam, P. J., Doney, S. C., and Bishop, J. K. B. (2011). The dynamic ocean biological pump: insights from a global compilation of particulate organic carbon, $CaCO_3$, and opal concentration profiles from the mesopelagic: the dynamic ocean biological pump. *Global Biogeochem. Cycles.* 25, n/a–n/a. doi: 10.1029/2010GB003868

Laurenceau-Cornec, E. C., Le Moigne, F. A. C., Gallinari, M., Moriceau, B., Toullec, J., Iversen, M. H., et al. (2020). New guidelines for the application of stokes' models to the sinking velocity of marine aggregates. *Limnol. Oceanogr.* 65, 1264–1285. doi: 10.1002/lno.11388

Liu, C. C. K., Dai, J. J., Lin, H., and Guo, F. (1999). Hydrodynamic performance of wave-driven artificial upwelling device. *J. Eng. Mech.* 125, 728–732. doi: 10.1061/(ASCE)0733-9399(1999)125:7(728)

Llinás, O., Rodríguez de León, A., Siedler, G., and Wefer, G. (1994). *ESTOC data report 1994*, ICCM, 77.

López-García, P., Gelado-Caballero, M. D., Patey, M. D., and Hernández-Brito, J. J. (2021). Atmospheric fluxes of soluble nutrients and fe: more than three years of wet and dry deposition measurements at gran canaria (Canary islands). *Atmospheric. Environ.* 246, 118090. doi: 10.1016/j.atmosenv.2020.118090

Lüdecke, D., Ben-Shachar, M., Patil, I., Waggoner, P., and Makowski, D. (2021). Performance: an r package for assessment, comparison and testing of statistical models. *JOSS* 6, 3139. doi: 10.21105/joss.03139

Maiti, K., Charette, M. A., Buesseler, K. O., and Kahru, M. (2013). An inverse relationship between production and export efficiency in the southern ocean. *Geophys. Res. Lett.* 40, 1557–1561. doi: 10.1002/grl.50219

Mari, X., Passow, U., Migon, C., Burd, A. B., and Legendre, L. (2017). Transparent exopolymer particles: effects on carbon cycling in the ocean. *Prog. Oceanogr.* 151, 13–37. doi: 10.1016/j.pocean.2016.11.002

Mayor, D. J., Sanders, R., Giering, S. L. C., and Anderson, T. R. (2014). Microbial gardening in the ocean's twilight zone: detritivorous metazoans benefit from fragmenting, rather than ingesting, sinking detritus: fragmentation of refractory detritus by zooplankton beneath the euphotic zone stimulates the harvestable production of labile and nutritious microbial. *BioEssays* 36, 1132–1137. doi: 10.1002/bies.201400100

McDonnell, A. M. P., Boyd, P. W., and Buesseler, K. O. (2015). Effects of sinking velocities and microbial respiration rates on the attenuation of particulate carbon fluxes through the mesopelagic zone. *Global Biogeochem. Cycles*. doi: 10.1002/2014gb004935

Obernosterer, I., and Herndl, G. J. (1995). Phytoplankton extracellular release and bacterial growth: dependence on the inorganic n: p ratio. *Mar. Ecol. Prog. Ser.* 116, 247–257. doi: 10.3354/meps116247

Olenina, I., Hajdu, S., Edler, L., Andersson, A., Wasmund, N., Busch, S., et al. (2006). *Biovolumes and size-classes of phytoplankton in the Baltic Sea* (HELCOM).

Ortiz, J., Arístegui, J., Taucher, J., and Riebesell, U. (2022). Artificial upwelling in singular and recurring mode: consequences for net community production and metabolic balance. *Front. Mar. Sci.* 8, 743105 doi: 10.3389/fmars.2021.743105

Oschlies, A., Pahlow, M., Yool, A., and Matear, R. J. (2010). Climate engineering by artificial ocean upwelling: channelling the sorcerer's apprentice. *Geophys. Res. Lett.* 37. doi: 10.1029/2009GL041961

Pan, Y., Fan, W., Zhang, D., Chen, J. W., Huang, H., Liu, S., et al. (2016). Research progress in artificial upwelling and its potential environmental effects. *Sci. China Earth Sci.* 59, 236–248. doi: 10.1007/s11430-015-5195-2

Ploug, H., and Grossart, H.-P. (2000). Bacterial growth and grazing on diatom aggregates: respiratory carbon turnover as a function of aggregate size and sinking velocity. *Limnol. Oceanogr.* 45, 1467–1475. doi: 10.4319/lo.2000.45.7.1467

Puigcorbé, V., Benitez-Nelson, C. R., Masqué, P., Verdeny, E., White, A. E., Popp, B. N., et al. (2015). Small phytoplankton drive high summertime carbon and nutrient export in the gulf of California and Eastern tropical north pacific. *Global Biogeochem. Cycles.* 29, 1309–1332. doi: 10.1002/2015GB005134

R Core Team (2021). *R: a language and environment for statistical computing.*

Riebesell, U., Czerny, J., von Bröckel, K., Boxhammer, T., Büdenbender, J., Deckelnick, M., et al. (2013). Technical note: a mobile sea-going mesocosm system – new opportunities for ocean change research. *Biogeosciences* 10, 1835–1847. doi: 10.5194/bg-10-1835-2013

Rijkenberg, M. J. A., Middag, R., Laan, P., Gerringa, L. J. A., Van Aken, H. M., Schoemann, V., et al. (2014). The distribution of dissolved iron in the West Atlantic ocean. *PloS One*, 9, e101323. doi: 10.1371/journal.pone.0101323

Riley, J. S., Sanders, R., Marsay, C. M., Le Moigne, F. A. C., Achterberg, E. P., and Poulton, A. J. (2012). The relative contribution of fast and slow sinking particles to ocean carbon export. *Global Biogeochem. Cycles*, 26. doi: 10.1029/2011gb004085

Ristow, G. H. (1997). Wall correction factor for sinking cylinders in fluids. *Phys. Rev. E.* 55, 2808–2813. doi: 10.1103/PhysRevE.55.2808

Roberts, E. C. (2003). Response of temperate microplankton communities to N:Si ratio perturbation. *J. Plankton. Res.* 25, 1485–1495. doi: 10.1093/plankt/fbg109

RStudio Team (2022). *RStudio: integrated development environment for r.*

Sanders, R., Morris, P. J., Poulton, A. J., Stinchcombe, M. C., Charalampopoulou, A., Lucas, M., et al. (2010). Does a ballast effect occur in the surface ocean. *Geophys. Res. Lett*, 37. doi: 10.1029/2010gl042574

Sarmiento, J. L., Gruber, N., Brzezinski, M. A., and Dunne, J. P. (2004). High-latitude controls of thermocline nutrients and low latitude biological productivity. *Nature* 427, 56–60. doi: 10.1038/nature02127

Sarmiento, J. L., Simeon, J., Gnanadesikan, A., Gruber, N., Key, R. M., and Schlitzer, R. (2007). Deep ocean biogeochemistry of silicic acid and nitrate. *Global Biogeochem. Cycles.* 21. doi: 10.1029/2006GB002720

Sarthou, G., Baker, A. R., Blain, S., Achterberg, E. P., Boye, M., Bowie, A. R., et al. (2003). Atmospheric iron deposition and sea-surface dissolved iron concentrations in the eastern Atlantic ocean. *Deep. Sea. Res. Part I.: Oceanogr. Res. Papers.* 50, 1339–1352. doi: 10.1016/S0967-0637(03)00126-2

Sharp, J. H. (1974). Improved analysis for "particulate" organic carbon and nitrogen from seawater. *Limnol. Oceanogr.* 19, 984–989. doi: 10.4319/lo.1974.19.6.0984

Siegel, D. A., DeVries, T., Doney, S. C., and Bell, T. (2021). Assessing the sequestration time scales of some ocean-based carbon dioxide reduction strategies. *Environ. Res. Lett.* 16, 104003. doi: 10.1088/1748-9326/ac0be0

Smetacek, V. (1985). Role of sinking in diatom life-history cycles: ecological, evolutionary and geological significance. *Mar. Biol.* 84, 239–251. doi: 10.1007/bf00392493

Smetacek, V. (1999). Diatoms and the ocean carbon cycle. *Protist* 150, 25–32. doi: 10.1016/s1434-4610(99)70006-4

Sommer, U. (1994). Are marine diatoms favoured by high Si:N ratios? *Mar. Ecol. Prog. Ser.* 115, 309–315. doi: 10.3354/meps115309

Taucher, J., Arístegui, J., Bach, L. T., Guan, W., Montero, M. F., Nauendorf, A., et al. (2018b). Response of subtropical phytoplankton communities to ocean acidification under oligotrophic conditions and during nutrient fertilization. *Front. Mar. Sci.* 5. doi: 10.3389/fmars.2018.00330

Taucher, J., Jones, J., James, A., Brzezinski, M. A., Carlson, C. A., Riebesell, U., et al. (2015). Combined effects of CO_2 and temperature on carbon uptake and partitioning by the marine diatoms thalassiosira weissflogii and *Dactyliosolen fragilissimus*: combined effects of CO_2 and temperature. *Limnol. Oceanogr.* 60, 901–919. doi: 10.1002/lno.10063

Taucher, J., Stange, P., Algueró-Muñiz, M., Bach, L. T., Nauendorf, A., Kolzenburg, R., et al. (2018a). In situ camera observations reveal major role of zooplankton in modulating marine snow formation during an upwelling-induced plankton bloom. *Prog. Oceanogr.* 164, 75–88. doi: 10.1016/j.pocean.2018.01.004

Tonnard, M., Planquette, H., Bowie, A. R., van der Merwe, P., Gallinari, M., Desprez De Gésincourt, F., et al. (2020). Dissolved iron in the north Atlantic ocean and Labrador Sea along the GEOVIDE section (GEOTRACES section GA01). *Biogeosciences* 17, 917–943. doi: 10.5194/bg-17-917-2020

Trainer, V. L., Bates, S. S., Lundholm, N., Thessen, A. E., Cochlan, W. P., Adams, N. G., et al. (2012). Pseudo-nitzschia physiological ecology, phylogeny, toxicity, monitoring and impacts on ecosystem health. *Harmful. Algae.* 14, 271–300. doi: 10.1016/j.hal.2011.10.025

Volk, T., and Hoffert, M. I. (1985). Ocean carbon pumps: analysis of relative strengths and efficiencies in ocean-driven atmospheric CO_2 changes. *Geophys. Monogr.* 32, 99–110. doi: 10.1029/GM032p0099

Wickham, H., Averick, M., Bryan, J., Chang, W., D'Agostino McGowan, L., François, R., et al. (2019). Welcome to the tidyverse. *J. Open Source Software.* 4, 1686. doi: 10.21105/joss.01686

Xiang, Y., Lam, P. J., Burd, A. B., and Hayes, C. T. (2022). Estimating mass flux from size-fractionated filtered particles: insights into controls on sinking velocities and mass fluxes in recent U.S. GEOTRACES cruises. *Global Biogeochem. Cycles.* 36. doi: 10.1029/2021GB007292

frontiers | Frontiers in Marine Science

TYPE Original Research
PUBLISHED 22 November 2023
DOI 10.3389/fmars.2023.1286899

OPEN ACCESS

EDITED BY
Alex J. Poulton,
Heriot-Watt University, United States

REVIEWED BY
Tron Frede Thingstad,
University of Bergen, Norway
Emilio Maranon,
University of Vigo, Spain

*CORRESPONDENCE
Kristian Spilling
kristian.spilling@syke.fi

RECEIVED 01 September 2023
ACCEPTED 02 November 2023
PUBLISHED 22 November 2023

CITATION
Spilling K, Arellano San Martín M, Granlund M, Schulz KG, Spisla C, Vanharanta M, Goldenberg SU and Riebesell U (2023) Microzooplankton communities and their grazing of phytoplankton under artificial upwelling in the oligotrophic ocean.
Front. Mar. Sci. 10:1286899.
doi: 10.3389/fmars.2023.1286899

Microzooplankton communities and their grazing of phytoplankton under artificial upwelling in the oligotrophic ocean

Kristian Spilling[1,2]*, Mirian Arellano San Martín[3], Mira Granlund[1], Kai G. Schulz[4], Carsten Spisla[3], Mari Vanharanta[1,5], Silvan Urs Goldenberg[3] and Ulf Riebesell[3]

[1]Marine and Freshwater Solutions, Finnish Environment Institute, Helsinki, Finland, [2]Centre for Coastal Research, University of Agder, Kristiansand, Norway, [3]Biological Oceanography, GEOMAR Helmholtz Centre for Ocean Research Kiel, Kiel, Germany, [4]Faculty of Science and Engineering, Southern Cross University, Lismore, NSW, Australia, [5]Tvärminne Zoological Station, University of Helsinki, Hanko, Finland

Ocean artificial upwelling has been suggested to boost primary production and increase harvestable resources such as fish. Yet, for this ecosystem-based approach to work, an effective energy transfer up the food web is required. Here, we studied the trophic role of microzooplankton under artificial upwelling via biomass and community composition as well as grazing rates on phytoplankton. Using mesocosms in the oligotrophic ocean, we supplied nutrient-rich deep water at varying intensities (low to high) and addition modes (a Singular large pulse or smaller Recurring pulses). Deep-water fertilization created a diatom-dominated bloom that scaled with the amount of inorganic nutrients added, but also *Synechococcus*-like cells, picoeukaryotes and nanophytoplankton increased in abundance with added nutrients. After 30 days, towards the end of the experiment, coccolithophores bloomed under recurring upwelling of high intensity. Across all upwelling scenarios, the microzooplankton community was dominated by ciliates, dinoflagellates (mixo- and heterotrophic) and radiolarians. Under the highest upwelling intensity, the average grazing rates of *Synechococcus*-like cells, picoeukaryotes and nanophytoplankton by microzooplankton were 0.35 d^{-1} ± 0.18 (SD), 0.09 d^{-1} ± 0.12 (SD), and 0.11 d^{-1} ± 0.13 (SD), respectively. There was little temporal variation in grazing of nanophytoplankton but grazing of *Synechococcus*-like cells and picoeukaryotes were more variable. There were positive correlations between abundance of these groups and grazing rates, suggesting a response in the microzooplankton community to prey availability. The average phytoplankton to microzooplankton ratio (biovolume) increased with added deep water, and this increase was highest in the Singular treatment, reaching ~30 (m^3 m^{-3}), whereas the phytoplankton to total zooplankton biomass ratio (weight) increased from ~1 under low upwelling to ~6 (g g^{-1}) in the highest upwelling but without a difference between the Singular and the Recurring mode. Several smaller, recurring upwelling events increased the importance of microzooplankton compared with one large pulse of deep water. Our results

demonstrate that microzooplankton would be an important component for trophic transfer if artificial upwelling would be carried out at scale in the oligotrophic ocean.

KEYWORDS

Atlantic Ocean, ciliates, tintinnids, dinoflagellates, radiolarians, dilution experiment

Introduction

Ocean primary production approximately equals primary production on land and forms the basis for higher trophic levels and harvestable marine resources (Field et al., 1998). In the ocean, we are currently harvesting too much of high trophic level resources, resulting in depleted fish stocks and impoverished biodiversity (FAO, 2022). With a global population recently exceeding 8 billion humans and still growing, we need to find new sources of food with minimal environmental footprint.

Vast areas of the ocean are oligotrophic and primary production is limited by inorganic nutrients. However, the ocean interior contains high concentrations of inorganic nutrients below the upper stratified surface water layer. That makes these nutrients mostly inaccessible for the microscopic phytoplankton that make up the bulk of ocean primary production. One way the nutrients become accessible is through physical mixing events at different scales (e.g. Gupta et al., 2022). This mixing is forecasted to decrease with warmer surface temperatures of the ocean as it increases the density difference between the upper ocean and underlying water layers. This will reduce the amount of inorganic nutrients reaching the sunlit surface and primary production limited by its availability (Moore et al., 2018).

A prominent form of mixing is natural upwelling. Wind and currents in combination with the earth's rotation (Coriolis force) may push coastal surface waters offshore and this surface water is replaced with upwelling deep water. Due to the inorganic nutrients in the deep water, upwelling areas are some of the most productive areas of the ocean and crucial for fisheries. With large regional, seasonal and temporal differences in upwelling, the effect of global warming is difficult to project but seems to be dependent on the location (Varela et al., 2015), but there is still a lot of uncertainty about how upwelling will be affected by global warming (e.g. Bograd et al., 2023).

With the importance of upwelling for productivity, and many fisheries being close to, or exceeding the carrying capacity, the prospect of artificial upwelling has been suggested to first increase primary productivity and then harvestable resources (Kirke, 2003). The first part of this assumption is reasonably well established. If the surface of the oligotrophic ocean is fertilized with deep water, there will be an increase in phytoplankton biomass (e.g. Sommer et al., 2002). This does not, however, automatically transfer to higher trophic levels such as fish: first, each trophic level reduces the amount of biomass available for higher trophic levels (Eddy et al., 2021); second, there could be a mismatch between primary producers and the grazing community e.g. increasing export rather than trophic transfer (Spilling et al., 2018); third, the food quality of the phytoplankton varies and may not be very suitable, or even toxic to higher trophic levels (Ianora and Miralto, 2010; Thomas et al., 2022).

The most effective route resulting in increased fisheries would be the classical food web model where large primary producers (e.g. diatoms) are grazed by mesozooplankton (e.g. copepods), and pelagic fish feeding on them. This type of short food chain with a close match between primary producers and grazers supports some of the richest fisheries in the world (Chavez and Messié, 2009). In contrast, food webs in the oligotrophic ocean typically have longer food chains, with the microbial loop being relatively more important and where microzooplankton play a major role in the trophic transfer (Calbet, 2008). Microzooplankton such as ciliates have a wide range of preferred grazing prey and could play an integral part in trophic transfer during artificial upwelling in particular in cases where there is a mismatch between primary producers and mesozooplankton grazers. Yet, the role of microzooplankton during artificial upwelling needs to be investigated before any conclusion can be made.

Technically, there are different ways artificial upwelling of deep water could be introduced to the surface. The introduction of deep water could either be stationary at one location or be placed on a floating platform that moves with a water parcel. This difference will have implications for the input of nutrient-rich water. Water masses moving past a stationary upwelling point will get one addition of deep water, whereas using a platform that floats with the water parcel would add a continuous stream of nutrient-rich water to planktonic communities in that water parcel. A single addition would presumably make one large bloom of primary producers whereas several additions of nutrients would produce a prolonged bloom with a less pronounced biomass peak. The different modes of upwelling could potentially affect the match/mismatch between primary producers and the grazers, but what effect, if any, different modes of artificial upwelling have on trophic transfer is still an open question.

Here we investigate the effect of upwelling on planktonic biomass, community, and trophic transfer. We set up a mesocosm experiment and manipulated both the amount of deep water added to the mesocosms and the mode of addition, comparing one singular addition with the same amount of inorganic nutrients added as several recurring additions.

Materials and methods

Experimental setup

The mesocosm experiment was set up off Gran Canaria (Gando Bay; 27° 55.673' N, 15° 21.870' W). The mesocosm bags, each containing ~38m^3, were set up and closed on 5th November 2018. The bags were circular (Ø = 2 m) and extended down to 15 m depth. At the bottom, there were conical-shaped sediment traps that enabled the collection of settling material. Further description of the bags can be found in Riebesell et al. (2013).

Nine mesocosm bags were used: one was left as an untreated control, and eight received different additions of deep water. These additions were done as a gradient, either in a single addition or eight smaller additions that in total equaled the nutrient gradient of the respective single addition (Table 1).

Deep water was collected on two occasions (26 Oct and 28 Nov) using a deep-water collector, which, in short, is a 100 m^3 bag that is filled at the desired depth and brought to the surface (Taucher et al., 2017). The original plan was to collect deep-water from 600 m depth, but due to technical difficulties, the water collected was from ~300 m depth on both occasions. As this water did not contain the targeted concentration of inorganic nutrients, we added nitrate, phosphate and silicate to a final concentration of 25 µmol NO_3 L^{-1}, 1.38 µmol PO_4 L^{-1} and 12.1 µmol DSi L^{-1} respectively. A more detailed description and outline of experiment events can be found in Baumann et al. (2021).

Sampling

Samples were taken every second day with an integrating water sampler (HYDRO BIOS), which collected an integrated sample from 0 – 13 m depth. The samples were stored in polycarbonate containers inside a cool box until they were processed. Samples were taken in the morning and were back in the laboratory around noon.

The plankton community was sampled and counted directly (no fixatives used) with a FlowCam (FluidImaging) using 4x magnification and a 300 µm flow cell. The camera was set to take 13 frames s^{-1} and all particles >3 µm were captured. Each sample was run for 10 min using the volumetric counting mode, equaling 10.1 mL of counted volume. Example of images taken are presented in the Supplementary Figure S1.

TABLE 1 The experimental setup with the percent original water exchanged with deep water during the addition(s), and the total addition of nitrate (sum of all additions in the Recurring treatment).

Control	Singular	Recurring (x8)
0%; 0 µM	–	–
–	6.4%; 1.6 µM	0.8%; 1.6 µM
–	12.0%; 3.1 µM	1.6%; 3.1 µM
–	22.4%; 5.6 µM	3.2%; 6.2 µM
–	39.2%//9.8 µM	6.4%//11.0 µM

Microzooplankton samples were fixed with acidic Lugol's solution and stored in a fridge until counting using a Utermöhl chamber (20 or 50 mL depending on how dense the sample was). Samples were settled overnight at room temperature before enumeration with an inverted microscope (Leitz labovert) using a 20x objective.

Mesozooplankton was collected with vertical net hauls with different sized Apstein nets (55/500 µm mesh size, ø 17/50 cm, HYDRO-BIOS Kiel) every four days. Mesozooplankton organisms were counted and categorized into different size classes (55-200 µm, 200-500 µm, > 500 µm). Based on their taxonomic identity, the most abundant species were handpicked, dried at 60°C for 24 h, packed into tin capsules and stored dry in a desiccator (GEOMAR Kiel, Thermo Scientific IRMS). Further details of sample processing can be found in Spisla (2021). Carbon content was determined by mass-spectrometry (GEOMAR Kiel, Thermo Scientific IRMS). Combining the carbon content of key species, covering different size groups, we converted the total abundance counts to mesozooplankton biomass in µg C L^{-1}.

For the comparison of ratios between different groups we also made a conversion of the biovolume of phytoplankton from the measured seston carbon concentration presented in Baumann et al., 2021. These samples were filtered, mesozooplankton removed, and the carbon content determined with a CN analyzer (Euro EA-CN, HEKAtech GmbH, Wegberg, Germany). Assuming this represented the phytoplankton, microzooplankton and detritus determined with the FlowCam, we calculated an average conversion factor of 50 µg C mm^{-3} to get a carbon estimate of phytoplankton, but noted some variability in this number with higher values outside the main biomass peaks. For microzooplankton, we used a conversion factor of 190 µg C mm^{-3} (Putt and Stoecker, 1989).

Fresh samples were run through a flow cytometer (Cytosense, Cytobuoy) using two different flow rates 1.34µl s^{-1} (180 s) and 10.86 µl s^{-1} (300 s). The first flowrate was used to determine *Synechococcus*-like cells, and the second to determine larger phytoplankton species. The flow cytometer was calibrated by running MQ water for various periods and measuring the mass loss with a high-precision balance, allowing the determination of flow rates from the slope of mass loss against time. The photomultiplier tube settings were 65 for sideward scatter (SWS), 90 for green/yellow (FLY), 90 for orange (FLO) and 93 for red fluorescence (FLR), and the trigger was set to FLR7 for the prokaryote and to FLR17 for the larger phytoplankton setting. Clustering of the data was performed in Cytoclus (version 4.8.2.8), using exclusive sets (Marie et al., 1999). Distinct clusters of *Synechococcus*-like cells were identified using average FLR against total FLY. Total FLR against total FLO was used to cluster picoeukaryotes and total FLR against total SWS was used to identify nanophytoplankton. More details on the flow cytometer methods including data on additional groups can be found in Schulz et al. (in prep).

Grazing rates

Grazing rates were determined by setting up dilution experiments (Landry and Hassett, 1982). We did dilution

experiments on every sampling day, but due to time constraints only for two mesocosms: Singular extreme and Recurring extreme.

Samples (5 L) were taken by the integrating water sampler. Half of the sample was filtered using a peristaltic pump and 0.2 µm filter cartridge (Pall). Care was taken to reduce shear stress in the sample water, e.g. by always homogenizing samples by gentle rotation of the bottle. The experiment was set up using 500 mL Tissue Culture flasks (Greiner), filled with 400 mL, leaving some headspace. The dilution series was set up using nine TC flasks. No dilution (100% sample water), and the most diluted (12.5% sample water + 87.5% 0.2 filtered water) were done in triplicates. In addition, bottles with 25%, 50% and 75% sample water, mixed with 0.2 µm filtered water of the same origin were set up.

Inorganic nutrients were added to the dilution series in F/20 medium concentration (Guillard and Ryther, 1962). The bottles were set up in a water reservoir with flow-through seawater keeping close to *in situ* temperature (20.7 - 21.5°C). The bottles were stored in random locations inside an open box to keep them in place. The box was submerged in the flow-through reservoir and covered with one layer of blue foil (172 Lagoon Blue, Lee filters) to bring the light spectrum closer to the one in the mesocosm bags. These incubations were done in the same way as the primary production measurements presented by Ortiz et al. (2022a); Ortiz et al. (2022b).

The counting of phytoplankton was done with a flow cytometer (Cube 8, Partec) with a connected autosampler taking samples from 96 well plates. The flow cytometer had two lasers (488 and 561 nm) and recorded forward and side scatter in addition to three fluorescence channels representing chlorophyll a (Chl a; 670/40 nm detection), phycoerythrin (610/30 nm) and phycocyanin (661/16 nm) pigment fluorescence. The original count was done right after the dilution series was set up and again after 24 h. Gating of the phytoplankton was done using FCS Express 6 software and main groups were identified as described above. The larger eukaryotes and coccolithophores were also excluded as we did not have the option of mounting the incubation bottles on a plankton wheel and these groups likely sank rapidly to the bottom of the incubation bottles.

Data analysis

Comparisons of treatments were done using added inorganic nitrate as explanatory variables and the mean of repeated measures of plankton biomass as response variables. Linear regressions with accompanying statistics were done in SigmaPlot 15. Comparisons between two groups were done with a Student's pairwise t-test. The effect of the treatment and temporal development on the microzooplankton community was also determined using ordination scores of the first and second axis of a nonparametric multidimensional scaling (NMDS) estimated with the metaMDS function in the vegan package in R software (Oksanen et al., 2022).

Results

Biomass

The addition of deep water stimulated a bloom of diatoms in the mesocosms, with the highest concentration in the singular extreme addition of deep water (Figures 1A, B). The largest abundance peak of diatom chains developed in the Singular extreme treatment on days 11-13, a week after the addition of deep water. Smaller diatom peaks occurred in Singular high and medium. In the Recurring extreme treatment, the diatom abundance peak developed later and was more prolonged compared with the Singular treatment (Figure 1B). In the Recurring high and medium treatments there was more diatom biomass that declined towards the very end of the experiment. Also, towards the end of the experiment, there was a bloom of coccolithophores that occurred in the Recurring extreme and, to a smaller extent, in the Recurring high treatment (Figure 1C).

Microzooplankton were dominated by ciliates, heterotrophic/mixotrophic dinoflagellates and radiolarians (Figures 1D–F). For ciliates, the abundance peaks varied temporally in the different mesocosms, with a first biomass peak at the same time as the diatom peak in the Singular high and medium treatments. This was followed by a biomass peak in the Singular extreme on day 19 followed by peaks in the Recurring extreme on day 25 and in the Recurring medium and high on days 31 and 25 respectively. There was also a second peak in ciliates biomass in the Singular extreme on day 31.

Large dinoflagellates (> 20 µm) had a peak at day 13 in the Singular extreme and high, with smaller abundance peaks in Singular medium and Recurring extreme at this time point. This dinoflagellate group became more abundant towards the end of the experiment (after day 25) in the Recurring extreme, high and medium treatments.

Radiolarians increased in biomass in most of the mesocosms with a peak around day 25, with a notable exception of Singular extreme where they were almost absent throughout the experiment. Also, in Singular low, radiolarians were at very low biomass during the main peak in other mesocosms, but there was a lower peak in this mesocosm at day 15.

There was also a clear effect of the deep-water addition on the smaller phytoplankton (Figure 2). *Synechococcus*-like cells increased in all mesocosm bags including the control, a week after the closure of the bags, but had the highest initial abundance peaks in the Singular treatment, in particular in Singular extreme and high. Picoeukaryotes and nanophytoplankton also increased rapidly in these same treatments after the addition of the deep water followed by lower abundance in all treatments after the initial peak.

The development in the mesozooplankton biomass varied between 10 to 20 µg C L^{-1} at the beginning of the experiment (Figure 3). There was one exception, Singular low, where the biomass was much lower due to the presence of small fish (data not shown). The highest peak of mesozooplankton was in the Singular high reaching 57 µg C L^{-1} (Figure 3).

Community composition

There was an effect of both deep-water addition and temporal development in the microzooplankton community composition (Figure 4). Ciliates were dominated by *Strobilidium* sp., *Strombidium* sp. and the tintinnids *Amphorides* sp. and

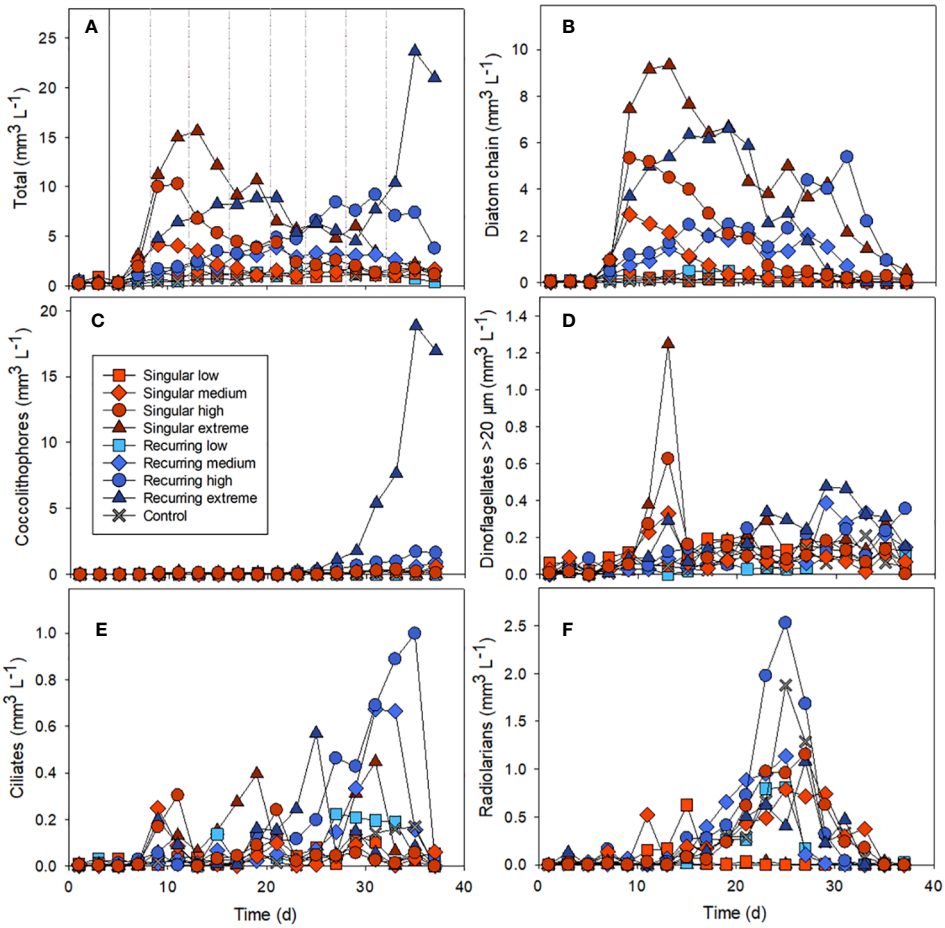

FIGURE 1
The biovolume over time of different nano- and microplankton groups: the total biovolume of all nano and microplankton **(A)**, diatom chains **(B)**, coccolithophores **(C)**, dinoflagellates >20 µm **(D)**, ciliates **(E)** and radiolarians **(F)**. Example images used in the biovolume determination can be found in the Supplementary Material (Supplementary Figure S1). The solid vertical line in Figure 1A denotes the time of addition of deep water in both singular and recurring treatments and the dashed vertical lines are addition of deep water in the Recurring treatment (similar for all graphs).

Dadayiella sp. during the first bloom of phytoplankton followed by an abundance peak in the tintinnid *Eutintinnus* sp. in the treatment with added deep water midway in the experiment. The main dinoflagellates present were *Protoperidinium* spp, *Gymnodinium* sp, *Gyrodinium* sp. *Scrippsiella* sp., *Peridiniella* sp. *Heterocapsa* spp and *Ceratium* spp. (Figure 4; Supplementary Table S1). *Protoperidinium* spp were mostly present in the Singular treatments and Recurring extreme, whereas some of the other dinoflagellates like *Gymnodinium* sp. increased in all mesocosms during the first half of the experiment. *Scrippsiella* sp. had the highest abundance peaks in the two extreme additions.

Using the microscopy abundance counts as input variables, a nonparametric multidimensional scaling plot showed that the temporal development was more important than the treatment effects for the microzooplankton community composition, but the Singular high and Singular extreme treatments were positioned a bit apart from the other treatments (Supplementary Figure S2).

There was a positive correlation between deep water added and ciliate biomass with the exception of the Recurring extreme treatment which had less ciliate biovolume than Recurring high treatment (Figure 5). The same positive correlation was found for heterotrophic dinoflagellates in the Recurring treatment, whereas the radiolarian biovolume was independent of the deep-water addition. Overall, the biovolume of microzooplankton was higher in the Recurring compared with the Singular treatment (Student's paired t-test; $p = 0.02$; Supplementary Figure S3). The mesozooplankton community was dominated by different copepods, but with a large peak of Oikopleura in some of the Singular treatments and in the Recurring high treatment towards the end of the experiment (data not shown). There was no detected difference in mesozooplankton biomass between Singular and Recurring modes of addition (Figure 6; $p = 0.5$).

There was a positive correlation between the ratio of phytoplankton to microzooplankton biomass and the deep-water addition, and the slope was steeper for the Singular compared with the Recurring treatment (Figure 7; $p = 0.016$). This ratio based on biovolume ($m^3\ m^{-3}$) was 3.26 in the control, and elevated to 30.65 and 16.12 in the Singular extreme and Recurring extreme respectively. Using biovolume converted to carbon for phytoplankton and microzooplankton, the calculated phytoplankton to zooplankton (sum of micro- and mesozooplankton) ratio was positively correlated with upwelling intensity, with an average ratio around 1

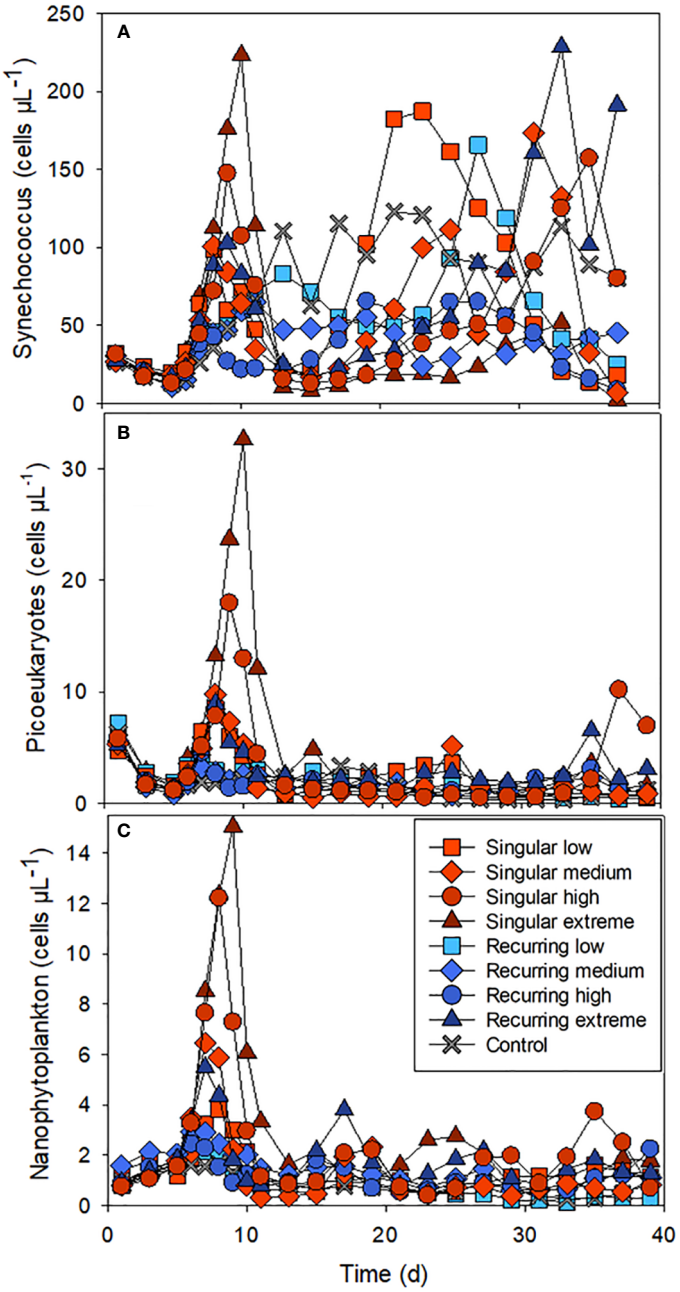

FIGURE 2
The abundance of *Synechococcus*-like cells **(A)**, picoeukaryotes **(B)** and nanophytoplankton **(C)** during the experiment. See Figure 1A for the timing of the deep-water addition.

in the control and low upwelling modes increasing to ~6 in the two extreme upwelling treatments (Figure 7), but there was no conclusive difference in the slope between Singular and Recurring upwelling ($p = 0.14$).

Grazing

The grazing rates of picoeukaryotes and nanophytoplankton increased after the addition of deep water in the Singular extreme and Recurring extreme treatments (Figures 8A, C). Grazing of *Synechococcus*-like cells were mostly present during the first half of the experiment. After this, grazing was not detectable apart from the very end of the experiment, in particular in the Recurring extreme treatment. Grazing rates of *Synechococcus*-like cells and picoeukaryotes had a higher peak in the Singular extreme compared with Recurring extreme treatment during the first half of the experiment. This was also taking place at the same time as a peak in large dinoflagellates (> 20 µm) in this treatment. Nanophytoplankton grazing was reaching the highest rates in the

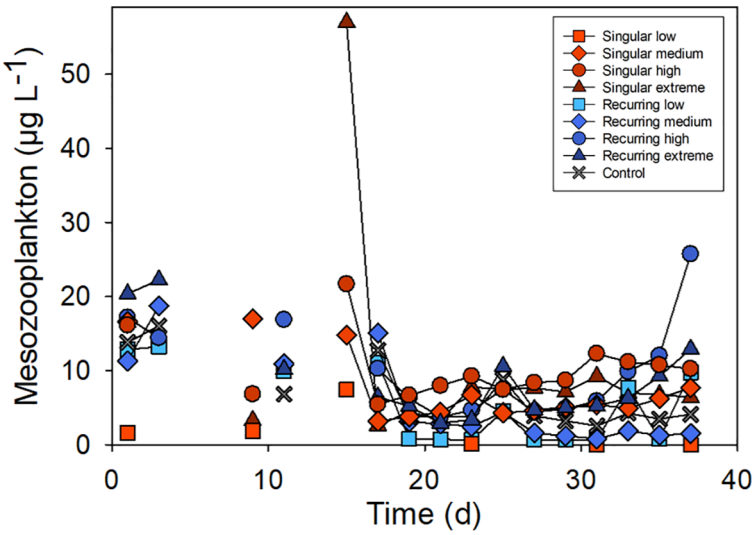

FIGURE 3
Temporal development in the total mesozooplankton biomass. See Figure 1A for the timing of the deep-water addition.

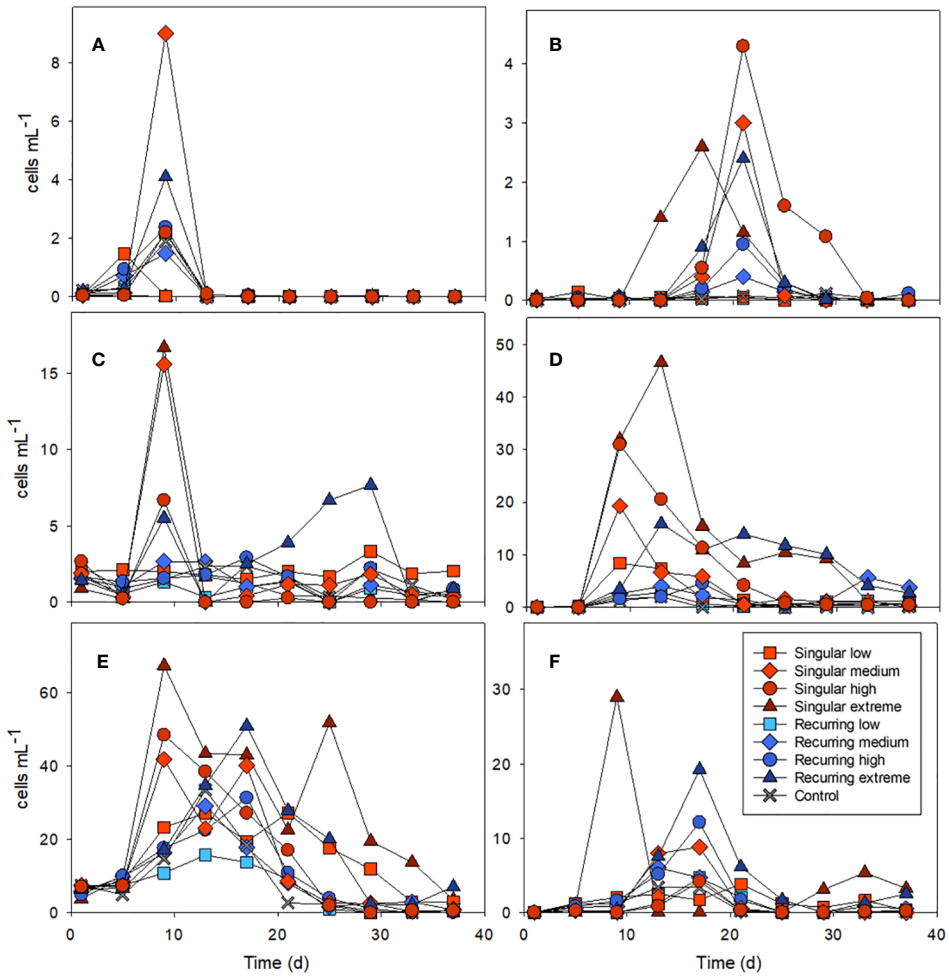

FIGURE 4
Examples of the abundance of key microzooplankton groups: ciliates combined *Amphorides* sp. plus *Dadayiella* sp. **(A)**; *Eutintinnus* sp **(B)**, combined *Strobilidium* sp. plus *Strombidium* sp **(C)**, and dinoflagellates *Protoperidinium* sp **(D)**, *Gymnodinium* **(E)** and *Scrippsiella* sp **(F)**. Abundance of all counted groups can be found in the Supplementary Table S1. See Figure 1A for the timing of the deep-water addition.

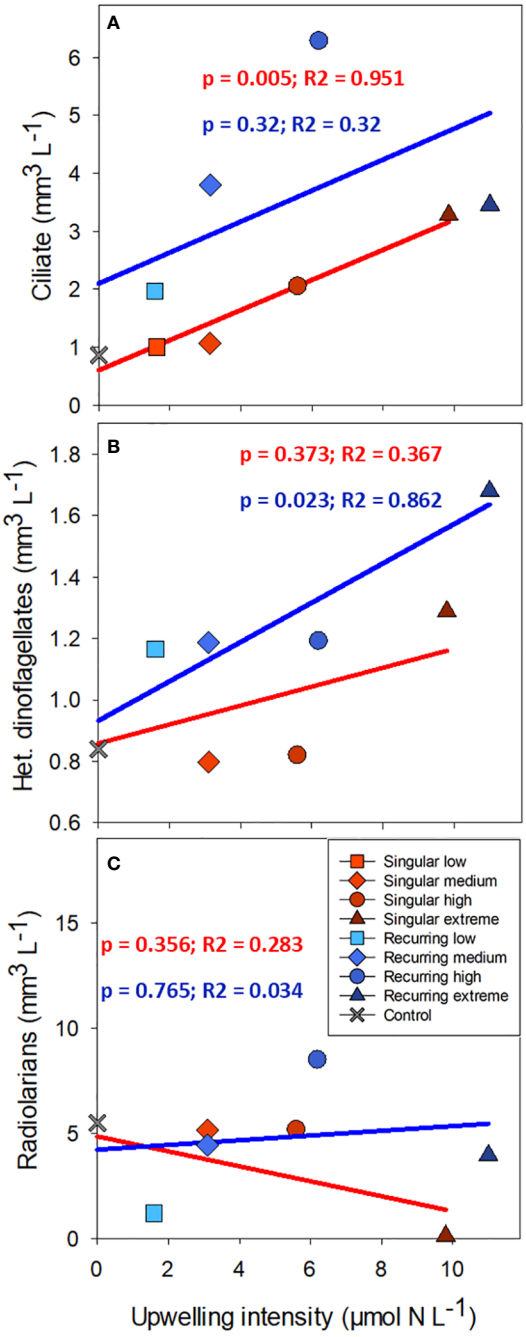

FIGURE 5
The average biovolume of ciliates **(A)**, heterotrophic dinoflagellates **(B)** and radiolarians **(C)** plotted against the addition of deep-water. Linear regression statistics for Singular mode is in red and for Recurring mode in blue.

Recurring extreme treatment on day 7 at 0.7 d^{-1}. For the rest of the experiment, grazing rates of nanophytoplankton were mostly between 0.2 to 0.6 d^{-1} in both treatments.

There was a connection between abundance and grazing rates in the Singular and Recurring extreme treatments (Figures 8A–F). Comparing the grazing rates of the three smallest autotrophic groups with their abundance counts in the respective mesocosm, revealed a positive correlation between *Synechococcus*-like cells and picoeukaryote abundance and grazing rate in the Singular extreme treatment (Figures 8B, D). The same positive correlation was found between nanophytoplankton abundance and grazing rates in the Recurring extreme treatment (Figure 8F).

Discussion

There was an effect of both increasing addition of deep water and mode of addition on the microzooplankton community and biovolume. Spreading the amount of inorganic nutrients over time provided more time for the microzooplankton community to

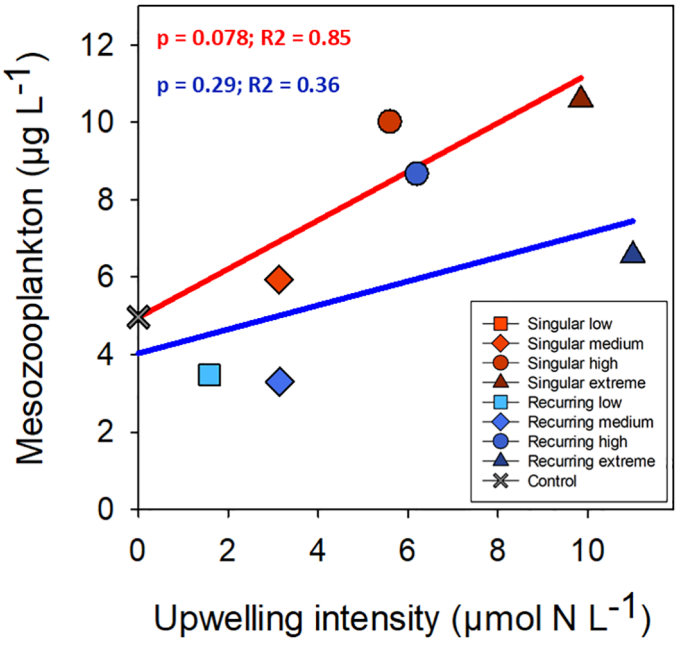

FIGURE 6
The average mesozooplankton biomass plotted against the addition of deep-water. Linear regression statistics for Singular mode is in red and for Recurring mode in blue.

respond with higher biomass overall in the Recurring treatment, but the response was different for different groups of microzooplankton. The key microzooplankton groups consisted of ciliates, heterotrophic and mixotrophic dinoflagellates and radiolarians. This is consistent with the plankton community in the area, apart from the radiolarians that are not that commonly reported (e.g. Schmoker et al., 2014).

There was a clear shift in the community of ciliates and some taxa were more affected by added nutrients than others. For example, *Strobilidium* sp and *Strobidium* sp are known to have high growth rates under favorable conditions (Montagnes, 1996) something we also observed. *Amphorides* sp. and *Dadayiella* sp, also increased rapidly after the first addition of deep water but disappeared rapidly at the end of the bloom, which to a large extent was exported out of the system (Baumann et al., 2021). Different groups of tintinnids were the main biomass of ciliates that became dominant after the initial bloom in the Singular extreme and in the Recurring treatments. The ciliate biomass in the Recurring extreme was much lower than in the Recurring high, perhaps an indication of a non-linear relationship between deep water addition and ciliate biovolume but no conclusion can be made based on one data point.

For dinoflagellates, the pronounced peak in biovolume in the beginning of the experiment was likely a response in the auto- and mixotrophic dinoflagellates benefitting from the inorganic nutrients. This was e.g. the *Gymnodinium* spp and *Scrippsiella* sp, which had a similar timing of the abundance peak after deep water addition. In the latter half of the experiment, the biovolume of heterotrophic dinoflagellates such as *Protoperidinium* spp increased in particular in the Recurring addition mode. Heterotrophic dinoflagellates typically ingest relatively large prey items (Hansen, 1991), and there is a temporal delay between food items becoming available until reaching maximum growth potential (Anderson and Menden-Deuer, 2017). The higher biovolume in the Recurring treatments suggested the increased duration of the algal bloom provided more time for heterotrophic dinoflagellates to build up biomass.

Radiolarians had a relatively high peak in biovolume in some mesocosms but were not counted in the microscopy method that was independently done. It is known that acid Lugol's solution does not work well with some microzooplankton groups as this fixative may affect both size and morphology (Stoecker et al., 1994), and the lack of microscopic counts suggest this preservation method does not work well with radiolarians. Radiolarians are well-known from the fossil records but surprisingly little is known about their ecology (Biard, 2022). Using imaging devices such as the FlowCam, that can be run without fixatives, could benefit the study of this group of protists. Interestingly, the radiolarian biomass was independent of deep-water additions. Some radiolarians are known to have photosymbionts (Decelle et al., 2015), and the driver for radiolarian growth in the mesocosms could be due to very specific grazing prey or relationships with symbionts deserving further study.

There was a clear effect of both the upwelling intensity and mode of upwelling on primary producers, and adding deep water with inorganic nutrients created a bloom of phytoplankton closely related to the concentration of nutrients added (see also Ortiz et al., 2022b). This bloom was dominated by diatoms for the first three weeks. This is not surprising as diatoms typically have an r-selected strategy with the ability to quickly take up inorganic nutrients and

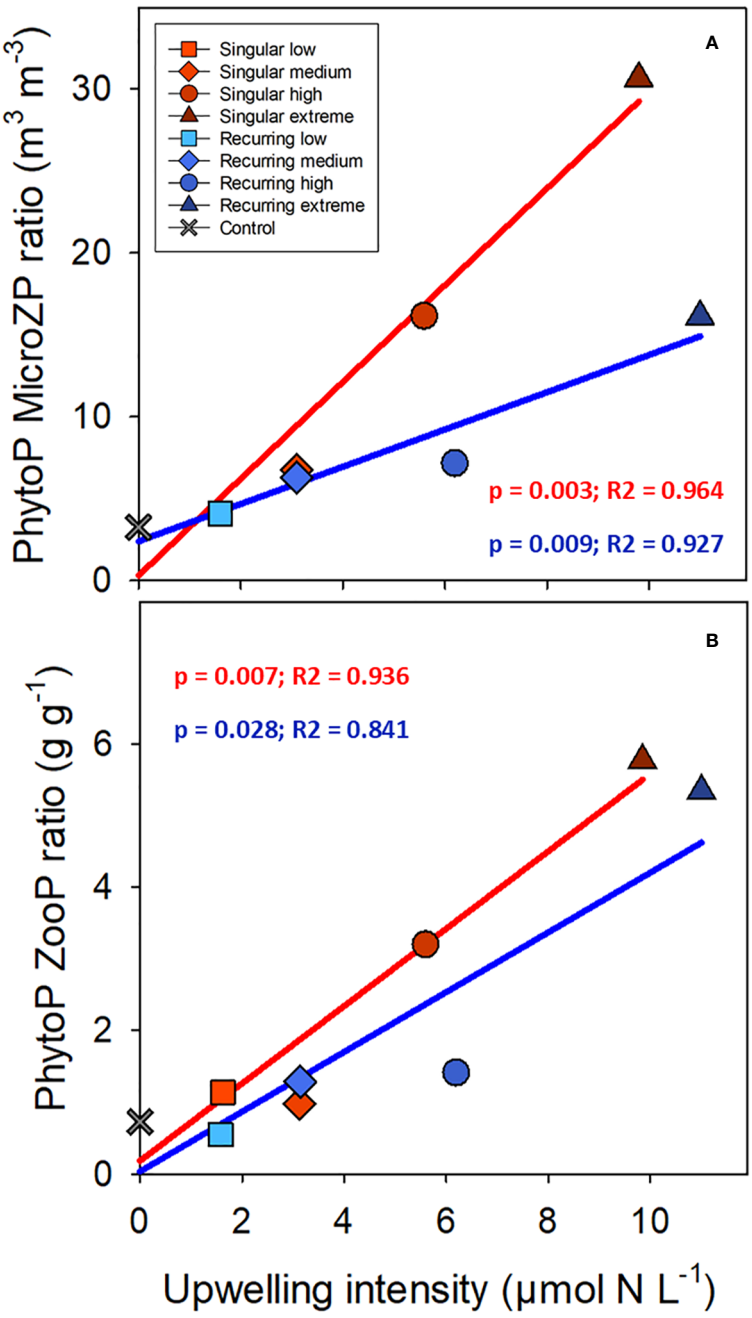

FIGURE 7
The average phytoplankton (PhytoP) to microzooplankton (MicroZP) ratio (biovolume; **A**), and phytoplankton to total zooplankton (ZooP = microzooplankton + mesozooplankton) ratio (weight; **B**) plotted against the deep-water additions. Linear regression statistics for Singular mode is in red and for Recurring mode in blue.

produce biomass under favorable conditions (e.g. Smayda and Reynolds, 2001). Making small but frequent additions of nutrients prolonged the phytoplankton bloom in comparison to adding all the nutrients at once in the beginning. In the last week of the experiment, a coccolithophore bloom was clearly visible inside the Recurring extreme mesocosm, with the water getting a milky tint. The biovolume presented for this group is likely a slight underestimation as most of the single-celled coccolithophores were not easily picked out in the FlowCam software and ended up in a group of unidentified <10 µm cells, but these would have contributed to the total biovolume.

The phytoplankton bloom that developed was also reflected in primary production, which positively correlated to nutrient additions and was higher in the Recurring treatment compared with the Singular treatment (Ortiz et al., 2022a). This difference was not detected in community respiration, suggesting that the autotrophs fixed more carbon with several smaller nutrient additions compared with the larger but shorter peak in primary

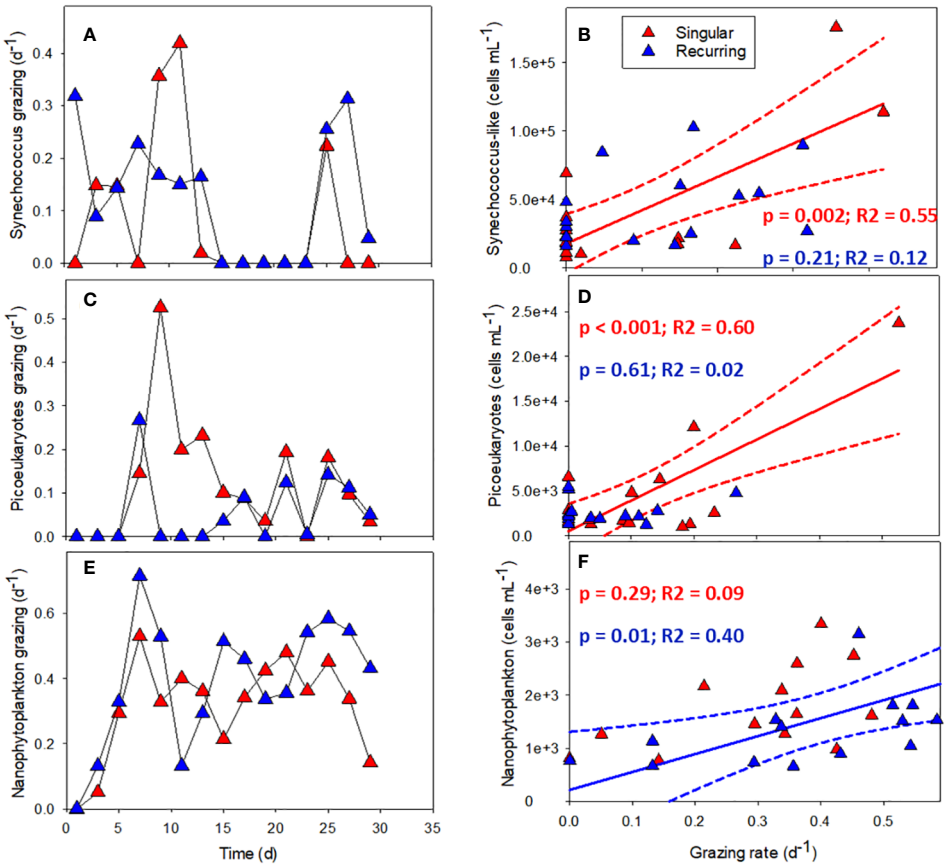

FIGURE 8
The grazing rates of *Synechococcus*-like **(A)**, picoeukaryotes **(C)** and nanophytoplankton **(E)** plotted against time in Singular and Recurring extreme, and the corresponding grazing rate plotted against abundance for the same groups: *Synechococcus*-like **(B)**, picoeukaryotes **(D)** and nanophytoplankton **(F)**. The solid lines in **(B, D, F)** represent the significant ($p < 0.05$) linear regression and dotted lines the 95% confidence interval. See Figure 1A for the timing of the deep-water addition.

production in the Singular treatments (Baños et al., 2022; Ortiz et al., 2022b).

The recorded grazing rates were in line with previous grazing rates for the coastal Atlantic Ocean (Schmoker et al., 2013), but what was a bit surprising was the sometimes low to absent grazing rates of the smaller phytoplankton groups: *Synechococcus*-like cells and picoeukaryotes. It was only the nanophytoplankton that were consistently grazed throughout the experiment. However, there was a positive correlation between grazing of *Synechococcus*-like cells and picoeukaryotes and their abundance in the Singular treatment, and nanophytoplankton grazing and its abundance in the Recurring treatment. This indicates that microzooplankton can regulate their grazing activity according to prey availability to some extent, but following low prey abundance, it might take some time for the grazers to start feeding on a particular food item again.

Dilution experiments are very elegant in theory but harder to carry out with several pitfalls when it comes to execution. Here we used relatively small volumes (about 5-orders of magnitude) compared with the mesocosms. It is clear that the conditions were not the same e.g. light, although we took steps to adjust e.g. the spectral composition of the light. We also did not have the option to place the incubation bottles on a plankton wheel and although there would be some advection due small changes in temperature in the flow-through pool where they were placed, larger non-motile organisms such as chain-forming diatoms were quickly settling to the bottom of the flasks. These were mostly >20 µm and too large for the flow cytometer to count and were not part of the nanophytoplankton group.

The diatom bloom was to a large extent exported after the inorganic nutrients were depleted (Baumann et al., 2021). Although microzooplankton did not effectively graze the diatom bloom that formed, some groups were positively correlation between deep-water addition suggesting that it was not a complete mismatch. Overall, the temporal difference in microzooplankton biomass was greater than the difference between Singular and Recurring treatments. However, the Recurring mode of addition produced higher microzooplankton biomass which gives an indication of this mode providing more time for microzooplankton to adjust to the phytoplankton food available and a better match between producers and microzooplankton consumers. There was likely also a top-down effect by mesozooplankton predation of microzooplankton. Spisla (2021) found higher trophic transfer to copepods in the Singular compared to the Recurring treatments based on ^{13}C incorporation. There were examples of rapid declines in

microzooplankton abundance that likely was due to top-down control. However, there was no overall difference in mesozooplankton biomass between Singular and Recurring treatments considering the average of the whole experiment suggesting that it was not large enough of a difference in the top-down control to make a measurable difference in mesozooplankton biomass.

Microzooplankton was particularly dominating the zooplankton biomass in the Recurring low and medium treatments suggesting it plays the biggest role under conditions with small and frequent additions of nutrients. Given additional time, microzooplankton might upgrade the food quality for larger crustacean mesozooplankton and increase the overall transfer to higher trophic levels (Campbell et al., 2009), but the experiment was too short to see any such effect here.

There are Some ocean models predict phytoplankton to zooplankton biomass ratio (P: Z ratio) in the range 0.1 – 10 with the highest values in nutrient-poor oligotrophic ecosystems that are bottom-up controlled, whereas lower ratios are found in more productive areas (Ward et al., 2012). However, other models point to an inverse relationship with the lowest P: Z ratio in less productive and increasing in more productive areas (ratio of 0.3 – 3.0; Negrete-Garcia et al., 2022). Our results are more in line with the latter in that the P: Z ratio increased with the nutrient input. The experiment was done in the oligotrophic ocean, and the duration was perhaps not enough to reach a new steady state. In other words, our high P: Z ratio in the high and extreme treatments could be a consequence of the initial mismatch between the phytoplankton and grazing communities.

Artificial upwelling would need to be done on a large scale to have any impact on ecosystem production, and bringing up such volumes of deep water would have other effects as well apart from fertilizing the surface ocean. The temperature of the upwelling water would be much lower than the surface water at low latitudes, and would itself have a cooling effect (Oschlies et al., 2010), which also affects gas solubility (Jürchott et al., 2023). Temperature was not something we addressed in this experiment, but could have practical implications for the community composition of both primary producers and zooplankton which have temperature optima that are species-specific. In addition, physiological responses are also greatly affected by temperature, and this should be studied further to understand what effect the lower temperature might have on the plankton community.

Conclusion

Grazing of the autotrophs by microzooplankton was consistent for nanophytoplankton but more variable for *Synechococcus*-like cells and picoeukaryotes, but there was a positive correlation between the abundance of these groups and grazing rates, suggesting a response in the microzooplankton community to prey availability. Some groups of microzooplankton biomass increased with deep-water addition, but the increasing P: Z ratio could be an indication that trophic transfer efficiency would be reduced with more nutrients added. Several smaller, recurring upwelling events increased the importance of microzooplankton compared with one large pulse of deep water. Our results demonstrate that microzooplankton would be an important component of trophic transfer if artificial upwelling would be carried out at scale in the oligotrophic ocean.

Data availability statement

The original contributions presented in the study are included in the article/Supplementary Material. Further inquiries can be directed to the corresponding author.

Ethics statement

The manuscript presents research on animals that do not require ethical approval for their study.

Author contributions

KS: Formal Analysis, Funding acquisition, Investigation, Methodology, Supervision, Writing – original draft. MM: Investigation, Writing – review & editing. MG: Investigation, Writing – review & editing. KGS: Formal Analysis, Investigation, Writing – review & editing. CS: Formal Analysis, Investigation, Writing – review & editing. MV: Investigation, Writing – review & editing. SUG: Formal Analysis, Investigation, Writing – review & editing. UR: Conceptualization, Funding acquisition, Investigation, Resources, Supervision, Writing – review & editing.

Funding

The author(s) declare financial support was received for the research, authorship, and/or publication of this article. This study was funded by an Advanced Grant of the European Research Council (ERC) to UR in the framework of the Ocean Artificial Upwelling project (Ocean artUp, No. 695094). Additional Transnational Access funds were provided by the EU project AQUACOSM (EU H2020-INFRAIA-project, No. 731065), which supported the participation of KS, MG and MV. KS and MV additionally got funding from Walter and Andreé de Nottbeck Foundation.

Acknowledgments

We would like to thank the Oceanic Platform of the Canary Islands (Plataforma Oceánica de Canarias, PLOCAN) and the Marine Science and Technology Park (Parque Cientiìfico Tecnoloìgico Marino, PCTM), from the University of Las Palmas (Universidad de Las Palmas de Gran Canaria, ULPGC), for support during this experiment. We are grateful for the KOSMOS team (GEOMAR) that took care of the logistics and technical work

necessary to conduct the mesocosm experiment. We would also like to thank Riina Klais-Peets at EcoStat Ltd that helped with statistics and NMDS plots. This study utilized research infrastructure provided by the Finnish Marine Research Infrastructure (FINMARI) network.

Conflict of interest

The authors declare that the research was conducted in the absence of any commercial or financial relationships that could be construed as a potential conflict of interest.

The author(s) declared that they were an editorial board member of Frontiers, at the time of submission. This had no impact on the peer review process and the final decision.

Publisher's note

Supplementary material

The Supplementary Material for this article can be found online at: https://www.frontiersin.org/articles/10.3389/fmars.2023.1286899/full#supplementary-material

References

Anderson, S. R., and Menden-Deuer, S. (2017). Growth, grazing, and starvation survival in three heterotrophic dinoflagellate species. *J. Eukaryotic Microbiol.* 64 (2), 213–225. doi: 10.1111/jeu.12353

Baños, I., Arístegui, J., Benavides, M., Gomez-Letona, M., Montero, M. F., Ortiz, J., et al. (2022). Response of plankton community respiration under variable simulated upwelling events. *Front. Mar. Sci.* 9, 1006010. doi: 10.3389/fmars.2022.1006010

Baumann, M., Taucher, J., Paul, A. J., Heinemann, M., Vanharanta, M., Bach, L. T., et al. (2021). Effect of intensity and mode of artificial upwelling on particle flux and carbon export. *Front. Mar. Sci.* 8, 742142. doi: 10.3389/fmars.2021.742142

Biard, T. (2022). Diversity and ecology of Radiolaria in modern oceans. *Environ. Microbiol.* 24, 2179–2200. doi: 10.1111/1462-2920.16004

Bograd, S. J., Jacox, M. G., Hazen, E. L., Lovecchio, E., Montes, I., Pozo Buil, M., et al. (2023). Climate change impacts on eastern boundary upwelling systems. *Annu. Rev. Mar. Sci.* 15, 303–328. doi: 10.1146/annurev-marine-032122-021945

Calbet, A. (2008). The trophic roles of microzooplankton in marine systems. ICES Journal of Marine Science. *J. du Conseil* 65, 325–331. doi: 10.1093/icesjms/fsn013

Campbell, R. G., Sherr, E. B., Ashjian, C. J., Plourde, S., Sherr, B. F., Hill, V., et al. (2009). Mesozooplankton prey preference and grazing impact in the western Arctic Ocean. *Deep Sea Res. Part II: Topical Stud. Oceanography* 56, 1274–1289. doi: 10.1016/j.dsr2.2008.10.027

Chavez, F. P., and Messié, M. (2009). A comparison of eastern boundary upwelling ecosystems. *Prog. Oceanography* 83, 80–96. doi: 10.1016/j.pocean.2009.07.032

Decelle, J., Colin, S., and Foster, R. A. (2015). "Photosymbiosis in marine planktonic protists," in *Marine protists*. Eds. S. Ohtsuka, T. Suzaki, T. Horiguchi, N. Suzuki and F. Not (Japan: Springer), 465–500. doi: 10.1007/978-4-431-55130-0

Eddy, T. D., Bernhardt, J. R., Blanchard, J. L., Cheung, W. W., Colléter, M., Du Pontavice, H., et al. (2021). Energy flow through marine ecosystems: confronting transfer efficiency. *Trends Ecol. Evol.* 36, 76–86. doi: 10.1016/j.tree.2020.09.006

FAO (2022). *The state of world fisheries and aquaculture. Towards blue transformation* (Rome: Food and Agriculture Organization of the United Nations).

Field, C. B., Behrenfeld, M. J., Randerson, J. T., and Falkowski., P. (1998). Primary production of the biosphere: integrating terrestrial and oceanic components. *Science* 281, 237–240. doi: 10.1126/science.281.5374.237

Guillard, R. R. L., and Ryther, J. H. (1962). Studies of marine planktonic diatoms. I. Cyclotella nana Hustedt, and *Detonula confervacea* (Cleve) Gran. *Can. J. Microbiol.* 8, 229–239. doi: 10.1139/m62-029

Gupta, M., Williams, R. G., Lauderdale, J. M., Jahn, O., Hill, C., Dutkiewicz, S., et al. (2022). A nutrient relay sustains subtropical ocean productivity. *Proc. Natl. Acad. Sci.* 119, e2206504119. doi: 10.1073/pnas.2206504119

Hansen, P. J. (1991). Quantitative importance and trophic role of heterotrophic dinoflagellates in a coastal pelagial food web. *Mar. Ecol. Prog. Ser.* 253–261.

Ianora, A., and Miralto, A. (2010). Toxigenic effects of diatoms on grazers, phytoplankton and other microbes: a review. *Ecotoxicology* 19, 493–511. doi: 10.1007/s10646-009-0434-y

Jürchott, M., Oschlies, A., and Koeve, W. (2023). Artificial upwelling—A refined narrative. *Geophysical Res. Lett.* 50, e2022GL101870. doi: 10.1029/2022GL101870

Kirke, B. (2003). Enhancing fish stocks with wave-powered artificial upwelling. *Ocean Coast. Manage.* 46, 901–915. doi: 10.1016/S0964-5691(03)00067-X

Landry, M., and Hassett, R. (1982). Estimating the grazing impact of marine micro-zooplankton. *Mar. Biol.* 67, 283–288. doi: 10.1007/BF00397668

Marie, D., Brussaard, C. P., Thyrhaug, R., Bratbak, G., and Vaulot., D. (1999). Enumeration of marine viruses in culture and natural samples by flow cytometry. *Appl. Environ. Microbiol.* 65, 45–52. doi: 10.1128/AEM.65.1.45-52.1999

Montagnes, D. J. (1996). Growth responses of planktonic ciliates in the genera *Strobilidium* and *Strombidium*. *Mar. Ecol. Prog. Ser.* 130, 241–254. doi: 10.3354/meps130241

Moore, J. K., Fu, W., Primeau, F., Britten, G. L., Lindsay, K., Long, M., et al. (2018). Sustained climate warming drives declining marine biological productivity. *Science* 359, 1139–1143. doi: 10.1126/science.aao6379

Negrete-García, G., Luo, J. Y., Long, M. C., Lindsay, K., Levy, M., and Barton, A. D. (2022). Plankton energy flows using a global size-structured and trait-based model. *Prog. Oceanogr.* 209, 102898. doi: 10.1016/j.pocean.2022.102898

Oksanen, J., Simpson, G. L., Blanchet, F. G., Kindt, R., Legendre, P., Minchin, P. R., et al. (2022) *R Package 'vegan': Community ecology package*. Available at: https://cran.r-project.org/web/packages/vegan/vegan.pdf.

Ortiz, J., Arístegui, J., Hernández-Hernández, N., Fernández-Méndez, M., and Riebesell., U. (2022a). Oligotrophic phytoplankton community effectively adjusts to artificial upwelling regardless of intensity, but differently among upwelling modes. *Front. Mar. Sci.* 9, 880550. doi: 10.3389/fmars.2022.880550

Ortiz, J., Arístegui, J., Taucher, J., and Riebesell, U. (2022b). Artificial upwelling in singular and recurring mode: Consequences for net community production and metabolic balance. *Front. Mar. Sci.* 8, 743105. doi: 10.3389/fmars.2021.743105

Oschlies, A., Pahlow, M., Yool, A., and Matear, R. J. (2010). Climate engineering by artificial ocean upwelling: Channelling the sorcerer's apprentice. *Geophysical Res. Lett.* 37, L04701. doi: 10.1029/2009GL041961

Putt, M., and Stoecker, D. K. (1989). An experimentally determined carbon: volume ratio for marine "oligotrichous". *ciliates Estuar. Coast. waters. Limnology oceanography* 34, 1097–1103. doi: 10.4319/lo.1989.34.6.1097

Riebesell, U., Czerny, J., v. Bröckel, K., Boxhammer, T., Büdenbender, J., Deckelnick, M., et al. (2013). Technical Note: A mobile sea-going mesocosm system–new opportunities for ocean change research. *Biogeosciences* 10, 1835–1847. doi: 10.5194/bg-10-1835-2013

Schmoker, C., Hernández-León, S., and Calbet, A. (2013). Microzooplankton grazing in the oceans: impacts, data variability, knowledge gaps and future directions. *J. Plankton Res.* 35 (4), 691–706. doi: 10.1093/plankt/fbt023

Schmoker, C., Ojeda, A., and Hernández-León, S. (2014). Patterns of plankton communities in subtropical waters off the Canary Islands during the late winter bloom. *J. Sea Res.* 85, 155–161. doi: 10.1016/j.seares.2013.05.002

Smayda, T. J., and Reynolds, C. S. (2001). Community assembly in marine phytoplankton: application of recent models to harmful dinoflagellate blooms. *J. Plankton Res.* 23, 447–461. doi: 10.1093/plankt/23.5.447

Sommer, U., Stibor, H., Katechakis, A., Sommer, F., and Hansen, T. (2002). Pelagic food web configurations at different levels of nutrient richness and their implications for the ratio fish production: primary production. *Hydrobiologia* 484, 11–20. doi: 10.1023/A:1021340601986

Spilling, K., Olli, K., Lehtoranta, J., Kremp, A., Tedesco, L., Tamelander, T., et al. (2018). Shifting diatom-dinoflagellate dominance during spring bloom in the Baltic Sea

and its potential effects on biogeochemical cycling. *Front. Mar. Sci.* 5, 327. doi: 10.3389/fmars.2018.00327

Spisla, C. (2021). *Marine zooplankton community responses to anthropogenic influences*. PhD thesis. (Kiel University). Available at: https://oceanrep.geomar.de/id/eprint/57680/. 162 pp.

Stoecker, D. K., Gifford, D. J., and Putt, M. (1994). Preservation of marine planktonic ciliates: losses and cell shrinkage during fixation. *Mar. Ecol. Prog. Ser.* 110, 293–299. doi: 10.3354/meps110293

Taucher, J., Bach, L. T., Boxhammer, T., Nauendorf, A., Consortium, G. C. K., Achterberg, E. P., et al. (2017). Influence of ocean acidification and deep water upwelling on oligotrophic plankton communities in the subtropical North Atlantic: insights from an in *situ* mesocosm study. *Front. Mar. Sci.* 4, 85. doi: 10.3389/fmars.2017.00085

Thomas, P. K., Kunze, C., Van de Waal, D. B., Hillebrand, H., and Striebel., M. (2022). Elemental and biochemical nutrient limitation of zooplankton: A meta-analysis. *Ecol. Lett.* 25, 2776–2792. doi: 10.1111/ele.14125

Varela, R., Álvarez, I., Santos, F., DeCastro, M., and Gómez-Gesteira, M. (2015). Has upwelling strengthened along worldwide coasts over 1982-2010? *Sci. Rep.* 5 (1), 10016. doi: 10.1038/srep10016

Ward, B. A., Dutkiewicz, S., Jahn, O., and Follows, M. J. (2012). A size-structured food-web model for the global ocean. *Limnol. Oceanogr.* 57 (6), 1877–1891. doi: 10.4319/lo.2012.57.6.1877

Frontiers in Marine Science

Explores ocean-based solutions for emerging global challenges

The third most-cited marine and freshwater biology journal, advancing our understanding of marine systems and addressing global challenges including overfishing, pollution, and climate change.

Discover the latest Research Topics

See more →

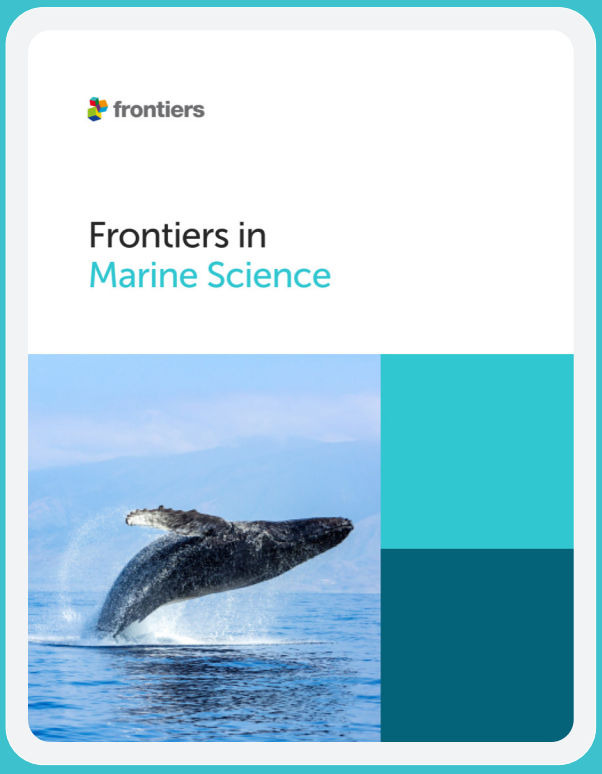

Frontiers

Avenue du Tribunal-Fédéral 34
1005 Lausanne, Switzerland
frontiersin.org

Contact us

+41 (0)21 510 17 00
frontiersin.org/about/contact